Karlsruhe Institute of Technology

Annual Report 2024/25

Institute for Nuclear Waste Disposal

By H. Geckeis, M. Altmaier, S. Fanghänel, V. Metz, J. Rothe (Eds.)

INE SCIENTIFIC WORKING DOCUMENTS 09

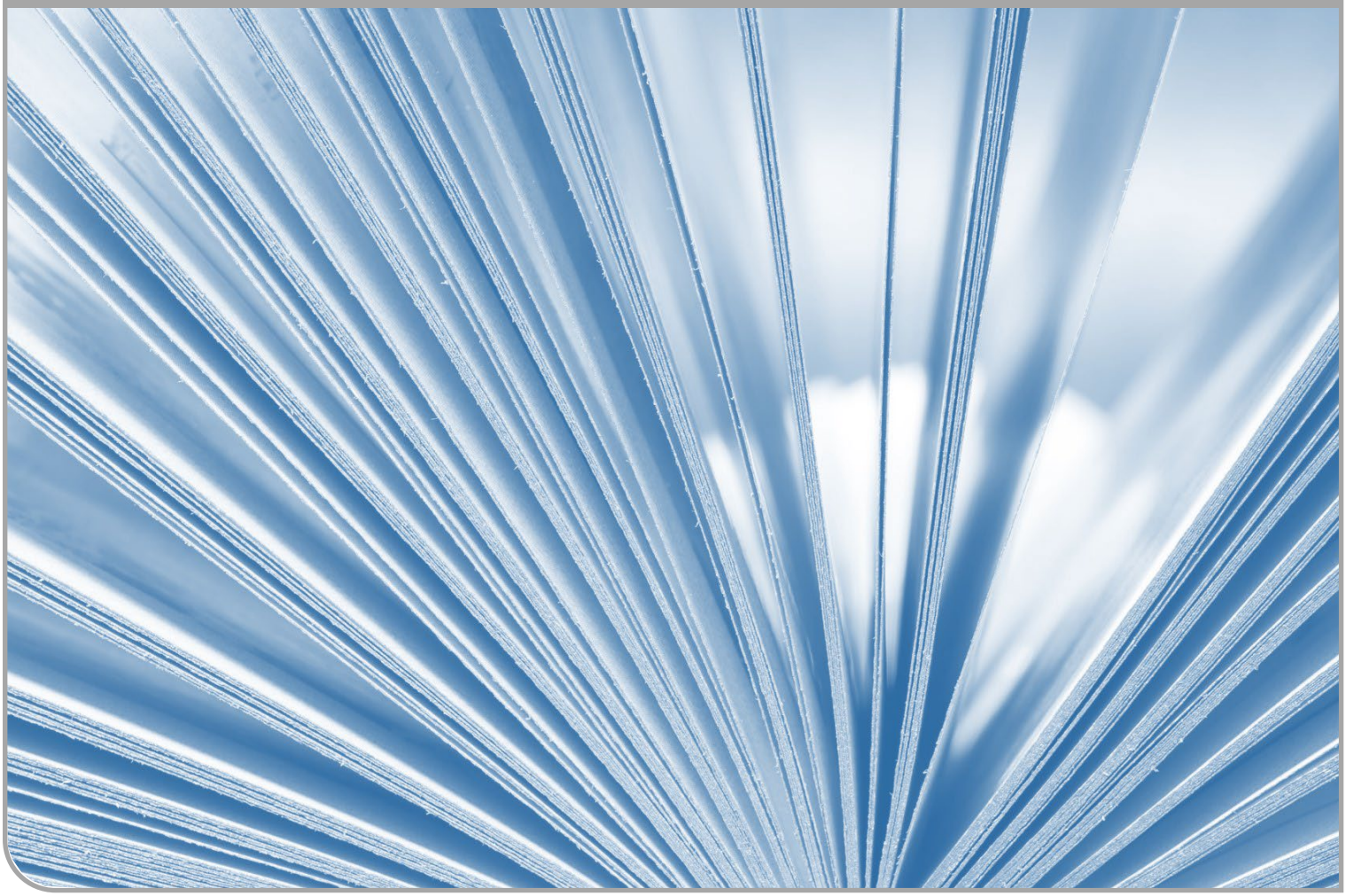

Institut für Nukleare Entsorgung (INE)

Hermann-von-Helmholtz-Platz 1
76344 Eggenstein-Leopoldshafen
www.ine.kit.edu

Impressum

Karlsruher Institut für Technologie (KIT)
www.kit.edu

2026

URL: http://www.ine.kit.edu/53.php
ISSN: 2701-262X
DOI: 10.5445/IR/1000192576

Foreword

The Institute for Nuclear Waste Disposal (INE) is part of the Karlsruhe Institute of Technology (KIT). A main part of KIT-INE's research covers nuclear aspects of the German Nuclear Waste Disposal programme, i.e. fundamental and applied studies on the behaviour of radioactive waste forms and radionuclides in environments typical to nuclear waste repositories. To do so, dedicated nuclear laboratory infrastructures equipped with state-of-the-art instrumentation are continuously developed and upgraded. INE operates one of the very few radiochemistry research laboratories equipped with a shielded box line ("hot cell") and a license acc. to §9 of the German atomic law (AtG), which allows to investigate i.a. highly radioactive materials such as irradiated nuclear fuel under repository and interim storage conditions. Those laboratories are in close vicinity to the Karlsruhe light source at the Karlsruhe Research Accelerator (KARA) facility where KIT-INE operates dedicated beamlines for the characterization of radioactive samples offering a wide range of synchrotron-based X-ray spectroscopic methods.

KIT-INE was using additional opportunities to further develop the already available analytical and technical infrastructure at KIT-INE within the HOVER project, funded by BMBF and the Helmholtz Association. After the official ground-breaking ceremony in October 2025, realisation of a new laboratory for high-precision accelerator mass spectrometry at KIT Campus North - a core infrastructure project of HOVER - is finally within reach and expected for 2027. HOVER is also providing new laboratory infrastructures for "predisposal" tropics: Within a dedicated laboratory it will be possible to investigate spent nuclear fuel cladding behaviour under extended interim storage conditions. Establishment of virtual laboratories and notably a Building Information Modelling (BIM) laboratory will enhance KIT research on the optimization of decommissioning processes significantly.

During the reporting period, KIT-INE continued research activities within large European projects, i.e. closing PREDIS and EURAD-1 and especially transitioning into a new EURAD-2 project phase. KIT-INE was significantly involved in developing the scientific work plan and contributed scientific research into these networks within various work packages (WP) as well as taking initiative as WP leader or Task leader. KIT-INE strongly contributed to the German site selection process by performing work on specific relevant topics under contract to the German Waste Management Organisation BGE. Project work related to the closure of the Asse II legacy site likewise continued to demand focused activities. Research funding provided by German ministries especially supported work by PhD students. INE researchers contributed to several events organized in Germany to discuss options and facts regarding waste disposal with the interested public and key institutional stakeholders. Providing scientific understanding and expertise is clearly at the core of decision-making and offers important feedback options to our research activities.

Ongoing efforts at INE to train students and early career researchers in the field of nuclear waste disposal importantly contribute to the availability of highly trained experts in the field. In this context it is especially positive that two colleagues from INE took significant new steps in their respective careers, Prof. Tonya Vitova was awarded with a professorship at the KIT faculty for Chemistry and Biosciences, and Dr. Frank Heberling successfully completed his habilitation at the faculty of Civil Engineering, Geo- and Environmental Sciences.

The institute is also active in organizing conferences in the nuclear field. In October 2024, KIT-INE was organizing "ATAS - AnXAS 2024", merging the 6th International Workshop on Advanced Techniques in Actinide Spectroscopy and the 10th International Workshop on Speciation, Techniques and Facilities for Radioactive Materials at Synchrotron Light Sources. The workshop attracted a total of 94 participants from 10 countries. Invited keynote lectures and contributed oral presentations were covering a broad range of radionuclide speciation methods and application fields - from radio-toxicology and medicine to the characterization of nuclear waste forms. INE scientists were decisively involved in the organization of the 19th International Conference on the Migration of Actinides and Fission Products in the Geosphere, Migration 2025 in New Orleans together with Clemson University and the Lawrence Livermore National Laboratory (LLNL). 185 participants from 16 countries contributed with oral and poster presentations on specific topics related to experimental and theoretical studies on radionuclide reactions under disposal conditions. Furthermore, interesting insight was provided into the specific developments within US legacy site and nuclear waste management programmes.

Research at KIT-INE goes beyond nuclear waste disposal topics. The challenging task of rebuilding the energy system in Germany requires a broad variety of technologies. Geoenergy can play an important role in respective systems. KIT has started to construct two major research infrastructures, in order to study relevant processes under realistic conditions: The GeoLab facility aims at integrating German research activities in a large underground research laboratory. The second facility DeepStor is planned to be established at the KIT-CN site and aims at developing high-temperature heat storage technologies. Both projects do not only concentrate on

technical issues with cutting-edge research tools but also consider close interaction with the public and decision makers.

KIT-INE research performed within the mid-term evaluation organised by the Helmholtz Association contributions to the NUSAFE and MTET programs was assessed very positively and received outstanding and excellent grades on an international level. We take this most positive high-level feedback as strong motivation and momentum to further develop our research into the future. In all KIT-INE activities, we are looking back to numerous excellent scientific results, successfully finished laboratory projects, master- and doctoral theses, and important newly acquired third party funded projects.

It must be emphasized, that the scientific success of KIT-INE research as well as the development and operation of unique and sophisticated infrastructure facilities in nuclear sciences and geoenergy were only possible due to the outstanding commitment of all technicians and scientists involved.

Prof. Dr. Horst Geckeis

Director of the Institute for Nuclear Waste Disposal

Table of contents

1 Introduction to the Institute for Nuclear Waste Disposal (INE)

The **Institute for Nuclear Waste Disposal** (INE), at the Karlsruhe Institute of Technology **KIT** performs R&D focusing on

(i) Long-term safety research for nuclear waste disposal (key focus of INE research)
(ii) Predisposal research
(iii) Geoenergy research

All R&D activities of INE are integrated into the program Nuclear Safety Research and Energy Storage within the KIT-Energy Center and the programs Nuclear Waste Management, Safety and Radiation Research (NUSAFE) and Materials and Technologies for the Energy Transition (MTET) within the Helmholtz Association. INE contributes to German provident research for the safety of nuclear waste disposal, which is the responsibility of the Federal Government.

Following the decision taken by Germany to phase out the use of nuclear energy, the safe disposal of long-lived nuclear waste remains as a key topic of highest priority. Calculations for Germany indicate that about a total of 17,770 tons of spent nuclear fuel have been generated. About 6,670 tons have been shipped to France and the UK until 2005 for reprocessing, to recover plutonium and uranium. Consequently, two types of high level, heat producing radioactive waste (HLW) have to be disposed of safely: spent nuclear fuel and vitrified high-level waste from reprocessing (HLW glass). The disposal of low- and intermediate level waste present in much larger quantities likewise needs to be addressed.

Over the last decades, a consensus within the international scientific/technical community was established, clearly emphasizing that final disposal in deep geological formations is the safest way to dispose of high level, heat producing radioactive waste. Disposal concepts with strong inherent passive safety features ensure the effective protection of the population and the biosphere against radiation exposure over very long periods of time. The isolation and immobilization of nuclear waste in a repository is ensured by the appropriate combination of redundant barriers (multi-barrier system).

Long term safety research for nuclear waste disposal at INE develops geochemical expertise and models to be used in the nuclear waste disposal Safety Case, focusing primarily on the detailed scientific description of aquatic radionuclide chemistry in the geochemical environment of a repository. Work concentrates on the disposal of spent nuclear fuel (SNF) and HLW-glass in the relevant potential host rock formations currently considered: rock salt, clay and crystalline rock formations. Actinides and long-lived fission and activation products play a central role, as they dominate HLW radiotoxicity and risks over long periods of time. Long-lived anionic fission and activation products are likewise investigated as significant contributors to the maximum radiation dose projected for relevant scenarios.

Relevant long-term scenarios for nuclear repositories in deep geological formations have to take into account possible radionuclide transport via the groundwater pathway. Possible groundwater intrusion into emplacement caverns may cause waste form corrosion and eventually radionuclide release. Radionuclide mobility is then determined by the various geochemical reactions in complex aquatic systems: i.e., dissolution of the nuclear waste form (HLW glass, spent nuclear fuel), radiolysis phenomena, redox reactions, complexation with inorganic and organic ligands, colloid formation, surface reactions at mineral surfaces, precipitation of solid phases and solid solutions.

Prediction and quantification of all these processes require fundamental thermodynamic data and comprehensive process understanding at the molecular scale. Radionuclide concentrations in relevant aqueous systems typically lie in the nano-molar range, which is exceedingly small in relation to main groundwater components. Quantification of chemical reactions occurring in these systems require the application and development of advanced tools and experimental approaches, to provide insight into the chemical speciation of radionuclides at trace concentrations. Innovative laser and X-ray spectroscopic techniques are continuously developed and applied to this end. A specialized working group performing state-of-art quantum chemical calculations for radionuclide chemistry supports both interpretation of experimental results and optimized experiment design.

The long-term safety of a nuclear waste repository must be demonstrated by application of modelling tools on real natural systems over geological time scales. Geochemical models and thermodynamic databases are developed at INE as basis for the description of radionuclide geochemical behavior in complex natural aquatic systems. The prediction of radionuclide migration in the geosphere necessitates coupled modelling of geochemistry and transport. Transferability and applicability of model predictions are examined by designing dedicated laboratory experiments, field studies in underground laboratories and by studying natural analog systems. This strategy allows to identify and analyze key uncertainties and continuously optimize the developed models.

Predisposal research activities deal with HLW interim storage issues and decommissioning of nuclear facilities. As the storage period for HLW is expected to exceed the originally licensed periods

by far and may be as long as 100 years, the evolution of these heat-generating waste types must be investigated under prolonged dry interim storage conditions. In particular it is essential to assess the structural integrity of rod claddings of spent nuclear fuel assemblies over such timescales to ensure safety during storage, handling, transport and safe reloading of SNF from storage and transport containers into a final disposal container. The work at INE focuses on the role of zirconium hydrides, which form in fuel rod cladding as a result of hydrogen absorption during reactor operation and hydride precipitation during cooling after irradiation, as well as on the role of halogenide-bearing precipitates that form at fuel pellet - cladding interfaces. Both hydride morphology / distribution and chemical pellet cladding interactions are crucial for the integrity of the cladding and the long-term safety of irradiated fuel rods.

The R&D topic **decommissioning of nuclear and conventional facilities** at INE expands the existing activities at the Institute of Technology and Management in Construction (KIT-TMB). Research in this field is focusing on a better understanding of the complete decommissioning process in Germany as well as on a global level.

For the environmentally-friendly use and monitoring of deep geothermal resources, the topic **geoenergy** at INE focusses on the development and testing of novel and integrative concepts for the management of the deep underground and of geophysical monitoring methods. Against this background, reservoir properties and processes and their influence on geophysical fields that are used for exploration and monitoring are crucial. To investigate this, experiments on different scales, from laboratory to reservoir scale, are carried out. Between 2024 and 2025, research work in the field of geoenergy was carried out in collaboration with the geoenergy division of the Institute for Applied Geoscience (KIT-AGW).

INE laboratories are equipped with all necessary infrastructures to perform radionuclide/actinide research, including a shielded box line enabling the investigation of spent nuclear fuel and nuclear waste glass, alpha glove boxes, inert gas alpha glove boxes and radionuclide laboratories. State-of-the-art analytical instruments and methods are applied for analysis and speciation of radionuclides and radioactive materials. Advanced spectroscopic tools exist for the sensitive detection and analysis of radionuclides. Trace element and isotope analysis is made by instrumental analytical techniques such as atomic absorption spectroscopy (AAS), ICP-atomic emission spectroscopy (ICP-AES) and ICP-mass spectrometry (Quadrupole-ICP-MS and high resolution ICP-MS). Methods available for characterization of solid bulk samples and surface sensitive analysis include X-ray powder diffraction (XRD) and atomic force microscopy (AFM). A modern X-ray photoelectron spectrometer (XPS) and an environmental scanning electron microscope (ESEM) are installed, recently augmented by focused ion beam – scanning electron microscopy (FIB-SEM) and X-ray microtomography (μ-CT). Laser spectroscopic techniques are developed and applied for sensitive actinide and fission product speciation such as time-resolved laser fluorescence spectroscopy (TRLFS), laser-induced breakdown detection (LIBD) and Raman spectroscopy. Insight into structural and electronic properties of radionuclide species is obtained by X-ray absorption fine structure (XAFS) spectroscopy and related techniques available at the INE-Beamline and the ACT experimental station at the KIT Light Source. INE's beamlines, in close proximity to INE controlled area laboratories, represent in combination with the other analytical methods a unique experimental infrastructure, which both profits from and contributes to INE's leading expertise in the field of actinide chemistry and spectroscopy. A 400 MHz-NMR spectrometer adapted to measuring radioactive liquid samples adds to the analytical and speciation portfolio of INE. State-of-the-art quantum chemical and molecular modelling calculations are possible on INE's high performance scientific computing cluster. The INE CAD workstations enable construction and planning of hardware components, process layout and flow sheets. The institute workshop is equipped with modern machine tools to manufacture components for specific experimental and analytical devices in hot laboratories.

In 2024 and 2025, the **Institute for Nuclear Waste Disposal** had around **100 employees** working in six departments and one cluster, which reflect the R&D and organizational tasks of the institute (Fig. 1).

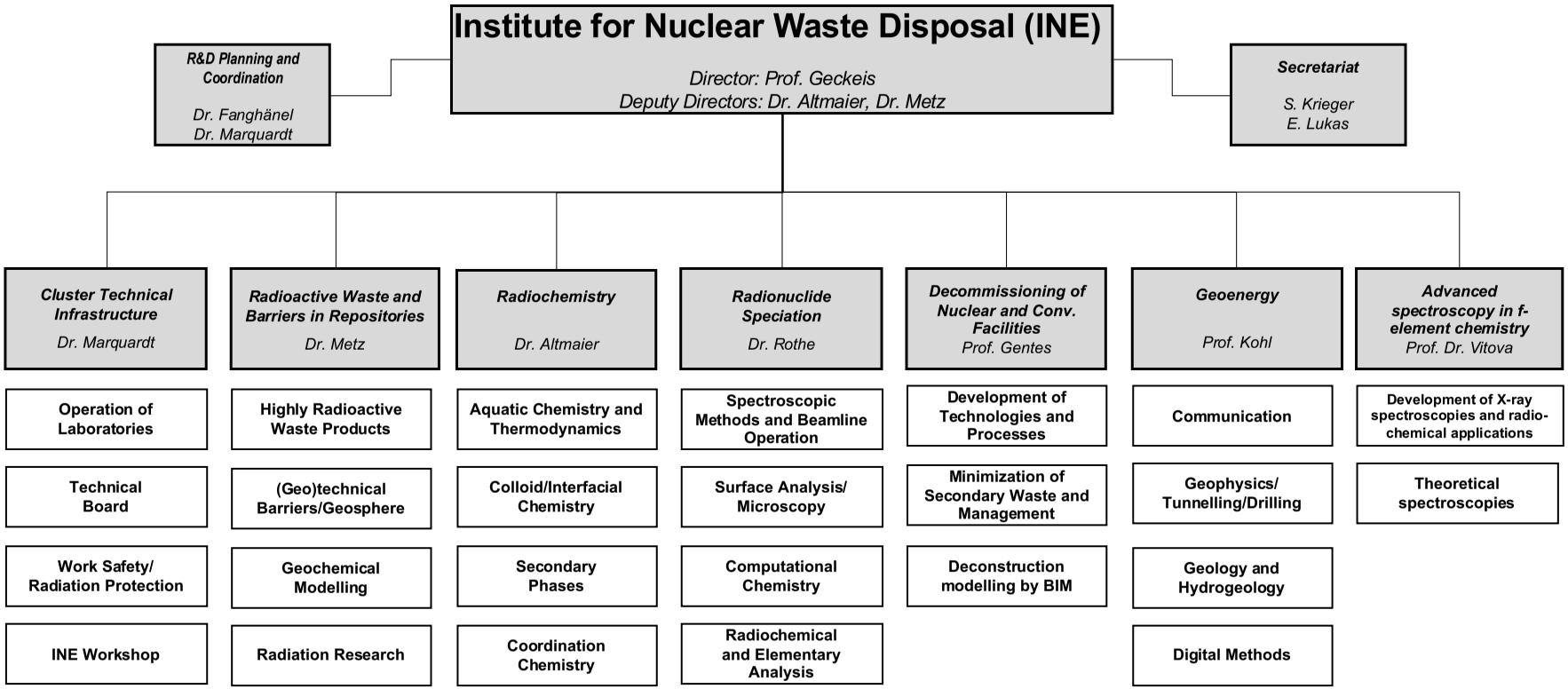

Fig. 1: Organizational chart of the Institute for Nuclear Waste Disposal (INE)

2 Education and training

Teaching of students and promotion of young scientists is of fundamental importance to ensure high-level competence and to maintain a leading international position in the fields of nuclear and radiochemistry. INE scientists are strongly involved in teaching at KIT and the University of Heidelberg.

Prof. Dr. **Horst Geckeis**, director of INE, holds a professorship for radiochemistry at KIT, Department of Chemistry and Biosciences. He teaches fundamental and applied radiochemistry for chemistry students in bachelor and master courses. A radiochemistry module consisting of basic and advanced lectures on nuclear chemistry topics and laboratory courses has been set up for master students in Karlsruhe. In addition, Dr. **Marcus Altmaier**, department radiochemistry, gives a lecture concerning the chemistry of f-elements.

Prof. Dr. **Sascha Gentes,** department decommissioning of nuclear and conventional facilities, holds a professorship at the Institute for Technology and Management in Construction at the KIT-Department of Civil Engineering, Geo and Environmental Sciences and gives lectures in the field of decommissioning of nuclear facilities, environmentally-friendly Recycling and Disassembly of Buildings, Machinery and Process Engineering as well as construction technology.

Prof. Dr. **Petra Panak**, heading a working group on coordination chemistry at INE, holds a professorship of radiochemistry at the Heidelberg University. A basic course in radiochemistry is offered for bachelor and/or master students. An advanced course comprised of the chemistry of f-elements and medical applications of radionuclides is also offered. The advanced radiochemistry lectures are supplemented by scientific internships at the INE radioactive laboratories.

Around 80 students from Karlsruhe and Heidelberg participated in three 3-week radiochemistry laboratory courses in 2024 and 2025 held at KIT Campus North in the FTU radiochemistry and the hot laboratories at INE. Some students are intensifying their knowledge in nuclear/radiochemistry topics during scientific internships at INE. Obviously, students are very interested in nuclear chemistry topics and appreciate the various semester courses.

Prof. Dr. **Tonya Vitova** gives lectures at KIT, Department of Chemistry and Biosciences, in the field of instrumental analytics. Dr. **Volker Metz** and Prof. Dr. **Ron Dagan** give lectures at the Department of Mechanical Engineering in the field of nuclear fuel cycle. Lectures and practical units taught by Dr. **Frank Heberling** and Dr. **Volker Metz** at KIT, Department of Civil Engineering, Geo and Environmental Sciences, focused in 2024 and 2025 on “geoscientific aspects of the disposal of radioactive and chemically toxic waste”.

Moreover, INE was involved in many schools and workshops concerning the education and teaching of students and young scientists.

Through this close cooperation with universities, students are educated in the field of nuclear and actinide chemistry, which most universities can no longer offer. Hence, INE makes a vital contribution to the intermediate and long perspective of maintaining nuclear science competence. Moreover, INE is involved in the education of trainees (chemical lab technicians, industrial mechanics and product designers) as well as student internships like BORS and BOGY.

PhD students

In 2024 and 2025, 18 doctoral students worked at INE on their dissertations; nine doctoral students were awarded their doctorate in 2024/2025.

Topics of the current doctoral students:

1. Extraction and speciation analysis for the separation of f-elements
2. Bentonite erosion: Mechanistic understanding and quantification
3. Solubility, hydrolysis and carbonate complexation of Fe(II) and Fe(III) in dilute to concentrated saline systems
4. Iron corrosion related bentonite alteration and its influence on the migration behavior of selected radionuclides
5. Investigations of the solubility, speciation, and solid phase formation of Pu(III/IV) and Np(IV/V) in citrate-containing solutions
6. Uptake of radionuclides (Ra(II), Sn(II/IV), Zr(IV), Nb(V)) by cementitious materials: quantitative description and mechanistic interpretation
7. Interrelations between bond covalency and bond stability of actinides
8. Investigation of the mechanical properties of irradiated cladding tubes under dry interim storage conditions
9. Development of radionuclide generators for short-lived α-emitters
10. Investigation of the interaction of cement degradation products with trivalent ions within the framework of the NORD site model
11. Binding behavior of lanthanide elements in molecular materials
12. Binding Properties of Lanthanide and Actinide Complexes Probed by High Resolution X-Ray Spectroscopic Techniques
13. Speciation of actinides and fission products by mass spectrometric methods.
14. Probing the electronic structure and binding of actinides by metal and ligand-based advanced X-ray spectroscopy

15. Uptake of radionuclides during metallic corrosion at the steel/bentonite interface
16. Numerical models for surface complexation and pore scale diffusion in clay: coupling surface chemistry and diffusion with nano-scale electrostatics
17. Investigations of actinide structural properties in solid, liquid and gas state applying high-energy resolution X-ray emission/absorption spectroscopy
18. Experimental determination of possible changes in reservoir properties caused by high-temperature thermal energy storage in DeepStor

Topics of the completed dissertations:

1. Impact of the heterogeneity of the sandy facies of Opalinus Clay on the retention of Cs, Co and Eu
2. Sorption of Eu(III) and Cm(III) on C-S-H phases and bentonite in presence of oxalate and EDTA at low to intermediate ionic strength conditions
3. Kinetics and interfacial processes in recrystallization of calcite and barite, and influence on radionuclide incorporation
4. Influence of Carbonate on the Radium Uptake by Barite and Witherite
5. Extraction and spectroscopic speciation of trivalent actinides and lanthanides with four-coordinate N-donor ligands
6. Extraction and spectroscopic speciation of trivalent actinides and lanthanides with bis(triazolyl)pyridine and bis(pyrazolyl)pyridine ligands
7. Investigations of the solubility, speciation, and solid phase formation of Pu(III) and Pu(VI) in dilute to concentrated carbonate-containing solutions
8. Inhibition of ferritic steel corrosion in the presence and absence of ionizing radiation
9. Metallic corrosion at the steel/bentonite interface under anoxic and water saturated conditions

3 National and international activities

3.1 National and international cooperation

INE R&D involves numerous national and international collaborations and projects. These are described in the following.

National

INE is involved in various bi- and multilateral collaborations with national research centers, universities and industrial partners on different topics. The projects are partly supported by the Federal Ministry of Research, Technology and Space (BMFTR, formerly Federal Ministry of Education and Research, BMBF), the Federal Ministry for the Environment, Climate Action, Nature Conservation and Nuclear Safety (BMUKN, formerly Federal Ministry for the Environment, Nature Conservation, Nuclear Safety and Consumer Protection, BMUV), the Federal Company for Radioactive Waste Disposal (BGE), the German Research Foundation (DFG) and the Helmholtz Association (HGF).

In the framework of measures for retrieval of radioactive waste and decommissioning of the **Asse II salt mine**, provisions for emergency preparedness are taken. The operator of Asse II, the Federal Company for Radioactive Waste Disposal (BGE), performed an exploration drilling in the overlaying sedimentary rocks of the salt diapir and coordinates studies with respect to the near-field of the radioactive waste. INE contributes both to the studies on radionuclide retention by rocks of the overlaying sediments as well as to studies on the geochemical milieu and radionuclide retention in the near-field of the radioactive waste. Based on the experimental results, sorption coefficients are derived, which are important input parameters for the assessment of the radionuclide retention capability. With respect to the near field of the waste within Asse II, INE performs experimental studies to improve the basis for assessing radionuclide transport and source terms.

With two completed projects and one ongoing project, INE participates in the representative preliminary safety analyses ("rvSU") of BGE for a deep geological repository for high-level radioactive waste in the ongoing **site selection procedure in Germany**. In the project **PARFREI**, reliable and robust quantitative state-of-the-art data for the rvSU with regard to the release, solubility, and sorption of radionuclides have been compiled and transparently documented with respect to the underlying process understanding for the derivation of these data. A simplified radionuclide scheme for the rvSU model calculations that takes all relevant radionuclides into account has been derived in project **RN-Schema**. Within the project relevance criteria for determining relevant radionuclides were developed and, based on this, a simplified radionuclide scheme that takes into account both the substance quantity and mass discharge criteria in accordance with §4 and the dose criterion in accordance with §7 of the Final Storage Safety Requirements Ordinance. Within the framework of the rvSU, BGE is required to examine whether selected site regions or sites for high-level radioactive could additionally accommodate a final repository for low- and intermediate-level radioactive waste. The most important requirement here is that the safety of the final repository for high-level radioactive waste is not compromised. In the ongoing **AbStand** project, a method is being developed to derive a minimum distance to rule out mutual negative interference between the inventories of two neighboring final repositories.

The **BARRIERS** Project started in May 2025. It is funded by the German research foundation (DFG). In the BARRIERS consortium INE is collaborating with the universities of Kiel and Paris (Sorbonne), as well as with the French geological survey (BRGM). The work of INE within BARRIERS aims at the development and parameterization of an electrostatic surface complexation model for Na-Montmorillonite. The porescale surface model will consider electrostatic spill-over and charge regulation between clay edges and basal planes as well as interactions between neighboring clay particles. Sorption and diffusion studies will be employed to study the sorption and surface mobility of Na^+ and Cs^+. With such a model and the detailed analyses of Na and Cs diffusion, the BARRIERS consortium aims at improving the understanding and the numerical modelling capabilities of specular induced polarization (SIP) phenomena in clay.

Goal of the ***f*-Char** project was to deepen the understanding of the coordination chemistry of actinide and lanthanide ions with so-called soft donor ligands. In particular, the subtle differences in the interaction of soft donor ligands with the chemically similar actinide vs. lanthanide ions were further characterized and quantified. An essential aspect was the training and promotion of young scientists in the field of nuclear safety research and nuclear chemistry in general and in actinide chemistry in particular. Thus, the project made an important contribution to the establishment, further development and maintenance of scientific-technical competence in nuclear safety research. *f*-Char terminated March 2024.

A direct follow-up to *f*-Char, **COORD*EX*** keeps the general scientific goal of improving the understanding of *f*-element coordination chemistry. However, in accordance with the TRANSPARANT program (see *International* below), a focus is put on the chemistry required to separate americium from curium and lanthanides. Again, training the next generation of scientist is an essential component of COORD*EX*. The former *f*-Char consortium of seven national partners is maintained. It is supported by two associated partners, Los Alamos National Laboratory and Universidad de Almería.

The aim of the collaborative project **EIKE**, funded by BMWi, was to develop an inhibitor combination that

helps increase the availability and sustainability of geothermal power plants. The economic efficiency of geothermal plants is often impaired by depositions of secondary minerals or corrosion damage. A promising countermeasure is the use of inhibitors, which can thereby improve the sustainability and economic use of geothermal plants. Geothermal plants in the North German Basin (NDB) extract highly saline thermal water from porous aquifers. Because of the small pore sizes (<100 µm), the flow parameters of such aquifers are sensitive to secondary mineral formation. If mineral deposition occurs near the injection well, the injectivity decreases. In geothermal plants, which extract thermal water from fractured aquifers - such as in the Upper Rhine Graben (ORG) - commercially available inhibitors are currently used in testing operation. In the long term, the harmlessness to water management as well as an expansion of the application to lower injection temperatures is essential, in order to enable sustainable and economic long-term operation. In EIKE an inhibitor combination was successfully developed and tested in the lab as well as in the geothermal power plant in Insheim. Its efficiency towards scaling inhibition and corrosion protection could be demonstrated. Large scale rock percolation experiments showed the efficiency towards a decrease in pore clogging. The EIKE project ended in May 2024.

The long-term safety of geological repositories in granitic host rock is investigated through the BMUKN funded **EVIDENT** project. The overarching goal of the project, of which INE, FSU and GRS are partners, is to enhance the mechanistic understanding of the processes critical to the integrity of the geotechnical barrier under near-natural, repository-relevant conditions in fractured granite systems and to provide a robust predictive model of the bentonite buffers and colloid-borne radionuclide transport. These questions underlie the various in-situ tests (LIT, i-BET, CFM Run 22-02) within the framework of the CFM project at the Grimsel Test Site (Switzerland) and are complementarily addressed with laboratory scale experiments. Topics include the mechanisms of bentonite erosion and colloid formation at the interface of the bentonite buffer to the crystalline rock, radionuclide speciation, the interactions between radionuclides and colloids, and their retention at the rock surfaces. The planned work builds partly on the findings obtained in Kollorado-e3, but also considers entirely new aspects, i.e., the characterization of crystalline rock heterogeneity and the influence of lamprophyre intrusions on the migration of radionuclides and colloids in the granodiorite rock. Several analytical methods are employed for radiation detection (gamma-spectrometry and LSC), mass spectrometry (ICP-MS) and surface/solid state analysis and microscopy (XRD and SEM) in the controlled area of INE, as well as ultra-trace analysis (AMS). Such experimental data are then merged with modelling results in order to acquire long-term performance-assessment for nuclear waste disposal in fractured crystalline host rock.

Within two projects of the Collaborative Research Center (CRC) **4f for Future** - "Activation and Stabilization of Small Molecules by Rare-Earth Compounds" and "Lanthanide-Based Multimetallic Clusters: Impact of f-Elements on Formation, Structure, Electronic Properties, and Reactivity", funded by the DFG — advanced high-energy-resolution X-ray spectroscopic techniques are developed and applied, in combination with quantum chemical studies, to elucidate the electronic structures of lanthanide (Ln) elements in molecular complexes with unusual Ln(II) and Ln(IV) oxidation states, as well as in multimetallic clusters incorporating lanthanides. The bonding properties of the lanthanide elements in these novel molecular compounds are directly related to their reactivity, magnetism, and luminescent behavior, which are investigated in collaboration with other projects within the CRC.

The BMFTR project "Digital Twin for Deep Geothermal Systems (**GeoDT**)", part of the German research program Geoforschung für Nachhaltigkeit (GEO:N), focuses on the development of digital twin concepts for deep geothermal systems as a strategic contribution to the energy transition in the subsurface. Its overarching objective is to enable an integrated, data-driven representation of geological structures, coupled thermo-hydro-mechanical processes and geotechnical operations across all phases of a geothermal site. Within GeoDT, INE concentrates on digital twin architectures, coupled process simulations and advanced virtualization methods for complex subsurface systems. In cooperation with national research partners, a prototypical digital twin is implemented for the potential GeoLaB site in the Odenwald region, providing a digital foundation for improved analysis, planning, design and implementation of experiments as well as stakeholder dialogues.

The project **"**Geotechnologies for a Turning Point in Germany's Energy Supply (**GEOZeit**)**"**, part of the **Helmholtz Zeitenwende initiative**, focuses on the development of energetic and material storage solutions in the deep subsurface as a strategic contribution to the German Energiewende. Its overarching objective is to accelerate the transfer of innovative subsurface technologies into practical implementation, in close collaboration with partners from industry. Within GEOZeit, INE concentrates on subsurface thermal energy storage, advancing the scientific and technical basis for scalable and reliable heat storage systems. In cooperation with Stadtwerke Karlsruhe, a case study has been carried out using the city of Karlsruhe as a model region, with the aim of effectively bridging the gap between research and real-world deployment. Specifically, this involves transferring insights from the DeepStor project at KIT Campus North to potential storage sites in Karlsruhe.

The **GRaZ II** project dealt with the migration of radionuclides in the near field of a repository for radioactive waste in clay formations with focus on the hyperalkaline water-cement-system. INE investigated the retention of actinides and lanthanides by clay minerals in presence of relevant inorganic and organic ligands. The project focused on carbonate, and cement additives (e.g. plasticizer and superplasticizer) like gluconate and citrate. The impact of these ligands on the sorption and solubility of actinides was studied in a wide pH range up to hyperalkaline pH values. One important aim of

the project was the consistent thermodynamic modelling of experimental solubility, complexation, and sorption data. Specific theory-based methods, such as molecular dynamics analyses, were also used to derive a detailed understanding of the interaction of Ln/An at C-S-H phases (relevant main phase in cement systems) and in the presence of organic ligands relevant to final nuclear waste disposal (Glu, EDTA, citrate). From all investigations reliable thermodynamic data were obtained that could later be implemented in the THEREDA thermodynamic reference database (www.thereda.de). The GRaZ II project thus provided basic knowledge and thermodynamic data needed in the frame of a long-term safety analysis of different repository concepts. The GRaZ II project was successfully terminated in 2024.

The **Helmholtz Climate Initiative** involves research on climate mitigation and adaptation. In the *ZeroNet-Zero-2050* Cluster, strategies and new approaches to achieve rapid and far-reaching reductions in emissions from all greenhouse gases including removal from the atmosphere and permanent storage or turning into high energy-density chemical energy carriers by renewable energy are scientifically examined and evaluated in four projects with regard to the German framework. In addition, two case studies are carried out with external stakeholders. The *Climate Neutral City*, is placed at the city of Karlsruhe. In the project *Potential and Integration of Subsurface Storage Solutions*, INE contributes to the topic of high-temperature heat storage. Technological storage solutions in the complex setting of urban areas requires intensive stakeholder dialogue. To this end, the geoenergy group collaborated with the KIT Center for People and Technology. Joint public engagement campaigns were developed and implemented.

The collaborative project **KURSIV** (2023-2026) focuses on experiments and modelling concerning competitive effects and reversibility in trivalent radionuclide/lanthanide adsorption on minerals. As a main hypothesis, aluminum ions e.g. from dissolution of clay or feldspar minerals could act as competitors when pH is changed and re-adsorption of Al occurs. The experimental studies were done on selected minerals and a new technique (Quartz-Crystal-Microbalance, QCM) was used to gain quantitative data. At the same time, electrokinetic studies were used to determine the charging of the minerals during these processes. The work led to the development of a cell, in which the zeta-potential determination and the QCM-experiments could be done simultaneously. The surface complexation modelling so far undertaken shows that the uptake of Al can be described by a simple inner-sphere-surface complex. However, the formation of secondary mineral phases cannot be excluded, and the mechanism needs to be clarified by AFM studies for example. The experimental work is further supported by various sets of experiments carried out by the partners at the German Association for Plant and Reactor Safety (GRS) and at HZDR.

Detailed knowledge of degradation processes occurring at the container/buffer interface is important input for the Safety Case of a nuclear waste repository. The project **IMKORB** (2021-2025) aims to provide an improved understanding of metallic corrosion and buffer alteration processes for conditions representative of clay-based disposal sites for heat generating waste. Modern microscopic and spectroscopic techniques are applied to decipher the underlying processes and their associated kinetics in dedicated experiments carried out in the laboratory. These experiments are complemented by in situ experiments under undisturbed conditions in underground research laboratory (see below). The ultimate goal is to identify the corrosion and alteration products likely to be present in the long-term and which may act as chemical barrier and reduce the radionuclide mobility.

The research topic of the collaborative project **KRIMI** relates to non-site-specific scenarios for safety assessments for deep geologic repositories for highly radioactive nuclear waste. Essential parameters for the description of the mobility of radionuclides in simulations for safety assessment are solubility limits and sorption coefficients of involved radionuclides under the respective geochemical conditions. An intermediate between sorption and precipitation is the incorporation of radionuclides into solid-solutions. In solid-solutions the whole mineral volume may be effective towards radionuclide retention. Thus, solid-solutions have a high potential for radionuclide sequestration compared to pure surface adsorption processes. Nevertheless, despite their retention potential, solid-solutions are nowadays rarely included in safety assessment simulations. This is due to the lack of necessary model parameters, which may serve to reliably describe the thermodynamics and especially also the kinetics of solid-solution formation. Scientific goal of KRIMI was the investigation of thermodynamics and formation kinetics of repository-relevant solid-solutions. Systems investigated within KRIMI included the radionuclides: Tc(IV), Pu(III), Se(IV), Np(V), and Ra(II) and the host minerals magnetite, calcite and barite. Studies included atomistic simulations, experimental studies, and investigation of natural analogue samples. An overarching societal goal of KRIMI was to contribute to the build-up and retention of competence in the field of radio-geochemistry. KRIMI was funded by BMBF, the project ended in February 2024.

The **NaMaSK** (2021-2024) joint project has developed a promising approach to reduce the amount of secondary waste generated by water jet abrasive cutting (WASS) during the decommissioning of nuclear power plants. In this project, funded by the German Federal Ministry of Research, Technology and Space (BMFTR, formerly Federal Ministry of Education and Research, BMBF), an existing pilot separation device was optimized and upgraded to demonstrate its feasibility for radioactive processes. At INE, a doctoral student conducted research on the use of corrosion inhibitors in ferritic steels as part of his dissertation, which was funded by the NaMaSK project. Corrosion inhibitors are intended for use in inhibiting corrosion in ferritic reactor pressure vessel steel during water jet cutting and post-cutting separation. The aim of the research was to de-

velop a method for the systematic selection of inhibitors based on their corrosion inhibition behavior, even in the presence of strong radiation fields. The dissertation includes a selection of suitable corrosion inhibitors for minimizing the corrosion of ferritic steel during and after WASS cutting processes in order to ensure efficient separation of steel and abrasive particles. Effects of ionizing radiation on the corrosion of ferritic steels in the presence and absence of inhibitors were investigated. It was shown that the selected inhibitors are ideally suited for the intended application. The project was successfully completed in 2024.

The collaborative project **RULET** (Rückhaltung und Löslichkeit dosisrelevanter Radionuklide unter den reduzierenden Nahfeldbedingungen eines Endlagers im Ton- oder Kristallingestein, 2024-2028) funded by BMUKN aims at improving the understanding of the physicochemical processes (complex formation, redox reactions, retention by sorption and solid-phase formation) leading to the retention of ^{99}Tc, ^{79}Se, ^{226}Ra and ^{14}C in carbonate, silicate and sulfide systems. The focus is on solid phases, oxidation states, and aqueous species expected in the immediate vicinity of the waste containers. Particular emphasis is placed on reactions and equilibria involving iron(II) corrosion phases. The work at INE targets the chemistry of ^{99}Tc (solubility, aqueous speciation, sorption) in silicate and sulfide systems, as well as the retention of small ^{14}C organic molecules (e.g., alkanes, alcohols, small carboxylic acids) by cement and clay systems. Building on the outcome of the work planned within RULET, the long-term safety of different repository concepts and scenarios will be assessed on a decisively improved scientific level.

The overall objective of the **SEPAM** project was the scientific investigation and further development of solvent extraction processes for the separation of americium from highly radioactive wastes, with a strong focus on basic chemistry. SEPAM terminated September 2024.

The collaborative project **SPIZWURZ** focused on experimental and theoretical studies on the behavior of hydrogen in fuel rod cladding materials and the stress state of Zircaloy-4 cladding in contact with high burn-up spent nuclear fuel to assess the impact on cladding integrity under dry interim storage conditions. For this purpose, long-term and detailed studies on non-irradiated cladding materials and samples were performed by other project partners within workpackage 1. In workpackage 2, INE determined the geometry of an irradiated nuclear fuel rod segment by means of a laser scan micrometer before and after removal of the fuel. The variation of the cladding geometry allowed to determine the hoop stress in the cladding, exerted by the fuel pellet. The experimental work was further supported by simulations and theoretical modelling performed by the German Association for Plant and Reactor Safety (GRS). Moreover, the Company for Interim Storage (BGZ) was involved in the project as an observer.

STAMINA (Stabilität von Mineralphasen des Eisens im Nahfeld eines Endlagers, 2023-2026) is a collaborative project funded by BMUKN involving INE and GRS. The project aims at deriving chemical, thermodynamic and (Pitzer, SIT) activity models for iron chemistry in the near-field of a radioactive waste repository. A multimethod approach is used for this purpose, involving solubility, isopiestic and spectroscopic (UV-vis, XAFS) measurements, in combination with existing literature data. The work at INE focuses on the solubility and aqueous speciation of Fe(II) and Fe(III) in water (hydrolysis), carbonate and silicate systems. The outcome of this project enables significantly improved modeling of iron chemistry in systems with high ionic strength, applying to the context of disposal in rocksalt, but also to clay formations in northern Germany characterized by high ionic strength pore solutions (>2 M). The developed thermodynamic data and Pitzer model parameters can subsequently be implemented in the German thermodynamic reference database THEREDA (www.thereda.de).

In the project **StInZyZwiLag**, funded by BMUKN, the mechanical properties of irradiated cladding under conditions of dry interim storage are studied. To prevent cladding failure during dry storage, stress and strain criteria are set by law. The hoop stress in the cladding tube depends upon its Young's modulus which is influenced by several phenomena, changing the response of the cladding to plastic deformation and leads to loss of ductility and embrittlement. The study of the variation of Young's modulus and hardness on a nanometric to micrometric scale will enable the forecast of the evolution of these properties during storage on a long timeframe and to single-out the factors contributing to properties changes. Two types of irradiated fuel rod segments are analyzed in these investigations: Zircaloy-4 cladding from the plenum and in contact with uranium dioxide fuel and Zircaloy-4 cladding in contact with mixed oxide fuel. In addition, non-irradiated Zircaloy cladding samples (with or without hydrogen loading) are studied.

Within the **THEREDA** project, INE provides thermodynamic data – complex formation constants, solubility data – for selected radionuclides from experiments and literature. The data are incorporated into a centrally managed and administered database of evaluated thermodynamic parameters after passing an evaluation process. This database is open for registered user. Thermodynamic data are required for environmental applications in general and radiochemical issues in particular. THEREDA, funded by the Federal Company for Radioactive Waste Disposal (BGE), is developed as a national (reference) standard and basis for future Safety Assessments for a national nuclear waste repository.

The collaborative project **TRANSENS**, funded by BMWi, was the first large-scale project in Germany for transdisciplinary research into the disposal of spent nuclear fuel and vitrified high-level radioactive waste. From 2019 to 2025, various technical, safety related and procedural aspects of disposal strategies for high-level radioactive waste were evaluated from the perspective of all scientific disciplines involved in TRANSENS, such as natural sciences, engineering, law, and

social sciences. A key objective of this transdisciplinary research project was the interaction between scientists from different disciplines and citizen scientists. Within the project, INE was responsible for a work package dealing with interdependencies between the current management of high-level radioactive waste in interim storage and future final disposal of this waste. In cooperation with research groups of Öko-Institut Darmstadt, Technical University Braunschweig and Leibniz University Hannover we published a study on interdependencies related to the reapproval of interim storage facilities for high-level radioactive waste after 40 years of operating license. Together with these research groups as well with social and political scientists of KIT-ITAS and university of Kiel, we conducted comparative path heuristics analyses for different disposal paths for nuclear waste management and an analysis on the role of uncertainties and narratives in the context of high-level radioactive waste disposal.

International

Coordinated by NAGRA (National Cooperative for the Disposal of Radioactive Waste, Switzerland), the Colloid Formation and Migration (**CFM**) project is an international platform aimed at investigating the stability of bentonite engineered barrier systems and the influence of colloids on radionuclide migration in crystalline host rocks. The project uses the unique experimental set-up at the generic URL Grimsel Test Site (Switzerland) featuring i) a megapacker flow control system that allows establishing hydrological boundaries close to repository relevant conditions and ii) a controlled area laboratory in which the use of radionuclide tracers, among them anthropogenic actinides, is permitted. INE plays a decisive role in the laboratory program as well as in the field activities, thanks to national funding (currently through the EVIDENT project) from BMUKN. Other project partners are BGE (Germany), KAERI (Republic of Korea), NUMO (Japan) and NWS (United Kingdom), joined by the Scientific Support Organizations CIEMAT (Spain), FS (UK), JAEA (Japan), PSI (Switzerland) and SAM (Switzerland). In the frame of the actual Phase 5 (2024 -2028), a Follow-up Integrated Test (FIT) as the successor to the Long-term In-situ Test (LIT) is planned. Focus is furthermore given to tracer migration tests to be performed in a water conductive feature at the interface between granodiorite and lamprophyre intrusions to investigate the influence of crystalline rock heterogeneity on retention and migration of radionuclides and bentonite colloids.

Experiments in the underground research laboratory (URL) **Mont-Terri** are organized as international research collaborations between voluntary research partners. INE is currently involved in three URL Experiments in Mont-Terri: DR-D, DR-C, and IC-A.

The **DR-D** Experiment, headed by INE, is a collaboration with the Helmholtz Centers GFZ in Potsdam, FZJ in Jülich, and HZDR in Leipzig, the German Federal Company for Radioactive Waste Disposal (BGE), the German Federal Institute for Geosciences and Natural Resources (BGR), as well as the Belgian Federal Agency for Nuclear Control (FANC). Aim of the DR-D experiment is to characterize the impact of rock heterogeneity on radionuclide diffusion in clay rock on a URL scale. A first step was the detailed investigation of a rock section of the sandy facies of Opalinus Clay by geophysical methods (borehole logging and seismic tomography survey), as well as by geochemical / mineralogical characterization of drill core samples. Secondly a diffusion setup was designed and installed into a particularly heterogeneous region of the sandy facies in collaboration with the Swiss company Solexperts. Next, radiotracers will be injected and diffusion will be monitored for two years. The plan is, to finalize the experiment by overcoring the diffusion experiment, in order to analyze tracer profiles around the contact zone between radiotracer solution and clay rock.

The **DR-C** experiment is closely related with DR-D as the two share many common features. However, DR-C is headed by FANC, and INE is one out of many partners. A particular focus of the DR-C experiment is the study of the impact of a temperature gradient on radionuclide diffusion in clay. To do so, two URL diffusion experiments were setup for DR-C, one reference experiment running at ambient temperature, and a heated experiment, where the central borehole is heated to 80°C, such that a temperature gradient will develop around the central borehole. The effect of the elevated temperature and the temperature gradient will be assessed by comparing diffusion around the two experiments. DR-C will provide essential information for the assessment of potential early canister failure scenarios.

Further, INE is partner of the **IC-A** experiment in Mont-Terri, headed by NAGRA. In IC-A metal coupons are embedded in bentonite and subjected to the ground water conditions of Opalinus Clay in Mont-Terri. After specific time intervals samples (bentonite with coupons) are retrieved from the IC-A boreholes, and analyzed by the partners of the IC-A experiment. Selected samples were analyzed at KIT, by SEM-EDX, μXRF and μXAFS, to learn about corrosion as well as secondary phase formation at the metal-bentonite interface.

Horizon 2020 and EJP

INE is substantially involved in large collaborative projects funded by the European Commission under the EURATOM frame. The European Joint Program on Radioactive Waste Management (EURAD) is a large-scale integrated research program dealing with various aspects of safe management of nuclear waste (www.ejp-eurad.eu/). After the first EURAD-1 project frame lasting until 2024, a new project phase named EURAD-2 (European Partnership on Radioactive Waste Management) was launched in 2024, again with a projected 5-year duration. Information on both EURAD-1 and EURAD-2 is available at the project website https://www.ejp-eurad.eu.

In the **EURAD-1** project frame, INE was strongly contributing to four workpackages: Cement-Organic-Radionuclide-Interactions (CORI), Fundamental understanding of radionuclide retention (FUTuRE), Spent Fuel Characterization and Evolution Until Disposal

(SFC) and Uncertainty Management multi-Actor Network (UMAN). INE was coordinating the WP CORI. CORI developed an improved understanding of the interaction of cementitious materials with organic matter and selected radionuclides. FUTURE contributed to the quantitative mechanistic understanding of radionuclide retention in the repository barrier system. The SFC workpackage aimed mainly to establish beyond state-of-the-art quantification of the characteristics and chemical processes of spent nuclear fuel assemblies from discharge of nuclear reactors, during interim storage until (pre-)disposal activities. UMAN was dedicated to the management of uncertainties possibly relevant at different stages of radioactive waste management and programs.

In the **EURAD-2** activities ongoing from 2024, INE again contributes to several workpackages, including: Release of safety relevant radionuclides from spent nuclear fuel under deep disposal conditions (SAREC), Innovative and new container/canister materials under disposal fields conditions: manufacturing feasibility and improved durability (InCoManD), Radionuclide mobility under perturbed conditions (RAMPEC) and Development and Improvement of Thermodynamic Understanding for use in Nuclear Waste Disposal Safety Case (DITUSC). Additional activities are linked to the Knowledge Management program. INE is coordinating RAMPEC, co-coordinates DITUSC and is Task Leader in SAREC. SAREC is working to improve the quantification and mechanistic understanding of the release of safety relevant radionuclides covering most representative types of spent nuclear fuel and of the fuel evolution both prior and posterior to contact with ground water to better predict the radionuclide source term for post-closure safety assessment. InCoManD is identifying and qualifying novel materials for the HLW containers/canisters, and provides a deeper knowledge of both traditional and novel materials long-term durability in, as realistic as possible, field conditions. RAMPEC improves the predictive capacity of models of disposal system chemistry and radionuclide mobility under perturbed conditions based on a combination of new experimental and modelling studies up to the cell scale. DITUSC is a strategic study focusing on thermodynamic understanding and quality assured data in support of the Nuclear Waste Disposal Safety Case, with special focus given to a transversal understanding.

With the **PREDIS** project, funded by the European Commission with a 4-year duration between 2020 and 2024, INE contributed to WP7 which was aiming to provide innovations in cemented waste handling and pre-disposal storage. PREDIS high-level objectives are to develop solutions (methods, processes, technologies and demonstrators) for future treatment and conditioning of waste, improving safety during next waste management steps or improve existing solutions with safer, cheaper or more effective alternative processes. In WP7, INE contributed to activities dedicated to adapt and demonstrate digital twin technologies. In this context, INE used advanced analytical techniques for the characterization of cement-based waste packages for calibration / validation.

Understanding the electronic structure and chemical bonding properties of the early actinide (An) elements (Th-Cm) poses a great challenge and scientific frontier in fundamental chemistry and physics. A deep insight into the An electronic structure and bond formation is also essential for developing innovative spent nuclear fuel conditioning strategies, to understand actinide environmental behavior - e.g., in contaminated legacy sites or the context of underground nuclear waste repositories - as well as for developing advanced pharmaceutical compounds for targeted cancer treatment. The ERC funded project **„The ACTINIDE BOND“** focuses on the link between covalency and strength of the chemical bond of the An elements in gas, liquid and solid state materials. The scientific challenges of these materials are tackled by combining highly innovative experimental setups, advanced synchrotron-based X-ray spectroscopy methods and state-of-the-art quantum chemical computations. X-ray based methodologies with high potential for a breakthrough in efforts have been developed, e.g., to select An materials or complexing agents with specific characteristics for the aforementioned application fields. Of essential importance for the success of the “The Actinide Bond” project are the ACT (CAT-ACT beamline) and X-Spec experimental stations at the KIT Light Source (KARA storage ring), situated within 10 minutes walking distance from INE with its state-of-the-art radiochemical laboratories.

The EURATOM program **TRANSPARANT** focuses on the efficient separation of americium from used fuel, on experimental and fuel performance code development work studying the behavior of americium-bearing fuel under irradiation and on the safety related research supporting the licensing process of MYRRHA in its role as dedicated accelerator driven transmuter demonstrator. TRANSPARANT joins communities working on partitioning, transmutation, and MYRRHA development from 21 research centers and universities from eight EU countries, the UK and Switzerland. KIT contributes to the hydrometallurgy work packages, developing and testing improved solvent extraction systems to separate americium from PUREX raffinate solutions.

VESTA is a collaborative research project on high-temperature heat storage in the deep underground. It involves five German partners from industry and science as well as the international partners GeoEnergie Suisse, Lawrence Berkeley National Laboratory (LBNL) and Idaho National Laboratory (INL). For thermal energy storage on a large scale and in the higher temperature range required for feeding into district heating networks and for industrial processes, novel high-temperature storage (HTS) systems in the deep subsurface are an option. However, many technical, regulatory, legal, environmental, and economic challenges need to be resolved to enable broader application of HTS. Within the scope of the VESTA project, it is planned to scientifically investigate the implementation of HTS systems by means of demonstration projects. Overarching goals of VESTA are to 1) demonstrate HTS at selected pilot sites including DeepStor, 2) evaluate technical and non-

technical barriers, 3) support development and implementation of commercial projects by providing process understanding, modeling and monitoring techniques, and optimized component design, 4) support agencies with scientific and technical knowledge as a basis for advancing regulatory provisions. The Helmholtz research infrastructure DeepStor is one of the pilot sites in VESTA. A first exploration well, currently under preparation, will give insights into the target formations.

3.2 Conferences

ATAS – AnXAS 2024 workshop

INE organized the international ATAS - AnXAS 2024 workshop, held at the FTU Auditorium at KIT Campus North, from October 7 to 11. ATAS - AnXAS 2024 has been the second joint workshop since merging the formerly separate ATAS and ActinideXAS series in 2022. ActinideXAS was launched in 1998 at the ESRF in Grenoble (France) to focus on work at emerging dedicated synchrotron labs licensed to handle radionuclide materials at beamlines. ATAS extended the scope in 2012 to other advanced, not solely synchrotron-based speciation methods, with an additional emphasis on quantum chemistry. The workshop attracted a total of 94 participants from 10 countries: Germany, France, United States, United Kingdom, Republic of Korea, Finland, Japan, Switzerland, Canada and China. The meeting featured 14 topical sessions structured by five invited plenary talks, 15 invited keynote lectures and 40 contributed oral presentations. These lectures were covering a broad range of radionuclide speciation methods and application fields (from radio-toxicology and medicine to the characterization of nuclear waste forms), where the unabatedly growing impact of high-resolution X-ray emission studies was remarkable. As well noteworthy was the high degree of maturity reached by computational chemistry tools in support of 5f element spectroscopies, e.g., to disentangle the wealth of transition features in resonant inelastic X-ray scattering. The conference program was complemented by an evening poster session held at the premises of the KIT Light Source.

Fig. 1: Workshop participants at the excursion to "Technik Museum Speyer"

Annual Meeting GDCh

From November 5 to 7 in 2024, INE co-organized the Annual Meeting of the Radiochemistry Subdivision of the German Chemical Society - GDCh (https://www.gdch.de/netzwerk-strukturen/fachstrukturen/nuklearchemie.html) together with JRC - Joint Research Centre, Karlsruhe. This conference series is organized bi-annually by subdivision members and offers a unique overview of research in this broad and interdisciplinary research field. Using a combination of three invited plenary presentations, 36 contributed oral presentations and a poster session, the conference was presenting excellent scientific results from several topical fields. A specific session was reserved to the award ceremony organized by the Subdivision in order to recognize and support young talent and presentations by the awardees. The Annual Meeting was attended by ~100 participants mainly from Germany.

Migration 2025 conference

The 19th International Conference on the Chemistry and Migration Behavior of Actinides and Fission Products in the Geosphere (Migration'25) took place from 21–27 September 2025 in New Orleans, USA. The conference was successfully organized by Clemson University and Lawrence Livermore National Laboratory in cooperation with INE, and supported by the International Steering and Scientific Committees. Continuing the tradition of previous meetings, Migration '25 provided a high-level international platform to discuss recent advances in understanding and predicting radionuclide migration processes. Almost 200 participants, including 55 students from 16 countries, underlined the sustained global interest in this field.

The conference opened on Sunday with an outstanding plenary session dedicated to "*Breakthroughs in Nuclear Waste Management*", featuring invited speakers Tim Vietor (Nagra), Kent Rosenberger (Savannah River Mission Completion) and Ping Yang (Los Alamos National Laboratory). The scientific program covered aquatic chemistry of actinides and fission products, radionuclide migration behavior, geochemical and reactive transport modelling, case studies, as well as two special sessions dedicated to the "*United States Department of Energy Environmental Management, Legacy Management, and Nuclear Waste Disposition programs*" and "*The intersection of nuclear security and radionuclide migration in natural and/or engineered systems*". Two extended poster sessions, showcasing more than 140 contributions, provided ample opportunity for in-depth scientific exchange, particularly for early-career researchers. In addition, 67 oral presentations including several invited talks emphasized key developments and emerging topics. Overall, Migration '25 demonstrated significant scientific progress and the

breadth and impact of current research and development in radionuclide migration. Marking both the 40th anniversary of the conference series and its 20th edition, Migration will return to Germany and, for the first time, will be hosted in Karlsruhe in September 2027.

3.3 Knowledge transfer and communication

Interaction with the public and stakeholders

In the context of management of radioactive waste, scientists at INE lead or participate in national expert groups, act as consultants for federal ministries and federal authorities in various project committees („Projektkomitee Zwischenlagerung / Abfallbehandlung“ (interim storage / waste treatment), "„Projektkomitee Endlagerung“ (final disposal)) and advise the BGE on geochemical and radiochemical issues in connection with the closure of the Asse II mine. They also make their expertise available to government waste disposal organizations abroad (Belgium, France, Sweden, South Korea). In addition, INE provides members to the following technical committees and advisory boards: Nuclear Waste Management Commission (ESK), ESK committee on Final Disposal (EL), Deutsche Arbeitsgemeinschaft Endlagerung (DAEF) and the German-Swiss Professional Association for Radiation Protection. Data compiled as part of INE research for final repository safety investigations is continuously fed into databases (e.g., THEREDA, OECD/NEA-TDB) and thus made publicly available. INE scientists were also involved in the joint project "TRANSENS," thereby establishing a link between science and society. During the reporting period, INE scientists were asked by the media for interviews and statements on current topics, thus contributing their expertise to informing the general public. INE scientists also participated in various public events with lectures and dialogue formats, such as the Baden-Württemberg Energy Transition Days in Stuttgart and the Forum on Final Storage Site Selection (“Forum Endlagersuche”) in Würzburg, 2024, and in Hannover, 2025, or a public panel discussion on the occasion of the opening of the exhibition “Who decides such things? Nuclear waste repositories and democracy”, organized by KIT-ITAS.

High ranking visitors

INE has welcomed several prestigious visitors from governmental departments, nuclear waste management organizations and national research institutions for discussions and informative lab-tours in the reporting period 2024/25.

On October 2, 2024, **Christian Kühn, president of the Federal Office for the Safety of Nuclear Waste Management (BASE)**, visited KIT and INE. He was informed about current research projects and the training of young professionals. Kühn was particularly impressed by the innovative approaches developed at INE for providing the scientific basis for the safe handling of high-level radioactive waste. "KIT's research is of great importance for addressing our task of managing the legacy of the nuclear age," Kühn pointed out during his visit. "The experiments conducted here and the insights gained make a significant contribution to ensuring the safety of radioactive waste disposal. It is particularly encouraging to see how theory and practice are combined at KIT to find solutions." Kühn visited laboratories and learned about scientific topics concerning the safety aspects of extended interim storage of nuclear fuel and the long-term safety of final repositories. Another focus of the visit was the training of the next generation of experts. Prof. Horst Geckeis, head of INE, explained the various training programs and emphasized the importance of fostering young talent: “Our students and doctoral candidates are the experts of the future. We place great value on providing them with a sound and practical education. Through the close integration of research and teaching, we ensure that they will contribute to the success of the nuclear waste disposal project as knowledge bearers in the coming decades.”

Dr. Andreas Volz from the division "Dismantling of Experimental Nuclear Installations; Dismantling Research" at the Federal Ministry of Research, Technology and Space (BMFTR) visited INE on February 5, 2025. After being welcomed by Prof. Geckeis and the head of the HGF program NUSAFE, Dr. Walter Tromm, Dr. Volz was accompanied on a tour of INE’s controlled area labs. At four selected stations - the shielded box-line (“hot cells”), the HOVER microscopy laboratory (cf. section 3.4), the actinide laboratory and the surface analysis laboratory - Dr. Volz was introduced to the essential methods of the institute's application-oriented basic research on the safe disposal and long-term safety of radioactive waste by doctoral students and INE staff.

In the context of awarding the 2025 Heinrich Hertz Guest Professorship at KIT, **Prof. Jürgen Mlynek - president of the Helmholtz Association of German research centers (HGF) from 2005 to 2015** - visited several controlled area laboratories of INE on October 20, 2025 under the heading "Safe Nuclear Waste Disposal - a Part of the Energy Transition in Germany." During the visit, Prof. Mlynek received comprehensive information about the unique research opportunities at KIT regarding the behavior of highly radioactive nuclear waste forms (irradiated nuclear fuel and nuclear

Christian Kühn (on the right), president of BASE, discussing with Prof. Geckeis (center) and Dr. Marquardt during his visit at the INE shielded box-line.

waste glasses) and possible mechanisms for the release or retention of long-lived radionuclides (actinides, fission and activation products) in a future underground repository. Current proposals for alternative disposal concepts and the waste forms generated in future fusion or fission reactors were also discussed.

The guided tour program on KIT Campus North and the visit to INE came about at the initiative of Prof. Anke-Susanne Müller, KIT Vice Provost “Research Infrastructures”, head of KIT-IBPT and member of the KIT Supervisory Board.

3.4 Large infrastructure projects

HOVER

The HGF centers FZJ, HZDR and KIT cooperating in the NUSAFE consortium are implementing the laboratory infrastructure "HOVER" (Helmholtz Research and Technology Platform for the Decommissioning of Nuclear Facilities and for the Management of Radioactive Waste) as a decentralized research infrastructure. HOVER is dedicated to support advanced scientific investigations and technical developments in the context of the German phase out of nuclear energy. To this end, HOVER provides state-of-the-art instrumentation to investigate radionuclides – including α-emitting actinides – and to study those processes which determine their behavior in interim storage facilities and deep geological repositories. As of today, in Germany such laboratories are not any more available at research facilities outside the Helmholtz Association. Moreover, HOVER is offering unique infrastructures for the development and demonstration of innovative decommissioning technologies. Thus, research performed within the HOVER platform covers scientific challenges and technical developments dealing with the entire chain of decommissioning, nuclear waste conditioning and final disposal.

At INE, facilities and infrastructures enabled through HOVER funding have been implemented and commissioned since 2022 or are approaching completion until 2027. The HOVER surface science and microscopy lab at INE is comprising state-of-the-art focused ion beam – scanning electron microscopy (FIB-SEM) and X-ray microtomography (μ-CT) instruments – augmented by an advanced atomic force microscope (AFM), e.g. allowing for fast video-rate-scanning. Capabilities at the new controlled area lab and examples of initial investigations are detailed in chapter 8.2 of this report.

A multi-isotope low-energy AMS (MILEA) system has been acquired from Ionplus AG (CH). MILEA features a 300 kV tandem accelerator and a compact setup that is optimized for analysis of ultra-trace levels of the long-lived radionuclides ^{10}Be, ^{14}C, ^{26}Al, ^{41}Ca, ^{129}I as well as actinides. A new building adjoining the main premises of INE on KIT Campus North is being built to host MILEA and an ISO 4 class cleanroom sample preparation laboratory. Sample handling and chemical treatment in such a cleanroom laboratory will allow for a significant decrease of the ubiquitous background from the global fallout of radionuclides and, hence, for a further increase in the analytical sensitivity. The ground-breaking ceremony for the new laboratory building took place in October 2025. Examples for ongoing AMS research projects are given in chapter 8.3.

As a result of the German energy transition policy, technical innovations are required in order to guarantee the safe and efficient decommissioning and dismantling of nuclear facilities. Research goals in this area at INE focus on the development of automation and remote handling technologies with the aim of waste minimization, reduction of radiation exposure for workers and the public and increasing the efficiency of decommissioning procedures. In order to adequately cover these topics in the frame of HOVER, a digitalization lab called BIM D² (Building Information Modeling Decommissioning & Deconstruction) has been conceived by the KIT Institute for Technology and Management in Construction (TMB), Department of Dismantling Conventional and Nuclear Buildings. BIM D² is currently established in refurbished premises at KIT Campus East.

4. Fundamental studies: Process understanding on a molecular scale

Fundamental studies on radionuclide chemistry and geochemistry contribute to the detailed understanding and reliable quantitative prediction of aqueous chemistry. In order to allow a comprehensive assessment of radionuclide behavior and mobility in aquatic systems relevant for nuclear waste disposal, studies with actinides and long-lived fission and activation products are performed. The investigated aqueous systems cover from dilute solutions to highly saline salt brine systems and establish essential site-independent data and process understanding. Work is focusing on both, detailed experimental investigations using the unique facilities available at KIT-INE and subsequently development of reliable chemical models and consistent thermodynamic data. This combined approach allows a systematic and reliable evaluation of key processes such as radionuclide solubility, radionuclide speciation, radionuclide retention and transport processes in relevant near- and far-field scenarios. The work summarized in this section is related to the (i) chemistry and thermodynamics of actinides and fission products in aqueous solution, (ii) radionuclide sorption on mineral phases, (iii) retention of radionuclides by secondary phase formation. The studies aim at identifying relevant radionuclide retention/retardation mechanisms on a molecular level and their robust thermodynamic quantification in support of the Nuclear Waste Disposal Safety Case. Fundamental studies on aqueous radionuclide chemistry are giving support to the applied studies performed at KIT-INE.

4.1 Chemistry and thermodynamics of actinides and fission products in aqueous solution

M. Altmaier, N. Cevirim-Papaioannou, K. Dardenne, S. Duckworth, D. Fellhauer, P. Fürst, X. Gaona, H. Geckeis, F. Greb, F. Häusler, C. Kiefer, P. Müller, T. Prüssmann, J. Rothe, D. Schild, A. Skerencak-Frech

In co-operation with:

P. Felipe dos Santos[a], K. Garbev[b], S. Hagemann[c], K. Kim[d], A. Lassin[e], B. Madé[f], W. Um[d]

[a] Amphos 21, Barcelona, Spain; [b] Institute for Technical Chemistry, Karlsruhe Institute of Technology, Karlsruhe, Germany; [c] Gesellschaft für Anlagen- und Reaktorsicherheit, Braunschweig, Germany; [d] Division of Advanced Nuclear Engineering, Pohang, Pohang University of Science and Technology, Republic of Korea; [e] Water, Environment, Process Development and Analysis Division, BRGM, Orléans, France; [f] Research and Development Division, ANDRA, Châtenay-Malabry, France.

Introduction

The aquatic chemistry of actinides and fission products is largely controlled by solubility phenomena, hydrolysis, complexation and redox behavior. In the context of nuclear waste disposal, an accurate knowledge of the radionuclide fundamental properties controlling these processes is of high relevance. Geochemical calculations and source term estimations require complete and correct chemical, thermodynamic and activity models, which are preferably based on sound and systematic experimental observations. This section highlights some outstanding examples of the research performed at KIT–INE within this field in the period 2024-2025.

In addition to the experimental R&D activities described in this chapter, KIT-INE contributes to several national and international projects, *e.g.* providing support and expert judgement to BGE with regard to the site selection process in Germany (Standortauswahlverfahren), participating in the development of the national thermodynamic reference database for actinides and fission products (THEREDA project) or contributing to several volumes of the OECD NEA-TDB thermodynamic series. Such contributions highlight the international leading role of KIT–INE in the field of aquatic chemistry and thermodynamics.

Solubility, speciation and thermodynamics of $PuCO_3OH(cr)$ in carbonate containing solutions

For the long-term safety assessment of nuclear waste repositories reliable predictions of the geochemistry of relevant radionuclides are required, considering the principal scenario of water contacting the waste packages. Important processes that control the mobility of radionuclides after an initial solubilization are solubility equilibria, complexation, interaction with mineral phases (sorption, incorporation), redox reactions, etc. Quantification and modelling of these processes as a function of different solution parameters like pH_m, ionic strength, redox potential is based on reliable chemical and thermodynamic models as well as consistent thermochemical databases, *e.g.*, NEA-TDB, THEREDA, Thermochimie, PSI-Nagra, etc. [1-4]. Plutonium is the main transuranium element in spent nuclear fuel. Pu is redox active and can exist as Pu(III)-Pu(VII) in aqueous solutions, with Pu(III) and Pu(IV) being the predominant oxidation states in reducing environments. In absence of complexing ligands, the behavior of Pu(III) and Pu(IV) is characterized by hydrolysis reactions. Whereas Pu(IV) is sparingly soluble from slightly acidic to hyperalkaline conditions due to the great stability of $PuO_2{\cdot}xH_2O(s)$, Pu(III) concentrations controlled by an equilibrium with the binary solid phase $Pu(OH)_3(s)$ are quite high in near-neutral pH_m

conditions. The carbonate system is ubiquitous in environmental systems and considered a highly relevant ligand in disposal systems as well. As demonstrated for Am(III) and the An(III)-analogue Nd(III), the presence of carbonate strongly impacts both the aqueous speciation of An(III) by formation of carbonate complexes, $An(CO_3)_n^{3-2n}$, as well as the formation of An(III) solid phases, where several binary An/Ln-CO_3 and ternary M-An/Ln-CO_3 phases have been described. $AnCO_3OH(cr)$ was found to have considerable stability in carbonate containing near-neutral solutions [5]. Whereas the hydrothermal synthesis and characterization of $PuCO_3OH(cr)$ was reported [6], no systematic study has been dedicated to revealing its solubility behavior and thermodynamic stability, despite the fact that it may have a significant impact on the Pu(III)-Pu(IV) redox borderline based on the available data for Am(III)/Ln(III). In the present work, we synthesized and characterized $PuCO_3OH(cr)$ under room temperature conditions and studied its solubility behavior in carbonate containing NaCl solutions as a function of pH_m and ionic strength.

For the synthesis of $PuCO_3OH(cr)$, $Pu^{3+}(aq)$ was obtained by electrochemical reduction from an initial PuO_2^{2+} stock solution, and precipitated as $Pu(OH)_3(s)$. The $Pu(OH)_3(s)$ was equilibrated in a Na-HCO_3-CO_3 solution with a pH_m near to 8. After about 10 months, the initial amorphous $Pu(OH)_3(s)$ had undergone transformation into a blue fine crystalline solid. The oxidation state of the fine crystalline solid was confirmed to be pure Pu(III) by digesting a small fraction of it in acid and recording a VIS/NIR absorption spectroscopy of the corresponding solution. The powder X-ray diffraction (XRD) pattern of the compound matches very well the ones of $PuCO_3OH(cr)$ [6] and $NdCO_3OH(cr)$ [7]. Analysis by scanning electron microscopy-energy-dispersive (SEM-EDS) revealed a C:Pu ratio of ~ 1:1 and a O:Pu ratio of ~ >3:1. The results confirm that the fine crystalline blue Pu(III) solid phase is $PuCO_3OH(cr)$. SEM pictures of $PuCO_3OH(cr)$ are displayed in Figure 1.

The solubility of the $PuCO_3OH(cr)$ was studied in 0.10-5.61 m Na-Cl-OH-HCO_3-CO_3 solutions at pH_m 5.0–8.0 at T = (23 ± 2)°C under inert argon atmosphere with 1% CO_2 in a glove box.

Figure 2 exemplarily shows the experimental solubility of $PuCO_3OH(cr)$ in 0.10 m Na-Cl-HCO_3-CO_3 solution. Between pH_m 5 to 7, the solubility systematically decreases with a slope ≈ -3 to -1 ($\log m_{Pu(III)}$ *vs.* pH_m),

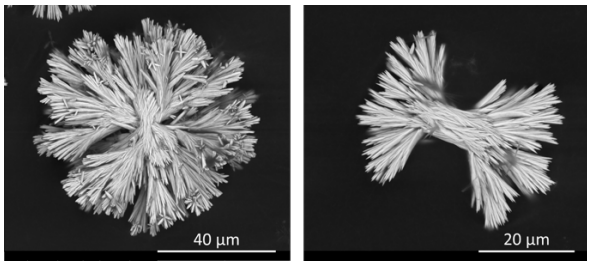

Fig. 1. Scanning electron microscope images of $PuCO_3OH(cr)$.

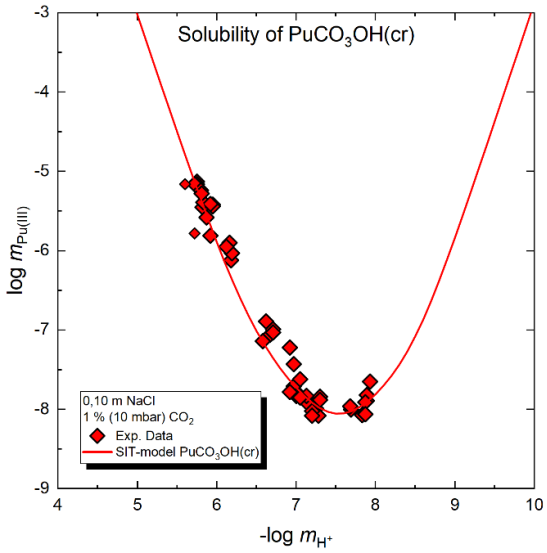

Fig. 2. Experimental molal solubility of $PuCO_3OH(cr)$ in 0.10 m NaCl solution and corresponding SIT model (solid line).

and remains at a rather constant level up to $pH_m \approx 8$. At the lowest point of the solubility curve at $pH_m = 7$ to 8, [Pu(III)] is about $1 \cdot 10^{-8}$ M, *i.e.*, about 4 orders of magnitude lower than for binary $Pu(OH)_3(s)$. The experimental and modelled (based on data for Am(III) with minor adaption of the solubility product) solubility curves are in very good agreement. With increasing [NaCl] = 0.1-5.61 m, the Pu(III) solubility systematically increases in the slightly acidic to neutral pH_m region due to the formation of Pu(III)-Cl complexes. The present work demonstrates that trace levels of carbonate can strongly decrease the solubility, and hence, mobility of Pu(III) by the formation of a carbonate containing solid phase compared to pure of hydrolysis compounds of Pu(III). The spontaneous formation of $PuCO_3OH(cr)$ in carbonate-containing solutions further proves that it can be realistically considered for geochemical model calculations and source-term estimations.

Acknowledgement: *This work was partially supported by the Bundesgesellschaft für Endlagerung (BGE).*

Solubility and hydrolysis of Fe(II) in reducing near-neutral to hyperalkaline, chloride-rich systems

For the long-term safety assessment of nuclear waste repositories, a reliable prediction of iron chemistry under reducing, alkaline, and in some cases chloride-rich conditions is essential. In case of water intrusion, corrosion of steel and cast-iron barriers can lead to the formation of Fe(II) solid phases, such as $Fe(OH)_2(cr)$ and $Fe_2(OH)_3Cl(cr)$. These iron phases act as redox buffers and thus govern the solubility and migration of redox-sensitive radionuclides and chemotoxic elements. However, predicted environmental geochemistry has long been hampered by uncertainties in the solubility products and hydrolysis equilibria of Fe(II) solids, par-

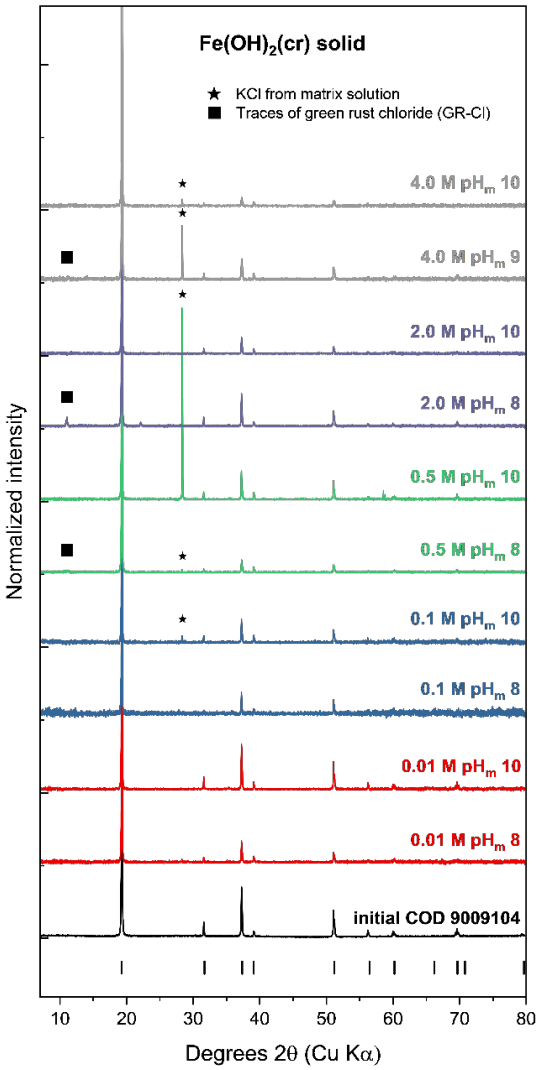

Fig. 3. XRD patterns for $Fe(OH)_2$(cr) solids before and after equilibration.

ticularly under chloride-rich and hyperalkaline conditions, which are common in cementitious repository environments. These uncertainties are reflected in the major thermodynamic databases (NEA-TDB [8-9], ThermoChimie [3], PSI/Nagra [4]), where equilibrium constants are often adopted from experiments with ambiguous solid phase identity or incomplete consideration of ionic strength effects. In particular, previous NEA reviews highlight a lack of reliable data for $Fe(OH)_2$(cr) and $Fe_2(OH)_3Cl$(cr), due to insufficient phase characterization and systematic investigation. To address these gaps, a comprehensive series of undersaturation solubility experiments with well-defined $Fe(OH)_2$(cr) and $Fe_2(OH)_3Cl$(cr) phases was conducted in KCl (0.01–4.0 M), KOH (0.1–4.0 M), and NaOH (up to 19 M, performed at GRS) solutions above pH_m 7.5 (T = 25 ± 2 °C), strictly excluding atmospheric O_2 and CO_2 (<0.1 ppm O_2). The solids were synthesized and aged in alkaline solutions and their purity was verified by XRD and Rietveld refinement. Redox purity of the supernatant solutions was confirmed by E_h measurements and CE-ICP-MS for selected samples (>95% Fe(II)). Equilibrated $Fe(OH)_2$(cr) exhibited excellent stability, although trace green rust chloride (GR-Cl) formation was observed at near-neutral pH_m and high KCl (>0.5 M), as shown in Figure 3. For $Fe_2(OH)_3Cl$(cr), transformation to $Fe(OH)_2$(cr) was observed at higher pH_m, especially at lower $[Cl^-]$. In mixed-phase samples, containing both $Fe(OH)_2$(cr) and $Fe_2(OH)_3Cl$(cr) as initial solid phases, the solid composition evolved with ionic strength, confirming phase boundaries and exchange reactions predicted from thermodynamic modeling.

Solubility measurements for $Fe(OH)_2$(cr) (Figure 4) and $Fe_2(OH)_3Cl$(cr) show log $[Fe]_{tot}$ decreasing as pH_m increases, with a slope of −2 at pH_m <9 (predominance of Fe^{2+}), and −1 at higher pH_m, indicating the increasing significance of the first hydrolysis species $FeOH^+$. Solubility constants were derived for both systems as follows using the SIT approach: $\log K°_{s,0}(Fe(OH)_2(cr)) = (12.32 \pm 0.05)$ and $\log K°_{s,0}(Fe_2(OH)_3Cl(cr)) = (16.38 \pm 0.20)$. Solubility behavior in mixed-phase experiments independently confirms the thermodynamic constants, describing the equilibrium $Fe_2(OH)_3Cl(cr) + H_2O \rightleftharpoons 2Fe(OH)_2(cr) + H^+ + Cl^-$, with SIT ion interaction coefficients derived for Fe^{2+}/Cl^-. The results of this work were published in Fürst et. al. (2025) [10]. In hyperalkaline NaOH and KOH systems, $Fe(OH)_2$(cr) solubility increases by several log units with increasing hydroxide concentration. Contrary to previous interpretations from Gayer and Woontner [11], detailed modeling of our dataset demonstrates that $Fe(OH)_3^-$ is the sole relevant Fe(II) hydrolysis species in solution under these conditions; no experimental support for higher order species such as $Fe(OH)_4^{2-}$ was found. The rapid solubility increase in saline, strongly alkaline media can be entirely described using SIT and Pitzer models, thereby improving reference constants and activity corrections for highly saline conditions. In conclusion, this work provides solubility products for $Fe(OH)_2$(cr) and $Fe_2(OH)_3Cl$(cr) from undersaturation solubility experiments with an extensive solid phase characterization using XRD in combination with Rietveld refinements and robust SIT and Pitzer modeling. The results can be used for an improved prediction of Fe phase evolution, redox control, and radionuclide migration

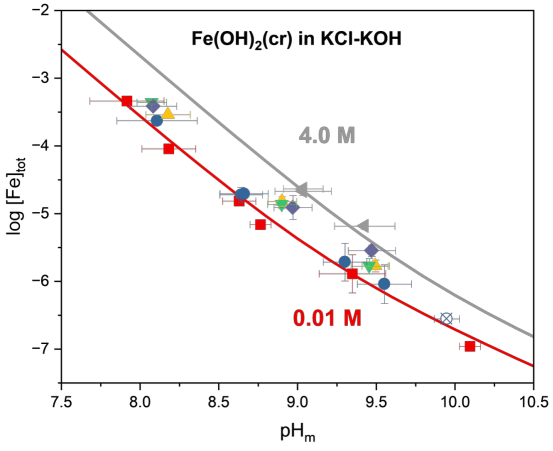

Fig. 4. Experimental Fe solubility of $Fe(OH)_2$(cr) in near-neutral to alkaline KCl/KOH system together with SIT model fits developed in this work.

under repository relevant conditions, and form the basis for ongoing database extensions performed in the framework of the STAMINA project in collaboration with GRS. Future work will further investigate the role of carbonate and silicate ligands, major components in cementitious and clay systems, on Fe(II) stability and solubility.

Acknowledgement. *This work was funded by the Federal Ministry for Environment, Nature Conservation and Nuclear Safety (BMUKN) within the STAMINA project under the contract number 02E12122B.*

Thermodynamic description of the Eu(III)-Na-NO_3-H_2O and Eu(III)-Mg-NO_3-H_2O systems

Eu(III) is, due to similar solution chemistry and aqueous speciation, considered an inactive analogue for trivalent actinides such as Am(III) and Pu(III), which play a predominant role in the field of radioactive waste disposal. Reprocessing techniques using nitric acid to recover radionuclides lead to considerable quantities of nitrate as part of the disposal inventory in specific L/ILW waste streams. Therefore, an understanding of the solution chemistry of nitrate systems is of importance to properly assess the chemical behavior of radionuclides under repository-relevant conditions. As continuation of the collaborative SUNI-RN project between BRGM, Andra, and KIT-INE, the present study investigates solubility and speciation phenomena within the ternary Eu(III)-Na/Mg-NO_3-H_2O systems. Samples were prepared by mixing ultrapure water (Milli-Q) with different amounts of $Eu(NO_3)_3{\cdot}6\ H_2O$, $NaNO_3$, and $Mg(NO_3)_2{\cdot}6\ H_2O$.

Solubility studies, carried out as batch experiments from undersaturation conditions, were performed at $T = (22 \pm 2)$ °C and $pH \leq 3.8$ over concentration ranges of 0.0-5.3 mol $NaNO_3$/kg H_2O and 0.0-4.3 mol $Mg(NO_3)_2$/kg H_2O, respectively. Periodic sampling of the solutions indicated that equilibrium conditions were obtained with constant Eu and Na/Mg concentrations determined via ICP-OES. The solid phases in equilibrium were identified by powder X-ray diffraction (XRD) and Schreinemakers' method. The combined results of solid and liquid phase analyses confirm the simple salts $Eu(NO_3)_3{\cdot}6\ H_2O$, $NaNO_3$, and $Mg(NO_3)_2{\cdot}6\ H_2O$, respectively, as equilibrium phases, while $2\ Eu(NO_3)_3{\cdot}3\ Mg(NO_3)_2{\cdot}24\ H_2O$ is indicated as metastable under the given conditions.

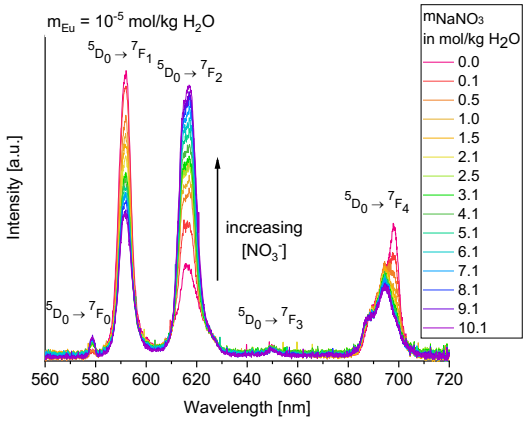

Fig. 5. Normalized (equal peak area) TRLFS spectra of Eu(III)-Na-NO_3-H_2O samples with 10^{-5} mol Eu/kg H_2O and 0.0-10.1 mol $NaNO_3$/kg H_2O at $T = (22 \pm 2)$ °C and $pH \leq 5.6$.

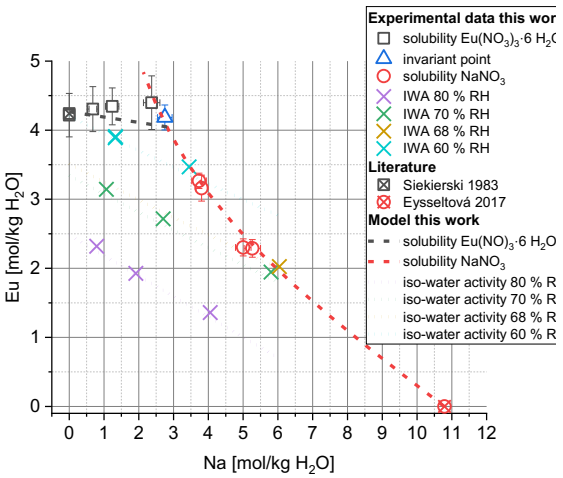

Fig. 6. Eu(III)-Na-NO_3-H_2O solubility and iso-water activity curves at 25 °C calculated with the partial dissociation Pitzer model (lines) compared to experimental data of this work and literature [17-18] (symbols).

The formation of aqueous Eu(III)-NO_3 complexes dependent on $NaNO_3$ concentration (0.0-10.1 mol/kg H_2O) was investigated with time resolved laser fluorescence spectroscopy (TRLFS) for 15 samples containing 10^{-5} mol Eu(III)/kg H_2O and pH adjusted to 5.0-5.6 (to prevent Eu^{3+} hydrolysis). Systematic changes in the intensity ratio of the transition peaks, best seen for the $^7F_1/^7F_2$ ratio (see Figure 5), verify changes in the coordination sphere of Eu(III) with increasing nitrate concentration and thus indicate Eu(III)-NO_3 complex formation.

Iso-water activity (IWA) and dynamic vapour sorption (DVS) experiments at T = 25 °C were conducted at BRGM for another set of samples to determine osmotic coefficients of different salt solutions at 50-80 % relative humidity (RH), which led to a reproducible increase in osmotic coefficient values with decreasing RH.

The comprehensive experimental data sets covering wide concentration ranges enabled us to derive thermodynamic models to describe the ternary systems as shown for the partial dissociation Pitzer model for Eu(III)-Na-NO_3-H_2O in Figure 6. We determined the missing complex formation constant $\beta^{\circ}_{Eu(NO_3)_2^+}$ and interaction parameters $\varepsilon_{i,j}$ (SIT formalism, Thermo-Chimie database [1]) as well as $\beta^{(0)}_{i,j}$, $\beta^{(1)}_{i,j}$, $\theta_{i,k}$, and $\Psi_{i,k,j}$ (Pitzer formalism, PhreeSCALE database [12]). Geochemical codes PhreeqC [13] (SIT) and PhreeSCALE [14] (Pitzer) were used for all modelling exercises combined with the parameter estimation software PEST [15].

This work continues a series targeting the thermodynamic description of Ln(III)/An(III)-SO_4-NO_3-H_2O systems of relevance in the context of radioactive waste

disposal. First calculations for the quaternary system Eu(III)-Na-SO_4-NO_3-H_2O with the parameters determined in the respective ternary sulphate [16] and nitrate systems show promising progress.

Solubility phenomena and thermodynamic description of the Tc(IV)-EDTA system in alkaline to hyperalkaline conditions

Technetium-99 (^{99}Tc) is a β-emitting radionuclide generated in nuclear reactors from the fission of ^{235}U and ^{239}Pu. Due to its long half-life ($t_{1/2} = 2.1 \cdot 10^5$ a) and differential chemical behavior of its main oxidation states (+IV and +VII), an accurate understanding of ^{99}Tc solubility and speciation is required in the context of nuclear waste disposal. Tc is primarily expected as sparingly soluble and strongly sorbing Tc(IV) in the very reducing conditions foreseen in underground repositories. Under weakly reducing to oxidizing conditions, Tc(VII) prevails as highly soluble and mobile pertechnetate anion. Ethylenediaminetetraacetate (EDTA) is commonly used as decontamination agent, and it is accordingly expected in specific waste streams in repositories for L/ILW, for which moderate ligand concentrations of up to ≈ 0.027 M are reported in the literature [19]. EDTA is known to form strong complexes with a variety of metal ions, including actinides and lanthanides [20]. Thermodynamic data for the complexation of EDTA with U, Np, Pu, Am, Tc, Ni and Zr were critically reviewed in volume 9 of the NEA-TDB project [21]. However, only a few experimental studies have previously investigated the interaction of Tc(IV) with EDTA, and no thermodynamic data for Tc-EDTA complexes were selected by the NEA-TDB reviewers. Although several studies were conducted thereafter [22-23], a thermodynamic description of the Tc-EDTA system remains incomplete.

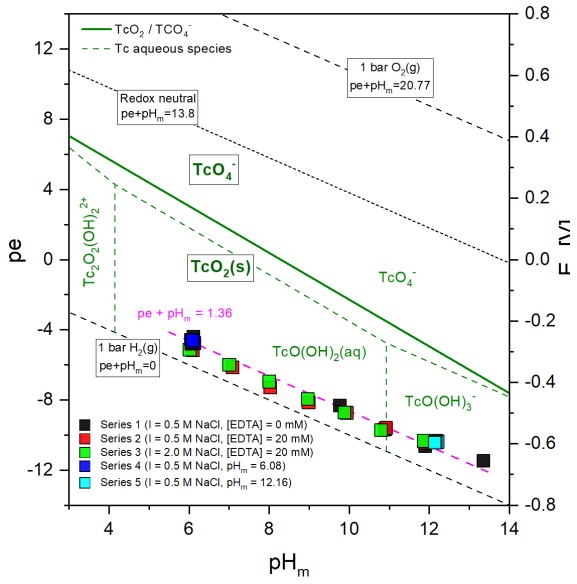

Fig. 7. Experimentally measured (pH_m + pe) values in the Tc–EDTA solubility experiments. Pourbaix diagram calculated for [Tc] = 10^{-5} M at I = 0.5 M NaCl using thermodynamic data selected in NEA-TDB [21].

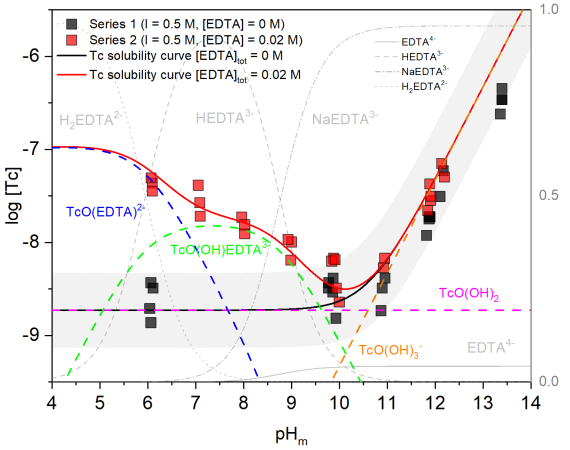

Fig. 8. Experimentally measured Tc concentrations at varying pH_m in the absence (black symbols) and presence (red symbols) of 0.02 M EDTA at I = 0.5 M. Solid lines correspond to the calculated TcO_2(am, hyd) solubility in the absence (black line, NEA-TDB) and presence (red line, this work) of EDTA.

All experiments were performed in Ar gloveboxes with < 3 ppm O_2 at T = (22 ± 2) °C. The solubility of Tc(IV) was investigated from undersaturation conditions with TcO_2(am, hyd). Reducing conditions were chemically maintained for each independent sample with 2 mM Sn(II). Solubility samples were prepared in 0.5 M and 2.0 M NaCl-NaOH-Na_4EDTA solutions at 6 ≤ pH_m ≤ 13.5, in the absence and presence of EDTA (with 10^{-4} M ≤ $[EDTA]_{tot}$ ≤ 0.1 M). pH_m, E_h and Tc concentrations were monitored for up to 124 days. The redox speciation of Tc in the aqueous phase of selected samples was investigated by solvent extraction. Selected solid phases were characterized by XAFS measurements performed at the INE-Beamline of the Karlsruhe Research Accelerator.

All measured (pe + pH) values are well below the redox borderline of $Tc^{IV}O_2$(am, hyd)/$Tc^{VII}O_4^-$, thus supporting the predominance of Tc(IV) solid phases and aqueous species in all samples (Figure 7). Solubility measurements in EDTA-free samples are consistent with the solubility of TcO_2(am, hyd) calculated with the current NEA-TDB thermodynamic selection [21] (Figure 8). The presence of EDTA promotes the enhancement of the Tc(IV) solubility in near-neutral to weakly alkaline conditions, i.e., 6 < pH_m < 10. Above this pH-range, a negligible impact of EDTA on the solubility of Tc(IV) is observed, suggesting that EDTA cannot outcompete the strong hydrolysis of Tc(IV) and the predominance of the anionic hydrolysis species $TcO(OH)_3^-$. At pH_m ≈ 6, the solubility of Tc(IV) is clearly enhanced by the formation of Tc(IV)–EDTA complex/es at $[EDTA]_{tot}$ ≥ 1 mM, possibly involving the formation of a 1:1 complex. Based on the slope analysis of solubility data (log [Tc] vs. pH_m and log [Tc] vs. log [EDTA]), redox speciation in the aqueous phase (solvent extraction) and solid phase characterization (EXAFS data), chemical, thermodynamic and SIT activity models were derived for the Tc(IV)–EDTA system (see solid red line in Figure 8). These

thermodynamic data can be implemented in geochemical calculations of relevance in the context of repositories for L/ILW.

References

[1] OECD-NEA. Thermochemical database project. https://www.oecd-nea.org/jcms/pl_22166/ thermochemical-database-tdb-project.

[2] German THEREDA database project. Website at: www.thereda.de.

[3] ThermoChimie database, v12a, https://www.thermochimie-tdb.com/

[4] PSI/Nagra Chemical Thermodynamic Database. www.psi.ch/en/les/database

[5] Grenthe, I., et al. Second Update on the Chemical Thermodynamics of Uranium, Neptunium, Plutonium, Americium and Technetium, Chemical Thermodynamics. OECD Nuclear Energy Agency, Boulogne-Billancourt, France (2020).

[6] Hagan, P.G., et al. J. Inorg. Nucl. Chem., 43, 1054-1055 (1981).

[7] Feng, W., et al. Acta Crystallographica Section E, E63, i174 (2007)

[8] Lemire, R. J., et al. NEA. Chemical Thermodynamics of Iron, Part 1; OECD Publishing: Paris (2013).

[9] Lemire, R. J., et al. NEA. Chemical Thermodynamics of Iron, Part 2; OECD Publishing: Paris (2020).

[10] Fürst, P. Q., et al. RSC Adv. 15 (54), 46308–46319 (2025).

[11] Gayer, K. H. and Woontner, L. J. Phys. Chem. 60 (11), 1569–1571 (1956).

[12] André, L., et al. PHREESCALE.DAT: A Thermodynamic Database for the PhreeSCALE Software. Version 1.0 (2020).

[13] Parkhurst, D. L., Appelo, C. A. J. US geological survey techniques and methods 6 (A43), 497 (2013).

[14] Lach, A., et al. Comput. Geosci., 92, 58-69 (2016).

[15] Doherty, J. Watermark Numerical Computing, Brisbane, Australia 3338, 3349 (2004).

[16] dos Santos, P. F., et al. Dalton Trans., 53 (14), 6323–6332 (2024).

[17] Siekierski, S., et al. IUPAC Solubility data series Vol. 13 (1983). (https://iupac.org/what-we-do/databases/solubility-data-series/)

[18] Eysseltová, J., et al. IUPAC-NIST Solubility Data Series Vol. 89; J. Phys. Chem. Ref. Data 46 (1), 013103 (2017).

[19] Wieland, E. Nagra Technical Report NTB 14-08 (2014).

[20] DiBlasi, N. A., et al. Environmental Science & Technology, 57(9), 3661-3670 (2023).

[21] Hummel, W., et al. Chemical thermodynamics of compounds and complexes of U, Np, Pu, Am, Tc, Se, Ni and Zr with selected organic ligands, OECD Publishing: Paris (2005).

[22] Boggs, M. A. et al. Radiochimica Acta, 101(1), 13-18 (2013).

[23] Evans, N. D. M. and Hallam, R. Mineralogical Magazine, 76(8), 3435-3438 (2012)

4.2 Sorption on mineral surfaces

M. Altmaier, I. Androniuk, X. Gaona, H. Geckeis, R. E. Guidone, N. Huber, J. Lützenkirchen, N. Palina, A. Skerencak-Frech, A. Thumm

In co-operation with:

L. Alcubierre[a], F. Bocchese[b], S. Brassinnes[b], K. Garbev[c], M. López-Garcia[a], B. Lothenbach[d]

[a] Amphos 21, Barcelona, Spain; [b] ONDRAF/NIRAS, Sint-Joost-ten-Node, Belgium; [c] Institute for Technical Chemistry, Karlsruhe Institute of Technology, Karlsruhe, Germany; [d] Laboratory Concrete & Asphalt, Empa, Swiss Federal Laboratories for Materials Science and Technology, Dübendorf, Switzerland

Introduction

The interaction mechanisms with mineral surfaces are key processes for the retention of radionuclides within the Safety Case of a nuclear waste repository. For their thorough quantification and implementation in safety performance calculations, a detailed mechanistic understanding of these processes is essential. This requires an in-depth knowledge of the mineral- water interfaces, and a reliable thermodynamic description of the sorption reactions.

The sorption of radionuclides on different relevant solid phases needs to be studied under systematic variation of experimental conditions, i.e., radionuclide concentration, pH values, composition and concentration of the electrolyte solution, and presence of other radionuclides and/or complexing aqueous ligands, which may both be able to compete/interfere during sorption onto the surface.

Besides classic batch and solubility studies, a variety of modern spectroscopic speciation techniques with a high analytical sensitivity are applied to study the sorption processes on a molecular level. In combination with a subsequent description by thermodynamic surface complexation models and molecular dynamic simulations, comprehensive information on the retention processes are determined, which are of high importance for the Safety Case.

In the present bi-annual report, various aspects of the interaction of different compounds with mineral surfaces are considered.

Sorption of Eu(III) and Cm(III) on C-S-H phases in presence of EDTA at intermediate to high ionic strength conditions

Clay rock formations in northern Germany are considered potential host rocks for the disposal of nuclear waste. A distinctive feature of these formations is their pore water, which is dominated by intermediate ionic strengths ($I = 1–3$ mol L^{-1}) of NaCl and $CaCl_2$. Calcium-Silicate-Hydrate (C-S-H) phases are the main component of cementitious materials and provide strong retention of tri- and tetravalent actinides.[1] In low- and intermediate-level waste (L/ILW) repositories, cementitious materials are extensively used as waste packages, overpacks, backfill, and for the solidification and stabilization of the waste.[2] Ethylenediaminetetraacetic acid (EDTA) is a powerful chelating ligand for tri- and tetravalent actinides (An(III/IV)) and is present in L/ILW owing to its widespread use as a decontamination agent.[3] The effect of EDTA on the retention of An(III) by C-S-H phases is not yet fully understood, and the influence of elevated ionic strength (NaCl and $CaCl_2$) has never been examined in detail. Consequently, this work investigates the uptake of Eu(III) and Cm(III) on C-S-H phases in the presence of EDTA and in NaCl and $CaCl_2$ solutions of intermediate ionic strength.

The study employed conventional batch sorption experiments together with Time-Resolved Laser Fluorescence Spectroscopy (TRLFS). EDTA concentrations were varied from 10^{-6} to 10^{-2} mol L^{-1}. Total concentrations of Eu(III) and Cm(III) were set to $2 \cdot 10^{-8}$ and $1 \cdot 10^{-7}$ mol L^{-1}, respectively, for the two analytical techniques. All experiments were carried out under an inert argon atmosphere ($O_2 \approx 2$ ppm) with a fixed solid-to-liquid ratio of 1 g L^{-1}. The calcium-to-silicon (C/S) ratio of the C-S-H phases was maintained at 1.1, yielding a pH of approximately 11.2–11.6. NaCl and $CaCl_2$ served as electrolyte solutions, providing an ionic strength of $I_m = 1.02$ mol $(kg \cdot H_2O)^{-1}$. Contact times were varied between 7 and 180 days.

In general, the ionic strength itself did not show any significant effect on the sorption coefficients (data not shown). Hence, further studies were conducted at a fixed ionic strength of 1.02 mol $(kg \cdot H_2O)^{-1}$, adjusted with either NaCl or $CaCl_2$. The $\log R_d$ values for Eu(III) uptake onto C-S-H phases over the EDTA concentration range $0 – 10^{-2}$ mol L^{-1} are shown in Figure 1.

For both electrolyte systems, very high $\log R_d$ values ($\approx 5–6$) are obtained at $[EDTA] \leq 10^{-3}$ mol L^{-1}, indicating near-quantitative adsorption of Eu(III) onto the solid phase and a negligible influence of EDTA. In contrast, at 10^{-2} mol L^{-1} EDTA the $\log R_d$ values drop markedly after 7 days of sorption for both electrolytes,

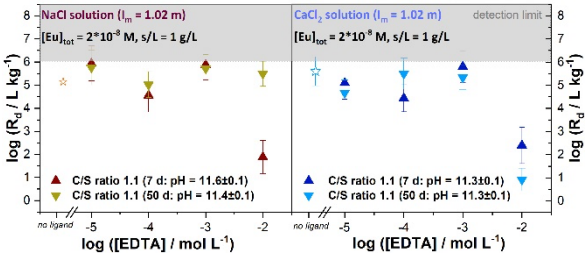

Fig. 1: Log R_d for the adsorption of Eu(III) on C-S-H phases (C/S = 1.1) with [EDTA] = 0 – 10^{-2} mol L^{-1} in NaCl (left) and $CaCl_2$ (right) solutions (I_m = 1.02 mol $(kg \cdot H_2O)^{-1}$) after 7 and 50 d. R_d given in $[L \cdot kg^{-1}]$.

reflecting the formation of stable Eu(III)–EDTA complexes in solution.

After 50 days, the log R_d for the NaCl system increases again, whereas it remains low in the $CaCl_2$ system. This behavior suggests that, in the presence of $CaCl_2$, very stable ternary (Ca–Eu(III)–EDTA) or quaternary (Ca–Eu(III)–OH–EDTA) complexes are formed, preventing Eu(III) from re-adsorbing onto the C-S-H phases.

The hypothesis was tested by applying Cm(III)-TRLFS. Figure 2 shows the emission spectra of Cm(III) in the presence of C-S-H phases at an EDTA concentration of 10^{-2} mol L^{-1}, measured in both NaCl and $CaCl_2$ solutions. Spectra were recorded for the suspension as well as for the supernatant liquid phase (no quantitative phase separation was performed for the latter).

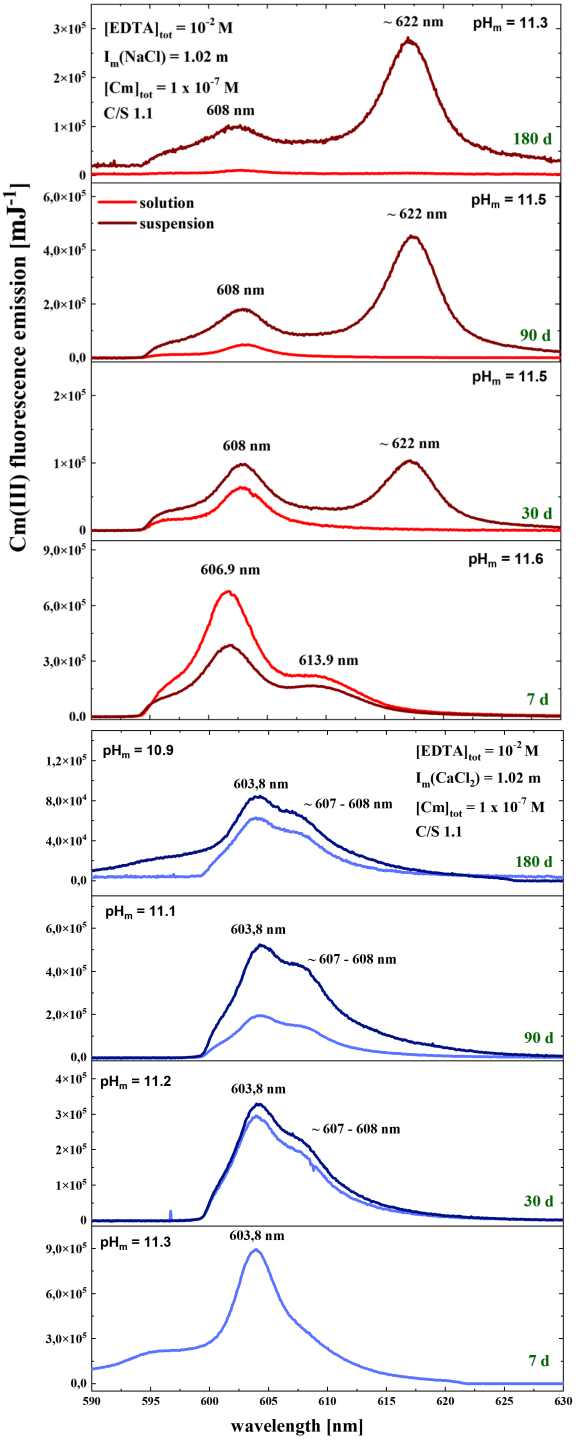

Fig. 2: Emission spectra of Cm(III) (10^{-7} mol L^{-1}) in presence of EDTA = 10^{-2} mol L^{-1} at 7 to 180 d of equilibration time. Red) $NaCl_{aq}$, Blue) $CaCl_{2,aq}$ (I_m = 1.02 mol (kg·H_2O)$^{-1}$ both). Light) measurement of the supernatant, Dark) measurement of the suspension

NaCl solution. After 7 days, the two ternary hydrolysis Cm(III)-EDTA species $Cm(OH)(EDTA)^{2-}$ and $Cm(OH)_x(EDTA)_{(x+1)}$ – located at 606.9 and 613.9 nm respectively – are observed in the aqueous phase. With longer contact times, a distinctly stronger red-shifted emission band appears at ≈ 622 nm. This band is attributed to Cm(III) that has become incorporated into the C-S-H phase. The simultaneous near-quantitative loss of fluorescence intensity in the liquid phase confirms that almost all Cm(III) has transferred to the solid.

Cl_2 solution. Throughout the entire sorption period the spectra are dominated by a band at 603.9 nm. This band is assigned to a ternary Ca–Cm(III)–EDTA complex, which is characterized by a significantly shorter fluorescence lifetime ($\tau = 160 \pm 20$ µs) compared with the binary Cm(III)–EDTA species ($\tau = 231 \pm 40$ µs).[4]. No emission feature around 622 nm – indicative of Cm(III) incorporated into C-S-H – is observed under these conditions.

These TRLFS results are fully consistent with the batch sorption experiments. In the absence of Ca^{2+} ions, Eu(III) and Cm(III) are initially stabilized in solution by complexation with EDTA and, over time, are gradually incorporated into the C-S-H structure. In contrast, when Ca^{2+} is present, very stable ternary Ca–Eu(III)/Cm(III)–EDTA (or Ca–Eu(III)/Cm(III)–OH–EDTA) complexes form, keeping the actinides in the aqueous phase for extended periods.

This work was performed within the GraZ II, funded by the BMWK under grant number 02E11860C.

Nb(V) uptake by calcite and carbonated cement paste in the absence and presence of ISA and chloride

^{94}Nb ($t_{½}$ = 20,400 a) is a β^-–γ emitting activation product generated by neutron irradiation of the naturally occurring, stable isotope ^{93}Nb present in structural components (e.g., Ni-based alloys) of nuclear reactors. ^{94}Nb is mostly present in streams resulting from the dismantling of nuclear power plants, as well as from the treatment of the primary cooling circuit, which may be disposed in cement-based repositories for low- and intermediate-level short-lived waste (L/ILW-SL). Isosaccharinic acid (ISA) is a polyhydroxycarboxylic acid forming upon degradation of cellulose in hyperalkaline conditions. ISA is known to form strong complexes with hard Lewis acids, thus potentially affecting radionuclide retention in cementitious systems [5-6]. High

concentrations of stable chloride (≤ 5 M) have been also described for specific waste streams containing evaporator concentrates. This study focuses on the uptake of Nb(V) by calcite ($CaCO_3$) and carbonated cement systems in the absence and presence of ISA and chloride. Both materials are taken as representatives of the degradation stage IV of cement, with relevance to near-surface disposal systems.

A combination of ^{93}Nb (stable) and ^{95}Nb ($t_{1/2}$ = 34.97 d) isotopes was used in systematic batch sorption experiments. Cement pastes (CEM I and III/C) were carbonated in a closed reactor using a CO_2/N_2 gas mixture (30/70%). Batch sorption experiments were performed under air-atmosphere at room temperature, using calcite and carbonated cement paste as solid phases in combination with their corresponding equilibrated waters (pH ≈ 8.2–8.5). Total niobium concentrations ranged within 10^{-11} M ≤ [Nb(V)]$_0$ ≤ 10^{-6} M (as ^{95}Nb or ^{93}Nb + ^{95}Nb), with S/L = 1–10 g·L^{-1}. Systems were investigated in the absence or presence of ISA ($1.0\cdot10^{-5}$ M ≤ [ISA] ≤ 0.1 M) and chloride ($8.4\cdot10^{-5}$ M ≤ [NaCl] ≤ 2.0 M). The aqueous niobium concentration after sorption was quantified by gamma spectroscopy after ultracentrifugation. Prior to the sorption experiments, oversaturation solubility experiments were conducted in the same equilibrated solutions to determine solubility limits. The solid phases obtained from the solubility experiments and used for the batch sorption experiments were characterized by means of XRD, Raman, ATR-IR, SEM-EDS, and BET.

The solubility of Nb(V) in calcite- and carbonated cement-equilibrated waters was quantified as ~10^{-6} M at t = 3 days, but decreased to ≤ 10^{-8} M at longer equilibration times (t = 13–121 days). This solubility limit is significantly lower than the one calculated assuming a solubility-control by Nb_2O_5(cr). XRD and Raman support that a Ca-Nb(V)-OH solid phase is responsible for the solubility-control of Nb(V) under these conditions, although no thermodynamic data for such solid phases is currently available in reference thermodynamic databases [7]. The uptake of Nb(V) by calcite shows moderate distribution ratios (R_d) at short contact times (t = 3 days, $R_d \approx 10^3$ L·kg^{-1}). An increase in R_d values is observed with time, resulting in $R_d > 2\cdot10^4$ L·kg^{-1} at t = 89 days. This observation may suggest a fast adsorption of Nb(V) on the calcite surface, followed by a slow incorporation into the calcite structure through the recrystallization process. A significantly stronger uptake is observed for both carbonated cement materials ($R_d \approx 8\cdot10^5$ L·kg^{-1} carb. CEM I; $R_d \approx 1\cdot10^6$ L·kg^{-1} carb. CEM III), as reflected in the sorption isotherms in Figure 3a. This differential behaviour is expectedly caused by the presence of amorphous phases with significantly larger specific surface area, i.e., $Si(Al,H)O_2$ gel or small fractions of low Ca C-S-H phases, as determined by means of Rietveld analysis, Raman and IR-spectroscopy and BET. The normalization of the distribution ratios by the surface area of the corresponding materials (calcite, carbonated cement) results in a much similar behaviour of the distribution ratios (see Figure 3b). This emphasizes the key role of surface area, as well as the need of an appropriate characterization of the individual phases present in complex sorbing materials (e.g., carbonated cement). The presence of stable ^{93}Nb in degraded cement paste suggests that isotopic exchange may also contribute in the retention of radioactive Nb isotopes (^{95}Nb in this work, ^{94}Nb in the waste) in carbonated cement materials.

ISA has a minor to moderate impact on the uptake of Nb(V), both for calcite and carbonated cement systems. The decrease in R_d values observed at high ligand concentrations is attributed to the formation of Nb(V)–ISA complexes. However, the impact on sorption is weaker compared to observations reported for the degradation stage I of cement at pH ≈ 13.6 [10]. Such differences could be partly explained by the greater stability of the Nb(V)-ISA complexes under hyperalkaline conditions, although other parameters (e.g., surface charge, concentration of Ca in the aqueous phase, sorption of ISA on the solid phase, etc.) can contribute as well to the observed differences. Chloride has a weak impact on sorption of Nb(V). The effect in R_d is more remarkable in calcite than in carbonated cement paste, which possibly reflects that a different mechanism is driving the uptake of Nb(V) in both systems.

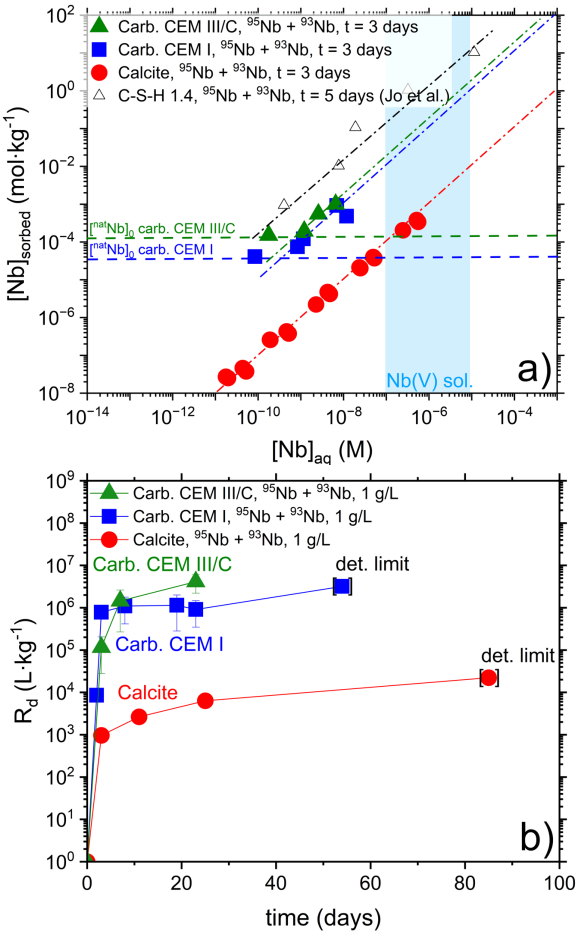

Fig. 3: (a) Nb(V) sorption isotherms for the uptake of Nb(V) by calcite, carb. CEM I and carb. CEM III/C at t = 3 days [8] and C-S-H 1.4 t = 5 days [9]. (b) Kinetics for the uptake of Nb(V) by calcite, carb. CEM I and carb. CEM III/C at t = 3 days [8].

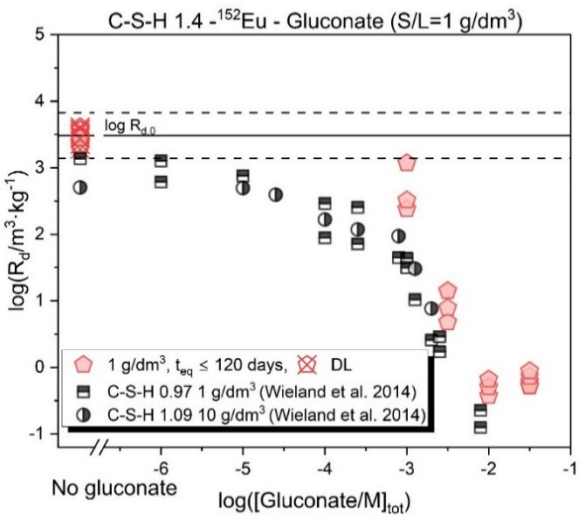

Fig. 4: Distribution ratios, R_d, determined for the uptake of Eu(III) by C-S-H 1.4 at increasing concentrations of gluconate. Experiments conducted at S/L = 1 g·dm^{-3} with up to 120 days of contact time (t_{eq}). X-crossed symbols refer to values at the detection limit. Data reported by Wieland [12] included for comparison purposes.

This work provides an improved quantitative description of Nb retention under conditions relevant for the cement degradation stage IV in repositories for L/ILW, in which the presence of ISA and chloride can be envisaged.

Acknowledgments: *This work was partly funded by ONDRAF/NIRAS under contract number CCHO 2015-0707/01/00.*

Impact of gluconate on the uptake of Eu(III) and Pu(III/IV) by cement phases

Cementitious materials are extensively used in repositories for low- and intermediate level waste (L/ILW), for construction purposes and stabilization of the waste. In this context, cement plays an important role acting as physical and chemical barrier minimizing the mobility of radionuclides. C-S-H phases represent the most abundant component in hydrated cement, and are known as main sink for the uptake of actinides. The presence of organics may have an impact on the radionuclide release due to the formation of stable aqueous complexes with higher solubility [5, 11-12]. Sodium gluconate is used as a cement-dispersing and retarding agent [11, 13], and thus can be expected in repositories for L/ILW.

Sorption experiments were carried out under Ar atmosphere with C-S-H phases at pH = 13.3 and varying gluconate concentrations (10^{-4} M ≤ $[GLU]_{tot}$ ≤ $10^{-1.5}$ M). C-S-H phases were synthesized with C/S = 0.8 and 1.4 and S:L = 1 and 25 g·dm^{-3}. Sorption experiments with plutonium were conducted with $[^{242}Pu]_0 = 10^{-8}$ M in presence of the redox buffers hydroquinone (HQ) or Sn(II), imposing mildly and strongly reducing conditions where Pu(IV) and Pu(III/IV) are expected to prevail, respectively [14]. Sorption experiments with Eu(III) were conducted using both inactive ($[^{nat}Eu]_0 = 10^{-7}$ M) and active ($[^{152}Eu]_0 = 10^{-9}$ M) europium isotopes. Sorption samples were monitored for equilibration times of up to 90 (Pu) and 120 (Eu) days.

A strong uptake of Pu(III/IV) by C-S-H was observed in the absence of gluconate (log R_d ~ 5.5, with R_d in dm^3·kg^{-1}), in good agreement with previous studies available in the literature [14]. Gluconate promoted a significant decrease in the R_d values at $[GLU]_{tot} > 10^{-4}$ M for both HQ and Sn(II) systems. A slightly enhanced Pu retention was observed in the very reducing conditions imposed by Sn(II). This observation is attributed to the possible formation of surface complexes involving Pu(III) and gluconate. A very strong uptake of Eu(III) by C-S-H phases was also observed in gluconate-free systems. Gluconate triggered a moderate decrease in the uptake of Eu(III) by C-S-H 0.8, but a significant decrease in the sorption was observed for C-S-H 1.4 systems (Figure 4). As confirmed by TRLFS, this observation can be explained by the formation of more stable Ca-Eu(III)-OH-GLU complexes in the porewater solution of C-S-H 1.4, which is characterized by Ca concentrations of *ca.* one order of magnitude higher than in C-S-H 0.8.

Molecular dynamic calculations were carried out to study the binding process occurring at the surface of C-S-H phases in both presence and absence of gluconate. Calculations were performed using the parameters reported for ClayFF [15] and Eu(III) [16].

The surface of C-S-H provides multiple possibilities for ion binding, among them the three most probable sorption sites were selected: "defect site" in the position of the missing bridging silicate tetrahedra in the silicate chain (DEF); "bridge site" – deprotonated silanol group of the bridging silicate tetrahedra in the silicate chain (BR); and "chain site" that includes coordination with one deprotonated silanol and bridging oxygens (CH). The performed PMF (Potential of Mean Force) calculations indicate that in the presence of gluconate in the coordination sphere of Eu(III) the strength of sorption is significantly decreased for the DEF and CH sites and shifted to the outer-sphere complexation in the case of the BR site (Figure 5). This validates the experimental data, and shows that gluconate mobilizes Eu(III) in C-S-H phases.

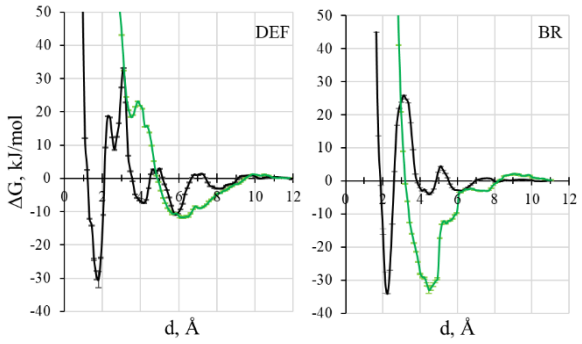

Fig.5: PMF curves for sorption of Eu(III) with (green) and without (black) gluconate on the selected sorption sites of the (001) C-S-H surface.

This work provides a comprehensive quantitative and mechanistic description of the uptake of Ln(III) and An(III/IV) by cement phases in the absence and presence of gluconate. The combination of experimental and theoretical methods provides key insights to understand the retention processes of these radionuclides in the context of repositories for L/ILW.

Acknowledgments: *The EURAD project leading to this application has received funding from the European Union's Horizon 2020 research and innovation programme under grant agreement no. 847593. This work was supported by the German collaborative GRAZ II project (Geochemische Radionuklidrückhaltung an Zementalterationsphasen, Teilprojekt 02E11860C), funded by the German Federal Ministry for the Environment, Nature Conservation, Nuclear Safety and Consumer Protection (BMUV). The authors likewise acknowledge support by the state of Baden-Württemberg through bwHPC and the German Research Foundation (DFG) through grant no INST 40/575-1 FUGG (JUSTUS 2 cluster)*

Uptake of trivalent cations by quartz: a re-evaluation

Two INE studies including surface complexation modelling have been published on the uptake of trivalent cations (Eu/Am/Cm, An(III)) on quartz. The first study was published in 2008 [17]. Due to the lack of titration data for the quartz sample in the surface complexation model (SCM), it was assumed that the surface had the same properties as standard silica. At the time surface titrations of the sample had been carried out, but the results were discarded since deprotonation was observed at very low pH. This was suspicious because the major part of published SiO_2 titration data shows no significant charge below pH 5. Some data from different communities however, suggested quite early that SiO_2 surfaces may exhibit a two step deprotonation [18]. Such charging curves were also reported in the second INE-study on An(III) on MINUSIL, another quartz sample [19]. In this second study, the modelling of An(III) surface speciation was adopted from the first paper. This was done, since that paper also involved spectroscopic data, that ultimately could only be fitted with the the equations

$$(\equiv SiOH)_2 + An^{3+} = (\equiv SiO)_2HAn^{2+} + H^+ \quad (1)$$

$$(\equiv SiOH)_2 + An^{3+} + H_2O = (\equiv SiO)_2An(OH)^\circ + 3H^+ \quad (2)$$

The SCM parameters obtained in the two studies were substantially different concerning the stability constants and the charge distribution parameters for equations (1) and (2). Here, we have reconsidered the titration data of the first quartz with respect to the sample used in Stumpf et al. [17] and a comparison is shown in Figure 6 with both the experimental data and the model published by Garcia et al. [19].

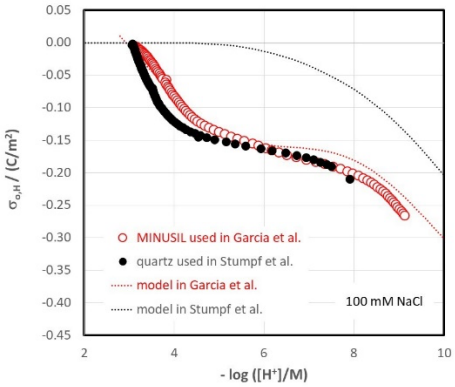

Fig. 6: Specific proton surface charge density of quartz samples used by Stumpf et al. [17] and Garcia et al. [19] and the respective models curves from the two papers for 100 mM NaCl.

The initially discarded charging data set obtained with the quartz simple used by Stumpf et al. [17] actually resembles very closely the results published by Garcia et al. [19]. As is also obvious, the simple silica model (black dotted line) used in Stumpf et al. [17] suggests only little charge at pH 6 and below, whereas the data and the model from Garcia et al. [19] involves high charge resulting in enhanced electrostatic factors.
Consequently, the An(III) uptake and spectroscopic data of Stumpf et al. [17] were remodeled using the acid base model of Garcia et al. [19].

Figure 7 shows that the data can be equally well described. The resulting log K values and charge distribution factors for the two models, i.e. the original model by Garciea et al. and (in brackets) the updated model for the data of Stumpf et al. are log K = -065 (0.58) and $\Delta z_{An,o}$ = 0.36 (0.77) for (1) and -10.02 (-8.76) and 0.02 (0.43) for (2).

It has been extensively discussed by Stumpf et al [17] that from surface species 1, equation (1) to surface species 2, equation (2), two protons were released, i.e. one intermediate hydrolysis species did not occur. The reason was the low charge on the silica (i.e. the black dotted line in Figure 6). With the acid-base model of Garcia et al. [19], the intermediate hydrolysis species

$$(\equiv SiOH)_2 + An^{3+} = (\equiv SiO)_2An(OH)^+ + 2H^+ \quad (3)$$

was combined with equation (1). The best fit results with this option are shown in Figure 8, with log K = -0.13 and $\Delta z_{An,o}$ = 1.20 for (1) and -4.10 and 1.25 for (3).

The fit is slightly worse compared to the combination of equations (1) and (2), which is mainly caused by the failure to reach 100 per cent uptake at the higher Am concentration (2 µM). This could be improved by including the precipitation of $Am(OH)_{3(s)}$, as was done in Stumpf et al. [17] for another series of measurements. The best fit charge distribution factors indicate a closer approach of An(III) to the surface in this model option as compared to the previously discussed option, and

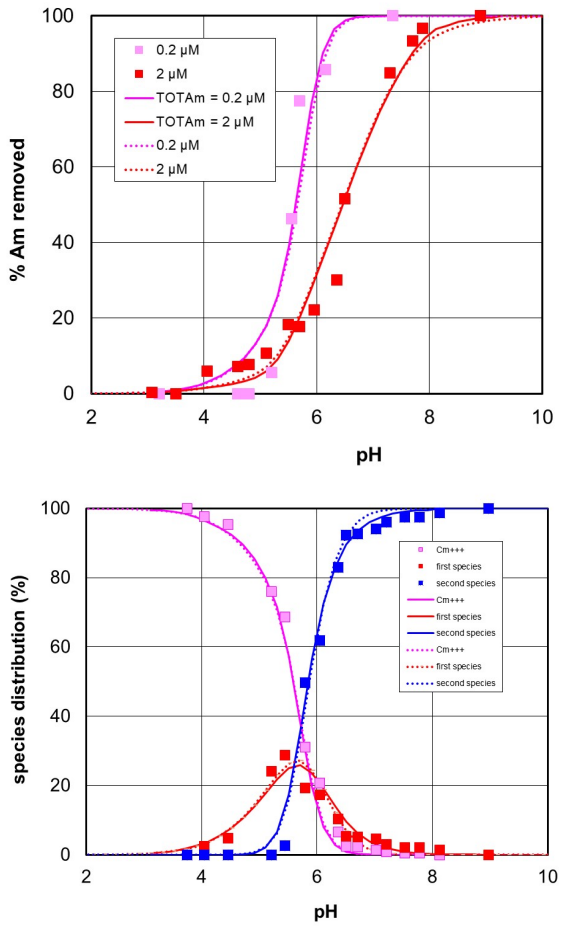

Fig. 7: Upper part: Adsorption data for An(III) on quartz by Stumpf et al. [17] remodeled as described in the text compared to the original model. Lower part: TRLFS data for An(III) in the presence of quartz by Stumpf et al. [17] remodeled as described in the text (dotted lines) compared to the original model (full lines). All in 100 mM NaCl.The model variants assume equations (1), labelled first species and (2), labelled second species.

might be in closer agreement with the notion of an inner-sphere surface complex that was found by Stumpf et al. [17].

A combination of equations (2) and (3) lead to an intermediate result, i.e. the original combination remains the numerically best fit. Ultimately refitting the data in Garcia et al. [19] could be useful to obtain more consistent charge distribution factors in that case as well. Moreover, one might refine the acid-base model for the black dots in Figure 6 to obtain a self-consistent set of surface parameters, but this is hampered by the absence of more data.

Overall, it becomes clear how important the electrostatic factors, as related to the potentiometric titrations of a given solid, can be.

References

[1] M. Ochs, D. Mallants, L. Wang, Radionuclide and metal sorption on cement and concrete, **Vol. 2**, Springer, (2016).

[2] M. L. Schlegel, I. Pointeau, N. Coreau, P. Reiller, Environmental Science & Technology, **38**, 4423-4431, (2004).

[3] W. Hummel, F. J. Mompean, M. Illemassène, J. Perrone, Chemical thermodynamics of compounds and complexes of U, Np, Pu, Am, Tc, Se, Ni and Zr with selected organic ligands, **Vol. 9**, Elsevier Amsterdam, (2005).

[4] M. Trumm, A. G. Tasi, A. Schnurr, N. A. DiBlasi, X. Gaona, Mol. Phys., **8**, e2033864, (2022).

[5] M. Ochs, D. Mallants, L. Wang, Radionuclide and metal sorption on cement and concrete, **Vol. 2**, Springer, (2016).

[6] Tits, J., Wieland, E., Bradbury, M. H. (2005), Applied Geochemistry, 20, 2082-2096.

[7] Rai, D., Kitamura, A. (2017), The Journal of Chemical Thermodynamics, 114, 135-143.

[8] N. Huber et al., Cem. Con. Res., **197**, (2025).

[9] Y. Jo et al., *Cem. Con. Res.*, **172**, (2023).

[10] N. Cevirim-Papaioannou et al, *Cem. Con. Res.*, **153** (2022).

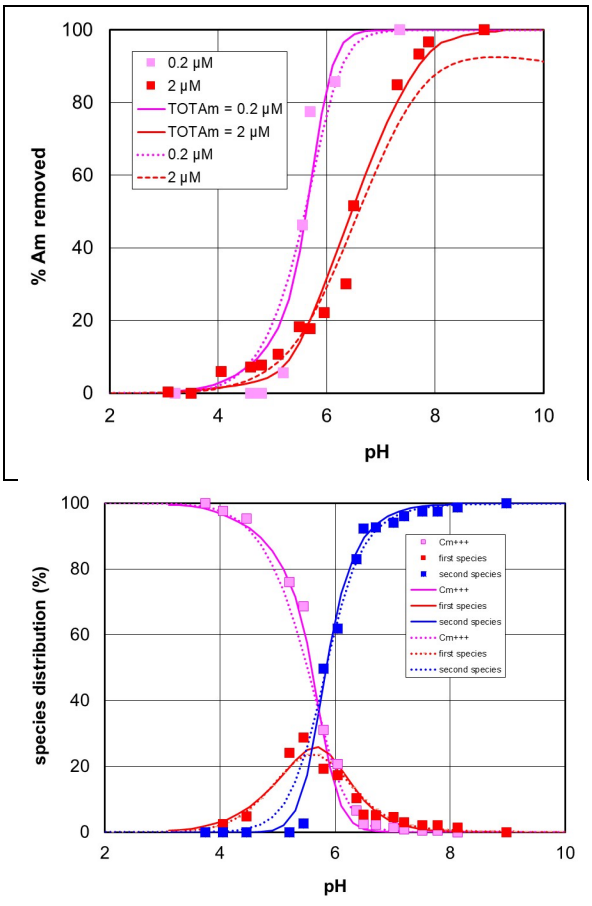

Fig. 8: Upper part: Adsorption data for An(III) on quartz by Stumpf et al. [17] remodeled as described in the text compared to the original model. Lower part: TRLFS data for An(III) in the presence of quartz by Stumpf et al. [17] remodeled (dotted lines) as described in the text compared to the original model (full lines). All in 100 mM NaCl. The model variants assume equations (1), labelled first species and (3), labelled second species.

[11] W. Hummel, F. J. Mompean, M. Illemassène, J. Perrone, Chemical thermodynamics of compounds and complexes of U, Np, Pu, Am, Tc, Se, Ni and Zr with selected organic ligands, Vol. 9, Elsevier Amsterdam, (2005).
[12] E. Wieland, Nagra Technical Report 14-08, (2014).
[13] R. E. Guidone et al., Applied Geochemistry, 175, 106145 (2024).
[14] A. Tasi, X. Gaona, D. Fellhauer, M. Böttle, J. Rothe, K. Dardenne, R. Polly, M. Grivé, E. Colàs, J. Bruno, K. Källström, M. Altmaier, H. Geckeis, Applied Geochemistry, 98, (2018).
[15] R. T. Cygan et al. J. Phys. Chem. B 108, 1255-1266, (2004).
[16] Y. An et al. J. Phys. Chem. A 104, 11243-11247 (2000).
[17] S. Stumpf et al., *J. Colloid Interface Sci.*, **318,** 5-14, (2008).
[18] S. Ong et al., Chem. Phys. Lett. **191**, 327-335, (1992).
[19] D. Garcia et al, Colloids and Surfaces A **578,** 123610, (2019).

4.3 Retention of radionuclides by secondary phase formation

M. Alzaydan, P. Cakir-Wuttke, O. Dieste Blanco, N. Finck, H. Geckeis, F. Heberling, V. Metz, R. Polly, T. Roth, D. Schild, A. Singh, M. Schorer, L. Zunftmeister

In co-operation with:

Ferdinand Kirchner [1], Martin Kutzschbach [1], Felix Brandt [2], Martina Klinkenberg [2]

1) Institute of Applied Geochemistry, Technische Universität Berlin, Ernst-Reuter-Platz 1, 10587 Berlin, Germany
2) Institute of Energy and Climate Research (IEK-6)-Nuclear Waste Management and Reactor Safety, Forschungszentrum Jülich GmbH, 52425 Jülich, Germany

Introduction

The final disposal in a deep geological repository (DGR) is a generally accepted strategy for dealing with long-lived high-level radioactive waste (HLW). In such a repository, HLW is planned to be surrounded by natural and engineered barriers capable to prevent or to retard groundwater from contacting the waste packages, and radionuclides (RNs) released from the altering waste matrix from being transported to the far-field. During the evolution of the repository system, groundwater may ultimately reach the waste packages, triggering various alteration and corrosion processes at the canister/engineered barrier interface. Metallic corrosion will limit the canister service life, but the neoformation of secondary phases will provide a new chemical barrier able to scavenge RNs released upon waste matrix alteration.

Various molecular scale processes can result in RN immobilization, ranging from surface adsorption to structural incorporation by solid solution formation. Among these mechanisms, incorporation within the bulk structure may occur when RNs are present during growth or recrystallization of secondary phases and result in very effective retention. In order to be implemented in the Safety Case, kinetic and thermodynamic models of RNs immobilization need to be developed. The development of such models usually relies on the application of complementary advanced microscopic and spectroscopic techniques combined with computational studies. This strategy is applied at KIT-INE to develop models describing the immobilization of key RNs by relevant secondary phases.

Examples of ongoing studies related to secondary phases formation and to RN uptake performed within national and international projects are presented in the following.

Metallic corrosion at the water-saturated steel/bentonite interface under anoxic conditions

In deep geological repositories, HLW is planned to be encapsulated in metallic containers and surrounded by engineered barriers. In some countries, the DGR may be hosted in crystalline or clay rock and bentonite can be used as backfill material because of low hydraulic conductivity and the ability to strongly sorb many radionuclides [1]. The intrusion of groundwater during the evolution of the repository system will trigger degradation mechanisms that will result in the formation of secondary phases at the water-saturated container/bentonite interface. The nature of the formed secondary phases is highly dependent on the nature of the selected materials and on the prevailing geochemical conditions.

Within a PhD thesis, a spheroidal graphite cast iron (SGI) and a low alloyed fine-grained carbon steel (C-steel) were selected to perform corrosion experiments in contact with MX-80 bentonite saturated by synthetic Grimsel groundwater under anoxic conditions. The C-steel microstructure consists of ferrite (α-Fe) and pearlite (alternating layers of ferrite and cementite (Fe_3C)) regions, while SGI has a pearlite structure with in addition graphite inclusions. The same steels and bentonite have been selected to perform corrosion experiments under *in situ* conditions at the Grimsel Test Site in Switzerland [2]. The goal is to compare results from experiments in the laboratory with that obtained for *in situ* conditions in order to conclude on the transferability of data between laboratory and field conditions. In addition, performing experiments in the laboratory allows investigating the effect of individual parameters (e.g., temperature) on the investigated degradation processes.

Steels were prepared as polished coupons. Separately, bentonite was contacted with the groundwater

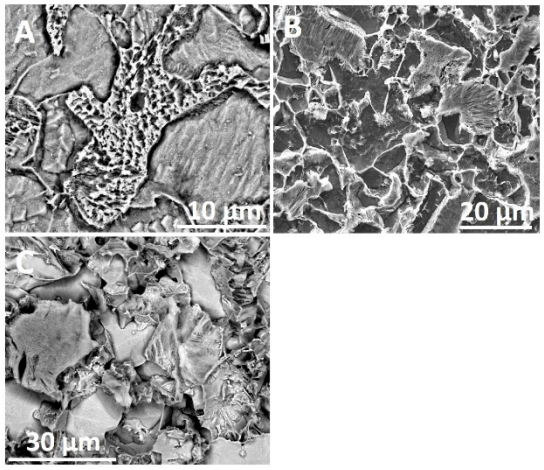

Fig. 1: Scanning electron micrographs of the C-steel corroded for 3 months at 25°C (A), 6 months at 25°C (B) and 3 months at 50°C (C).

and left to equilibrate under anoxic conditions. Coupons were then contacted with the equilibrated bentonite suspension in closed vessels in an Ar-filled glove box.

After 3 months at 25°C, the surface of the C-steel is made of domains or grains of various textures (Fig. 1A). Results from SEM-EDXS analysis rule out any significant difference in chemical composition between the grains, and further indicate a composition close to that of the starting steel. After 6 months, the surface looks rougher with grain boundaries clearly visible and some bentonite aggregates sticking on the surface (Fig. 1B). After 3 months at 50°C, the surface also looks made of grains, with the very occasional exposure of cementite lamellas and presence of some fine grained material at grain boundaries (Fig. 1C). The corrosion rate decreases with exposure time and increases with temperature.

Cementite lamellas are clearly visible at the surface of the SGI coupon corroded for 3 months at 25°C, suggesting a preferential removal of ferrite from the surface (Fig. 2A). Comparable observations can be made for the experiment performed at 50°C, however, with a corrosion damage growing into preferential directions (Fig. 2B). In a parallel experiment at 25°C, hematite was present (0.5 wt. %) during corrosion in order to mimic the presence of oxic corrosion products forming during handling and emplacement of canisters into the repository before conditions turn anoxic (Fig. 2C). The presence of this ferric compound resulted in a higher redox potential (+87±50 mV vs S.H.E) and higher corrosion rate (4.5±0.3 µm/a) compared to the experiment in the absence of hematite (-441±50 mV and 3.4± 0.3 µm/a). It is very likely that hematite absorbs and oxidizes ferrous ions [3] produced upon steel corrosion and thus acts as a redox buffer. The affinity of Fe_2O_3 for dissolved Fe^{2+} ions certainly prevents the formation of a protective passivation layer at the surface of the coupon that thus corrodes faster than in the absence of added hematite. After 6 months at 25°C in the presence of added hematite, the surface damage becomes more pronounced around graphite inclusions (Fig. 2D). A possible explanation would be the spatial separation of anodic and cathodic reactions sustaining the corrosion [4], with effects more pronounced after longer reaction time. Both the presence of hematite and an increase of temperature increase the corrosion rate.

For both steels, most frequently detected secondary phases are iron (hydr)oxides and iron silicates (TO type). Further detail can be found in the PhD thesis [3].

Fate of radionuclides during steel corrosion

The intrusion of groundwater into the repository near-field will result in corrosion and alteration processes at the container/buffer interface. During the long-term evolution of the DGR system, these processes will proceed until a possible container failure and subsequent waste matrix alteration resulting in RN mobilization. It is reasonable to assume that container corrosion and RNs mobilization would then occur concomitantly. Steel corrosion (or iron oxidation) is coupled to water reduction, and these reactions significantly impact the

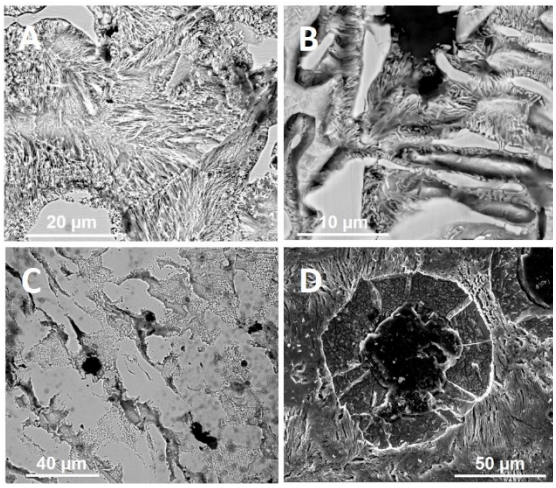

Fig. 2: Scanning electron micrographs of SGI corroded for 3 months at 25°C (A), 3 months at 50°C (B), 3 months at 25°C in the presence of added hematite (C) and 6 months at 25°C in the presence of added hematite (D).

local geochemical conditions. Under these constantly evolving conditions, several mechanisms can contribute to the immobilization of RN in a DGR near-field. To get further insights into these processes, corrosion experiments are being performed in the presence of RNs (or RNs simulants) using the same steels, bentonite and groundwater as in the previous study: SGI or C-steel, MX-80 bentonite and synthetic Grimsel groundwater. Selected RNs are Se(IV), Tc(VII) and U(VI) (or Ni(II), Re(VII) and Lu(III) as simulants). Experiments are performed in gastight containers in an Ar-filled box, at room temperature. A bentonite slurry is first prepared then spiked with the RNs (or simulants) before contacting the metallic coupons. The preparation of parallel experiments allows obtaining information on time dependency of the investigated processes.

For experiments with RN simulants reaction times ranged from 1 month to 1.5 year. For both steels, the *in situ* pH hardly varies with time and is around 8.5, likely buffered by bentonite. In contrast, the redox potential (vs S.H.E) significantly decreased to reach about -250 mV for SGI and -350 mV for the C-steel after 1.5 year. For both steels, the corrosion rate obtained by gravimetric method is around 10 µm/a after 1 months and decreases with increasing time.

SEM-EDXS analyses revealed the presence of Re and Ni at the surface of all coupons, with contents increasing with reaction time. Furthermore, XPS and X-ray absorption spectroscopy indicated the presence of Re(0) at the C-steel surface after 8 months. It is very likely that iron oxidation provided the electrons necessary to reduce perrhenate ions at the steel surface.

For C-steel corroded for 1.5 year, information on the structure of the corrosion layer was obtained by SEM-EDXS analysis of the sample prepared as crosscut. The corrosion layer has a duplex structure made of an inner and an outer corrosion product layer (iCP and oCP, respectively, Fig. 3). The iCP layer is 15-30 µm wide and is mostly made of iron and oxygen, with lower amounts of silicon (2 at. %) suggesting the presence of iron

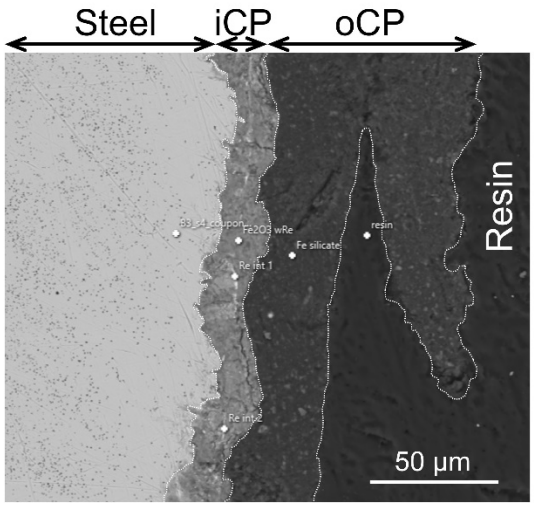

Fig. 3: scanning electron micrograph of the crosscut prepared from C-steel corroded for 1.5 year and embedded in resin

(hydr)oxides in contact with the metal. This layer has cracks and only some of them are filled. A detailed analysis of the filled cracks indicates the presence of Ni (8-15 at. %) and Re (4-8 at. %) in significant amounts as well as lower Ca (2 at. %) contents. Apart from these cracks, the iCP layer contains only trace amounts of Re or Ni, but no Lu could be found in any part of this layer. Findings may suggest that Re and Ni were not taken up during the iCP formation, but rather that the iCP layer formed first and cracks formed subsequently, then water containing Re and Ni entered the cracks.

The iCP layer is covered by a thick (30-80 µm) layer mostly made of iron and silicon with a mole ratio close to 1:1, hinting at the presence of iron silicate (e.g., greenalite). No Re, Ni or Lu could be found associated with this layer.

The composition of the iCP and oCP layers suggest that ferrous ions released upon corrosion precipitated as Fe (hydr)oxide at the steel surface, and that a fraction of Fe ions diffused through this layer to react with Si coming from the contacting bentonite to produce iron silicates. The exact structure of the phases present in the iCP and oCP layers remain to be determined, but based on chemical compositions, results agree with the usually reported corrosion layer structure [4].

Experimental data further suggest that RNs simulants were not incorporated in the structure of the neoformed secondary phases during their formation. RN simulants were added to the bentonite suspension before contacting the coupon. Trivalent elements have high affinity for montmorillonite, which is the main component of the bentonite, implying that Lu(III) must have been taken up quantitatively by the bentonite. The retention of divalent cations by montmorillonite is slightly weaker, while the uptake of anionic species such as Re(VII) by montmorillonite is very weak. These considerations suggest that at the start of the corrosion experiment, the porewater contained no dissolved Lu(III) ions, only low amounts of Ni(II) and nearly all of Re(VII) added to the suspension. This would explain the absence of Lu association with the corrosion products, in contrast to Ni and Re.

Experiments with RNs remain to be opened and analyzed to determine whether these elements are associated with the corrosion products. In these experiments, all RNs were added to the bentonite suspension as anionic species, meaning the largest fraction may remain dissolved in the porewater and thus be available for uptake by the corrosion products. The analysis of the samples will allow determining whether RNs can be immobilized at the canister/bentonite interface during corrosion.

Barite transformation to witherite in presence of carbonate and its impact on radium retention

Ra-226 presence in HLW imposes important considerations in terms of long-term safety aspects for DGRs. Due to its relatively short half-life (1600 years), Ra-226 can attain secular equilibrium relatively rapidly with its long-lived parent nuclide U-238, making it a critical radionuclide. The groundwater intrusion to the DGR near-field and subsequent HLW matrix corrosion can lead to Ra-226 mobilization and migration through different barriers of the DGR. These processes can last for long time spans due to Ra-226 dependency on U-238.

Barium isotopes are present in HLW as decay products of the highly abundant fission products Cs-134 and Cs-137, and can amount to a few kg per HLW package [5]. Ba can also be released upon HLW matrix corrosion and its interaction with dissolved sulfate present in the groundwater can result in the precipitation of barite ($BaSO_4$) [8, 9]. The mobilization of Ba from the corroding HLW matrix is expected to follow that of Ra, implying that Ra-226 released from HLW may to some extent be retained by barite as a $(Ba,Ra)SO_4$ solid solution due to recrystallization processes in barite-saturated pore water [5].

Another scenario that ought to be considered is the consequences of groundwater with high carbonate concentrations and elevated pH. Carbonate is ubiquitous in groundwater [7], whereas pH can be elevated due to alteration of cementitious materials inside a DGR. As a result, it is likely that high carbonate concentration combined with elevated pH alter the chemical behavior of barite particles, either by mixing at the surface, formation of a witherite ($BaCO_3$) layer at the barite surface, or the complete or partial dissolution of barite particles through interface-coupled dissolution–precipitation reactions [8].

The aim of the present study was to investigate the thermodynamics and kinetics of barite transformation into witherite and the subsequent fate of Ra-226 upon such a transformation. Different barite initial materials were used: natural barite, as powders and as 3×3×3 mm cubes, from the Androvo mine in Bulgaria (AR) and from the Western Harz Mountains, Iberg, Germany (IB) with 1.8 ± 0.36 at. % Sr; one commercial high purity barite powder from Sachtleben (SL); Ra-226 doped

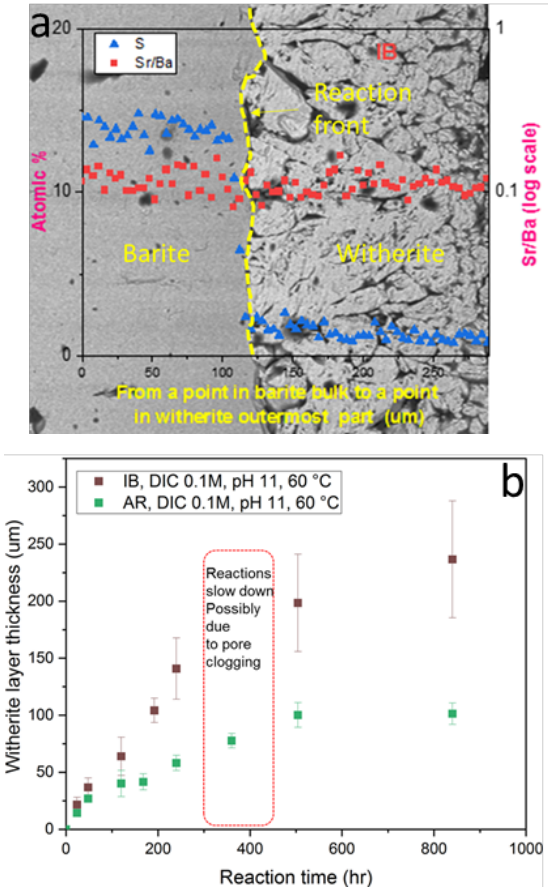

Fig. 4: (a) IB witherite porous layer formed at reaction front. Sharp S drop at the interface indicates two phases of different compositions. Though Sr tends to partition preferably in $BaCO_3$ [9], Sr/Ba ratio is constant demonstrating that Ba is consumed in witherite likely due to uptake kinetics ruling over partitioning thermodynamics. (b) Rapid reaction rates followed by a slowdown, which affects IB less than AR.

barite (RSL) from [6]. Cubes and powders were pre-equilibrated with NaCl and then contacted with carbonate solutions (1-100 mM, pH 9.50-11).

Cubes reacted with carbonate solutions and formed porous witherite layers only with 100mM Na_2CO_3, pH 11 and at 60 °C (Fig. 4). The formation rate of both cube types was rapid at early stages then slowed down, with IB cubes reacting faster that AR. Slowing down of the reaction is likely due to increasing diffusion length through the porous witherite layer, which forms at the barite surface. Additionally, subsequent clogging of initial pores in the witherite layer is indicated, and may for AR cubes lead to a complete passivation of the surface.

All barite powders formed hexagonal witherite particles after reacting with carbonate at 25 °C (Figure 5) at high carbonate concentration (0.1M) and high pH (11). SL and IB show a considerably faster transformation than AR (Fig. 5). Though SL witherite formation decreased with the decrease of carbonate concentration and pH, it was higher than AR and IB, which showed rather low transformation rates at carbonate concentration 0.01M – 0.05M and pH 9.50 (not shown).

RSL powders were contacted with carbonate at high carbonate concentration (0.1M) and pH (11), however, no witherite formation was observed. One possible explanation is that RSL reactivity is rather low since this barite powder has been pre-equilibrated + equilibrated with Ra-226 for 9 years [9, 13] prior to the present experiments. This seems to confirm the hypotheses that high energy sites on the barite crystals, like attached fine crystal grains, nano- and micro pore structures [10] or high energy surfaces (e.g. on cut crystals) are a prerequisite for effective recrystallization reactions even if the solution provides a significant chemical driving force (high carbonate concentration and pH).

The interplay of growth inhibition and incorporation of impurity ions – a mechanistic approach to describe interactions of SeO_3^{2-} with calcite

Understanding the interaction between SeO_3^{2-} and calcite is of great importance in the context of nuclear waste disposal, specifically for the retention of radioactive Se isotopes in potential repositories. If respective partitioning coefficients suggested in the published literature (D = 0.02 [11]) can be applied to real word scenarios, solid solution formation bears a great potential for the sequestration of radioactive Se(IV) isotopes, but if not, sequestration may be greatly overestimated.

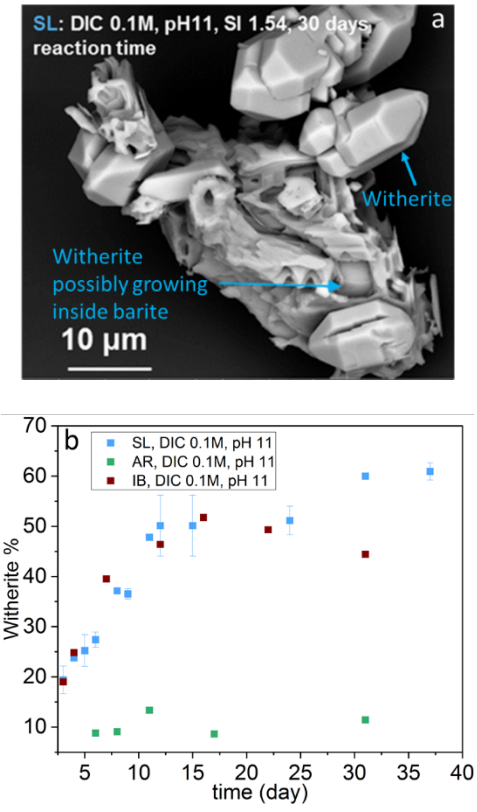

Fig. 5: (a) SL barite shows non-uniform surfaces, since witherite grows inside openings resulting from dissolution of small inter-grown particles (b) SL and IB recrystallize relatively fast. Similar as in the cube experiments, AR exhibits the lowest reactivity.

For Se(IV), which is not well compatible with the calcite structure though it matches with the stoichiometry of carbonate (SeO_3^{2-} vs. CO_3^{2-}), this partitioning coefficient is only applicable and relevant if calcite grows at sufficiently high supersaturation. This study uses the entrapment model to describe the SeO_3^{2-} uptake into calcite. The entrapment model predicts a high dependency of the SeO_3^{2-} uptake on the supersaturation with regards to calcite, present in the contact solution. Past studies [12] have shown that the SeO_3^{2-} moiety is significantly more stable in the relaxed surface monolayer compared to the bulk calcite crystal. In the literature, log K_{SP} values of -6.7 and 0.5 have been suggested as hypothetical $CaSeO_3$ endmember solubilities for a thermodynamic description of the surface solid solution and the bulk solid solution, respectively. Based on the theoretical supersaturation (Eq. 1) of different solid solution compositions, a first assumption for the precipitating solid solution composition from a solution with given $[Ca^{2+}]$, $[CO_3^{2-}]$ and $[SeO_3^{2-}]$ activities can be made.

$$\boldsymbol{\sigma_{solid-sol.}} = \frac{a(Ca^{2+}) * a(CO_3^{2-})^{(1-X)} * a(Se0_3^{2-})^{(X)}}{(K_{SP}(Calcite) * (1-X))^{(1-X)} (K_{SP}(CaSeO_3) * (X))^{(X)}} \quad (1)$$

Calculated or measured Ca^{2+} and CO_3^{2-} activities can be used to produce a supersaturation curve with the mole fraction of Se in the surface solid solution as abscissa for a given SeO_3^{2-} activity. The most highly supersaturated solid solution serves as an average assumption for the actual precipitate and coincides with the equilibrium composition of the solid solution. In this study Ca^{2+} and CO_3^{2-} activities were assumed to be consistent with an equilibrium towards aragonite. Batch recrystallization experiments at different Se concentrations were conducted in order to study the entrapment process in detail. Aragonite was chosen as reactant since its dissolution provides a constant and well-defined supersaturation with respect to calcite (SI(Cc) = 0.14). An energy balance between the Gibbs free energy required for the entrapment of one mol of the respective solid solution of composition X ($X_{Se/ca} * (41 \pm 8 \frac{kJ}{mol})$ [11]) and the Gibbs free energy provided by the supersaturation ($|\Delta G_{\text{supersaturation}}| = |RT \ln(\boldsymbol{\sigma})|$) can be used to determine at which conditions the entrapment will take place. The critical solid solution composition for which entrapment is expected, can be visualized if the energy balance equation is solved for the mole fraction $X_{Se/ca}$ (Fig. 6).

Aforementioned thermodynamic considerations suggest that a stable surface solid solution in equilibrium with SeO_3^{2-}-containing solutions can be entrapped (at an SI of 0.14) until SeO_3^{2-} concentrations reach ~50-60 µmol/L. The SeO_3^{2-} activity and respective solid solution composition for given samples can be used to test the entrapment model. A stagnation of the SeO_3^{2-} uptake by calcite above 50 µmol/L SeO_3^{2-} was observed, which is in good agreement with the entrapment model proposed in the literature [11]. We propose a refinement of the incorporation threshold proposed in the literature [11] (red error band vs grey error band). From

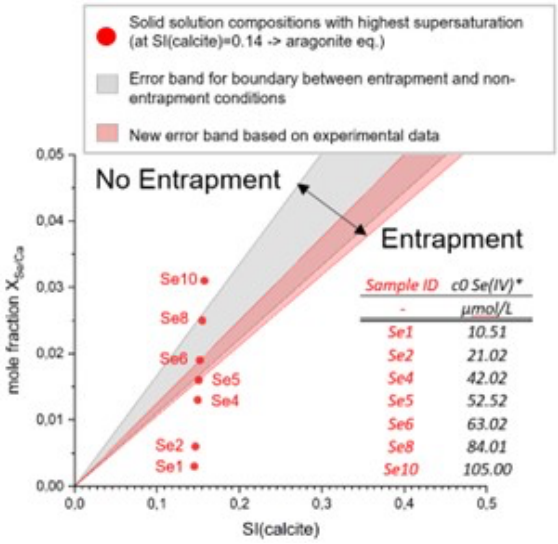

Fig. 6: Entrapment threshold (grey band) based on an energy balance between the Gibbs free energy required for entrapment and the Gibbs free energy provided by the supersaturation. Samples from batch recrystallization experiments investigated in this study were grown at a constant SI of 0.14, but with differing Se concentration and are thus arranged in an approximately vertical line (cf. Eq.1). Their stoichiometric composition can be calculated from the respective D (using $C_0(SeO_3^{2-})$) [11]. The red error band is based on the highest SeO_3^{2-} concentration at which uptake (and thus the entrapment process) was observed (50 µmol/L). No uptake into calcite was observed at 60 µmol/L (upper limit).

a thermodynamic perspective, systems that are close to the concentration limit for the entrapment effect should bear the highest potential for SeO_3^{2-} sequestration. However, this potential is limited by a kinetic growth inhibition effect (and therefore limited calcite precipitation) caused by the presence of SeO_3^{2-}. Our observations indicate that a high SeO_3^{2-} mole fraction within the surface solid solution leads to a significant decrease in growth rates.

LA-ICP-MS mappings (Fig. 7) of Se in calcite (from batch recrystallization experiment Se2, Fig. 6) show a heterogeneous SeO_3^{2-} distribution within the produced calcites, which is consistent with inter-sectoral zoning

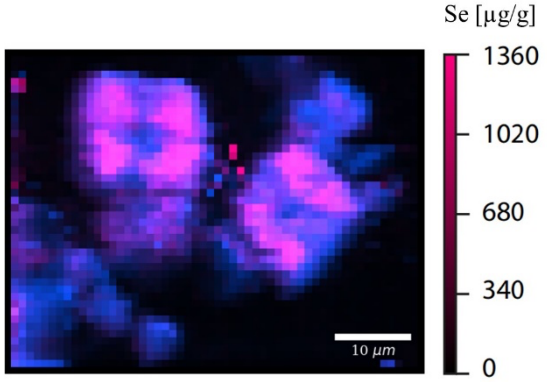

Fig. 7: Composite image of calcite grown at 20 µmol/L *SeO_3^{2-} and mapped for Ca (blue) and Se (magenta) using LA-ICP-MS. Ca is used to identify the outlines of calcite and aragonite crystals. This Ca mapping is overlaid by a Se mapping. Selenium is heterogeneously distributed within different growth sectors of the (104) surface.*

caused by preferred incorporation at facets of growth hillocks at the calcite (104) surface made up by acute edges.

Acknowledgements*. The work presented in this chapter received partial financial support by the German Federal Ministry for the Environment, Nature Conservation, Nuclear Safety and Consumer Protection (02E11981B) and the European Union's Horizon 2020 research and innovation program 2014-2018 under grant agreement N°847593 (EURAD-ConCorD). The acknowledgment extends to King Abdulaziz City for Science and Technology (KACST), funding M. Alzaydan's PhD work, and to the German federal ministry for education and research (BMBF) for funding through the collaborative project (KRIMI), grant agreement 02NUK056A.*

References

[1] Gates, W. et al., *Elements*, 5, 105-110 (2009).
[2] Reddy, B et al., *Mater. Corros.*, 72, 361-382 (2020).
[3] Singh, A. R. *Metallic corrosion at the steel/bentonite interface under anoxic and water saturated conditions.* KIT, Germany (2025). DOI: 10.5445/IR/1000184722
[4] Schlegel, M.L., et al., *Corros. Sci.*, 109,126-144 (2016).
[5] Curti, E., et al., *Geochim. Cosmochim. Acta,* 74, (12), 3553-3570 (2010).
[6] Heberling, F. et al., *Geochim. Cosmochim. Acta*, 232, 124-139 (2018).
[7] Stober, Ingrid., *Geothermal Energy,2, (1), 978-3* (2014).
[8] Putnis, A. and Putnis C.V., *J. Solid State Chem.*, 180, 1783-1786 (2007).
[9] Prieto, M., et al., *Geochim. Cosmochim. Acta* 61. (16), 3383-3397 (1997).
[10] Weber, J., et al., *Chem. Geol.* 466: 722-732, (2017)
[11] Heberling, F., et al. *Geochim. Cosmochim. Acta*, 134, 16-38., (2014)
[12] Polly, R., et al. *J. Phys. Chem. C* 121.37, 20217-20228. (2017)

5 Applied studies: radioactive waste behavior and radionuclide retention in the multi-barrier system

Long-term safety of a deep geological repository for nuclear waste depends on a multi-barrier system which consists of technical and geo-technical barriers such as the waste form, the canister, backfilling and sealing of the mined openings as well as on the natural barrier function of the host rock. Currently, a series of studies on various subsystems with respect to potential multi-barrier systems in argillaceous or crystalline host-rocks are performed. These experimental studies cover a variety of components of the multi-barrier systems such as spent nuclear fuel as waste form, bentonite as geo-engineered barrier material and the interface between an iron-based canister and bentonite. Experiments are conducted on migration of radionuclides at a generic near-field/geosphere interface consisting bentonite and granitic rock as well as on radionuclide diffusion in Jurassic clay stone (i.e. Opalinus Clay, Switzerland). Moreover, the distribution of natural organic matter in Oligocene clay (i.e. Boom Clay, Belgium) are analyzed. In the context of dry interim storage of spent nuclear fuel in surface facilities, the integrity of the cladding of fuel rods as technical barrier is investigated. Our investigations deal with the role of zirconium hydrides, which form in within the claddings as a result of hydrogen absorption during reactor operation and hydride precipitation during cooling after irradiation. Moreover, the role of halogenide-bearing precipitates that form at fuel pellet / cladding interfaces are studied. Radiation research at KIT-INE focuses on the assessment of radiation exposure by estimating doses from external radiation fields and on the effects of ionizing radiation on materials. The research is based on recording and evaluation of radiation exposure from radiation sources. Current experimental and numerical studies deal with age determination curves of Cf-sources and improving dosimetry assessments in the context of occupational radiation protection.

5.1 Highly radioactive waste forms

M. Herm, T. König, Y. Lin, A. Walschburger, M. Böttle, R. Dagan, K. Dardenne, M. Fuss, V. Metz, T. Pruessmann, J. Rothe, D. Schild

Investigations related to cladding integrity during prolonged dry interim storage

Introduction

As interim storage durations for spent nuclear fuel (SNF) are expected to extend well beyond originally licensed periods, potentially up to 100 years, it is essential to assess the structural integrity of fuel rod cladding over such timescales to ensure safety during storage, handling, and transport.

As the first barrier against the release of radionuclides, the mechanical properties of Zircaloy-4 cladding may evolve as a result of manufacturing history, hydrogen uptake, and irradiation effects. Moreover, accumulation of cladding degrading elements, such as chlorine, iodine and tellurium, present in fuel-cladding interface layers of irradiated UO_X and MOX fuels could potentially lead to stress corrosion cracking of the cladding.

Understanding how these factors influence cladding behavior at the microstructural level is crucial for reliable safety assessments of long-term dry storage of SNF. Accordingly, the main objective of this work is to systematically study these effects.

To this end, mechanical (nanoindentation) and crystallographic (EBSD) characterization methodologies are being developed and validated using non-irradiated model materials, with the goal of applying the refined approaches to irradiated Zircaloy cladding from medium- and high-burnup spent fuel currently stored in the shielded box line (ABL) of INE.

Additionally, spectroscopic investigations of the fuel-cladding interfaces of irradiated UO_X and MOX fuels for possible cladding degrading elements, such as chlorine, iodine and tellurium was performed to scrutinize the composition and individual elemental speciation of the fuel cladding interfaces, X-ray absorption spectroscopy (XAS) at the KIT Light Source was utilized. The outcomes of this study aim to reduce uncertainties on chemically assisted degradation processes in irradiated SNF rods.

Materials and irradiation history

The investigated fuel and cladding specimens were sampled from high burn-up UO_X (50.4 GWd/t_{HM}) and MOX (38.0 GWd/t_{HM}) fuel rod segments, both in ownership of KIT-INE. Both fuel types were irradiated during the 1980s in commercial pressurized water reactors (PWR) in Switzerland and Germany, respectively.

Experimental and analytical methods

UO_X and MOX specimens were cut from the respective fuel rod segment in the ABL by use of a diamond wavering blade (IsoMet, 15LC, Buehler Ltd.) mounted on a low-speed saw (IsoMet, 11-1180, Buehler Ltd.). From each fuel rod segment, an approximately 2 mm thick disk was cut and subsequently defueled with a punch, in order to obtain fuel fragments and cladding specimens. The cutting and defueling process is shown in Figure 1.

Thereafter, respective cladding and fuel specimens were removed from the ABL and transferred into a ventilated fume hood for further preparation.

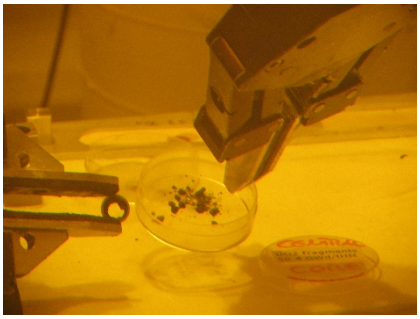

Fig. 1: Defueling process of the SNF specimens.

For mechanical investigations the samples were grinded, polished or electropolished using various grit sizes and suspensions.

Thereafter, respective cladding and fuel specimens were removed from the ABL and transferred into a ventilated fume hood for further preparation.

For mechanical investigations the samples were grinded, polished or electropolished using various grit sizes and suspensions.

For Cl-K (2822 keV) and I-K edge (33169 keV) XAS measurements, cladding and fuel specimen of both fuel types were mounted on aluminum sample holders with circular immersions. Each sample holder was then sealed with a double layer of 8 µm polyimide foil (KAPTON®, DuPont, USA) in order to obtain a double-sealed containment. Subsequent to the sample preparation, the specimens were sent to the INE and CAT/ACT beamlines at the KIT Light source for analysis. Data treatment for XAS measurements was performed using the Demeter IFEFITT program pack as well as PyMCA software package [1,2].

Results and discussion

Zircaloy-4 exhibits pronounced microstructural heterogeneity driven primarily by tube fabrication processes and hydrogen content. EBSD inverse pole figure maps show wide variations in grain size and deformation features associated with its manufacturing procedures (see Figure 2). These features provide a necessary baseline for distinguishing hydrogen- and irradiation-induced effects. In hydrogenated Zircaloy-4, hydrogen further introduces localized regions of increased lattice curvature and geometrically necessary dislocations near

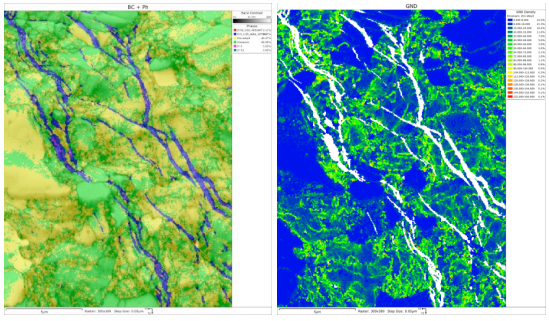

Fig. 2: Phase and band contrast (left) and Geometrically Necessary Dislocation (GND) map (right) of hydrogenated Zircaloy-4 (300 ppm H).

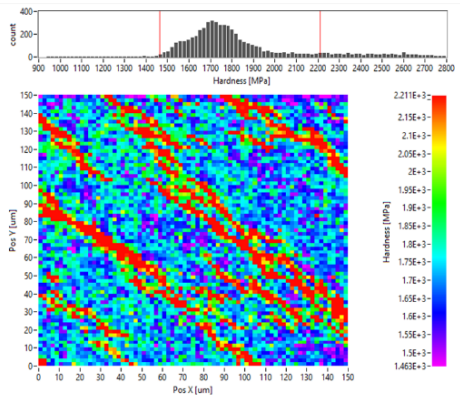

Fig. 3: Hardness Intensity Map of Hydrogenated Zircaloy-4 Cladding (300 ppm H).

hydride packets, consistent with strain accommodation arising from hydride–matrix misfit.

Nanoindentation measurements indicate clear local variations in hardness across the cladding, with clustered regions of elevated hardness observed in hydrogenated samples (Figure 3).

Data-driven clustering methods were successfully applied to separate the mechanical response of the zirconium matrix from that of hydride regions, enabling a more quantitative comparison than traditional mapping approaches (Figure 4). The results show that hydrides exhibit systematically higher hardness than the surrounding matrix, while the overall deformation state of the cladding remains largely governed by manufacturing-related features.

XAS was used to examine specimens of the irradiated SNF and SNF-Zircaloy cladding interfaces of UOx and MOX fuel rod segments irradiated in the Gösgen and Obrigheim nuclear power plants. Iodines K-edge spectra of theses specimens and several reference compounds were analyzed. As predicted by Cubicciotti and Sanecki as well as Yaggee, Mattas and Neimark, it is conceivable, that the iodine species formed within the irradiated fuel as well as at the fuel-cladding interface resembles precipitated CsI [3,4]. CsI is expected to accumulate in the colder, cladding adherent region of the SNF due to a vapor transport process of cesium and iodine along its thermal gradient during irradiation. Yet, as stated by Burns et al. and summarized by Sidky, the prevailing oxygen potential within the fuel-cladding

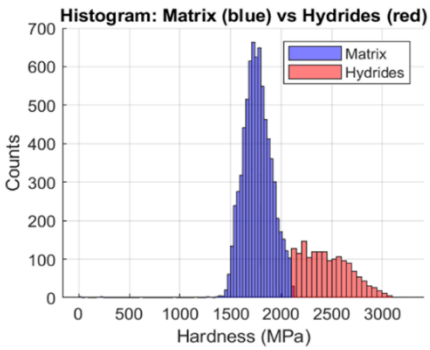

Fig. 4: Hardness distribution of Zircaloy-4 matrix and hydrides derived from nanoindentation.

interface is not sufficient to indicate a stress-corrosion cracking process of CsI due to its chemical stability, i.e., the required $p(I_2)$ to enable reactions with the Zircaloy cladding is not reached [5,6]. However, regarding the immense local radiation field within the SNF pellet, a radiolytical dissociation of CsI and thus the build-up of sufficient $p(I_2)$ could be conceivable [7].

Chlorine K-edge spectra for the fuel and fuel-cladding interface specimens are compared to those of a sample of unirradiated reactor grade Zircaloy-4 as well as a CsCl reference compound. In comparison to the unirradiated Zircaloy specimen as well as the CsCl reference, the irradiated samples exhibit less features after the white line, which might be the result of the strong (re)absorption in the UO_2 matrix or due to the formation of another chlorine compound during the irradiation of the fuel. Furthermore, an elevated amount of ruthenium was detected within the MOX specimen, resulting in the intense L3 peak next to the K-edge chlorine peaks. Two explanations for this feature are conceivable: For once, Pu-239 has a higher fission yield for the respective ruthenium isotopes in comparison to U-235 and secondly, the analyzed MOX specimen contained a higher quantity of noble metal bearing ε-particles (Mo, Tc, Ru, Rh, Pd containing alloys) present on the measured areas.

Experimental investigation on the dissolution of spent nuclear fuel samples and consecutive radionuclide release in high pH solution under anoxic / reducing atmosphere

Introduction

Within the assessment period of one million years, the safety assessments for deep geological repositories consider the access of water and, subsequently, the failure of the emplaced canisters in conjunction with the loss of cladding integrity of the SNF. Therefore, a thorough process understanding of the chemical interactions between intruded aqueous solution and the waste form, the SNF dissolution rate, as well as the quantification of the radionuclide release from the SNF matrix is of utter importance to scrutinize the performance of the highly radioactive wastes in the reducing environment of an underground repository.

This study aims at the characterization and quantification of the chemical durability and radionuclide release behavior of spent, medium and high burn-up UO_X fuel within the context of a deep geological repository in argillaceous host rock. In the event of groundwater intrusion to the emplaced waste structure and prior water saturation of the surrounding engineered barriers, the initial pore water composition will be altered due to interaction with e.g., concrete buffer material in the repository system. As a consequence, the altered groundwater solution will shift to higher pH regions in its early stages (> 12) and be comprised of highly alkaline NaOH, KOH and $Ca(OH)_2$ as main components. Thereby, the SNF will encounter a highly alkaline cement water solution. In order to scrutinise the behavior of spent UO_X fuel upon contact with the alkaline solution, six long-term autoclave leaching experiments for up to 1400 days are currently performed within this work.

Materials and irradiation history

All SNF specimens utilized in this work were approximately 23 mm long segments, cut by tube cutter to maintain the natural pathways for radionuclides. Four of the SNF specimens were sampled from a fuel rod which was irradiated in the PWR Gösgen (KKG, Switzerland) to an average burn-up of 50.4 GWd/t_{HM} for 1226 consecutive full power days in four cycles. A fission gas release of (8.4 ± 0.9) % was determined by dividing the measured amount of fission gases derived from a puncturing test by the total fission gas inventory of the fuel.

Furthermore, two SNF specimens of a medium burn-up fuel rod were prepared. The fuel rod was utilized in the PWR Biblis-A (KWB, Germany), reaching an average burn-up of 46.9 GWd/t_{HM} during its 1554 full power days in five cycles with an approximate fission gas release of 2 %.

Experimental procedure

All experiments are conducted in poly ether-ether ketone (PEEK)-lined stainless-steel autoclaves (Berghof Products + Instruments, Eningen, Germany). The autoclaves have a capacity of 250 mL and are equipped with three valves in the lid to allow the sampling of gaseous and liquid aliquots. In addition, six sample holders were manufactured out of PEEK to ensure the contact of both pellet surfaces with the solution at any time. As leachant, a young cement water with calcium (YCWCa) with a pH of 13.7±0.3 is used. All autoclaves are pressurized to 40 bar with either pure argon gas (anoxic conditions) or a Ar/H_2 mixture (reducing conditions) with a $p(H_2)$ of 0.3 bar. The denotation of each autoclave experiment, i.e., the four experiments utilizing the high burn-up (HBU) KKG fuel as well as two experiments with medium burn-up (MBU) KWB fuel, is given in Tab. 1.

Throughout the experimental duration, periodical samplings of gaseous and aqueous phase were performed to determine the amount of released fission gases (i.e., Xe, Kr) as well as radionuclide concentration (e.g., Sr-90, I-129, Cs-137, U-238, Pu-239) in solution.

Table 1: Denotation of the autoclave experiments (HBU: High burn-up UOX; MBU: Medium burn-up UOX).

Experiment	HBU-red-A	HBU-red-B	HBU-anox-A	HBU-anox-B	MBU-red	MBU-anox
Fuel	KKG	KKG	KKG	KKG	KWB	KWB
Atmosphere	Ar/H_2	Ar/H_2	Ar	Ar	Ar/H_2	Ar

Results and discussion

To evaluate the fraction of safety relevant radionuclides released into the aqueous phase throughout the leaching experiments, an attempt is made to correlate them with the fraction of fission gas inventory in the head space of the autoclaves. The fraction of ^{129}I or ^{137}Cs released upon fuel rod failure in a repository is often correlated with the fission gas release determined upon puncturing of the respective fuel rod. In previous leaching experiments performed with various fuels, e.g., the European Commission projects FIRST-Nuclides project and DISCO, it was indicated, that this correlation is often biased depending on the fuel type and irradiation conditions. However, with the accessibility of fission gas release data throughout leaching of a SNF specimen, a direct correlation of released fractions during the autoclave experiments is possible. A compilation of the cumulative released inventory fractions into the aqueous phase (CumFIAP) of I-129 and Cs-137 in comparison to the cumulative amount of fission gases released (CumFIGP) is shown in Figure 5.

For the duplicate experiments HBU-red-A as well as HBU-red-B, performed under reducing conditions, the cumulative fraction of ^{129}I approaches the cumulative fraction of fission gases released during the leaching experiments after approximately 100 days. At the end of the experiments after approximately 320 days, both released fractions are comparable with each other, i.e., CumFIGP (Xe+Kr) amounts to 17 % for HBU-red-A and 19 % for HBU-red-B in comparison to the CumFIAP (^{129}I) of 17 % for HBU-red-A and 15 % for HBU-red-B. The obtained cumulative values demonstrate the good reproducibility of the leaching experiments within a comprehensive experimental uncertainty of ± 1 % for both the fission gases (in CumFIGP (Xe+Kr) units) and for ^{129}I (in CumFIAP (^{129}I) units). For the cumulative fraction of ^{137}Cs released into the aqueous phase, a lower release is observed when comparing it to the released fraction of fission gases (Xe+Kr). For ^{137}Cs, a CumFIAP of 8 % for HBU-red-A and 7 % for HBU-red-B were determined which would correlate to half of the fission gas fraction released during leaching. Again, the obtained cumulative values demonstrate the good reproducibility of the leaching experiments within a comprehensive experimental uncertainty of ± 1 % for ^{137}Cs (in CumFIAP (^{137}Cs) units.

In the duplicate experiments performed under anoxic conditions, HBU-anox-A as well as HBU-anox-B, a to some extent similar behaviour can be observed when comparing the CumFIGP (Xe+Kr) with the CumFIAP of ^{129}I. However, it should be mentioned, that some data points for ^{129}I were below detection limit, therefore the data should be treated with a larger uncertainty. It is shown, that the CumFIAP (^{129}I) approaches the CumFIGP (Xe+Kr) with proceeding time for experiment HBU-anox-A eventually amounting to 13 % of ^{129}I in the aqueous phase as well as 14 % of Xe+Kr in the gas phase after about 320 days of leaching. For experiment HBU-anox-B, two concentration values for ^{129}I were below detection limit, resulting in a data gap. Thus the derived CumFIAP (^{129}I) is lower than the CumFIGP (Xe+Kr) with values of 7 % for ^{129}I (with a quite small number of experimental data) and 14 % for the fission gases. For the comparison of the CumFIGP (Xe+Kr) to the cumulative fraction of ^{137}Cs in the aqueous phase of the anoxic duplicate experiments HBU-anox-A as well as HBU-anox-B, a similar observation to the experiments under reducing conditions can be made. Both CumFIAP (^{137}Cs) values correlate about half of the cumulative fraction of fission gases released during leaching.

Similar to experiment HBU-anox-B, concentration values for ^{129}I determined in experiment MBU-red were largely below detection limit thus subsequently biasing the CumFIAP (^{129}I). The correlation between cumulative released fission gas fraction with the ^{129}I fraction equals to about a third, i.e., significantly lower in comparison to the Gösgen fuel experiments. For the anoxic experiment using the Biblis-A fuel, MBU-anox, all ^{129}I concentrations were below detection limit and therefore no conclusions can be drawn. For both experiments utilizing the MBU fuel, ^{137}Cs could be determined and for both MBU fuel experiments, the aqueous fraction of ^{137}Cs inventory corresponds to about one third of the respective released fission gas release fraction, i.e., a significant lower ratio is observed when comparing it to the HBU experiments.

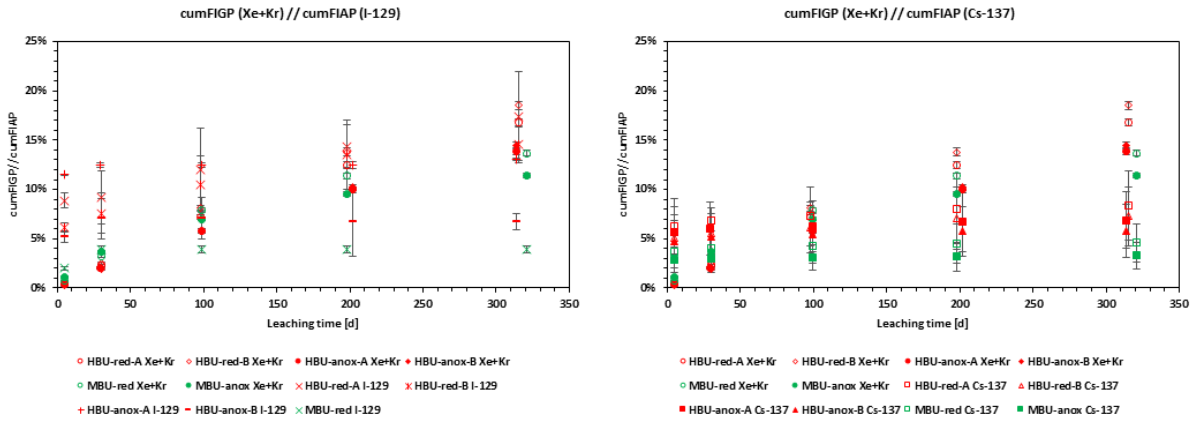

Fig. 5: Comparison of CumFIGP with CumFIAP of I-129 and Cs-137 for all autoclave leaching experiments.

Acknowledgements

The authors greatly acknowledge the funding from the Federal Ministry of Environment, Climate Action, Nature Conversation and Nuclear Safety (FKZ 1501645), the Belgian waste management organization (ONDRAF/NIRAS), as well as the European Union's Horizon 2020 research and innovation program under grant agreement N°847593. Furthermore, we would like to thank M. Große and M. Steinbrück (both KIT-IAM) for the provisioning of reactor-grade Zircaloy for XAS measurements.

References

[1] B. Ravel, M. Newville, ATHENA, ARTEMIS, HEPHAESTUS: data analysis for X-ray absorption spectroscopy IFEFFIT, J Synchrotron Radiat 12 (2005) 537–541. https://doi.org/10.1107/S0909049505012719.

[2] V.A. Solé, E. Papillon, M. Cotte, P. Walter, J. Susini, A multiplatform code for the analysis of energy-dispersive X-ray fluorescence spectra, Spectrochim Acta Part B At Spectrosc 62 (2007) 63–68. https://doi.org/10.1016/j.sab.2006.12.002.

[3] F.L. Yaggee, R.F. Mattas, L.A. Neimark, Characterization of Irradiated Zircaloys: Susceptibility to Stress Corrosion Cracking, NP-1557, 1980.

[4] D. Cubicciotti, J.E. Sanecki, Characterization of deposits on inside surfaces of LWR cladding, Journal of Nuclear Materials 78 (1978) 96–111. https://doi.org/10.1016/0022-3115(78)90508-1.

[5] P.S. Sidky, Iodine stress corrosion cracking of Zircaloy reactor cladding: Iodine chemistry (a review), Journal of Nuclear Materials 256 (1998) 1–17. https://doi.org/10.1016/S0022-3115(98)00044-0.

[6] R.G.J. Ball, W.G. Burns, J. Henshaw, M.A. Mignanelli, P.E. Potter, The chemical constitution of the fuel-clad gap in oxide fuel pins for nuclear reactors, Journal of Nuclear Materials 167 (1989) 191–204. https://doi.org/10.1016/0022-3115(89)90442-X.

[7] D. Cubicciotti, J.H. Davies, The Release of Iodine from Iodide Salts by Gamma Radiolysis, Nuclear Science and Engineering 60 (1976) 314–319.

5.2 Geo-engineered barrier material

C. Beiser, M. Bouby, Z. Chen, A. Fried, F. Geyer, Y. Kouhail, S. Kraft, S. Kuschel, V. Metz, S. Moisei-Rabung, M. Plaschke, F. Quinto, A. Shelyug, H. Geckeis.

In co-operation with:

T. Schäfer[a]
[a] *Institute of Geosciences, Applied Geology, Friedrich-Schiller-Universität Jena, Germany*
I. Blechschmidt[b], *A. Martin*[b] *R. Schneeberger*[b]
[b] *NAGRA National Cooperative for the Disposal of Radioactive Waste, Wettingen, Switzerland*
U. Noseck[c]
[c] *Gesellschaft für Anlagen- und Reaktorsicherheit (GRS) GmbH, Braunschweig, Germany*

Introduction

Bentonite is planned to be used as an engineered barrier for deep geological disposals of high-level radioactive waste in crystalline rocks [1]. Steel canisters containing the spent fuels rods will be emplaced in the crystalline host rock with bentonite surrounding the canisters as a backfill material. In some scenarios of long-term safety analyses intrusion of glacial melt water through fractures in the crystalline host rock is considered. Such an intrusion of low-mineralized water would lead to the swelling and the erosion of the bentonite, with consecutive formation of bentonite colloids that could act as carrier for radionuclides (RN) in case they would have been released from the waste product. Thus, laboratory and in-situ experiments are of paramount importance to understand the bentonite erosion processes in order to properly assess its long-term barrier function.

The present experiments are performed in the framework of the BMUKN funded project EVIDENT (duration 2023-2026), and is related to the international Colloid Formation and Migration (CFM) project performed at the Grimsel Test Site (GTS) [www.grimsel.com]. These activities are conducted with the support and in close collaboration with NAGRA, the Swiss nuclear waste management agency. GTS is NAGRA´s generic underground research laboratory located within the crystalline Aar Massif in Switzerland. It provides unique location and infrastructures for the study of physicochemical processes that are expected to influence the performance of bentonite engineered barrier systems and the migration of RNs in fractured crystalline host rock.

At the GTS, the Long-term In-situ Test (LIT), was dedicated to the diffusion of RNs through compacted bentonite and the release of bentonite colloids into a region of fractured granodiorite rock over a 4.5-year time period. In this way, LIT represents a complex and holistic approach to the study of the performances of the multi-barrier system in deep geological disposal. While the in-situ erosion of the LIT compacted bentonite was investigated by our EVIDENT partner, the Institute of Geosciences at the Friedrich-Schiller Universität Jena, in this chapter, we report on the progress in the post-mortem analysis of the LIT and an analogous laboratory experiment carried out at INE, the so-called mock-up test [2].

Concerning laboratory investigations, former experiments with the GMZ bentonite (Gao-Miao-Zi, Inner Mongolia, China) – which is discussed for Chinese disposal concepts – were performed in the framework of the BMWi/BMWK project "ELF-China-Pilot" [3]. New laboratory investigations are presented following our previous work at KIT-INE with the Volclay® MX80 bentonite (Wyoming, USA) [4].

RN diffusion through the LIT and corresponding mock-up test

LIT consisted of compacted FEBEX bentonite rings and compacted Zn-labelled montmorillonite rings in which 16 glass vials containing a bentonite slurry mixed with a RN tracer cocktail (including ^{99}Tc, ^{233}U, ^{237}Np, ^{242}Pu and ^{241}Am) were emplaced. Such a bentonite source was installed in a water conducting fracture at the GTS [2,5]. The analogous mock-up test consisted of a ring of the same compacted bentonite emplaced between two Plexiglas plates spaced by a 1 mm height aperture to simulate a parallel fracture and containing 3 vials with the RN tracer cocktail vials and an inactive one. A Grimsel groundwater flow equal to ca. 44 µL/min and similar to that of the LIT was established through the mock-up for ca. 5 years [2,5].

In order to investigate the diffusion profiles of RNs tracers through the bentonite of the mock-up test and LIT, segments of bentonite adjacent to chosen tracer vial were collected and embedded in Epofix® resin, then thin layers of bentonite (20 to 100 µm thick) were obtained via abrasive peeling starting from the extremity at ca. 2 cm distance from the vial (distal extremity).

A selected group of samples representative for the entire segments was then submitted to analysis. After desorption of the RNs from the bentonite samples, the concentration of the actinide tracers was analyzed by SF-ICP-MS.

Fig. 1 a) and b) represent the concentration of ^{237}Np and ^{233}U in bentonite samples from the mock-up test adjacent to a tracer vial that broke down during bentonite expansion. These values range between 1 and 10 ng/g and 0.1 and 1.2 ng/g, respectively and the concentration profiles appear to be constant within the experimental scattering of the data, except for one sample corresponding to a distance of ca. 430 µm that reaches levels of 318 and 43 ng/g for ^{237}Np and ^{233}U, respectively (indicated in Fig. 1 a) and b) with a green

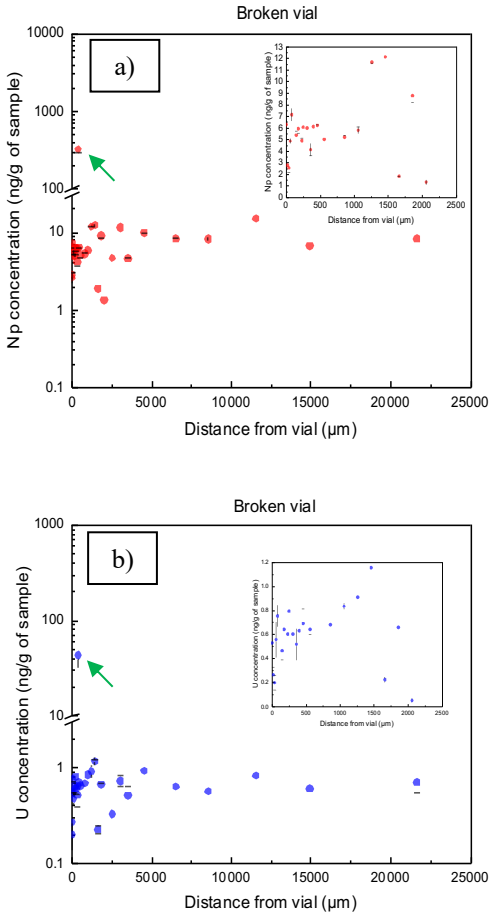

Fig. 1: *a) ^{237}Np and b) ^{233}U concentration profile in a bentonite sample of the mock-up test adjacent to a broken tracer vial (log scale) for a distance up to 25 000 µm from the vial. In each plot the insert shows a zoom of the ^{237}Np and ^{233}U concentration profiles (linear scale) until 2500 µm, see text.*

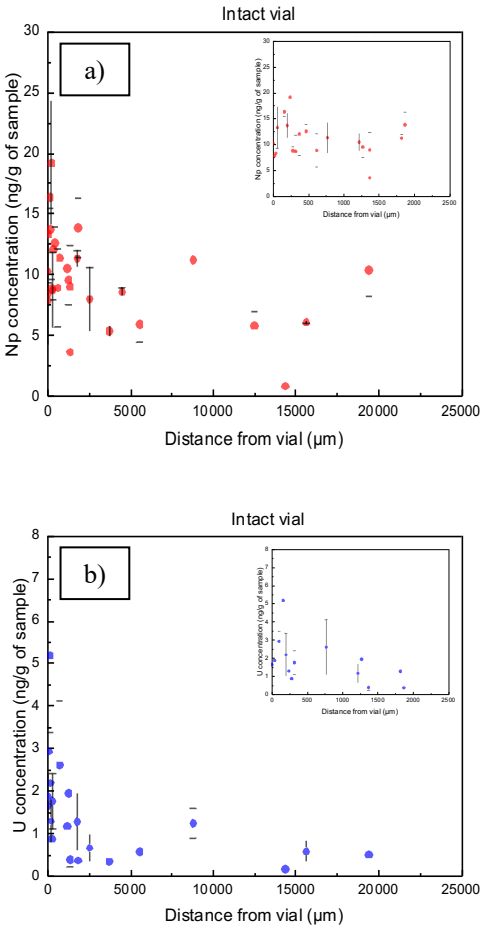

Fig. 2: *a) ^{237}Np and b) ^{233}U concentration profile in a bentonite sample of the mock-up test adjacent to an intact tracer vial over a distance of up to 25 000 µm from the vial. In each plot the insert shows a zoom of the ^{237}Np and ^{233}U concentration profiles (linear scale) until 2500 µm, see text.*

arrow). This sample was enriched also in iron with a concentration of 599 µg/g, compared to levels of 1.2 to 20.5 µg/g in the other samples. The enhanced actinide levels in this sample might be explained by a preferential sorption to an iron mineral, potentially pyrite.

Similar results were obtained from the analysis of a bentonite segment adjacent to a vial that remained intact during bentonite expansion (*note that vials were emplaced without their cover caps, so that the RN tracers could in any case diffuse even if the vial was not broken*). As shown in Fig. 2, the concentrations of a) ^{237}Np and b) ^{233}U in these bentonite layers range between 0.7 and 19 ng/g and between 0.1 and 5 ng/g, respectively. Data show significantly stronger scattering as compared to the samples collected at the vicinity of the broken vial. However, RN concentrations 2 cm away from the vial lie in a similar range for both segments, at 8 and 10 ng/g for ^{237}Np and at 0.7 and 0.5 ng/g for ^{233}U, respectively.

These similar concentration profiles characterized by a rather flat plateau can be qualitatively reproduced by diffusion model simulations [5] and indicate that a steady state for the diffusive transport and outflow of ^{237}Np and ^{233}U from the vials is achieved over the 5 years duration of the experiment. These results are supported by the observation of a breakthrough of both

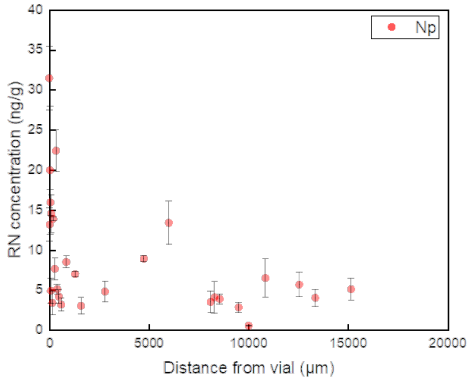

Fig. 3: *^{237}Np concentration profile (linear scale) in a bentonite sample of LIT adjacent to a tracer vial over a distance of up to ca. 15 000 µm from the vial.*

RNs in the outlet of the mock-up test during the experiment [2].

The high mobility points to the existence of Np and U in their oxidized states V and VI, respectively, indicating that redox conditions are at least not reducing enough to transfer all Np and U into the tetravalent state.

In Fig. 3, first results on ^{237}Np diffusion profile in a sample from the LIT are depicted. As it can be seen, ^{237}Np concentrations range over the same orders of magnitude and show a similar distribution as in the mock-up test. These results point towards an initial diffusive transport of Np(V) before the expected reducing condition in the LIT would have been established [6].

Laboratory Investigation: Erosion of GMZ bentonite

The potential erosion behavior of the GMZ bentonite was first studied in contact with a water of composition close to a groundwater from the Beishan region (Gansu Province, China) [7]. The synthetic carbonated water (SBPW) presents a high ionic strength (IS); IS = 39 mM with $[Ca^{2+}]$ = 2 mM and a slightly basic pH (pH = 8.5). Details are given in Tab.1.

Table 1. Composition of the simulated Beishan and Grimsel (glacial-melt or meteoric) type groundwaters.

Cations	mg.L^{-1}	Anions	mg.L^{-1}
Synthetic Grimsel ground water (SGW, glacial melt or meteoric type)			
Na^+	28.4 ± 3 %	F^-	2.80 ± 3 %
K^+	-	Cl^-	2.32 ± 5 %
Mg^{2+}	-	NO_3^-	-
Ca^{2+}	1.31 ± 1 %	SO_4^{2-}	4.12 ± 5 %
		HCO_3^{2-}	84 ± 1 %
pH	8.4	IS	1.6 mmol/L
Synthetic Beishan Pore Water (SBPW) adapted from [3]			
Na^+	567 ± 3 %	F^-	0.80 ± 3 %
K^+	7.8 ± 1.2 %	Cl^-	585 ± 5 %
Mg^{2+}	21.2 ± 1.7 %	NO_3^-	4.8 ± 4 %
Ca^{2+}	80 ± 1 %	SO_4^{2-}	570 ± 5 %
		HCO_3^{2-}	125 ± 1 %
pH	8.5	IS	39 mmol/L

The first phase of the experiment lasted 9 months after which the SBPW was exchanged by a low mineralized water simulating the intrusion of glacial-melt water (meteoric-type, SGW). A second erosion phase continued then during one year. In addition, and for comparison, the erosion was studied for GMZ pellets placed in contact with the meteoric type water directly. This synthetic water (SGW) has been used in previous work [4,8] and has a composition (see Tab.1) similar to the natural water from the Grimsel Test Site.

Experiments were conducted by using the GMZ provided during the "ELF-China-Pilot" project [3]. It contains montmorillonite (71-78%) and some accessory minerals like quartz, plagioclase, feldspar, cristobalite and carbonates in higher amount (wt.%)

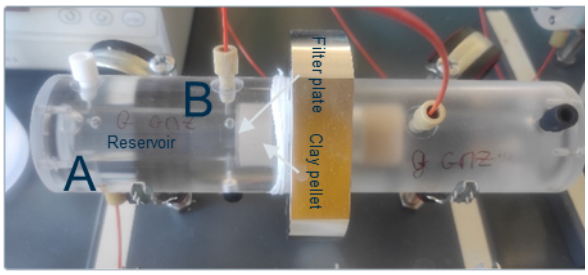

Fig. 4. Double-sided reactors used in the erosion experiments. A: water introduction port, B: collection, the water is circulating from A to B.

than the previously used MX80 bentonite [4]. It has a cationic exchange capacity of 71-78 meq/100g [9,10]. As in [4], for each erosion tests, two GMZ bentonite cylindrical pellets (19 mm diameter, 10 mm height and dry density of 1.6 g/cm^3) were prepared using a hydraulic press. The pellets were emplaced into the two separate compartments of a translucent double-sided reactor (Fig.4). The pellets were confined between a stainless-steel filter plate (19 mm diameter, 1.6 mm height, 20 µm pore width) and a PEEK spacer. The filter was emplaced to allow the GMZ pellets to be hydrated by the synthetic groundwater and to simulate a fracture filled with porous fracture filling material.

The compartments of the reactor were filled with 11.6 mL of the synthetic Beishan type water or with the meteoric-type water immediately before the start of the experiment. The synthetic groundwater was circulated with a peristaltic pump at a flow rate of 3 µL/min, at room temperature and under aerobic conditions. A visual inspection of the pellets indicated that they were hydrated within 3 days.

The effluents were collected every 3 days in the first month of each experiment (later on, samples were collected circa every 10 days) to measure pH and to analyze the composition with ICP-OES for major cations, ICP-MS for trace elements and ionic chromatography for the anionic composition.

The presence of clay colloids was revealed by the detection of their main (Si, Al, Mg, Fe) or trace constituents (Th, U). The entire erosion experiments extended over 2 years. The comparison of data obtained in the two parallel experiments showed an excellent reproducibility (Fig.5, open and closed symbols).

Na-Ca exchange reaction was clearly observed. Na^+ in raw GMZ bentonite exchanges with Ca^{2+} from the SBPW in this experiment but no significant erosion was detected during the contact of the GMZ bentonite pellets with the high IS SBPW as observed by the constant concentrations of the effluent collected. The results in these experiments with SBPW ($[Ca^{2+}]$ = 2 mM) are in-line with previous studies suggesting that Na^+ and Ca^{2+} concentrations larger than critical coagulation concentrations (CCC_{Na} = 10-100 mM; CCC_{Ca} = 0.1-1 mM, in [11,12]) prevent bentonite erosion.

The erosion (clay colloid detachment) via a low mineralized groundwater flow was quantified by

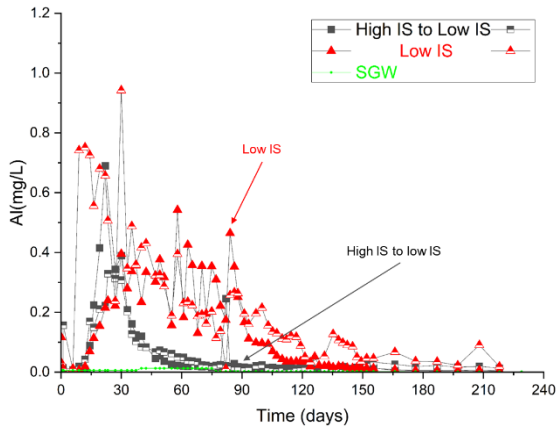

Fig. 5. Al mass concentration evolution (as clay colloid erosion indicator) during the erosion experiment directly in contact with a low IS groundwater (meteoric type) or after 9 months contact time with the high IS GW (Beishan type water), see Tab.1 for GW details.

Table 2: AMLR for the various conditions tested

Pellets composition	Eluent	AMLR (kg/(y·m²))	
		0-100 d	0-365 d
Raw MX80	Directly in SGW	0.08 ± 0.03	0.03 ± 0.01
Raw GMZ	Directly in SGW	0.043 ± 0.006	0.012 ± 0.003
	Step 1 SBPW, high IS (9 months)	Not detectable C_{Na}(25 mM)> (CCC_{Na}(10-100 mM) C_{Ca}(2mM)>CCC_{Ca}(0.1-1 mM)	-
	Step 2: SGW	0.014 ± 0.001	0.005 ± 0.001

determining an average eluted mass loss rate (AMLR, Tab. 2).

For comparison, AMLR values are integrated over the same period of time. Compared to raw MX80 bentonite, raw GMZ bentonite showed lower AMLRs (0.012 ± 0.003 kg/(y·m²) compared to 0.03 ± 0.01 kg/(y·m²) for MX80) within the same erosion time period (365 10 days) when contacted with a low IS SGW. This might be explained by a higher content of less soluble accessory mineral, like quartz and feldspar, in agreement with [13]. The erosion inhibiting effect of quartz or feldspars is most likely caused by clogging of the filters simulating a fracture filled with secondary minerals, which does not occur in experiments with an open fracture [14]. Nonetheless, for greater erosion time (> 500 days) the difference became less and less significant. Contacting first the raw GMZ bentonite with a high IS (I = 39 mM) groundwater (SBPW) for 9 months and then interacting with low IS SGW significantly reduced the eroded mass, leading to a decrease of AMLR from 0.012 ± 0.003 kg/(y·m²) to 0.0051 ± 0.0001 kg/(y·m²). Apparently, the exchange of the Na^+ from the raw GMZ bentonite with the Ca^{2+} from the SBPW reduced the swelling and thus later, the erosion. The addition of 10 mg/L humic acid, simulating the presence of natural organic matter in groundwater, did not significantly influence GMZ erosion in low IS SGW (AMLR = 0.016 ± 0.001 kg/(y·m²) compared to 0.012 ± 0.003 kg/(y·m²) w/o humic acid). At the given pH around 8.4, the interaction of humic acid with clay minerals is weak and, thus, is not able to induce an enhanced stabilization of clay colloids in SGW.

Care should be taken by using these erosion data. Actually, using short-term erosion rates for performance assessment analyses might overestimate long-term bentonite erosion, as the influence of groundwater composition and accessory minerals on bentonite erosion weakens over time.

Important is that assuming erosion via GW flow from a single fracture intersecting a deposition hole filled with bentonite at an angle of 90° and with fracture aperture of up to 200 µm, neither the Raw GMZ nor the Raw MX80 reach the acceptable mass loss limit of 1200 kg bentonite during the first 10^6 years [15] under the present conditions.

Actual work is focusing on the modeling of the data obtained so far according to [16].

Acknowledgments:

The research related to the Long-term In-situ Test and corresponding mock-up test was supported by BMUKN in the framework of the EVIDENT project and research on the erosion of GMZ bentonite was funded by BMWi/BMWK in the framework of the "ELF-China-Pilot". We express our gratitude to the China Scholarship Council (grant no. 201908220157) for funding Z. Chen's contribution to the study on erosion of GMZ bentonite.

References

[1] Shelton et al. SKB Technical report, TR-17-17. (2018).
[2] Kollorado-e2 Final Report. KIT publications, Editors: Noseck, U. and Schäfer, T. (2019).
[3] Deutsch-Chinesische Entsorgungsforschung-Pilotprojekt: Reanalysis of BRIUG THM Mock-up Test (ELF-China-Pilot), funded by BMWi/BMWK under grant numbers 02E11850A-E.
[4] Bouby, M. et al. App. Clay Sci., 198, 105797, (2020).
[5] Nagra Technical Report NTB 23-10 (2025).
[6] Montoya, V. et al., J. Hazard. Mat., 424 127733, (2022).
[7] Zhu et al. Coll. Surfaces A: Physicochem. Eng. Aspects, 640, 128374 (2022).
[8] Norforrs et al., App. Clay Sci., 114, 179–189, (2015).
[9] Kaufhold, S. et al. Vibrational Spectroscopy, 59, 29-39, (2012).
[10] Kaufhold, S. et al. Corrosion Science, 171, 108716, (2020).
[11] García-García, S. et al. J. Coll. Int.Sci., 315, 512-519, (2007).
[12] Seher, H. et al. Coll. Surf., 4, 16, (2020).
[13] Yan H., et al., doi: 10.1016/j.enggeo.2022.106800, (2022).
[14] Schäfer T. et al., NAGRA Technical Report NTB 23-10, (2025).

[15] Johansson B. et al. POSIVA working report, FI-27160, Finland, (2002).

[16] Yan H.et al., Géotechnique, 75(13), 44-53, (2025).

5.3 Colloid impact on radionuclide migration

C. Beiser, M. Bouby, A. Fried, F. Geyer, S. Kraft, S. Kuschel, A. Lunz, M. Plaschke, F. Quinto, H. Geckeis

In co-operation with:

S. Brassines[a],
[a] *ONDRAF/NIRAS, Belgian Agency for Radioactive Waste and Enriched Fissile materials, Geological Disposal, R&D, Avenue des Arts, 14, 1210 Bruxelles, Belgium*
I. Blechschmidt[b], *R. Scheeberger*[b], *A. Martin*[b]
[b] *National Cooperative for the Disposal of Radioactive Waste, Wettingen, Switzerland*
T. Schäfer[c]
[c] *Institute of Geosciences, Applied Geology, Friedrich-Schiller-Universität Jena, Germany*

Introduction

The influence of colloidal/nano-scale phases on the radionuclide (RNs) solubility and migration behavior is one of the uncertainties in certain scenarios of long-term safety analyses for deep geological repositories. [1, 2]. In our work, we aim to 1) identify the presence and the formation of relevant colloids in some argillaceous rocks, 2) determine their stability as a function of geochemical parameters, 3) elucidate the thermodynamics and kinetics of the colloid interaction with radionuclides, 4) perform laboratory and field experiments to quantify the colloid mobility and their interaction with surfaces. Laboratory and in-situ migration experiments need the use and development of highly sensitive and sophisticated analytical techniques [3-6]. The final goal is to state on the relevance of the nanoparticles (NPs) / colloids for the radionuclide migration in natural geochemical conditions and to implement our experimental data into reactive transport modelling codes.

Our present activities are conducted with the support and in close collaboration with international nuclear waste management agencies, like ONDRAF/NIRAS, (Belgium) and NAGRA (Switzerland).

The collaboration with the ONDRAF/NIRAS is related to the characterization of natural organic matter (NOM) derived from different layers within the Belgian Boom Clay (BC) formation and its interaction with RNs [7].

Characterization of Boom Clay (BC) dissolved organic matter (DOM)

In Belgium, poorly indurated clay formations like the Boom Clay (BC) are the subject of research activities related to deep geological disposal of high-level and/or long-lived radioactive waste. The BC contains up to 1 to 5 wt.% immature organic matter (OM) [8,9]. The transport of radionuclides (RNs) might be thus influenced.

This report concentrates on the determination of the size distributions of dissolved organic matter (DOM) and associated naturally abundant metal ions in real BC pore waters (BCPW) collected from the HADES underground research laboratory (Mol, Belgium) and taken as representative for different layers of the BC formation. Leachates from solid BC samples were also examined.

To prepare the leachates, some inner-pieces of small clay discs are suspended for 1 week under atmospheric conditions in a synthetic Boom Clay water (SBCW) consisting of 15 mM $NaHCO_3$ at a solid/liquid ratio of 0.2 kg/L. The suspension obtained from this leaching experiment is then ultra-centrifuged at 15,000 rpm (g_{max} = 16162) for 90 min. The leachates are the supernatants collected after the centrifugation.

The Asymmetrical Flow Field-Flow Fractionation coupled to a UV-Vis spectrophotometer (AsFlFFF-UV) [3,4] as well as the Liquid Chromatography coupled to Organic Carbon Detection, UV and ICP-MS (LC-OCD-UV-ICP-MS) [5,6] are used for DOM and elemental association characterization. Results are presented Figs. 1,2,3 and 4.

Small sized OM fractions (< 7 nm) are detected in all BCPWs where the maximum of the DOM species distribution is at a hydrodynamic diameter of ~1.8 nm (Fig. 1).

The pore waters originating from or influenced by the double band (DB) structure (i.e. here Morpheus-F8) exhibits a multimodal size distribution ranging to larger sized colloidal entities up to ~30 nm.

In the leachates (Fig. 2), a small-sized fraction with a maximum at ~ 1.8 nm or somewhat larger is also visible like in BCPW samples.

However, the main fraction appears in the larger colloid size region with a broad distribution up to 30 nm and a maximum at ~ 15-16 nm. The findings support the outcome of earlier investigations [10]

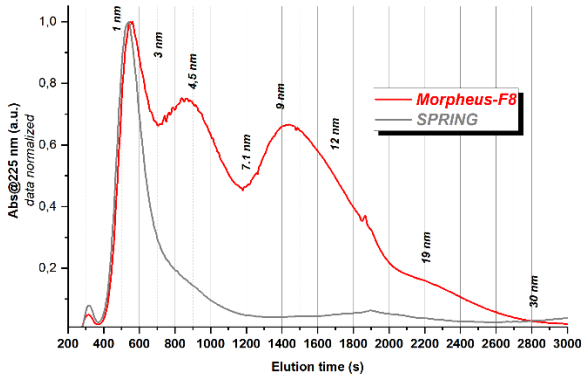

Fig. 1: AsFlFFF-UV-fractograms as obtained after the injection of the SPRING and Morpheus-F8 BCPW, mean of 3 successive injections of 100 µL; eluent $NaHCO_3$ 15 mM.

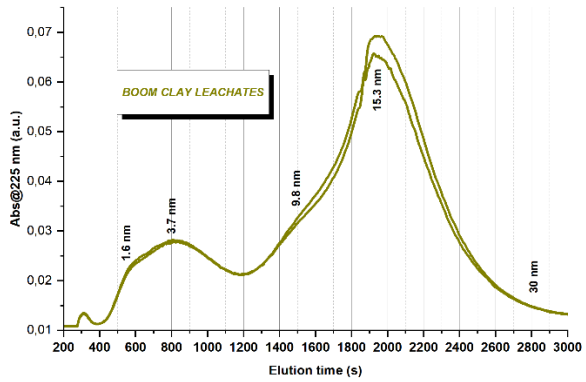

Fig. 2: AsFlFFF-UV-fractograms as obtained after the injection of the BC leachates; 2 successive injections of 100 µL; eluent $NaHCO_3$ 15 mM.

stating that the inter layer mobility of DOM in BC apparently is restricted to species with a diameter of < 6 nm.

Trace elements (Fe, Ni, lanthanides, Th, U) reveal a variable and complex association with colloidal species in BCPW and BC extracts where inorganic species such as FeOOH nanoparticles play a role besides DOM (Fig. 3 and 4).

A preliminary attempt to derive in-situ K_d-values for the naturally abundant lanthanides and actinides in the BC system is found to be consistent with laboratory K_d-values reported in the literature for Eu, U, Pu and Th (log K_d=3.5 – 4.5) [11].

Even though in-situ K_d-values are derived under certain simplified assumptions, the similarity of in-situ and laboratory K_d-value ranges increase confidence in the applicability of such data for long-term safety analyses.

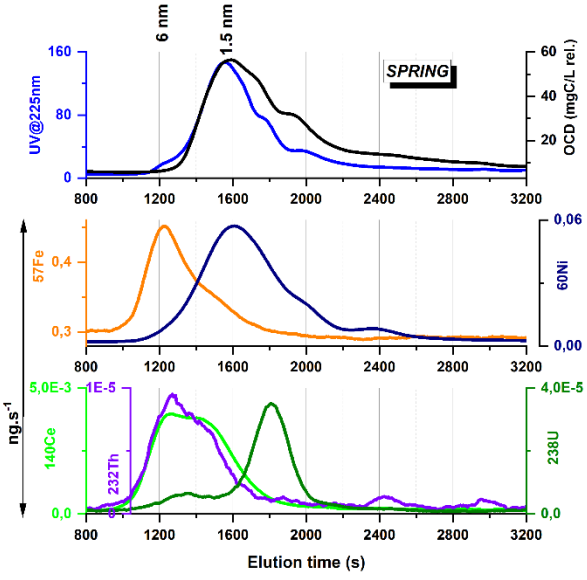

Fig. 3: LC-OCD-UV-ICP-MS chromatograms as obtained after injection of the raw SPRING BCPW. Mean of 3 successive injections of 1mL, on-line filtration at 450 nm.

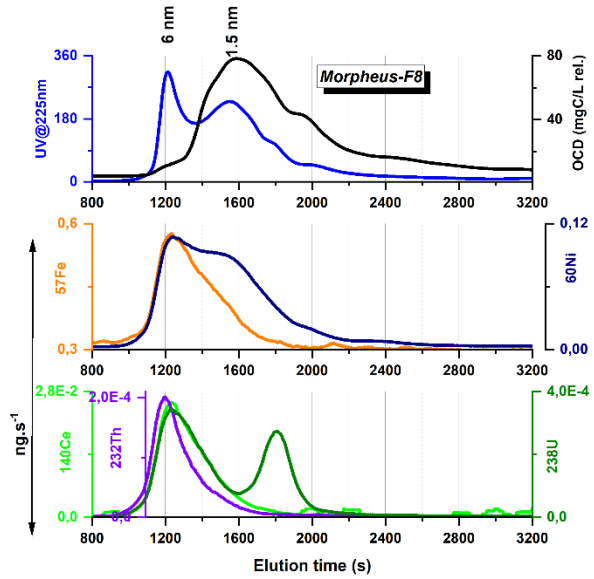

Fig. 4: LC-OCD-UV-ICP-MS chromatograms as obtained after injection of the raw Morpheus-F8 BCPW. Mean of 3 successive injections of 1mL, on-line filtration at 450 nm.

Influence of groundwater residence time on RNs and colloids retention at the GTS

In the framework of the international CFM project performed at the generic underground research laboratory GTS (Grimsel Test Site, Switzerland) a series of in-situ RN tracer tests have been carried out in advective groundwater flow. These field tests aimed to study the retention and migration of bentonite colloids and RNs through a water conducting fracture of the granodiorite rock. The GTS groundwater is a Na^+/Ca^{2+} -HCO_3^- -SO_4^{2-} type with a pH of 9.6, an E_h(SHE) of ca. -220 mV and an ionic strength 1.6 mM, providing conditions for high stability and mobility of bentonite colloids [12,13]. The latest of such tests, named CFM Run 22-02, focuses on the kinetics of colloids and RNs retention mechanisms in the granodiorite fracture.

Over the last 25 years three in-situ RN tracer tests were carried out at the GTS within the same hydrological dipole, named CRR (2.23 m length). A cocktail of RN tracers (among them ^{233}U(VI), ^{237}Np(V), ^{242}Pu(IV) or ^{244}Pu(IV) and ^{241}Am(III) or ^{243}Am(III)), bentonite colloids and a conservative tracer prepared in Grimsel groundwater was injected into the CRR dipole at different injection and extraction rates in order to accomplish a certain groundwater residence time. The first of these tests, CRR Run 32 [12,13] was characterized by a short groundwater residence time of ca. 114 min. In 2009, after the installation of a pressure and groundwater flow control megapacker system, a second experiment, the CFM Run 13-05 [14], was conducted with a much longer residence time of ca. 8400 min, a value closer to the expected slow groundwater flow in repository conditions. While the fraction of actinide tracers and bentonite colloids migrating out of the granodiorite fracture was between ca. 70 % and ca. 100 % in CRR Run 32, a much lower recovery spanning ca. 4 % to 36 % was observed in

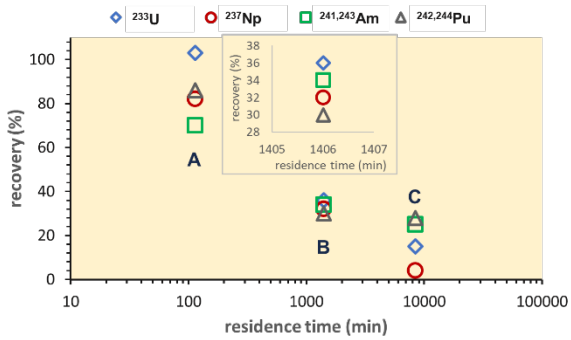

Fig. 5: *Recovery (%) of ^{233}U (blue rhombus), ^{237}Np (red circle), $^{241,243}Am$ (green square) and $^{242,144}Pu$ (grey triangle) for the three field tests carried out in the CRR dipole as function of groundwater residence time (logarithmic scale). The letters "A, B and C" indicate the recoveries for CRR Run 32, CFM Run 22-02 and CFM Run 13-05, respectively. The insert with light grey border shows a zoom of the actinides recovery for CFM Run 22-02.*

CFM Run 13-05 (see Fig. 5). For the latest field test, named CFM Run 22-02, an intermediate groundwater residence time of ca. 1410 min was chosen. Current results of this test, partially presented in chapter 9 and sub-chapter 8.4, corroborate the previous observations of an inverse correlation between residence time and colloids/RNs migration through the fracture. As it can be seen in Fig. 5, the recovery for all the actinide tracers, ranging between 30 % and 36 %, is intermediate between those obtained for the fast CRR Run 32 and the slowest CFM Run 13-05. In the geochemical conditions of the Grimsel groundwater, different mechanisms are responsible for actinide retention. Namely, for the colloid borne Pu(IV) and Am(III): colloid filtration through the pores of the granodiorite fracture and dissociation from colloids and adsorption to rock surfaces; for U(VI), stabilized in solution as ternary calcium-uranyl-carbonate complexes [15]: isotopic exchange with natural uranium bearing minerals/surface sorption; and for the redox sensitive Np(V): reduction to Np(IV) with consequent precipitation of NpO_2(am) or surface sorption of Np(IV) species [15].

The results of this study highlight how the far-field migration of actinides in fractured crystalline host rock is strongly dependent on the groundwater flow rate. In particular, the kinetics of the afore-mentioned retention mechanisms favor actinide retention for lower fluxes that are expected in a deep geological repository.
Further investigation is ongoing in order to estimate the bentonite colloid recovery for CFM Run 22-02. Furthermore, an additional field test is planned in which Np(IV) is stabilized in the cocktail and injected instead of Np(V).

Acknowledgments:

The authors greatly acknowledge the funding from the Belgian waste management organization (ONDRAF / NIRAS) for the study on colloids in Boom Clay. The research related to the Long-term In-situ Test and corresponding mock-up test was supported by BMUKN in the framework of the EVIDENT project.

References

[1] Geckeis, H., *Geological Society Special Publication*, 236, 529-543, (2004)
[2] Schäfer, Th. et al., *Appl. Geochem.*, 27, 390-403, (2012)
[3] Bouby, M. et al., *Anal. Bioanal. Chem.* 392:1447-1457, (2008).
[4] Gopalakrishnan, A. et al., *Sci. Tot. Env.* 855, 158891, (2023).
[5] Huber, S.A. et al., *Wat. Res.,* 45, 879-885, (2011).
[6] Tasi, A. et al., *Appl. Geochem.* 169: 106015, (2024).
[7] M. Bouby et al., *Appl. Geochem.* (*submitted*).
[8] De Craen, M. et al. Geochemistry of Boom Clay pore water at the Mol site, Status Report 2004, SCK.CEN-BLG-990, (2004).
[9] Bruggeman, C. and M. De Craen (2012). Boom clay natural organic matter. Status report 2011, SCK.CEN-ER206, (2012).
[10] Durce, D., et al., *J. Cont. Hydrol.* 208: 27-34. (2018).
[11] Bruggeman, C. and Maes, N. Radionuclide migration and retention in Boom Clay, SCK-CEN ER-0345, Table 3-8, (2017).
[12] Möri, A. et al., *Coll. Surf. A,* 217, 33−47, (2003).
[13] Geckeis, H. et al., *Radiochim. Acta.* 92, 675−674 (2004).
[14] Quinto, F. et al., *Anal. Chem.* 89, 7182- 7189 (2017)
[15] Montoya, V. et al., *J. Hazard. Mat.*, **424** 127733, (2022).

5.4 Diffusion

F. Heberling, N. Gill, Y. Kouhail, S. Kraft, V. Metz, F. Quinto, S. Ratnayake, F. Steegborn, H. Geckeis

In co-operation with:

J. Göttlicher[a]

[a] Institute for Photon Science and Synchrotron Radiation (IPS), Karlsruhe Institute of Technology (KIT), Hermann-von-Helmholtz-Platz 1, 76344 Eggenstein-Leopoldshafen.

Introduction

Final disposal in a deep geological repository is a generally accepted strategy for the long-term management of high-level radioactive waste (HLW). Geologic formations that are considered as potential host rocks for HLW repositories in Germany and other European countries are clay rock, crystalline rock (e.g. granite or granodiorite), and rock salt. In clay and crystalline rocks, many common repository concepts consider a geotechnical barrier made of bentonite. In clay and crystalline rocks, groundwater intrusion into the HLW repository needs to be considered, which will lead to canister corrosion and may finally induce radionuclide release. Due to the small particle sizes of clay minerals, leading to small pore sizes, advective water flow is very limited in bentonite and considered argillaceous host rocks. Thus, diffusion is the main transport process in these geo-materials, and may eventually lead to quite slow radionuclide migration out of the containment-providing rock zone, towards adjacent aquifers.

Diffusion in pristine, unaltered, and homogeneous clay materials has been studied for decades. Relevant processes have been identified and can be readily included in numerical transport simulations [e.g. 1-3].

Recent studies at KIT-INE, which were initiated in the frame of the iCross project and are presented as part of this report, focus on effects of bentonite alteration, e.g. in the presence of Fe(II), released from corroding waste canisters, effects of elevated temperature and temperature gradients, or effects of clay rock heterogeneity on radionuclide diffusion.

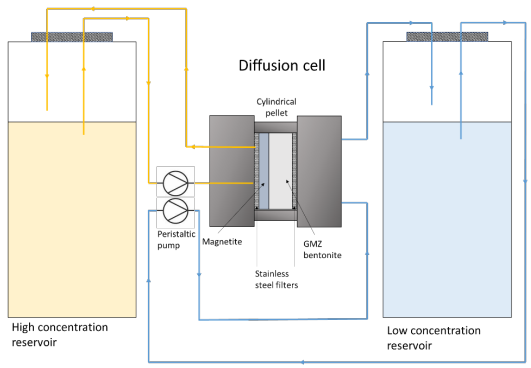

Fig. 1. Through-diffusion setup for experiments on radionuclide diffusion through a mixed magnetite (2 mm) – GMZ bentonite (8 mm) sample, mimicking a corrosion product - bentonite interface in a multi barrier system after canister corrosion.

Impact of dissolved iron on the diffusion of radionuclides in bentonite

In a first attempt to mimic the effect that corrosion induced bentonite alteration may have on diffusion of radionuclides, two through diffusion experiments were set up, in which the diffusion cells were packed with a 2 mm thick layer of magnetite, an expectable corrosion product of steel at anoxic conditions, and 8 mm of GMZ bentonite (Gaomiaozi, Inner Mongolia, China). Both materials were compressed to a dry density of 1.6 g/cm^3. A schematic sketch of the experimental setup is shown in Figure 1. For comparison two more cells were prepared containing only 10 mm GMZ bentonite (also 1.6 g/cm^3).

The synthetic pore water composition followed the recipe from Wu et al. [4]. In experiments with magnetite, 12 µM $FeCl_2$ were added to the high concentration reservoir (HCR) to prevent magnetite dissolution. The pore water was preequilibrated with bentonite (and magnetite) before the experiment. During the experiments with magnetite, the Fe(II) concentration in the HCR increased to 18 µM, indicating some minor magnetite dissolution.

High concentration reservoir (HCR) and low concentration reservoir (LCR) solutions were circulated though the diffusion cell at a flow rate of 0.4 mL/min.

After 3 weeks equilibration of the packed diffusion cells with the porewater, non-sorbing HTO and $^{36}Cl^-$ tracers were added to the HCR for the first diffusion tests. At selected time intervals, the HCR was sampled, and/or the LCR was sampled and exchanged with fresh solution. HTO and $^{36}Cl^-$ concentrations were analyzed by liquid scintillation counting using an LSC Ultima Gold XR cocktail (Perkin Elmer). Diffusion data for non-sorbing tracers were analyzed with an analytical solution of the diffusion equation, assuming constant inlet and zero outlet concentration after Crank (1975) [5], and a least-squares fitting routine. The results are summarized in Table 1.

Concerning HTO diffusion, the cells with magnetite and bentonite exhibit higher diffusion coefficients and slightly increased rock-capacity factors (= porosities for non-sorbing tracers) for HTO, indicating differences in the pore structure between magnetite and bentonite. For $^{36}Cl^-$, the pure bentonite cells show the

expected anion exclusion effect, i.e. diffusion coefficients and porosities are about a factor of 4-6 lower compared to HTO. The magnetite-bentonite cells exhibit a strongly suppressed anion exclusion. Diffusion coefficients for $^{36}Cl^-$ are decreased by a factor of 3 only, and porosities are about half as high as for HTO. We attribute this effect to the adsorption of Fe(II) at smectite surfaces increasing their surface charge (making it less negative) and thereby decreasing anion exclusion [6].

Table 2. Results from through-diffusion tests with layered magnetite / GMZ bentonite- and pure GMZ bentonite cells. Numbers provided in each cell are effective diffusion coefficient D_e and rock capacity factor α.

		HTO	$^{36}Cl^-$
GMZ			
Cell 1	D_e (m^2/s): α:	$(5.79 \pm 0.06) \times 10^{-11}$ 0.54 ± 0.04	$(1.37 \pm 0.01) \times 10^{-11}$ 0.09 ± 0.01
Cell 2	D_e (m^2/s): α:	$(5.54 \pm 0.05) \times 10^{-11}$ 0.45 ± 0.04	$(1.24 \pm 0.01) \times 10^{-11}$ 0.08 ± 0.01
magnetite / GMZ			
Cell 3	D_e (m^2/s): α:	$(1.47 \pm 0.01) \times 10^{-10}$ 0.63 ± 0.04	$(4.63 \pm 0.03) \times 10^{-11}$ 0.42 ± 0.02
Cell 4	D_e (m^2/s): α:	$(1.44 \pm 0.01) \times 10^{-10}$ 0.58 ± 0.03	$(4.28 \pm 0.01) \times 10^{-11}$ 0.30 ± 0.01

Bentonite alteration in the presence of iron at elevated temperature

The expected anaerobic corrosion in the repository initiates the release of dissolved mobile Fe(II) species. This may lead to the iron induced alteration of smectite minerals in the bentonite buffer. Such processes may lead to pore space alterations in the bentonite and changes in transport- and adsorption properties. Especially, the formation of secondary phases like Fe-smectites or Fe bearing 1:1 phyllosilicates (berthierine, cronstedtite, greenalite, odinite) could lead to a reduced swelling capacity and cation exchange capacity (CEC). Dedicated experiments are being carried out to examine secondary clay alteration phase formation and the effect of such alterations on transport properties.

In autoclaves, GMZ bentonite, MX-80 reference bentonite (Wyoming, USA) and KGa-2 reference kaolinite were mixed with different iron sources ($FeCl_{2(aq)}$, Fe-Powder), a 0.03 M NaCl solution and stored at 90 °C in an oven within an Argon-filled Glovebox for 4 months. The solid/liquid ratio (g/L) amounted to 15 for the bentonites and 15 or 20 for kaolinite. The Fe/Clay ratio was set to 0.5 (mass/mass). Afterwards, samples were analyzed via Infrared Spectroscopy (IR), X-ray Diffraction (XRD) and X-ray Absorption Spectroscopy (XANES).

IR results show for the original bentonites GMZ, MX-80 and kaolinite absorption bands (1000 cm^{-1} - 800 cm^{-1}), which are related to the octahedral ions. These decrease in intensity upon alteration. Samples treated with Fe-Powder display higher decrease in absorption bands than samples treated with $FeCl_2$. Thus, IR results indicate structural decomposition of the octahedral sheets of clay minerals.

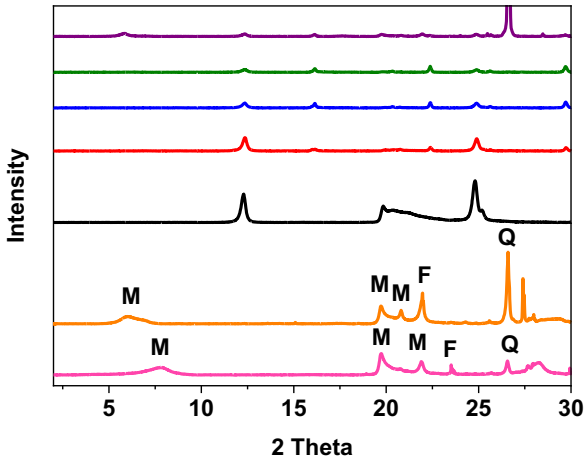

Fig. 2: X-ray diffraction results. Diffractograms of untreated samples (pink, orange and black line) compared with samples treated with Fe-Powder (picture above). Samples: red KGa-2 s/L 15; blue KGa-2 s/L 20, green MX-80, purple GMZ.

XRD data (Fig.2) show complete replacement of 2:1 phyllosilicates from GMZ and MX-80 after alteration (peaks labelled with M in Fig. 2). Peaks of further bentonite components like quartz and feldspars disappeared. The appearance of new peaks at 7.15 Å (d(001), ca. 12.5°, 2 Theta) and 3.57 Å (d(002)) is independent of the educts tested in this study and indicates formation of a 1:1 phyllosilicate. In addition, all samples treated with $FeCl_2$ exhibit a new d(060) peak at 1.52 Å. This indicates a change in octahedral occupancy, alteration from the original dioctahedral clay mineral to a mixed di-/ trioctahedral clay mineral.

XANES data exhibit pre-edge features, characteristic of octahedrally coordinated iron. In general, edge positions indicate about 30±20% Fe(III) and 70±20% Fe(II). In conclusion, the mineral phase odinite ($(Fe^{3+}, Mg, Al, Fe^{2+})_{2.4}(Si_{1.8}Al_{0.2})O_6(OH)_4$) shows the best crystal chemical and crystallographic agreement with the reaction product, as characterized by IR, XRD and XANES.

The results of these batch mineral syntheses experiments show complete transformation of smectites in bentonite and of kaolinite in the presence of iron to a newly formed 1:1 phyllosilicate.

Large scale diffusion studies in the underground research laboratory Mont-Terri

INE became partner in a diffusion experiment, named DR-C, in the underground research laboratory (URL) Mont-Terri and initiated another diffusion experiment, named DR-D, in the same URL. The location of the two diffusion experiments is highlighted in the map of the Mont-Terri URL in Figure 3. Both experiments are located in the new gallery 18 of the URL and both will investigate radionuclide diffusion in the upper sandy facies of Opalinus clay.

The upper sandy facies of Opalinus clay is a dark grey clay stone. Compared to the shaly facies it is higher in quartz and lower in clay content, and contains more sandy components. It is also characterized by a higher degree of heterogeneity, with whitish calcite

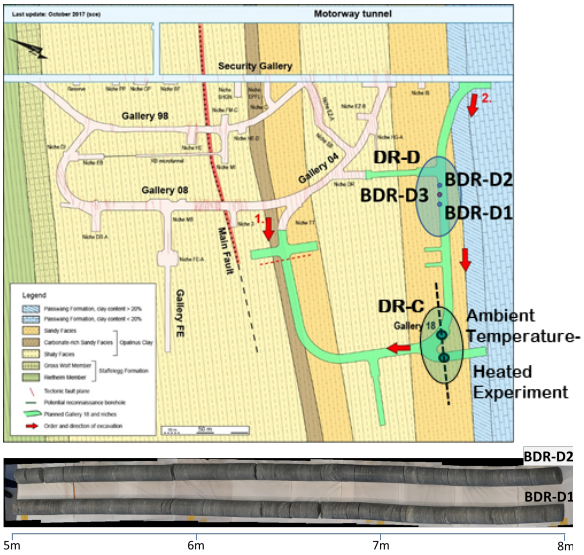

Fig. 3. Map of the URL Mont-Terri indicating the location of the two diffusion experiments DR-C and DR-D, both in the new gallery 18, and both in the upper sandy facies of Opalinus clay. The lower image shows the 5 – 8 m sections of two drill cores, recovered from the bore holes BDR-D1 and BDR-D2.

and quartz enriched intercalations and limestone concretions. The drill core photography in the lower image in Fig. 3 gives an impression of the rock heterogeneity.

The experimental location was chosen to mimic potential German clay host rocks, which are as well expected to be more heterogeneous compared to the shaly facies of Opalinus clay, the host rock candidate in Switzerland.

Aim of the DR-C experiment is to study diffusion in a thermal gradient (80°C to ca. 15°C), compared to diffusion at ambient temperature (ca. 15°C). Therefore, two diffusion experiments are setup 10 m apart from each other in similar rock sections along the strike of the clay rock bedding.

Aim of DR-D is to study the effect of rock heterogeneity on radionuclide diffusion. Therefore, the injection interval of the experimental setup is placed at the intersection of two different subfacies (SF2 and SF3 [7]) of the sandy facies Opalinus Clay, ca. 10 m below the gallery. This transition area has been identified by drill core analyses and bore hole logging, and could be visualized after a cross hole seismic tomography survey between bore holes BDR-D1 and BDR-D2 [8].

Both experiments have been successfully installed, and the heated experiment of DR-C was heated up in a step-wise procedure during 2025. Ca. 12L synthetic porewater have been circulation in the experiment for several months in order to ensure equilibration of solution and rock. Tracer injection is foreseen for January 2026. In a first step the strongly sorbing tracers Cs-137, Co-60 and Ba-133 will be injected. After 18 months, non- and weakly sorbing tracers Na-22, HTO and Cl-36 will be added. Expected runtime of the experiments is two years until beginning 2028. The solution compositions will be monitored throughout the runtime. After the experiment the tracer profiles will be analyzed from overcoring samples of the rock around the diffusion boreholes.

Acknowledgements

We acknowledge funding via the iCross project, BMBF grant 02NUK053C, and Helmholtz Association, grant SO-093. We thank all the partners of the Mont-Terri experiments, and especially swisstopo and the Mont-Terri project, for the good collaboration, help, and support.

References

[1] Yu, J.W., Neretnieks, I. *Diffusion and sorption properties of radionuclides in compacted bentonite*. No. SKB-TR--97-12. Swedish Nuclear Fuel and Waste Management Co., 1997.

[2] Van Loon, L. R., et al. *Applied Geochemistry* 18.10 (2003): 1653-1662.

[3] Glaus, M.A., Frick, S., Van Loon, L.R. *Diffusion of selected cations and anions in compacted montmorillonite and bentonite*. No. NTB-17-12. Paul Scherrer Institute PSI, 2017.

[4] Wu, T., et al. *Applied Clay Science* 101 (2014): 136-140.

[5] Crank, J. "The mathematics of diffusion. Oxford." *England: Clarendon* (1975).

[6] Zhang, C.-L., et al. in: Shao, H., et al. (Eds.), Thermo-Hydro-Mechanical-Chemical (THMC) Processes in Bentonite Barrier Systems. Springer Nature, Switzerland (2024): 41-90.

[7] Lauper, B. et al., *Frontiers in Earth Science* 9 (2021).

[8] Lüth, S. et al., *Geophys J Int* 236 (2024): 1342-1359.

5.5 Radiation research

F.B.E. Becker, R. Dagan, C.M. Marquardt, K. Wu

In co-operation with:

A. Benali, R. Bouwman, J. Campani, J. Dabin, J. Eakins, P. Ferrari, F. Fioroni, K. Hürkamp, F. Jansen, Z. Jovanović, D. Krstić, P. Mariotti, A. McCann, E. Michaś-Majewska, P. Teles, K. Tymińska, G. Venturi[a]

[a] Working Group 12 of the European Radiation Dosimetry Group (EURADOS).

Experimental confirmation of new theoretical findings on the age determination of Cf sources

This study provides an experimental confirmation of new theoretical findings on the age determination of Cf sources. The age determination of Cf sources by gamma spectroscopy, first proposed by Gehrke [1], requires the fitting of the Cs-137 peak at 662 keV and the I-132 peak at 668 keV. The underlying idea is to evaluate their age-dependent peak intensity ratios according to the different life-times of the nuclides. The calculated ratio of the γ-ray emission rates of 662 keV to 668 keV, plotted as a function of the age of the Cf source ("age-determination curve"), makes it possible to determine the age of a Cf source from the corresponding ratios determined in measured spectra. However, in one of our previous investigations on Cf sources [2], discrepancies concerning the age determination curve were observed. Our theoretical studies using the Nucleonica toolkit [3] showed deviations for sources older than 30 years, with deviations increasing quite strongly with age. To check the deviating theoretical predictions, experiments were carried out with a 49-year-old Cf source [4].

Experimental procedure

γ-ray spectra of a 49-year-old Cf source were measured in the KIT-INE controlled area using a coaxial HPGe Germanium detector. A portable well-type HPGe detector system manufactured by Mirion Technologies (Canberra) was employed. The source was placed at a distance of 20 cm to achieve a high-count rate with an acceptable low dead time for the detector. Figure 1 shows the experimental setup used. The calibration of the detector itself was performed with an Eu-152 source in the control area of KIT-INE.

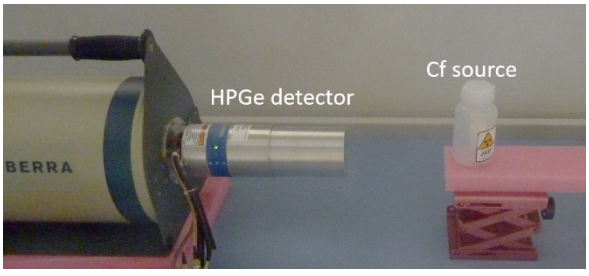

Fig. 1: Experimental setup with HPGe detector and Cf Source.

Results and Conclusions

From the intensity of the γ-ray lines in the measured spectra, we determined the 662 keV/668 keV activity ratio of the 49-year-old source. This measured data point does not agree with Gehrke's age determination curve, but follows the trend of the curve from our Nucleonica simulations, which we determined in our earlier study [2]. The activity ratio according to Gehrke's age determination curve is predicted to be about 20000, while the experimental result indicates a ratio of 1000, which agrees with our theoretical predictions.

With our gamma spectroscopic investigation with a 49-year-old Cf source, we were able to confirm our theoretical predictions on the age determination curves for Cf sources. Our results for old sources differ from those proposed by Gehrke. These discrepancies are probably because Gehrke, due to simplified assumptions, did not take into account all the decay channels that produce the isotopes Cs-137 and I-132. Obviously, complex decay channels play an important role from an age of the source of more than 25 years, as they were considered to a greater extent in our simulations with Nucleonica.

Activities in cooperation with the Working Group 12 of the European Radiation Dosimetry Group

KIT-INE contributes to activities of the Working Group 12 of the European Radiation Dosimetry Group (EURADOS). This group focuses on occupational radiation protection and individual monitoring in X-ray and nuclear medicine practices. In this field, numerous studies have been conducted, especially for workplaces in interventional radiology and cardiology. The complexity of the inhomogeneous radiation fields makes radiation protection and monitoring of the medical staff during interventional procedures exposed workers a challenging task.

Wearer Position-dependent Dose Recording of Personnel Dosimeters in Interventional Cardiology

We briefly report here on one of the latest studies by the EURADOS Working Group 12, which deals with the recording of doses from personal dosimeters in interventional cardiology [5,6]. The possible effects on the registered doses in a stray field in connection with

the actual wearing position of a dosimeter were investigated by Monte Carlo simulations and validated by measurements.

Materials and methods

To simulate a “typical” interventional cardiology procedure with femoral access, the Monte Carlo N-Particle (MCNP) Monte Carlo code [7] was employed. A modified version of the MIRD model was used as computational human phantom to imitate the patient and the two operators. Furthermore, lead aprons and the collar protectors were added to the model, and the operators' arms were angled to obtain a more "realistic" configuration. 35 simulation dosimeters were placed equidistant on the chest of each operator. In this way, a 5 x 7 dosimeter matrix (vertical x horizontal) was created on the chest. The X-ray tube beam qualities and positioning of the phantoms were simulated according to the experimental specifications.

Measurements were performed with a Philips Allura Xper FD20 irradiation device. A plastic Rando phantom was used to mimic the operator and a PMMA slab phantom to represent the patient. The absorbed dose was measured at different positions on the Rando phantom with an active dosimeter system.

Results and Conclusions

From the Monte Carlo simulations for a 70 kV beam, with reference to the horizontal middle row of the matrix higher dose values are observed in the upper rows of the dosemeter matrix while the lower rows show decreasing values. From the vertical middle row to the right side, the doses decrease by about a factor of 0.3 to 0.4. A strong decrease was observed for the dosimeters on the far left in the range of the factor 0.4 to 0.5. This decrease is attributed to the fact that the arms partially shield the respective dosimeters. Simulations without arms confirm this hypothesis, since in this case an increase in dose instead of a decrease is observed for the dosimeters on the far left. The measurement results with the phantom without arm show a similar behavior as the corresponding simulations without arms. From the breast center to the right a decrease of about 50% is observed and from the breast center to the upper positions the dose is reduced by about 60%.

The complexity of the different scenarios sets limits to this study. The exact mapping of the measurements into the simulations is not an easy task. In real situations, moreover, the static simulation and measurement scenarios are confronted with motion sequences. In a supplementary study [6], the potential shielding effect of the arms on dosimeters placed above the apron on the operator's chest was investigated through measurements in the hospital using a suitable anthropomorphic thoracic phantom. Overall, these results confirm the trends predicted in the associated Monte Carlo simulations.

Investigation of the exposure of the eyes of medical personnel when administering Sc-47 and Cu-67 labelled radiopharmaceuticals

Here a summary of a study of the EURADOS Working Group 12 dealing with the exposure of medical personnel when administering Sc-47 and Cu-67 labeled radiopharmaceuticals is given [8].

Materials and methods

To determine the exposure of the eye lens and thyroid gland of personnel during the administration of radiopharmaceuticals in a typical scenario of peptide receptor radionuclide therapy, Monte Carlo simulations were performed using a modified ICRP voxel model in the Monte Carlo N-Particle (MCNP) Monte Carlo code [7]. The simulations were validated by comparing the results with TLD measurements performed in a hospital using Lu-177-labeled compounds.

Results and conclusions

The doses for the eye lens and thyroid gland were derived from the photon emissions, whereby the beta contribution, which is three orders of magnitude smaller, was neglected. The agreement be-tween the simulation and measurement results obtained for Lu-177 suggests that, within the limits of the simulation approach, the simulation results for Sc-47 and Cu-67 can also be followed.

The dose to the eye lens for personnel is in the order of 2 µSv/GBq per patient application for Lu-177 compounds. Applied to Sc-47 and Cu-67, this amounts to approximately 8 µSv/GBq due to the different energies and yields of these radiopharmaceuticals. This information is useful for optimizing radiation protection for medical personnel in nuclear medicine and for assessing the appropriate workload for personnel in such practices.

References

[1] R. J. Gehrke et al., Nucl. Instr. and Meth. in Phys. Res. B, 213, 10–21, (2004).

[2] K. Wu, F. Becker, R. Dagan, Characterization of young Californium sources by means of γ-ray spectroscopy, NIM A, Vol. 1028 (2022) 166388.

[3] Nucleonica GmbH, 2017, Nucleonica Nuclear Science Portal (www.nucleonica.com), Version 3.0.269, Karlsruhe.

[4] F. B. E. Becker, R. Dagan, Ch. M. Marquardt, Investigation of 252Cf Sources with a Ge Gamma-Ray Detector, Radiat. Prot. Dosim. 199, Issue 15-16, October 2023, Pages 1674–1679, https://doi.org/10.1093/rpd/ncad135

[5] P. Ferrari, F. Becker, L. Campani, J. Jansen, Z. Jovanović, D. Krstić, F. Mariotti, P. Teles, G. Venturi, On the Placement of Apron Dosemeters and Dose Assessment in Interventional Cardiology Procedures: Preliminary Results, Radiat. Prot. Dosim. 199 Issue 4 (2023) 383, https://doi.org/10.1093/rpd/ncad065

[6] P. Ferrari, G. Venturi, L. Campani, F. Mariotti, F. Becker, J. Jansen, Z. Jovanović, D. Krstić, P.

Teles, Medical staff monitoring in interventional cardiology: over apron dosemeter placement based on measurements and simulations, Radiat. Prot. Dosim. 200, Issue 8, June 2024, Pages 802–807, https://doi.org/10.1093/rpd/ncae125

[7] D. B. Pelowitz (editor) MCNP6 User's Manual. Los Alamos National Laboratory Tech. Rep. LA-CP-13-00634. Los Alamos, NM, USA. May 2013.

[8] P. Ferrari, F. Becker, J. Dabin, J. Eakins, Z. Jovanović, D. Krstić, E. Michaś-Majewska, K. Tymińska, A. Benali, R. Bouwman, A. McCann, K. Hürkamp, F. Fioroni, Monte Carlo study of the eye lens exposure of medical staff administering Sc-47 and Cu-67 labelled radiopharmaceuticals, Physica Medica, 137, 2025, 105077, https://doi.org/10.1016/j.ejmp.2025.105077

6 Coordination chemistry

KIT-INE performs coordination chemistry studies in solution related to actinide separations by solvent extraction. These studies address the interactions and the speciation between actinide ions (and other ions) and ligands potentially useful for separating actinides and other metal ions. Recent activities involve solvent extraction and spectroscopic studies with a variety of ligands (see Fig.).

A. Geist, U. Müllich, P. J. Panak, R. Polly, T. Sittel, J. Stracke

In co-operation with:

G. Baruth,[a] K. Becker,[a] M. Maag,[a] P. Weßling,[a] G. Modolo,[b] F. Sauerwein,[b] A. Wilden[b]

[a]Heidelberg University, Institute of Physical Chemistry, Heidelberg, Germany; [b]Forschungszentrum Jülich GmbH, Institut für Fusionsenergie und Nukleare Entsorgung (IFN-2), Jülich, Germany

Introduction

In recent years, our primary research focus has been *f*-element coordination chemistry, with particular emphasis on actinide coordination chemistry. We use a complementary set of experimental methods, including nuclear magnetic resonance spectroscopy (NMR), time-resolved laser fluorescence spectroscopy (TRLFS) and solvent extraction experiments. These methods have proven highly efficient for analyzing and describing the coordination chemistry of trivalent *f*-element ions. Moreover, this approach can be extended to other elements of the periodic table, such as alkali metals, which are of importance in the context of nuclear waste disposal.

Solvent extraction is a highly selective and versatile method to separate metal ions. An organic phase containing an extracting agent (*i.e.* a lipophilic complexing agent) is brought into contact with an aqueous phase containing metal ions. The extracting agent forms hydrophobic complexes with selected metal ions, transferring them into the organic phase, while metal ions that do not form complexes remain in the aqueous phase. N-donor ligands such as bis-triazinyl-bipyridines (BTBP) efficiently separate trivalent actinide ions from trivalent lanthanide ions.[1,2] Using a similar strategy, calix[4]arene crown-ethers are known to efficiently separate radiocesium from spent nuclear fuel.[3]

A molecular understanding of extraction processes requires detailed knowledge of coordination chemistry in solution. To achieve this, we combine TRLFS and NMR. TRLFS is used to determine complex stoichiometries, thermodynamic parameters, and stability constants of Cm(III) and Eu(III) complexes. NMR provides insight into metal-ligand interactions, molecular structure and speciation of *f*-element complexes. For example, TRLFS studies have demonstrated that Cm(III) forms complexes with N-donor ligands that show stability constants up to two orders of magnitude higher than those of the corresponding Eu(III) complexes, while NMR investigations further elucidate the nature of these interactions.

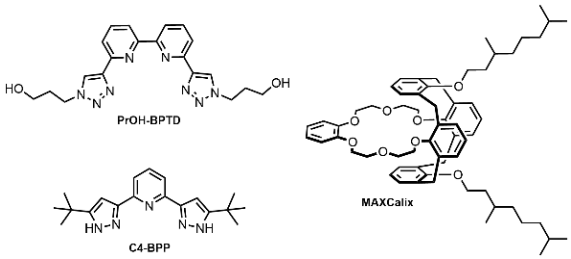

Fig. 1: Ligands studied, PrOH-BPTD, C4-BPP, and MAX-Calix.

Extraction studies for An(III)/Ln(III) with hydrophilic PrOH-BPTD

In EURATOM programs, several solvent extraction systems have been developed to separate minor actinides, with a particular focus on Am(III). One such system is the AmSel process, in which Am(III), Cm(III) and Ln(III) are co-extracted into an organic phase containing the extracting agent TODGA. In a subsequent step, Am(III) is selectively back-extracted from the organic phase using a dedicated complexing agent. One suitable complexing agent is PrOH-BPTD.[4]

Fig. 2 presents the distribution ratios of Am(III), Cm(III) and the light lanthanides (La–Eu) as a function of nitric acid concentration. For all metal ions, the distribution ratios increase with increasing HNO_3 concentration, indicating a solvating extraction mechanism consistent with the formation of $[M(TODGA)_3]^{3+}$ complexes in the organic phase. Effective Cm(III)/Am(III) separation requires a distribution ratio $D_{Am} < 1$ and $D_{Cm} > 1$. This condition is fulfilled in the nitric acid concentration range of $0.33\ M < [HNO_3] < 0.39\ M$. Within this window, the separation factor ranges from 2.0 to 2.3. In contrast to SO_3-Ph-BTBP studied earlier,[5] PrOH-BPTD contains only C, H, O, and N atoms, minimizing secondary waste generation.

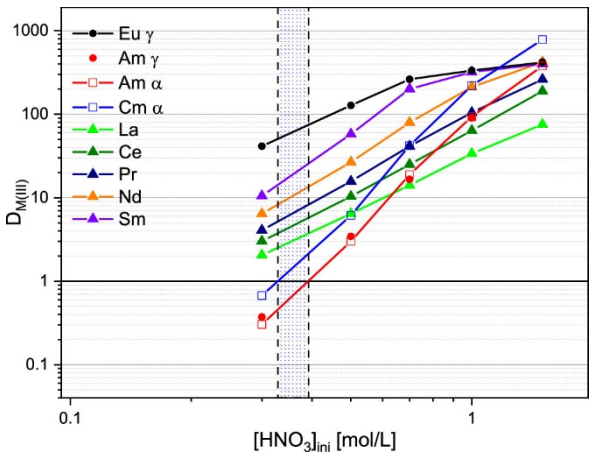

Fig. 2: Distribution ratios for the extraction of ^{241}Am(III), ^{244}Cm(IIII), ^{152}Eu(III), and La(III)–Sm(III) from solutions containing 0.04 M PrOH-BPTD in HNO_3 into 0.2 M TODGA dissolved in kerosene/1-octanol (5 vol %).[4]

This work has received funding from the European Research Council (ERC) under the European Union's Horizon 2020 research and innovation program (project PATRICIA, grant agreement no. 945077) and the German Federal Ministry for Research and Education (grant agreement nos. 02NUK059A, 02NUK059C, 02NUK059D).

TRLFS studies with hydrophilic PrOH-BPTD

The coordination chemistry of PrOH-BPTD is of fundamental interest. Accordingly, the complexation of Cm(III) and Eu(III) with this ligand has been systematically investigated using TRLFS. Fig. 3 shows the normalized emission spectra of Cm(III) as a function of ligand concentration. In the absence of PrOH-BPTD, the emission spectrum corresponds to the Cm(III) aquo ion. Upon addition of the ligand, a bathochromic shift of the emission band to 604.4 and 614.6 nm is observed. These emission bands are assigned to the formation of $[Cm(PrOH\text{-}BPTD)_n]^{3+}$ complexes, with n = 1–2.

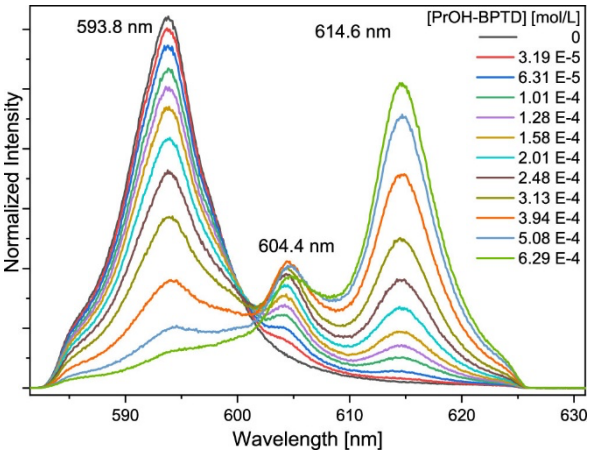

Fig. 3: Normalized Cm(III) emission spectra of the complexation of Cm(III) with PrOH-BPTD in 10^{-3} M $HClO_4$.[4]

As highlighted in Fig. 2, PrOH-BPTD shows pronounced selectivity for An(III) over Ln(III) ions. Therefore, the investigation of Eu(III) complexation with PrOH-BPTD is also of considerable interest. In this case, only a 1:2 complex is formed, as supported by slope analysis and lifetime measurements.

The corresponding stability constants are summarized in Table 1. PrOH-BPTD forms stronger complexes with Cm(III) than with Eu(III), consistent with the observed separation of Cm(III) and Eu(III) in solvent extraction experiments.

Table 1: Comparison of the stability constants log β of Cm(III) and Eu(III) complexes with PrOH-BPTD.[4]

$[M(PrOH\text{-}BPTD)_n]^{3+}$	log β_1	log β_2
Cm(III)	3.0 ± 0.1	6.7 ± 0.3
Eu(III)	–	6.2 ± 0.4

Cesium separation from brine solutions by extraction

A wide range of elements are produced during the nuclear fission of uranium and plutonium. Among the most significant fission products is ^{137}Cs, which may be present in considerable amounts in low- to intermediate-level nuclear waste. In this context, the development of potential effective decontamination strategies for concentrated chloride brines is investigated.

Fig. 4 shows Cs(I) distribution ratios for its extraction from various chloride salts into MAXCalix as a function of chloride concentration. Na(I), Mg(II), and Ca(II) are not co-extracted. In contrast, K(I) competes with Cs(I) extraction, which is expected given the strong affinity of 18-crown-6 ethers for K(I) ions. NH_4^+ behaves similarly.

As summarized in Table 2, Cs(I) is selectively extracted from mixed brine solutions containing Mg(II), Ca(II), Na(I), and K(I), with D_{Cs} values between 4 and 6, and excellent selectivity over K(I), Na(I), Mg(II), and Ca(II). The separation factors for Cs(I) over the other metal ions, *SF*, range from 10^2 to 10^4.

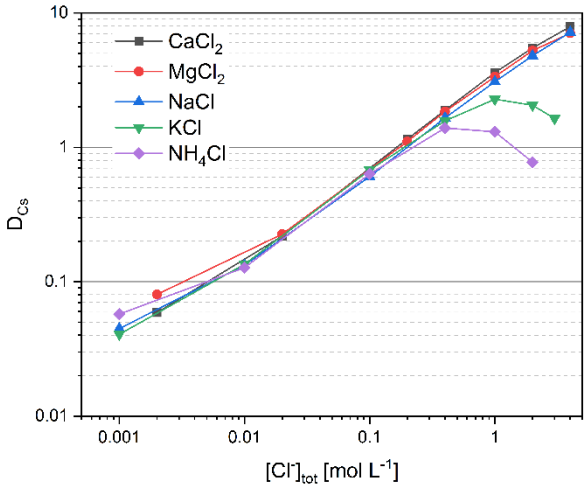

Fig. 4: Cs(I) distribution ratios as a function of the chloride concentration in presence of Na(I), K(I), Mg(II), Ca(II) and NH_4^+. 0.05 M MAXCalix in 1-octanol/kerosene 75/25%v.[6]

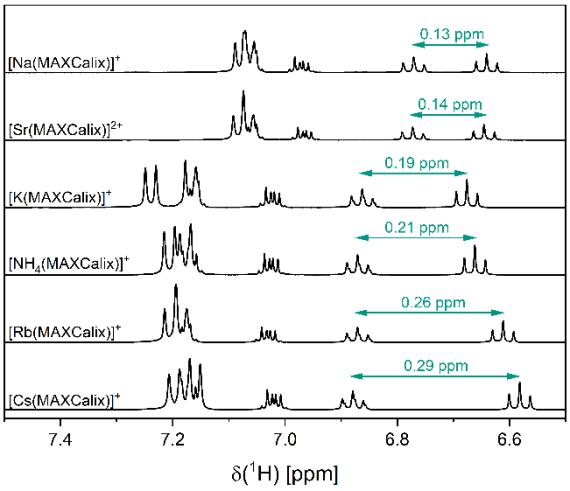

Fig. 5: ^{1}H-NMR spectra of the aromatic region of various $[M(MAXCalix)]^{n+}$ (M = Cs, Rb, NH_4, K, Sr, Na) complexes.[7]

Table 2: Distribution ratios *D* for the extraction of Cs(I), Mg(II), Ca(II), Na(I), and K(I) from mixed brine solutions S1 and S3 into MAXCalix in 1-octanol/kerosene 75/25 %vol. [MAXCalix] = 0.05 M, $[Cl^-]_{tot}$ = 4.45 M, pH_m = 3, A/O = 1:1.[6]

	S1	S3	*SF*
D_{Cs}	5.71	4.72	
D_{Mg}	0.0004	–	10^4
D_{Ca}	–	0.0002	10^4
D_{Na}	0.0033	0.0016	10^3
D_{K}	0.038	0.031	10^2

Overall, these results enabled proposing a robust laboratory-scale extraction procedure for the efficient separation of radioactive Cs(I) from concentrated brine solutions. While the process is somewhat sensitive to the presence of K(I), it shows substantial tolerance toward other alkali and alkaline earth metal ions, which is essential given the variable composition of potential feed solutions.

Speciation study in the MAXCalix system using NMR

Above observations appear counterintuitive given the well-established coordination chemistry of 18-crown-6-ethers, highlighting a gap in the understanding of their interactions with chemically related ions. This underscores the need for a systematic and comprehensive study of the coordination behavior of MAXCalix.

As shown in Fig. 5, MAXCalix efficiently coordinates large ions such as Cs(I) but also forms complexes with smaller ions, including Na(I), demonstrating the versatility of the ligand. Complex formation induces pronounced changes in the chemical shifts of both the aromatic and crown ether regions in the ^{1}H NMR spectra. In the Cs(I) complex, most aromatic signals shift downfield, except for one triplet. As a result, the chemical shift difference between the aromatic protons of the calix[4]arene backbone increases to 0.29 ppm. This indicates a substantial redistribution of electronic density between the metal-facing and metal-opposing rings of the 1,3-alternating calix[4]arene, suggesting the presence of π-interactions between the metal-facing benzene rings and the cation. In the crown ether region, significant changes in signal multiplicity, relative to the free ligand, point to a conformational rearrangement of the crown ether substructure. In contrast, complexation with Sr(II) results in comparatively minor shifts in the aromatic region, while more pronounced effects are observed in the crown ether region. Here, the triplet signals shift downfield relative to the free ligand, indicating a different crown ether conformation in the Sr(II) complex. Overall, a clear correlation between ionic size and complexation emerges from these observations.

Additional structural insight was obtained through quantum chemical calculations. Representative structures of Cs(I), K(I) and Ra(II) complexes are shown in Fig. 6. In the Cs(I) complex, the cation is located within the plane of the 18-crown-6 moiety and is nearly symmetrically coordinated by the crown ether oxygen atoms. A top-view perspective reveals that the Cs(I) ion is slightly displaced beneath the calix[4]arene rings, suggesting possible π-interactions between the benzene rings and the cation. Furthermore, the terminal benzene ring tilts out of the coordination plane, indicating substantial ligand reorganization to accommodate the metal ion.

The K(I) complex shows similarities to the Cs(I) complex but displays a more pronounced distortion of the crown ether substructure. The terminal oxygen atoms and the terminal benzene ring are significantly tilted, leading to a half-boat conformation. This distortion shifts the K(I) ion above the coordination plane, while it remains slightly beneath the calix[4]arene framework, resulting in preferential interaction with a single benzene ring.

Substituting alkali metals with alkaline earth metal ions leads to more drastic structural changes. In the Ra(II) complex, the crown ether adopts a twisted conformation, and the terminal benzene ring is rotated nearly 90° relative to the coordination plane. Although the Ra(II) ion remains close to the coordination plane,

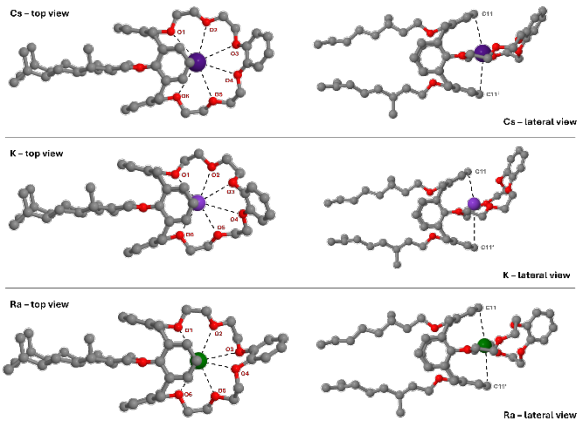

Fig. 6: Top and lateral view of the DFT-optimized structures of $[M(MAXCalix)]^{n+}$ complexes (M = Cs(I), K(I), Ra(II)). Hydrogen atoms are omitted for visual clarity.[7]

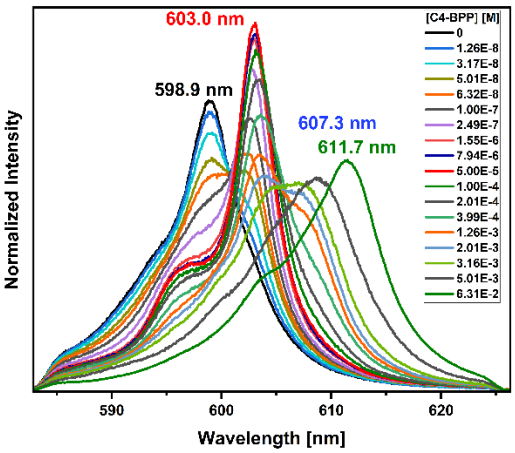

Fig. 7: Normalized fluorescence spectra of Cm(III) in methanol containing 1.5 vol % water as a function of the C4-BPP concentration.[9]

it is drawn further towards the underside of the calix[4]arene framework compared to the Cs(I) and K(I) complexes.

Based on these representative examples, two distinct structural subtypes can be identified. Subtype I features an almost planar crown ether substructure and includes complexes of Na(I), K(I), Rb(I), Cs(I), and Fr(I). Subtype II is characterized by a twisted crown ether substructure and is formed by Sr(II), Ba(II) and Ra(II). The results presented here complement existing structural and theoretical studies on Cs(I) complexation with calix[4]crown ethers. Furthermore, they provide a foundation for improving established extraction protocols or developing new strategies for radionuclide decontamination and related applications.

This work was funded by the German Federal Ministry for Research and Education (grant agreement No. 02NUK059A, 02NUK059C).

An(III)/Ln(III) complexation studies with C4-BPP

Variations in the side chains lead to pronounced differences in extraction behaviour.[8] While these effects can be partly attributed to steric factors, the specific influence of side-chain architecture remains insufficiently understood. Consequently, systematic studies employing structurally and electronically modified ligands are required to address these questions. This work deals with the synthesis of a new 2,6-substituted (1H-pyrazol-3-yl)pyridine derivative and the question how modifications of the side moieties affect complex stability, speciation and selectivity.

TRLFS was used to investigate the speciation of Cm(III) and Eu(III) with C4-BPP in solution. Cm(III) was dissolved in methanol containing 1.5 vol.% water and the concentration of C4-BPP was gradually increased. The corresponding normalized emission spectra are shown in Fig. 7. In the absence of C4-BPP, the solvent spectrum of Cm(III) shows an emission band at 598.9 nm. Upon increasing the C4-BPP concentration, a bathochromic shift of the emission band is observed, and three new emission bands appear at 603.0, 607.3 and 611.7 nm. These bands are assigned to the formation of $[Cm(C4\text{-}BPP)_n]^{3+}$ complexes with $n = 1–3$.

A comparison of the conditional stability constants of C5-BPP and C4-BPP reveals increasing deviations with higher coordination numbers. While the stability constants of the 1:1 complexes agree within experimental uncertainty, those of the 1:2 and 1:3 complexes differ by one and three orders of magnitude, respectively. In contrast to C5-BPP, which contains a neopentyl side chain, C4-BPP features a directly attached tert-butyl group. The observed differences originate primarily from increased steric strain within the complexes caused by the higher steric demand and limited conformational flexibility of the tert-butyl substituents. As the coordination number increases, steric hindrance between C4-BPP molecules becomes increasingly significant, leading to a pronounced decrease in overall complex stability. In the case of C5-BPP, this effect is mitigated by the additional methylene groups, which provide greater flexibility and reduce the effective spatial demand of the tert-butyl moieties.

Table 3: Stability constants of C4-BPP and C5-BPP for Cm(III) in methanol containing 1.5 vol % water.[9]

	$\log \beta_1$	$\log \beta_2$	$\log \beta_3$
C4-BPP	7.2 ± 0.4	10.1 ± 0.5	11.8 ± 0.6
C5-BPP	6.9 ± 0.2	11.2 ± 0.3	14.8 ± 0.4

To obtain further insights into the interaction of C4-BPP with Ln(III) and An(III) ions, a series of complexes was investigated using NMR. The complexes were characterized by ^{1}H-^{15}N HMQC. In comparison to the ^{15}N chemical shifts observed for the corresponding Ln(III) complexes, the Am(III) complexes show a pronounced upfield shift of approximately 270–280 ppm for the coordinating nitrogen donor atoms.

These large shifts cannot be explained solely by the paramagnetism of Am(III), as Sm(III), which has a comparable paramagnetic character, shows ^{15}N chemical shifts similar to those observed for the diamagnetic complexes. The pronounced upfield shift is therefore attributed to fundamental differences in the metal-nitrogen interaction. While bonding between An(III) ions and ligands is generally dominated by electrostatic interactions, the altered coordination behavior observed here suggests a higher degree of covalency in the Am(III)-N interaction.

This work was supported by the German Federal Ministry for Economic Affairs and Climate Action (BMUV) under contract number 02E11921B and the German Federal Ministry of Education and Research (BMBF) under contract numbers 02NUK059A and 02NUK059C.

References

1. P. J. Panak, A. Geist, *Chem. Rev.* **2013,** *113,* 1199–1236.
2. A. Geist, P. J. Panak, *Solvent Extr. Ion Exch.* **2021,** *39,* 128–151.

3. M. Simonnet, L. Muller, T. Sittel, P. Weßling, U. Müllich, A. Geist, P. J. Panak *Radiochim. Acta* **2023**, *111*, 597–600.
4. P. Weßling, M. Maag, G. Baruth, T. Sittel, F. S. Sauerwein, A. Wilden, G. Modolo, A. Geist, P. J. Panak, *Inorg. Chem.* **2022,** *61,* 17719–17729.
5. C. Wagner, U. Müllich, A. Geist, P. J. Panak, *Solvent Extr. Ion Exch.* **2016,** *34* (2), 103–113.
6. T. Sittel, K. Becker, A. Geist, P. J. Panak *Solvent Extr. Ion Exch*. **2024**, *42*, 118–132.
7. T. Sittel, K. Becker, R. Polly, U. Müllich, A. Geist, P. J. Panak *Chem. Eur. J.* **2025**, e202501065.
8. J. Stracke, P. Weßling, T. Sittel, P. Meiners, A. Geist, P. J. Panak *RSC Adv.* **2024**, *14*, 28415.
9. J. Stracke, P. Weßling, T. Sittel, C. Adam, F. Rominger, A. Geist, P. J. Panak, *Inorg. Chem.* **2024**, *63*, 13214-13222.

7 Deconstruction and decommissioning of conventional and nuclear buildings

In Germany, the last nuclear power plants in operation were finally shut down on 15.04.2023. After the operational use of the nuclear power plants, decommissioning and dismantling of the plants to a greenfield site follows. Depending on the size of the plant, dismantling of nuclear facilities is associated with costs of around 1 billion euros and takes 10 - 15 years. [1] In conjunction with the research reactors, dismantling in Germany will take many more decades and will therefore also require skilled workers.
A very high proportion of manual work is still required for technical dismantling and very little automation, digitalization and robotics are available. This is where the present research work comes in. The focus of the R&D work is on digitalization, the modelling of nuclear power plants with Building Information Modeling (BIM) and the adapted and coordinated dismantling. Individual processes are being optimized and new technologies are being developed and patented. These processes are integrated into the digital dismantling chain in order to minimize manual work and to digitize and automate data processing. In cooperation with other research departments, processes are being developed to reduce waste volumes and increase recycling volumes. Projects are being carried out at European level to provide further training and maintain skills as well as firmly establishing these topics nationally in lectures of KIT. The R&D work is carried out in close cooperation with industry, so that junior staff are introduced directly into practice during their doctorate.

Reference

[1] Bavarian State Ministry for the Environment and Consumer Protection (year unknown):„FAQS zum Rückbau von Kernkraftwerken“, online at: https://www.stmuv.bayern.de/themen/reaktorsicherheit/stilllegung_abbau/faq.htm, accessed on 23.10.2025.

7.1 Digital twins and ontology for robot assisted decommissioning operations

J. Ridao Cabrerizo
In co-operation with:

Technical Research Centre of Finland Ltd. (VTT); Institute of Energy Technology (IFE); Wai.blue; SPIX Industry; Centre d’Etude de l’Energie Nucléaire (SCK CEN); Autorité de Sûreté Nucléaire et de Radioprotection (ASNR); iUS GmbH consultants & advisors; CATENDA AS; Université de Strasbourg (Unistra); Amphos 21 consulting SL

Introduction

Dismantling and Decommissioning (D&D) is a necessary step for facilities reaching the end of their life cycle. This is the case for many nuclear facilities worldwide that are being shut down in the coming years. However, data may be incomplete or missing in the case of facilities that were built several decades ago. The lack of historical information – operational records, original designs… – represents a challenge for nuclear decommissioning projects, so current and reliable data must be acquired and digitized to make it available to the different stakeholders that participate in D&D tasks.

The project DORADO (Digital twins and Ontology for Robot Assisted Decommissioning Operations) [1], funded by the Euratom (European Atomic Energy Community) program between September 2024 and August 2027, brings together 12 partners from 8 European countries. During 36 months, the partners are combining different technologies around a dedicated nuclear decommissioning ontology using the DORADO platform. Following the footsteps of PLEIADES [2], a previous Euratom project in which a digital platform was created but software integration was just started, the consortium aims to go further with next steps: expanding the coverage of the supported ontology and supporting decommissioning planning activities, as well as continuing the development of the ontology and the API (Application Programming Interface). Therefore, eight new technologies will be integrated into the server: sensor data mapping with temporal dimension; environment data comparison against BIM (Building Information Modeling); point-cloud and 3D model change detection; digital twins based ALARA (As Low As Reasonably Achievable) dose estimation; server-based integration with IFC (Industry Foundation Classes) file format and extended data queries; mission control, robot route optimization; human-to-system smart voice assistant interface; and standardization using the common ontology. Many of these technologies may be connected to involve AI (Artificial Intelligence), robotics, and sensor networks.

In Work Package 4, led by KIT, technologies will be linked to demonstrations using data from real use cases. Therefore, the DORADO platform will use different data formats: point clouds, historical photogrammetry, dose rate survey, 3D models, robot data as LiDAR, RGB-D (Red Green Blue-Depth), SLAM,

inventory data, etc. This data may come from the Halden Research Reactor (HRR) in Norway, the Otaniemi Research Reactor (FiR1) in Finland, and the Belgian Reactor 3 (BR3) in Belgium, among others.

The DORADO consortium is inviting all interested stakeholders in D&D projects (operators, regulators, technological experts...) to join the end users group. The value for the end users is the opportunity to increase their understanding on each technology and hence, gain a better understanding on how these technologies can be used in their own business. This may include the use of the technologies, benefits, applications, and many other aspects in order to support nuclear decommissioning projects.

References

[1] https://dorado-project.eu/

[2] https://pleiades-platform.eu/

[3] A. Räty, J. A. Ridao, O. Zahra, P. Honkamaa, D. Daniska, S. Gentes: DIGITAL TECHNOLOGIES IN EUROPEAN NUCLEAR DECOMMISSIONING PROJECTS. 51st Annual Meeting of the Spanish Nuclear Society (Cáceres, 24.09.2025 – 26.09.2025)

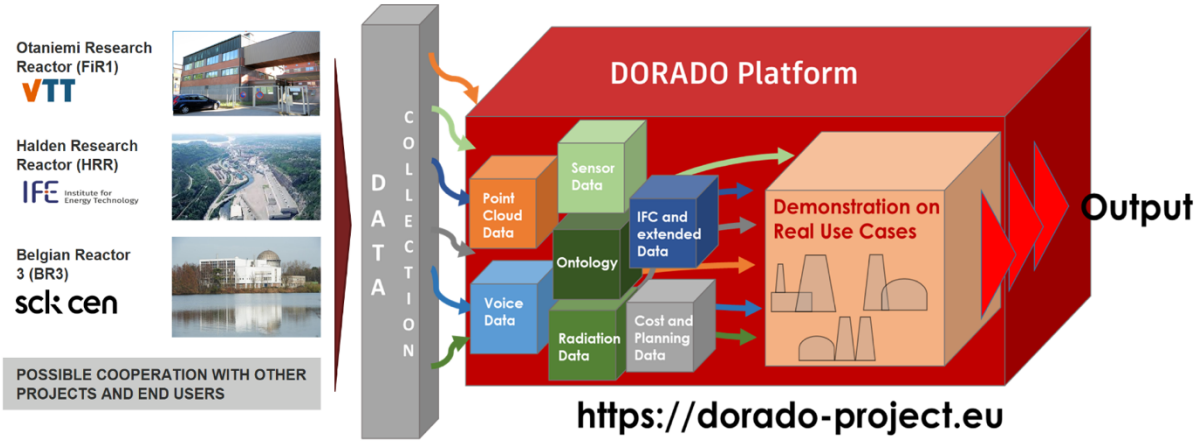

Fig. 1: Demonstrations on real use cases

7.2 Visualization of trouble spots for decontamination work and decision measurements with the help of BIM

M. Müßle, K. Clintworth

Introduction

Following the shutdown of a nuclear power plant, the operator is obliged to dismantle the plants. In order to be able to remove plant components from nuclear power plants and release them in accordance with the Radiation Protection Ordinance, their activity must be below a limit value. Typical nuclear power plants in Germany have 100,000 m² to 450,000 m² of concrete surfaces [1] that need to be processed for clearance.

An accurate acquisition of the spatial data, in particular all surfaces as well as the disturbing objects contained therein, such as anchor plates under the decontamination coating or pipe penetrations, is essential for the planning and execution of the decision measurements. Currently, spatial data acquisition is done manually. This means that no digital building models or similar data are available for the further procedural steps.

The aim of the "Visualization of trouble spots for decontamination work and decision measurements with the help of BIM" (ViSDeMe) project, which was funded by the German Federal Ministry of Research, Technology and Space (BMFTR), is digital recording and visualization of building structures with various disturbing objects in nuclear facilities with the help of Building Information Modeling (BIM). In the project, a Scan2BIM process was developed, starting with recording of the premises including all relevant trouble spots, evaluation and analysis of the collected data and visualization in a digital model (see figure 2).

For every step of the Scan2BIM process, digitalization methods were investigated and partly methods of automation have been developed. The focus of the research project was on the localization of the trouble spots in the premises to be released, including visually invisible or barely visible anchor plates, which are hidden under the decontamination coating and the exact location of these in the digital model. Visible objects were recorded by laser scanning together with the rooms themselves. In order to capture hidden objects several measuring techniques have been tested, with active thermography proving to be the most suitable. Fused data from laser scanning and thermography served as a basis for creating the 3D building model and for automated data analysis. In this step, all relevant disturbing objects, have been extracted from the data by means of AI and Computer Vision methods. In the last step, algorithms were developed to integrate all extracted objects automatically into the building model. Based on this integrated model, the planning of decontamination works and decision measurements can be carried out digitally.

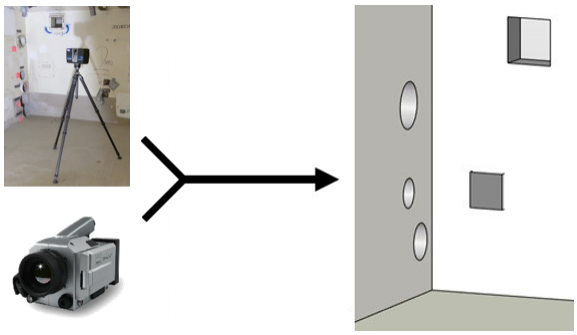

Fig. 2: Scan2BIM process: data recording → BIM model (© ViSDeMe joint project, 2024)

Digitization of the process, among other things, reduces the effort required for spatial data acquisition as well as the execution and documentation of decontamination work and decision measurements for users in nuclear facilities. By digitizing the entire process of spatial data acquisition and measurement planning or at least relevant process steps, resources and costs as well as the radiation exposure of personnel can be reduced. In addition, the susceptibility to errors in data collection and documentation can be reduced.

The process is being investigated and evaluated in cooperation with the project partner RWE Nuclear GmbH using the example of the power plant in Mülheim-Kärlich.

The research project ViSDeMe was funded by the BMFTR and listed under the sponsoring number 15S9435A. The research project ran from July 2022 to September 2025. Building on the findings and results of the ViSDeMe project, the ViMPoG project, which is also funded by the BMFTR, started in October 2025. The aim is to improve and expand the developed methods in order to support the entire clearance process.

References

[1] Gentes, S.; Aminy, A.; Gabor, N.; Reinhardt, S.: Internationale Rückbautechniken und Managementmethoden für kerntechnische Anlagen - Eine wissenschaftliche Analyse aufbauend auf dem internationalen Stand der Technik (IRMKA). Final report of the research project with the funding code: 02S8851, 2015.

7.3 Validation of a continuous magnetic filter and sieving system for the treatment of particulate mixtures

Introduction

While the projects DORADO and VISDEME focus on digitisation, the KOMASI project (Validation of a continuous magnetic filter and sieving system for the treatment of particulate mixtures) aims to reduce waste during decommissioning. In the decommissioning of nuclear facilities, dismantling of the reactor pressure vessel and its internals poses a major challenge. One dismantling method that offers many technical and radiation protection advantages over other methods is water abrasive suspension cutting (WASS). In this process, water and abrasive are brought into suspension at high pressure, pushed through a nozzle and directed on the material to be cut. This process generates large quantities of radioactive secondary waste, which leads to very high disposal costs. A separation plant has been developed for use in the nuclear sector to significantly reduce the amount of radioactive secondary waste. The separation plant is based on a special sieving process combined with magnetic filtration, which allows intact abrasive particles to be re-introduced into the cutting process and reused. [1]

The separation units were subjected to experimental investigations involving the sieving component and the magnetic filter. The scientific and technical results of these investigations are summarised below. Initially, separation tests were carried out in the batch mode. The tests with the magnetic filter were evaluated on the basis of the separation efficiency of the steel and the steel concentration in the reusable abrasive. For sieving, the focus was on the removal of small particles, smaller than the mesh size. The percentage of these particles was considered as sieving error. During sieving with a mesh size of 150 µm, separation efficiencies of approximately 97% were achieved with a steel concentration of the reusable abrasive of approximately 0.03–0.06 % by mass. During separation with 250 µm, a separation efficiency of approx. 99 % and a steel concentration of less than 0.01 % by mass of the reusable fraction were achieved. In all separation tests, the sieve error of the undersize particles was less than 7 % by mass. [2,3,4]
The plant was then modified for continuous operation. The flow chart was modified and individual components (sieve and magnetic filter) were redesigned.

Figure 3 shows the newly developed sieve. The sieve error in continuous operation with a mesh size of 180 µm was less than 5% by mass.
In Figure 4, the newly developed and patented magnetic filter is shown. The magnetic filter consists of a pipe divider, referred to as an r-divider. This r-divider consists of a pipe section in which the suspension passes through the magnetic filter and a separator pipe filled with a stationary liquid. The magnetic rods move along the pipe section and the inner side of the curved separator pipe. As the particle suspension flows through the pipe section, it passes through the magnetic field of the magnetic rods. This causes the magnetic particles to be attracted by the magnetic field. These particles are then discharged into the separator pipe by the rotation of the magnetic rods. To determine the separation efficiency, tests were carried out with this magnetic filter using only steel particles. Figure 4 c) shows the reduction in steel particles over time. A comparison of this result with the theoretical results shows that the magnetic filter can filter between 0.5 and 1 % of the steel particles in a single pass. [4]

References

[1] Heneka, Alexander, et al. “A new technical approach for the minimization of secondary waste produced by water abrasive suspension cutting during disassembling of nuclear facilities.” atw Vol. 66, Januar 2021: 37-42.

[2] Heneka, Alexander. “Abrasivaufbereitung aus dem Wasser-Abrasiv-Suspeneka, Alexanensionsschneideverfahren mittels Nasssiebung und Magnetseparation.” Karlsruhe, 2024.

[3] Becker, Frank, et al. Magnet-Seperation von Korngemischen zur Minimierung von Sekundärabfällen im Rückbau kerntechnischer Anlagen (MaSK), Magnetic separation method for the reduction of secondary waste from the water abrasive suspension cutting technique (MaSK). Abschlussbericht, Karlsruhe: Karlsruher Institut für Technologie, 2019.

[4] Heneka, Alexander, M. J. Chaudhry, Sascha Gentes and Carla Olivia Krauß. Nasssiebung und Magnetseparation von Korngemischen zur Minimierung von Sekundärabfällen im Rückbau kerntechnischer Anlagen. Abschlussbericht, Karlsruhe: Karlsruher Institut für Technologie, 2022.

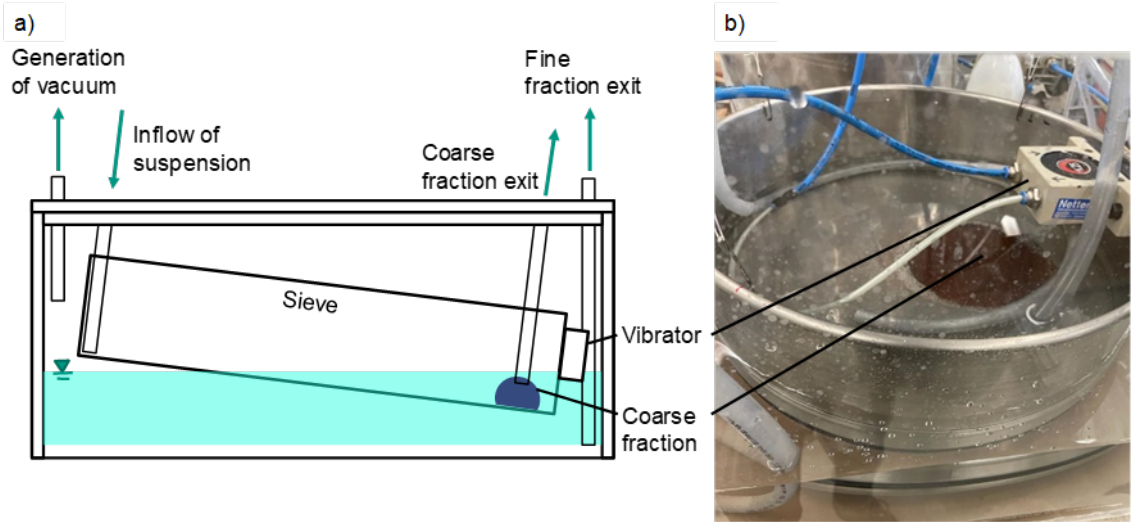

Fig. 3: a) Functional principle of the continuously operating sieve. b) Photograph of the sieve (© KoMaSi, 2024)

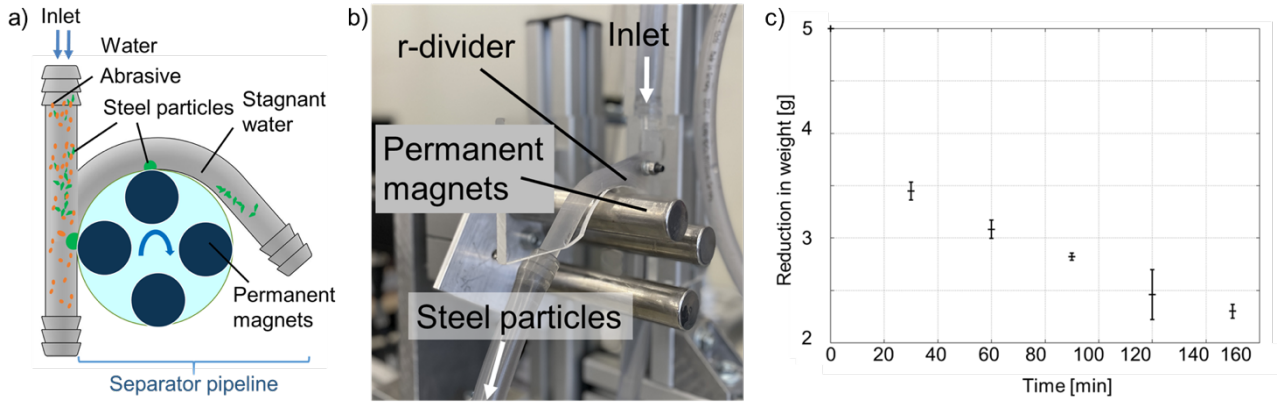

Fig. 4: a) Technical implementation of the magnetic filter b) Photograph of the magnetic filter c) Decrease in steel particles in grams plotted against time in minutes (© KoMaSi, 2024)

8 Development of radionuclide speciation methods

Developing and maintaining a state-of-the-art portfolio of radionuclide speciation tools encompassing surface science and spectroscopy methods is an important R&D activity at INE, as these methods are indispensable for advancing our understanding of radionuclide (geo)chemistry or the behavior of nuclear waste forms under different storage conditions. Radionuclide speciation methods available at INE's controlled area laboratories and the ACT and INE-Beamline stations at the KIT Light Source are continuously adapted to serve the requirements of *in house* and HGF/NUSAFE R&D programs or national and international cooperation partners. A major effort during the reporting period was the complete redesign and reconfiguration of the ACT experimental station within the 'NEXT' project (NEXT generation probe of chemical bonding properties of actinides and lanthanides). The new instrument offers improved capabilities for high-resolution X-ray emission spectroscopy (e.g., HR-XANES, RIXS, NIXS) in the tender to hard X-ray regime and for conventional hard X-ray XAFS (cf. section 8.1). The Helmholtz research and technology platform HOVER enabled us to expand INE's method portfolio by two major, state of the art instruments for surface and bulk analysis (cf. 8.3). To serve the former application field, a focused ion beam scanning electron microscope (Zeiss FIB-SEM, model CrossBeam 350 KMAT) with integrated laser ablation module was procured and commissioned in the new HOVER microscopy lab. The FIB-SEM features energy dispersive X-ray spectrometry (EDS), the detection of electron backscattering diffraction patterns (EBSD) and a workflow for the production of TEM lamellae. Capabilities in the latter area have been significantly strengthened by the installation of a Zeiss Xradia 620 Versa X-ray microscope in the same lab, enabling 3D micro-tomography of bulk objects with a theoretical resolution down to 400 nm. In a different low-resolution optics configuration, larger samples like drill cores up to 200 mm diameter and 100 mm height with a weight up to 25 kg can be scanned. Accelerator mass spectrometry is applied by INE researchers in a broad variety of ultra-trace level experiments to study migration or retention of radionuclides in engineered barrier systems, crystalline and clay host rock or environmental samples (cf. 8.3). In a recent study, AMS contributed to the determination of soil/porewater partitioning coefficients in lysimeter experiments mimicking the transport and transfer behavior of long-lived radionuclides possibly released from an underground repository along the groundwater – soil – plant chain. Another study has focused on the multi-actinide analysis in seawater samples collected in the vicinity of the La Hague nuclear fuel reprocessing plant. Computational chemistry methods are assisting and increasingly complementing experimental investigations at INE in the fields of nuclear waste disposal and fundamental radionuclide studies (cf. 8.4). Recent projects highlighted in this report have been focusing on molecular dynamics (MD) simulations of the bonding of trivalent lanthanides and actinides at C-S-H surfaces, the use of *ab initio* methods to describe the speciation of Tc(IV)-gluconate complexes and the calculation of core-excited states probed at the U $M_{4,5}$ manifold of uranyl.

8.1 Development of spectroscopic radionuclide speciation methods

K. Dardenne, N. Finck, T. Hippel, T. Platte, T. Prüßmann, J. Rothe, B. Schacherl, A. Skerencak-Frech, T. Vitova

Introduction

Spectroscopic speciation techniques for radioactive materials belong to INE's key assets to secure *in situ* molecular scale structural information on radionuclides (Rn - i.e., actinides (An) or fission and activation products) in solid and liquid phases or at surfaces. In this section the term 'speciation' is applied in the sense of determining Rn physicochemical states (encompassing both electronic bonding states and molecular structures). The applied spectroscopic speciation methods have in common that they are based on deciphering the effects of the interaction of electromagnetic waves (i.e., photons) with the Rn electronic shell in a wide energy range - from the infrared over the visible light to the ultraviolet and X-ray regime (thus exciting different electronic levels of the molecular systems or solids). Next to laboratory techniques like IR and Raman spectroscopy or UV-Vis absorption, which are common in many branches of chemical analysis (adapted to specific sample environments and safety protocols for handling radioactive specimens), INE applies technically more demanding, partially home-built speciation methods, notably laser (visible, UV) and synchrotron radiation (tender to hard X-rays) based absorption and emission spectroscopies.

The 'INE-Beamline for radionuclide science' at the KIT Light Source (KARA electron storage ring) had its 20th anniversary as a flexible experimental platform for X-ray based Rn speciation investigations in 2025. The hard X-ray beamline 'CAT-ACT' for CATalysis and ACTinide research was commissioned at an adjacent beam port in 2016. Both the INE-Beamline and ACT experimental stations are licensed to handle radioisotopes with activities up to one million times the (isotope specific) exemption limits, or 200 mg each of the fissile isotopes ^{235}U and ^{239}Pu. These stations are the only facilities of their kind in Europe offering direct access to onsite radiochemistry laboratories on the same research campus [1], primarily serving the INE/NUSAFE *in house* R&D program. Limited access by external cooperation partners (national and international) may be granted via individual agreements and service contracts or in the frame of the EURATOM/SNETP project OFFERR.

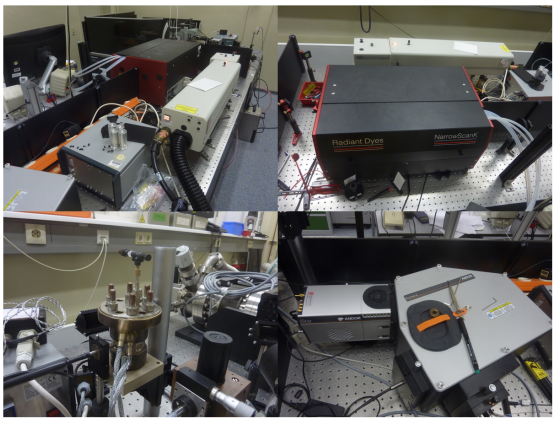

Fig. 1: TRLFS setup in the new laser applications lab.

Time-resolved laser fluorescence spectroscopy (TRLFS) is a method routinely applied at INE controlled area laboratories for the chemical speciation of Ln and An cations (e.g., Eu(III), U(IV), U(VI), Am(III) or Cm(III)) at trace level concentrations. Following excitation by pulsed laser light, Ln/An luminescence decay kinetics can be recorded on the ns to ms time scale. From the luminescence decay lifetime of aqueous complexes the number of water molecules in the first coordination sphere is derived, allowing to obtain structural information of the complex. In conjunction with the shift or splitting of the emission peaks, different Ln and An species present in the sample are discernible.

Reorganization of laser spectroscopy laboratories

Following the implementation of the new HOVER laboratory for surface and solid phase analysis at INE controlled area (cf. section 8.2), existing laboratories for laser absorption and TRLFS studies had to be partially reorganized. Method development activities have been bundled in a new laser applications lab (Fig. 1). The lab features a new Nd-YAG/dye laser source (Radiant Dyes NarrowScanK) variably coupled into different sample cells for ambient temperature measurements or cryo and high-T (up to 200° C) conditions. The detection system has been upgraded by a new Andor Kymera 328I-C spectrograph (4 optical gratings: 300, 900, 1200, 1500 l/mm) and a new Andor gen. 3 CCD camera with fast USB 2.0 connection. Additionally, the optical table has been fitted with a Nd-YAG driven setup optimized for optical uranium luminescence detection by the same spectrometer.

INE-Beamline and ACT: operation and upgrades in 2024/25

Due to limited funds for covering increasing electricity costs and the additional shortage of technical staff required for KARA operation, KIT Light Source availability in the remaining PoF-IV period has been limited to a maximum of 100 user and special user operation days per year. Note that beamtime at ACT amounts to 50% of the total annual UO days due to the sharing of the beamline optics for catalysis experiments at CAT station conducted by KIT-IKFT/ITCP.

As in previous years, INE *in house* and cooperative projects in the two-year period 2024/25 covered the investigation of a broad range of materials containing An, chemically homologue Ln or fission product species in the context of nuclear waste disposal safety research or basic radionuclide sciences. Projects conduced in responsibility of the new INE department "Advanced spectroscopy in f-element chemistry" (on average 52% in 2024 and 42% in 2025 of available beamtime at both stations) are separately covered in chapter 9 of this report.

Besides others, *in house* projects at INE-Beamline and ACT station included XAFS investigations of the retention mechanism of Nb(V) by calcite and carbonated cement paste, Sn K-edge XAFS to study the uptake of tin by cement systems, the speciation of Pu(III) in carbonate containing NaCl solutions, Ca K-edge µ-XANES and µ-XRF investigations of the speciation of Ca accumulated in bentonite contacting corroding steel, the speciation of Fe associated with bentonite at the corroding steel/bentonite interface by µ-XANES and µ-XRF, Fe K-edge XAFS for Fe speciation analysis in the presence of $CaCl_2$ in concentrated saline solutions, Pu L_3-edge and alkaline earth K-edge XAFS of solid phases forming in alkaline aqueous Pu solutions, Pu/Np L_3-edge XAFS to investigate Pu/Np-complexation by citrate and carbonate in aqueous solutions, U L_3-XAFS based speciation of U(VI)-NO_3 com-

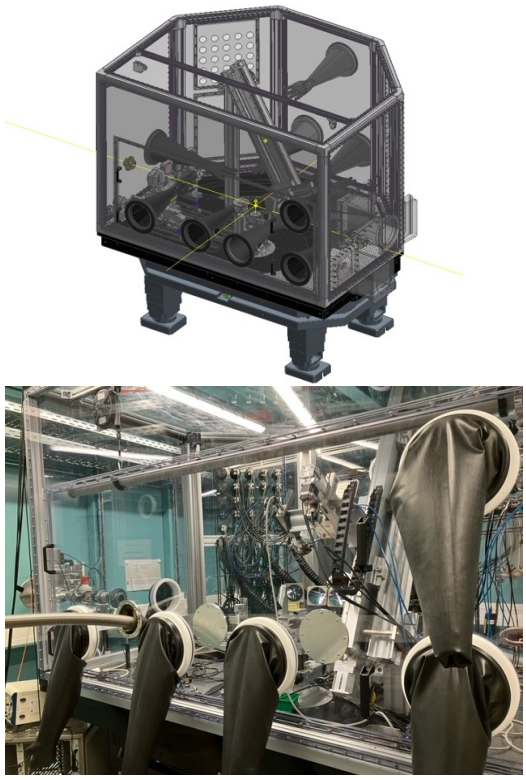

Fig. 2: top – 3D CAD drawing of the NEXT spectrometer implemented at the ACT station, bottom – photo taken during the commissioning of the new setup.

plexes in aqueous, highly concentrated electrolyte solutions – later on complemented by WAXS/total scattering measurements at ACT to derive pair distribution functions of local molecular environments, Fe, Cu and Zn K-edge µ-XANES and µ-XRF investigation of secondary phase formation and Cu diffusion within compacted bentonite upon copper corrosion, exploring the speciation of Fe(III) by Fe K-XAFS in silicon containing hyperalkaline electrolytes or the retention of Tc-99 by Fe(II) hydroxide and silicate solid phases based on Tc K-edge EXAFS.

An increasing number of Rn speciation projects relies on multi-edge studies conducted sequentially at both beamline stations - benefitting from the complementary energy ranges for EXAFS data and advanced spectral resolution in the tender X-ray regime. Noteworthy for the reporting period, these are a newly established cooperation between INE and PNNL (Washington State, USA) on the characterization of non-pertechnetate species in Hanford Tank Waste samples by combining Tc K- and L_3-edge XAFS or the investigation of Tc solid phases in the presence of EDTA and sorption on C-S-H phases.

Some of the aforementioned studies are presented in more detail elsewhere in this bi-annual report, see as well chapter 9 for high energy resolution X-ray emission spectroscopy applications.

Researchers and cooperation partners from the following German and international institutions conducted experiments at the INE-Beamline and ACT station in 2024/25:

- Joint Research Center Karlsruhe, European Commission
- PNNL, Washington State, USA
- EPFL Lausanne, Switzerland
- Helmholtzzentrum Dresden-Rossendorf, IRE, Germany
- Forschungszentrum Jülich, IFN, Germany
- TU Delft, The Netherlands

As in previous years, a considerable share of *in house* beamtime at INE-Beamline and ACT was spent for experiments conducted by internship, master and graduate students in the frame of their thesis work.

Within the ERC grant project 'The Actinide Bond' (cf. chapter 9), the entire reconfiguration of the ACT experimental station – termed the 'NEXT' project (i.e., NEXT generation probe of chemical bonding properties of actinides and lanthanides) – was implemented in 2023 summer shutdown and fully commissioned until 2024. The advanced 5-crystal HR-XES (high resolution X-ray emission spectrometer) setup features a custom-made (KIT-IBG-2) motorized (height, lateral position) support structure and an optimized inert gas box housing all spectrometer components (sample, analyzer crystal and detector stages) to provide all beam paths enclosed in He atmosphere for tender X-ray measurements, s. Fig. 2. Compared to the previous setup described in [2], the modified experimental station offers:

- a motorized rotation stage allowing for variable emission angles between 90° (standard) and 180° (backscattering) geometry,
- variable Rowland circle diameter (0.5 m – 1 m),
- faster and concerted positioning scans (e.g., for X-ray emission energy involving multiple axes) with new Phytron motion controllers,
- a pulley system for easy mounting and unmounting the vacuum tubing bridging the ACT station during CAT operation,
- optional installation of poly-capillary focusing optics.

The 180° backscattering position of the rotation stage and a detachable lid on the backside of the box give as well access to mounting positions for standard high energy XAS detection equipment.

I K-edge XAFS to study iodine retention by iron phases

The superconducting 2.5 T wiggler serving the CAT-ACT beamline delivers a sufficiently hard X-ray spectrum to reach K-edges of safety relevant nuclear fission products such as iodine (33.17 keV) or cesium 35.98 keV), which are often difficult to analyze at their shallower L-edges due to spectral overlap with matrix elements in waste forms or sorbent materials. A recent study on the retention of iodine by iron phases [3] has demonstrated the potential of such high-energy XAFS measurements.

Anoxic steel corrosion in a deep geological repository is expected to lead to the formation of various Fe (hydr)oxide phases (e.g., magnetite, ferrous hydroxychloride, green rust). The nature of these phases depends on parameters such as pH, E_h, temperature or the ion content of the contacting pore- or groundwater. Chloride green rust (GR-Cl) exhibits a permanent positive layer charge enabling retention of anionic fission product species such as $^{129}I^-$. The iodide uptake has been shown to strongly depend on the anion's concentration and that of chloride - competing with iodide for uptake - in the contacting water. The ability of GR-Cl to retain iodide as a function of pH_m and $[Cl^-]$, $[I^-]$ was systematically investigated, where sorption equilibria were achieved within a day of contact time between iodide and the preformed GR-Cl in suspension with an iodide adsorption coefficient R_d of 0.18 ± 0.05 kg/g in the pH_m range of 7.5−8.5. The I K-edge XAFS spectra in conventional I K_α fluorescence detection mode depicted in Fig. 3 have been recorded for GR samples prepared at varying pH_m and ionic strength conditions. The XANES spectra of all GR samples and that of the NaI(aq) reference are very similar, indicating the same oxidation state (-1) and short-range coordination environment of iodine. This implies that variations of pH_m or ionic strength have no influence on the iodine speciation. This result is corroborated by the analysis of the corresponding EXAFS data. Fit results confirm that iodine is surrounded by 6 O atoms at d(I−O) = 3.52(2) Å in all samples. According to these results, changes of

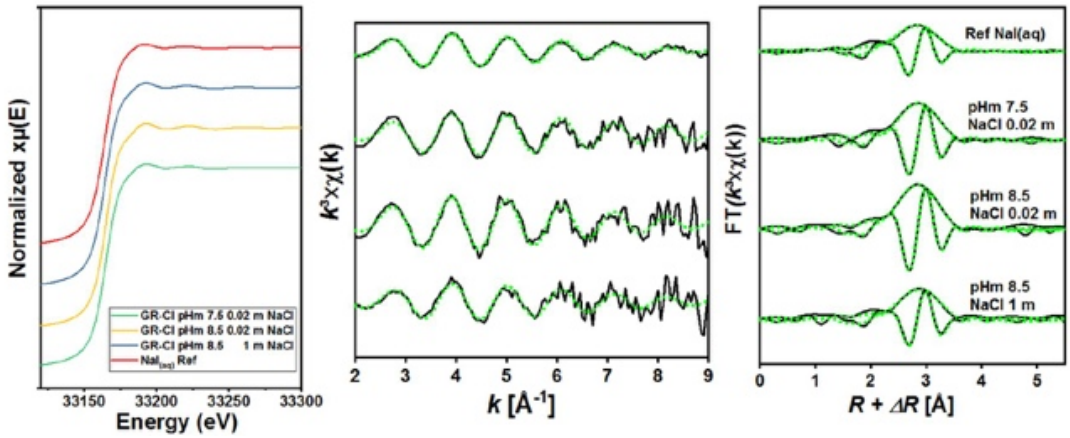

Fig. 3: Iodine K-edge XANES (left) and EXAFS (middle and right panel – experimental data plotted as solid black lines and fits as dashed green lines) of GR-Cl samples and a NaI(aq) reference (reproduced with kind permission from pubs.acs.org/est).

pH_m or ionic strength do not affect the hydration shell made of six water molecules binding iodide via H atoms to the positively charged GR-Cl layers. Overall, XAFS data are consistent with a weak electrostatic interaction with the Fe octahedral sheet, comparable to that reported in earlier studies of iodide uptake by formation of a GR-$Cl_{1-x}I_x$ solid solution [4].

References

[1] Rothe, J. et al., *Geosciences* **9**, 91 (2019).

[2] Schacherl, B. et al., *J. Synchrotron Rad.* **29**, 80 (2022).

[3] Platte, T. et al., *Environ. Sci. Technol.* **57**, 9376 (2023).

[4] Platte, T. et al., *Inorg. Chem.* **60**(14), 10585 (2021).

8.2 New instrumentation for surface and solid phase analysis

N. Müller, T. Prüßmann, D. Schild, A. Shelyug, F. Quinto, T.-Y. Lin, M. Herm, T. König, J. Rothe, H. Geckeis

Introduction

Helmholtz Association (HGF) research centers: Jülich Research Centre (FZJ), Helmholtz-Zentrum Dresden-Rossendorf (HZDR) and Karlsruhe Institute for Technology (KIT) cooperating in the NUSAFE consortium are implementing the laboratory infrastructure "HOVER" (Helmholtz Research and Technology Platform for the Decommissioning of Nuclear Facilities and for the Management of Radioactive Waste) since 2020 as a decentralized research infrastructure.

Within the HOVER project, waste form behavior and radionuclide migration in the near field of a repository with focus on deciphering the impact of material heterogeneity of real waste forms, geo-engineered barriers and host rocks are studied. Analyses on the centimeter to nanometer scale are enabled by combination of a new focused ion beam scanning electron microscope (FIB-SEM) and a 3D X-ray microscope. Features identified in samples by the X-ray microscope can be dissected inside the scanning electron microscope by laser ablation and/or focused ion beam milling followed by elemental and crystallographic characterization.

Focused Ion Beam Scanning Electron Microscope

With the recent upgrade capabilities for surface analytics at INE had been extended to correlated utilization of FIB-SEM - Zeiss model CrossBeam 350 KMAT, with integrated laser ablation module (Figure 1, A). The FIB-SEM consists of field emission gun and GEMINI 2 electron optical column (Figure 1, B), FIB column with focused Ga ion beam (Figure 1, C) and various detectors (Figure 1, D). The GEMINI objective lens generates a fine focused electron beam, with resolution of 0.9 nm at 15 kV and 1.7 nm at 1 kV without beam deceleration. Accelerating voltage ranges from 0.02-30 kV, beam current from 1 pA - 100 nA.

FIB-SEM operation

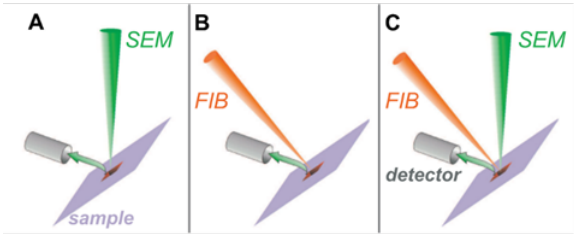

Fig. 2: Schematic representation of different imaging modes. (A) SEM imaging (scanning electron beam is active, high-resolution imaging), (B) FIB imaging (scanning ion beam is active, contrast imaging, defining milling patterns, grain analysis) and (C) CrossBeam operation: imaging by SEM and milling by Ga FIB.

Different imaging modes (detectors) are available to operate the microscope (Figure 2). Secondary electrons (SE) for imaging the sample surface and backscattered electrons (BSE) for imaging compositional/material contrast are measured by various detectors. An InLens and/or ESB detector inside the electron column is used at low working distances or during FIB milling. Electron transparent samples like TEM lamellae or particles on a TEM grid are imaged by a retractable STEM detector.

Femtosecond-laser module

Integrated femtosecond laser system enables to gain access to deeply buried structure and to prepare large cross-sections with minimal heat affected zones. The laser wavelength is 515 nm and pulse duration 350 fs at variable repetition rate in the range of 100 Hz to 1 MHz. The maximal pulse energy is 10 µJ at 1 MHz. Example of patterning is shown in Figure 3.

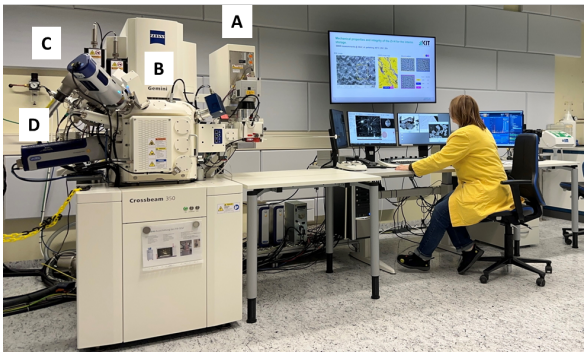

Fig. 1: New Zeiss FIB-SEM CrossBeam 350 KMAT at INE and its components: fs laser (A), GEMINI electron column (B), FIB gun (C) and EBDS detector (D).

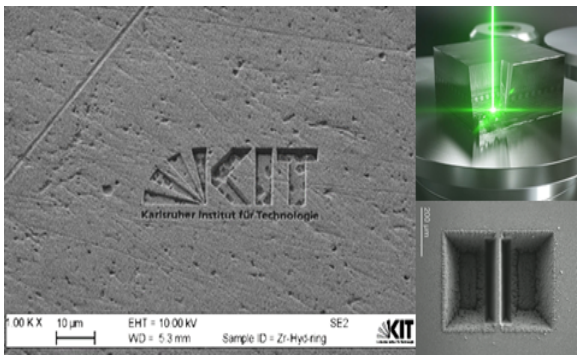

Fig. 3: Example of 515 nm fs-laser patterning.

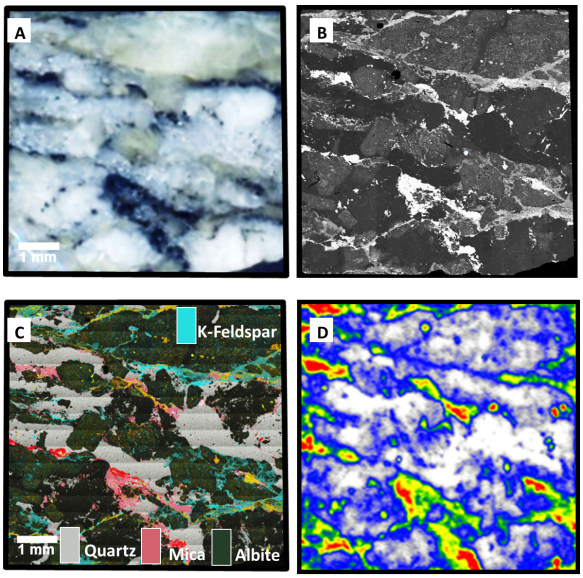

Fig. 4: SEM-EDS large area map (LAM). 238 individual maps are stitched with 1024 x 768 pixel each which corresponds to about 58 million spectra in total. Optical image (A), backscattering electron image (B), overlay of selected phases in false colours (C) and autoradiography image (D).

Energy dispersive X-ray Spectrometry (EDS)

Energy dispersive X-ray spectrometry (EDS) is performed by an UltimMax100 mm^2 silicon drift detector. X-ray spectral maps are recorded pixel-by-pixel resulting X-ray spectra over the sample area. Regions of similar spectra can be segmented to differentiate chemical phases present in the sample. Live chemical imaging of the distribution of elements allows interactive microscopy. SEM-EDS data acquisition and processing is done using AZtec 6.2 software by Oxfords Instruments.

As an example, a sample studied in the framework of EVIDENT project is shown in Figure 4. Here a 7 mm x 7 mm cross section of polished granodiorite crystalline rock from the Grimsel Test Site (Switzerland) was analyzed by SEM-EDS (Figure 4, A&B) and autoradiography (Figure 4, D) after being in contact with solution containing ^{241}Am. Combination of EDS phase analysis and autoradiography results points towards higher sorption of ^{241}Am at the Fe (mica) and Ca (areas colored in yellow) bearing phases.

TEM lamellae workflow

Another feature of Zeiss FIB-SEM CrossBeam 350 is a possibility to create a TEM lamella. The microscope allows to execute workflow which benefits from: (i) quick allocation of ROIs and keeping the eucentricity when tilting the sample. A gaseous injection system and micromanipulator ensure attachment and lift out of the lamellae and consequent attachment of it to the TEM-grid. Last few steps of lamellae preparation workflow are depicted in Figure 5.

After attachment of the lamella to a TEM-grid a final thinning and polishing can be monitored live benefiting from the signals of several detectors simultaneously. The SE signal allows to monitor lamella thickness and Inlens SE signal helps to control surface quality.

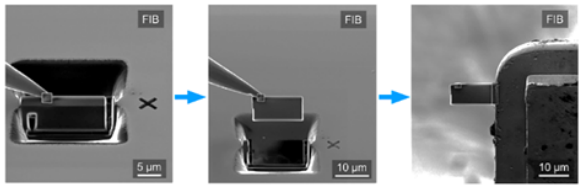

Fig. 5: Selected steps of the lamellae preparation workflow, from left to right: attachment of the micromanipulator needle to lamellae, lift out of the lamellae and attachment of lamellae to the TEM-grid.

Electron backscatter diffraction (EBSD)

Microstructural analysis is obtained by detection of backscattered electrons from a plane surface of a crystalline sample tilted to 70°. The electron backscatter diffraction pattern, also named backscatter Kikuchi diffraction is recorded by a detector equipped with a plane phosphor screen in front of a CMOS sensor. The recorded diffraction pattern is analyzed by Hough transformation and the Kikuchi lines are indexed by Bravais-Miller indices of the diffracting crystal planes which generate them. Together with EDS, elemental composition, crystal structure and orientation are recorded at every point during electron beam scanning resulting unique identification. The information volume of EBSD is about (10-40) nm^3 at 20 kV beam energy and hence is much less than the information volume of characteristic X-rays (EDS). To achieve good diffraction patterns, a well-polished crystalline surface is mandatory.

An example of the EBSD phase analysis of hydrogenated Zircaloy-4 (Zr-H) cladding of spent nuclear fuel (SNF) is shown in Figure 6. EBSD analysis reveals that fraction of δ-phase of zirconium hydride is higher compared to γ-phase.

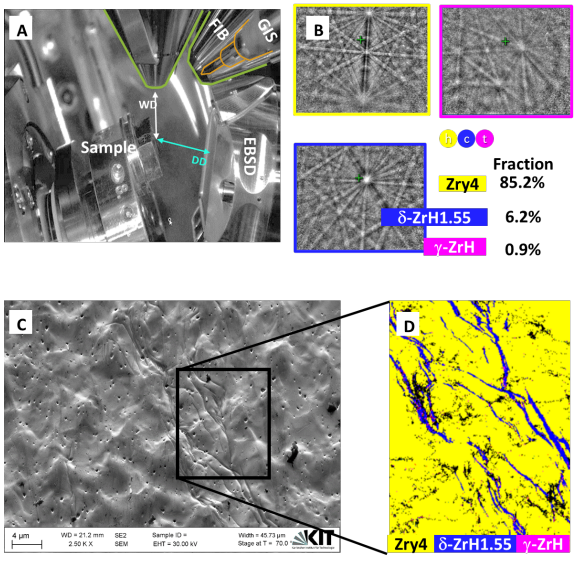

Fig. 6: (A) Chamber view of EBSD mode. (B) Kikuchi patterns recorded for Zr-H. (C) Backscattering electron (BSE) image of the Zr-H. (D) EBSD phase map of the Zr-H from the area marked in (C).

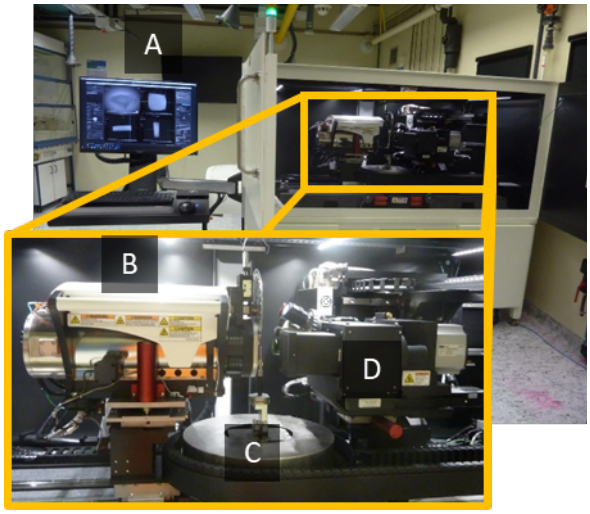

Fig. 7: Zeiss Xradia 620 Versa X-ray microscope and its components: acquisition software (A), X-ray source and filter wheel (B), sample stage (C), detector array (D).

3D X-ray microscope

A Zeiss Xradia 620 Versa X-ray microscope has been installed in the controlled area of KIT-INE, Figure 7. It is equipped with a sealed transmission, fast activation X-ray source with a voltage range of 30-160 kV and a maximum output of 25 W. A set of filters can be used to harden the X-ray spectrum.

Images are initially magnified via geometric projection. The projected image is cast onto a scintillator, converting X-rays to a visible light image, which is then optically magnified by microscope optics before acquisition by a CCD detector. The Xradia 620 Versa is equipped with objectives for 0.4x to 40x magnification. An additional Flat Panel X-ray detector (FPX) with only geometric magnification can be used for larger samples.

Theoretical resolutions down to 400 nm (2x Voxel size) can be reached. The actual resolution depends on the sample size (Table 1) and the sample composition. Low resolution measurements can be performed for samples up to 200 mm diameter and 100 mm height with a weight up to 25 kg. A wide field mode can be used with the 0.4x and 4x objectives to increase the horizontal field of view (FOV) while not changing the resolution. An increased vertical FOV can be achieved by stitching together multiple measurement collected at different sample heights.

An optional in-situ flow cell for elevated pressures and temperatures is currently being prepared.

Data acquisition and treatment (background correction, reconstruction, etc.) is run on a dual GPU (CUDA based) workstation. Data treatment is by default performed automatically within the Zeiss software suite, but adjusted manually if necessary. For data analysis, the Dragonfly software (Object Research Systems) is provided on the main workstation and on a second, identical workstation. As an application, SEM (top) and 3D X-ray microscope images (bottom) of $Rb_2UO_2Cl_4 \cdot 2H_2O$ (left) and $Rb_2UO_2Br_4 \cdot 2H_2O$ (right) single crystals are depicted in Figure 8. Note that 3D X-ray microscope images were recorded with single crystals encapsulated in epoxy resin and affixed to the tip of a capillary. A few cracks resulting from the loss of the crystal water are observed by both microscopy techniques. Partial smoothing of the crystal surface is observed in 3D X-ray microscope images of $Rb_2UO_2Br_4 \cdot 2H_2O$ as a result of encapsulation.

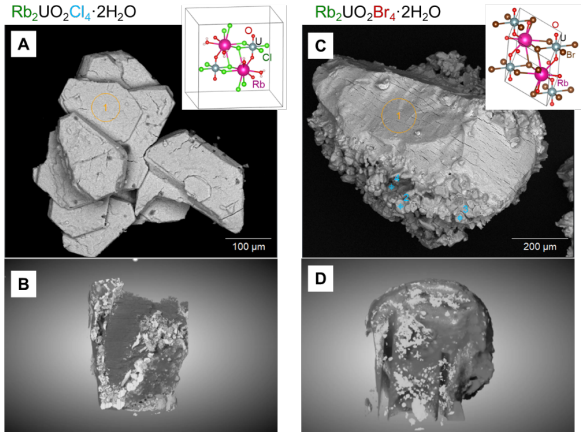

Fig. 8: An example of SEM imaging (A and C) and 3D X-ray microscopy (B and D) images of $Rb_2UO_2Cl_4 \cdot 2H_2O$ (left) and $Rb_2UO_2Br_4 \cdot 2H_2O$ (right) single crystals.

Table 1: Estimated Voxel size depending on objective, geometric magnification and sample size

Objective	Geometric Magnification	Sample Size (mm)	Voxel Size (µm)
FPX	~1.3 – 13x	15 - 140	6 - 57
0.4X	~1.1 – 11x	6 - 50	3 - 30
4X	~ 1.1 – 10x	2 - 20	0.7 - 3
20X	~1.1 – 2.7x	0.5 - 4.0	0.3 - 0.6
40X	~1.1 – 2x	0.3 - 2.0	0.2 - 0.3

With the combination of a Zeiss FIB-SEM CrossBeam 350 workstation and a Xradia 620 Versa X-ray microscope the capabilities of microscopy and surface analytics at INE are now extended to correlated studies of material morphology at high-resolution - encompassing phase and compositional analysis - including access to deeply buried structures as well as a fast large area mapping and patterning along with possibility to execute full workflow for TEM lamellae preparation. Combination of electron and X-ray analyzers allows to perform nondestructive investigation - where applicable also including studies of radioactive materials.

8.3 Accelerator mass spectrometry (AMS)

F. Quinto, T. Roth, H. Geckeis, S. Kraft, M. Plaschke

In co-operation with:

M. Böhm[a], Marcus Christl[b], K. Hain[c], H. Pérez-Tribouillier[b], T. Schäfer[a], P. Steier[c]

[a]Institute of Geosciences, Applied Geology, Friedrich-Schiller-Universität Jena; [b]Laboratory of Ion Beam Physics, ETH Zürich (Switzerland); [c]VERA Laboratory, Faculty of Physics, University of Vienna (Austria)

Introduction

The analytical capability of determining ultra-trace levels of long-lived actinides and fission products is a relevant asset to studies addressing the safety of geological disposal of radioactive waste. AMS is one of the most sensitive mass spectrometric techniques offering detection efficiency for actinide nuclides and ^{99}Tc at the level of ca. 1×10^4 atoms (25 ag) and ca. 3×10^6 atoms (0.5 fg) in a sample, respectively [1, 2]. We apply AMS to a variety of experiments investigating the retention and migration behavior of radionuclides (RNs) in the EBS-bentonite [2], crystalline host rock [3, 4], clay host rock [5, 6, 7] as well as environmental samples [8, 9].

In the actual chapter we report on our recent contribution to the study of soil-porewater partitioning coefficients for actinides at the ultra-trace levels. This study was carried out at the Institute of Geosciences of the Friedrich-Schiller University of Jena in the frame of the BMBF funded TransLARA project that investigated the transport and transfer behavior of long-lived RNs along the causal chain groundwater - soil surface - plant, considering long-term climatic changes. In particular, the actual study addresses the concern for the contamination of the biosphere from the possible release of long-lived RNs from a deep geological nuclear waste repository in crystalline environment and their transport in natural fractures/shear zones and subsequently through the vadose zone [9].

Furthermore, we describe our recent progress on the development of sample preparation methods enabling the concurrent determination of ultra-trace levels of several actinides, with the application of Actinide resin to seawater samples. In this way, we aim to set up a chemical separation of the actinide´s group from liquid samples with high content of matrix elements, like seawater and highly saline groundwaters that could offer higher analytical sensitivity than the $Fe(OH)_3$ co-precipitation [10].

Finally, we present the investigation of the long-term release of ^{242}Pu and ^{243}Am tracers from a granodiorite fracture during CFM Run 22-02. This is the latest *in-situ* RN tracer test carried out at the generic URL Grimsel Test Site, GTS (CH), in the frame of the international CFM Project that is introduced in chapters 5.2 and 5.3.

The samples investigated in the first two aforementioned studies were analyzed with AMS at the 3 MV tandem accelerator of the VERA laboratory (AT), while the samples from the third study were analyzed with AMS MILEA at the Laboratory of Ion Beam Physics of the ETH Zürich (CH).

Ultra-trace analysis of actinides in soil and porewater samples

In this mesoscale laboratory experiment, three reference top soil substrates were emplaced in lysimeters and fed from below with groundwater from the GTS, to mimic a contamination scenario of the vadose zone from groundwater arising from crystalline rock formations. The Grimsel groundwater contained ultra-trace levels of the RN tracers ^{233}U, ^{237}Np, ^{242}Pu and ^{243}Am artificially introduced in the frame of the CFM in-situ RN tracer tests at the GTS [3]. Furthermore, since the used reference soils are environmental samples that have been exposed to the global fallout, they contain ^{236}U, ^{239,240}Pu and ^{237}Np, namely the most abundant actinide nuclides produced by the past atmospheric testing of thermonuclear devices, offering the possibility to try and analyze also the partitioning of these global fallout RNs in the studied system.

Porewater was regularly sampled, and finally a soil core was taken from each lysimeter to obtain depth dependent information on the RNs associated with the solid phase in the established anoxic/suboxic and oxic horizons.

With adapted analytical procedures [9], it was possible to determine ultra-trace RN concentrations in the solid phase (ca. 3 to 18 g dry mass) and porewater

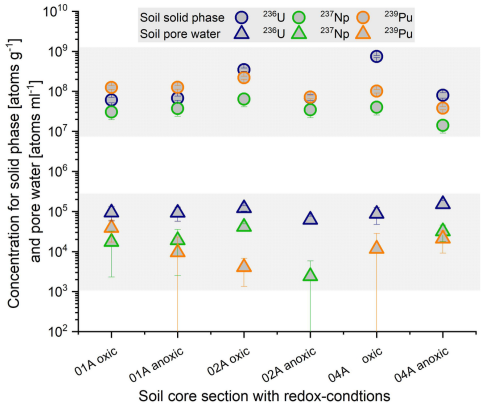

Fig. 1: ^{236}U (blue markers), ^{237}Np (green markers) and ^{239}Pu (orange markers) concentration in the solid phase (circles) and corresponding pore water phase (triangles) of soil samples from three reference soil – lysimeter systems.

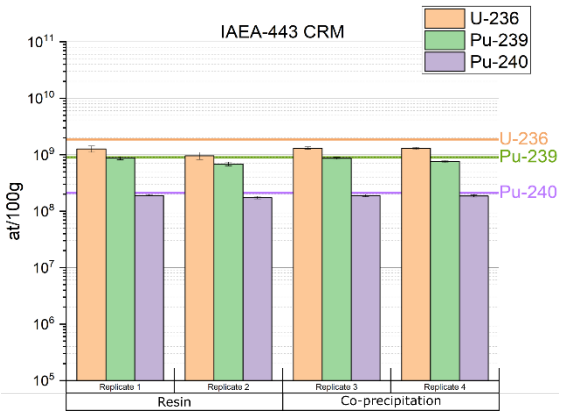

Fig. 2: Concentration of ^{236}U (orange bars), ^{239}Pu (green bars) and ^{240}Pu (purple bars) in four replicates of the CRM IAEA-443 (100 g, each), prepared with AC Resin (left) and $Fe(OH)_3$ co-precipitation (right). Horizontal lines indicate the corresponding literature values.

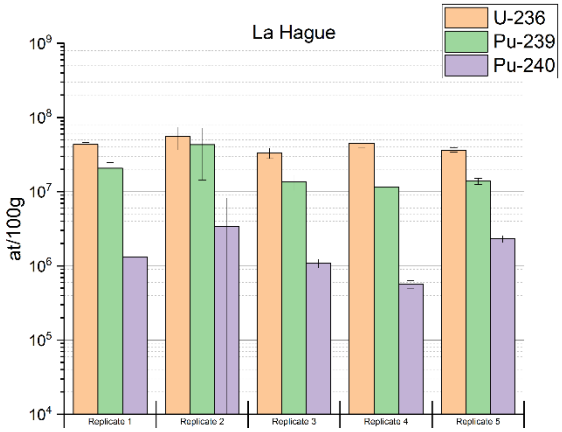

Fig. 3: Concentration of ^{236}U (orange bars), ^{239}Pu (green bars) and ^{240}Pu (purple bars) in five replicates of the La Hague sample (100 to 250 g, each) prepared with AC Resin.

phase (ca. 4 to 31 mL) of the soil samples, as exemplarily depicted in Fig. 1 for the global fallout derived ^{236}U, ^{237}Np and ^{239}Pu.

As it can be seen in Fig. 1, RN concentrations in porewater were generally 2 to 4 orders of magnitude lower than the corresponding solid phase concentrations and ranging between 10^4 and 10^5 atoms/mL. These results show depth patterns pointing to an enrichment in the upward soil sections in two of the three investigated cores, indicated as 02 and 04, that could be associated to a gradient in redox condition as well as to possible transport mechanisms, as extensively addressed in [9].

Multi-actinide analysis in seawater samples

Multi-actinide analysis with AMS after $Fe(OH)_3$ co-precipitation is an effective method for small and/or low matrix samples, like lowly saline groundwater [10], river water [8] and soil pore water [9]. It is, however, unselective and the resulting AMS target may contain relevant portions of matrix elements like Al, Si and Ca. This hampers the overall detection efficiency of AMS analysis of high matrix samples, because the sputtering rate of RNs in the AMS ion source would be lower compared to samples with a lower matrix in a process partly described as a dilution effect on the RN count rate [6]. A further influence of certain matrix elements on the ionization efficiency of RNs cannot be excluded and should be object of further studies.

Multi-actinide analysis with AMS after Actinide Resin™ (AC Resin, Triskem, Bruz, FR) separation has been recently developed and applied to river water samples, providing results consistent with $Fe(OH)_3$ co-precipitation for ^{236}U, ^{237}Np and $^{239,240}Pu$ determination [8]. The novel procedure was applied also to highly saline water samples, namely the Certified Reference Material (CRM) IAEA-443 (Radionuclides in Irish Seawater) and seawater samples collected in the vicinities of the La Hague nuclear fuel reprocessing plant (FR), aiming to compare it to samples prepared with $Fe(OH)_3$ co-precipitation [8].

As it can be seen in Fig. 2, the ^{236}U, ^{239}Pu and ^{240}Pu concentration determined after Actinide separation (replicate 1 and 2) and $Fe(OH)_3$ co-precipitation (replicate 3 and 4) are mostly consistent with each other and with the corresponding literature values [10], proving in this way the accuracy of the AC Resin method for AMS analysis of U and Pu nuclides in seawater samples.

Fig. 3 shows the ^{236}U, ^{239}Pu and ^{240}Pu concentration determined with the AC Resin method in five aliquots (100 to 250 g) of a La Hague seawater sample. Mostly consistent results among the aliquots and significantly lower levels of the RNs were estimated, indicating that the method can be successfully applied to environmental samples with RN concentrations orders of magnitude lower than those of the CRM IAEA-443.

Furthermore, from the analysis of the CRM IAEA-443, we have found indication that for samples where a significant amount of matrix would precipitate together with $Fe(OH)_3$, causing a dilution effect, the use of AC Resin can improve the signal count rates of the AMS detector, enabling shorter measurement times. Further experiments will focus on the analysis of sample systems with significantly higher matrix content than sea water, such as soil leachates, solid sample digestions and brine solutions, to investigate if use of AC Resin for these systems could indeed significantly increase analytical sensitivity.

Long-term release of ^{242}Pu and ^{243}Am in CFM Run 22-02

The extreme sensitivity of AMS has been required when investigating ultra-trace levels of RN tracers in field experiments, frequently as a complementary analytical technique to ICP-MS [2, 4, 10]. Also, in the frame of the latest *in-situ* RN tracer test at the GTS, CFM Run 22-02, AMS has been applied to analyze groundwater samples in which RN tracer concentration was below the detection limits of the employed SF-ICP-MS, as mentioned in chapter 10.

In fact, as depicted in Fig. 4, following the maximum of the RN breakthrough curves and after ca. 240 h from the starting of the experiment, the concentration of

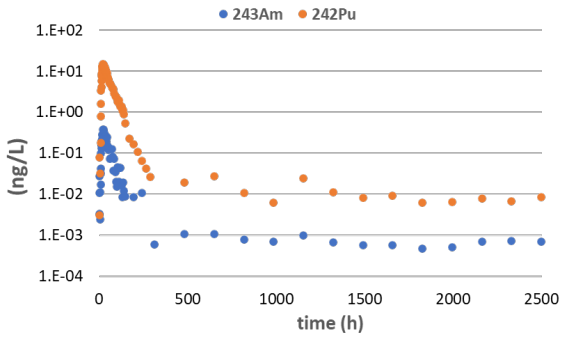

Fig. 4: Concentration of ^{242}Pu (orange spots) and ^{243}Am (blue spots) in collected Grimsel groundwater samples during CFM Run 22-02. A tailing, starting at ca. 240 h for the two RNs, was monitored with AMS until ca. 2500 h.

^{242}Pu and ^{243}Am decrease to levels below ca. 0.05 ng/L (50 ppq).

Groundwater samples were however regularly collected until ca. 2500 h (*i.e.*, 3.5 months from the injection of the RN cocktail). Such samples, after an appropriate chemical separation of the Pu and Am fractions, were analyzed with AMS. As it can be seen in Fig. 4, starting from ca. 240 h, a tailing of the RN breakthrough curves is observed, with concentrations laying on the orders of magnitude of ca. 10 ppq (10^7 atoms/mL) for ^{242}Pu and generally lower than ca. 1 ppq (10^6 atoms/mL) for ^{243}Am.

In this way, it was possible to investigate the long-term release of the ^{242}Pu and ^{243}Am tracers from the water conductive shear zone at the GTS. These experimental data will help evaluating the retention capability in the far field of fractured crystalline rock and support reactive transport modelling in predicting long-term migration of RN in deep geological repositories in crystalline host rock.

More details on CFM Run 22-02 are given in chapters 5.3 and 10 from this report.

References

[1] Steier P. et al., (2010), Nucl. Instrum. Methods Phys. Res., Sect. B, 268, 1045.

[2] Quinto F. et al., (2019), Anal. Chem., 91, 4585.

[3] Quinto F. et al., (2017), Anal. Chem., 2017, 89, 7182.

[4] Schäfer T. et al., (2025) NAGRA technical report NTB 23-10.

[5] Glückman, D., (2023), "Investigation of the diffusion of U(VI) and Am(III) through Opalinus Clay down to ultra-trace levels", PhD thesis. Karlsruhe Institute of Technology, Karlsruhe, Germany.

[6] Glückman D. et al., (2022), J. Anal. At. Spectrom., 37, 1696.

[7] Glückman D. et al., (2025), Environ. Sci. Technol., 59, 8694–8702

[8] Roth T. et al., "First application of Actinide Resin in the preparation of water samples for multi-actinide analysis with accelerator mass spectrometry". Manuscript under review at J. Anal. At. Spectrom. (2026).

[9] Böhm M., (2024) "The role of natural colloidal phases on migration of trace and ultra-trace elements in soil ecosystems - Laboratory lysimeter case studies on natural topsoil materials (Refesols)." Ph. D. thesis, Friedrich-Schiller-University Jena.

[10] Quinto F. et al., Anal. Chem., 2015, 87, 5766.

8.4 Computational chemistry

J. Androniuk, K. Dardenne, S. Duckworth, X. Gaona, R. Polly, J. Rothe

In co-operation with:

P. Bagus[a]

[a] Department of Chemistry, University of North Texas, Denton, Texas 76203-5017, United States

Introduction

Computational Chemistry is established as a reliable additional tool to investigate chemical systems relevant for nuclear waste disposal at KIT-INE. The theoretical methods applied are Molecular Dynamics (MD), Density Functional Theory (DFT) or various *ab initio* methods. They provide valuable fundamental insights on a molecular scale, strongly supporting spectroscopic investigations in the field of nuclear waste disposal. The considered systems vary from molecular species in the gas phase over small complexes in solution to bulk phases and mineral/liquid interfaces at ambient conditions. The synergistic effects - combining theoretical and experimental research - at KIT-INE in one research institution are enormous. A lot of effort is devoted on systematic theoretical studies of various radionuclides such as Tc, lanthanides (Eu^{3+}), actinyls (UO_2^{2+}, NpO_2^{2+}, NpO_2^{+}) as well actinide (U^{4+}, Pu^{3+}, Am^{3+}) ions in various systems from bulk phases to solutions and gas phase species. Especially the calculations reproducing the actual experimental spectra for X-ray Absorption Near Edge Structure (XANES) or Resonant Inelastic X-ray Scattering (RIXS) are one of the main focus points of the theoretical research at KIT-INE.

During the past decades, relativistic multireference *ab initio* quantum chemistry methods have developed into a powerful tool supporting X-ray spectroscopy techniques. Because of the complexity of the detected signals, theoretical calculations are very important for the interpretation of the experimental data.

8.4.1 Molecular dynamics (MD) study of trivalent lanthanides and actinides at C-S-H surfaces with additional gluconate in solution

Molecular dynamics is a method that allows precise description of the interface processes at the molecular scale. Classical MD simulations and the potential of mean force (PMF) calculations were used to obtain a mechanistic understanding of the surface sorption process for Eu^{3+} species on the surface of C-S-H in the presence of gluconate. Based on their similar charge-to-size (z/d) ratios, Eu^{3+} was considered as representative of key trivalent actinides expected in nuclear waste, *i.e.* Pu^{3+} and Am^{3+}. The representative C-S-H interface models were developed.

The surface of C-S-H provides multiple possibilities for ion binding, among them the three most probable sorption sites were selected: “defect site” in the position of the missing bridging silicate tetrahedra in the silicate chain (DEF); “bridge site” – deprotonated silanol group of the bridging silicate tetrahedra in the silicate chain (BR); “chain site” that includes coordination with one deprotonated silanol and bridging oxygens (CH); and “interchain site” (INTER) – sorption in the space between silicate chains. A series of PMF calculations were performed to study the sorption mechanisms in detail for the binary and ternary systems, with C-S-H parameters taken from ClayFF [1], Eu^{3+} parameters from [2], and gluconate parameters from GAFF [3]. Interaction of both 1:1 and 1:2 Eu^{3+}/gluconate complexes with the C-S-H surface was considered.

The comparison of the PMF curves of Eu^{3+} sorption at the two sites with and without gluconate is shown in Fig. 1. It can be seen that in the presence of gluconate in the coordination sphere of Eu^{3+} the strength of sorption is significantly decreased, the formation of the inner-sphere complexes is hindered on the DEF site, and in the case of 1:2 complex no sorption can be seen. Meanwhile, sorption on the CH and INTER sites was found to be insignificant. This validates and supports the experimental data, and shows that presence of gluconate increases Eu^{3+} mobility on the surface of C-S-H phases.

8.4.2 Ab initio speciation of Tc(IV)-gluconate complexes

A recent study of Tc(IV) complexes [4] revealed a significant change of the Tc L_3-edge XANES of Tc(IV) bound by two gluconate ligands. While Tc(IV) hydrous oxide, Tc(IV)O_2(am, hyd), shows a XANES spectrum with one broad peak, the XANES of Tc(IV) interacting with gluconate ligands reveals a very distinct splitting into two peaks [4].

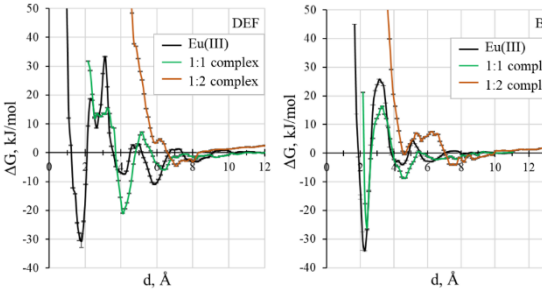

Fig. 1: PMF curves for sorption of the 1:1 and 1:2 Eu^{3+}/GLU complexes, and Eu^{3+} without gluconate on two sorption sites of the (001) C-S-H surface.

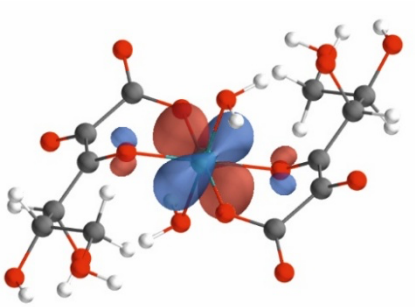

*Fig. 2: [Tc(IV)-(Glu$_{-2H}$)$_2$(H$_2$O)$_2$]$^{2-}$+4H$_2$O complex **(2)**.*

This initially puzzling observation was finally reproduced by means of two-step ab initio speciation calculations for various Tc(IV)-gluconate complexes conceivable to form in this sample [5].

In a first step, the structures of some proposed complexes were optimized and compared with the available experimental data of the Tc-O distance obtained from Tc K-EXAFS measurements. All structures with Tc-O distances deviating from the experimental value were excluded, for the remaining candidates the Tc L$_3$-edge XANES spectra were calculated.

The five different Tc(IV)-gluconate complexes considered at last are **(1)** [Tc(IV)-(Glu)$_1$]$^{1-}$, **(2)** [Tc(IV)-(Glu$_{-2H}$)$_2$(H$_2$O)$_2$]$^{2-}$(+4H$_2$O) (s. Fig. 2), **(3)** [Tc(IV)-(Glu$_{-H}$)$_2$(OH)$_2$]$^{2-}$(+4H$_2$O), **(4)** [Tc(IV)-(Glu$_{-2H}$)(Glu$_{-H}$)$_2$(OH)$_2$]$^{3-}$(+4H$_2$O) and **(5)** [Tc(IV)-(Glu$_{-2H}$)$_2$(OH)$_2$]$^{4-}$(+6H$_2$O).

Optimization of the complexes using the Møller-Plesset perturbation theory of second order (MP2) revealed that the [Tc(IV)-(Glu)$_1$]$^{1-}$ **(1)** can be excluded immediately. For all other complexes we calculated the Tc L$_3$-edge XANES with restricted active space self-consistent field (RASSCF) and the multiconfigurational perturbation theory of second order (RASPT2) methods including Spin-Orbit coupling (RASSI, AMFI). With this sound theoretical approach, multiconfigurational and relativistic effects are fully accounted for.

The calculated XANES spectra of species **(2)**, **(3)** and **(5)** and a comparison with the experimental data are shown in Fig. 3. This result helped to narrow down the number of possible candidates which are present in the sample. Finally, we singled out one species with a calculated Tc-O distance close to the EXAFS results and Tc L$_3$-edge XANES very close to the experimental spectra: [Tc(IV)-(Glu$_{-2H}$)$_2$(H$_2$O)$_2$]$^{2-}$(+4H$_2$O) **(2)**.

This shows how helpful and beneficial accurate ab initio calculations are for the identification of unknown species in the sample. Therefore, we coin the term *ab inito speciation* for this procedure outlined in [5].

The question remains why there is such a significant change in the XANES spectrum going from hydrous oxide Tc(IV)O$_2$(am, hyd) (single broad peak) to the Tc(IV)-(Glu)$_2$ spectrum (peak splitting)? This was finally answered by performing accurate RASPT2 calculations of the XANES spectra. The

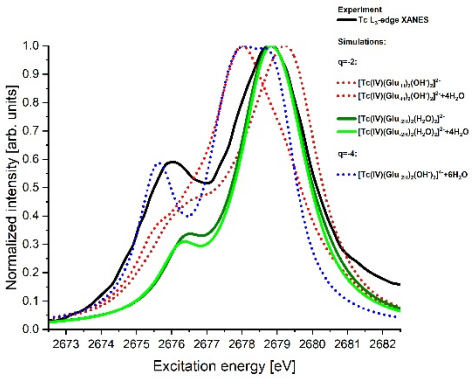

Fig. 3: Tc L$_3$-edge XANES spectra of Tc(IV)-(Glu)$_2$ complexes [5].

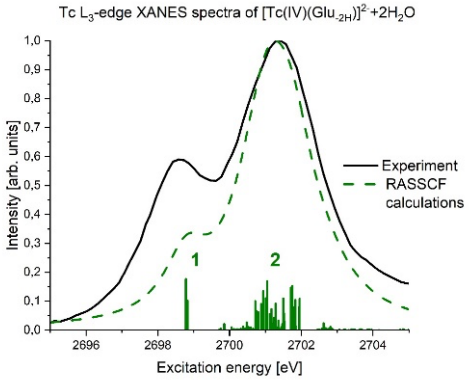

Fig. 4: Tc L$_3$-edge XANES spectra of Tc(IV)-(Glu)$_2$ complexes and different transitions (vertical bars) contributing to the Tc L$_3$-edge XANES [5].

electronic configuration of the Tc(IV) ground state is 4d^3. In Tc(IV)O$_2$(am, hyd) the ground state of Tc(IV) is a quartet state with all spins of the 4d electrons parallel, whereas in the [Tc(IV)-(Glu$_{-2H}$)$_2$(H$_2$O)$_2$]$^{2-}$(+4H$_2$O) **(2)** complex we found the ground state to be a doublet state. The reason for the significant differences of Tc L$_3$-edge XANES spectra obtained for both Tc(IV) species is that the six oxygen anions interacting with Tc(IV) are distorted from an ideal octahedral structure in the Tc(IV)-gluconate complex. Therefore, a doublet state becomes energetically more favorable. This insight can only be provided by multiconfigurational *ab initio* calculations and proves the power of this sophisticated theoretical approach. Due to the doublet ground state the core excited states split up into two groups as indicated in Fig. 4.

8.4.3 Core-excited states of the U M4,5 manifold of Uranyl

Recently a number of experimental and theoretical publications addressed the U M$_4$-edge XANES spectra and 3d4f RIXS map of uranyl [6-8]. The Uranyl U M$_4$-edge XANES spectra show three pronounced peaks which can be assigned to excitations from 3d core orbitals to 5f valence orbitals of uranium [6]. The first peak is assigned to excitations into non-bonding 5fδ and 5fϕ valence orbitals, the second peak to excitations into anti-bonding 5fπ* and the

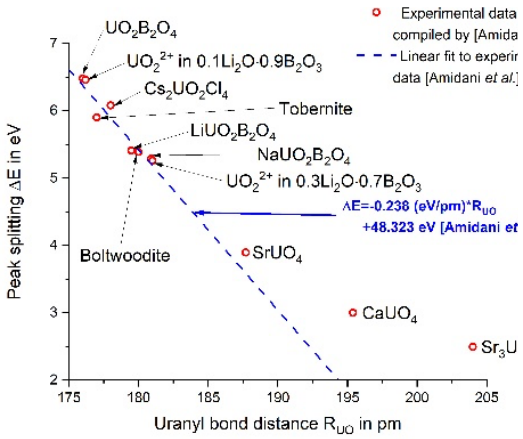

Fig. 5: Uranyl peak splittings [9] for various uranyl systems and empirical correlation between the peak splittings and the bond length.

third peak into anti-bonding 5fπ* valence orbitals of uranyl.

Amidani *et al.* [9] made a very interesting observation by investigating the relation of the peak splittings with the uranyl bond length for different uranyl systems (see references in [9]). They found an empirical linear correlation between the peak splittings in the U M_4-edge XANES and the bond lengths of uranyl (Fig. 5).

A key information required for the understanding of this empirical correlation are the potential energy curves of the core-excited states. We calculated these potential energy curves with the RASSCF and RASPT2 methods as outlined above.

The three branches of the potential energy curves of the core excited states shown in Fig. 6 belonging to the U $M_{4,5}$-edge manifold can be assigned to excitations from the 3d core-orbitals of uranium into either non-bonding (5fδ, 5fϕ) or anti-bonding (5fπ* or 5fσ*) valence orbitals. The shapes of these three branches are quite similar comparing both edges (U M_5 and U M_4), but differ significantly among each other for the same edge. The highest branch with the occupied anti-bonding 5fσ* valence orbital shows a repulsive shape in the considered range, whereas the other two branches display a shape almost parallel to the ground state of uranyl. The reason why the 5fσ* branch reveals this repulsive shape is that the occupation of the anti-bonding 5fσ* valence orbital introduces additional negative charge along the bond axis leading to additional repulsive coulomb interaction with the negatively charged oxygen ions.

With this theoretical information we are able to calculate the peak splittings of uranyl for different bond lengths and find an excellent agreement between the calculated peak splittings (see Fig. 7) and the relation proposed by Amidani *et al.* [9]. This proofs that our simple model of a bare uranyl moiety in the gas phase already reproduces this effect observed for many different uranyl compounds. The reason for the linear correlation between the peak splittings and the bond lengths is the relative shape of the potential energy curves of the core-excited states. Calculating the difference between the core-excited states by subtracting the respective energies shows that they are almost on a straight line (see Fig. 8).

This shows clearly that the empirical linear correlation as found by Amidani *et al.* [9] is due to the relative shapes of the involved potential energy curves of the core-excited states. Our results reproduce the magnitude of the peak splittings as well as the slope of the peak splittings depending on the uranyl bond length with very high accuracy.

Another important finding of Amidani *et al.* [9] is that at bond distances significantly longer than 180 pm the linear relation is lost (see Fig. 5). As can be seen from Fig. 6 the core excited states of the highest branch (5fσ* occupation) starts to mix with the second branch (5fπ* occupation) for longer bond distances and therefore this highest branch is not anymore characterized by an occupation of the anti-bonding 5fσ* valence orbital. This loss of linearity can be clearly seen in Fig. 8. The difference potential energy curve does not display anymore a linear slope in the range >180 pm.

An important question remains – why can the simple model system of the bare uranyl ion reproduce the linear trend observed for many different uranyl compounds with completely different chemical environments?

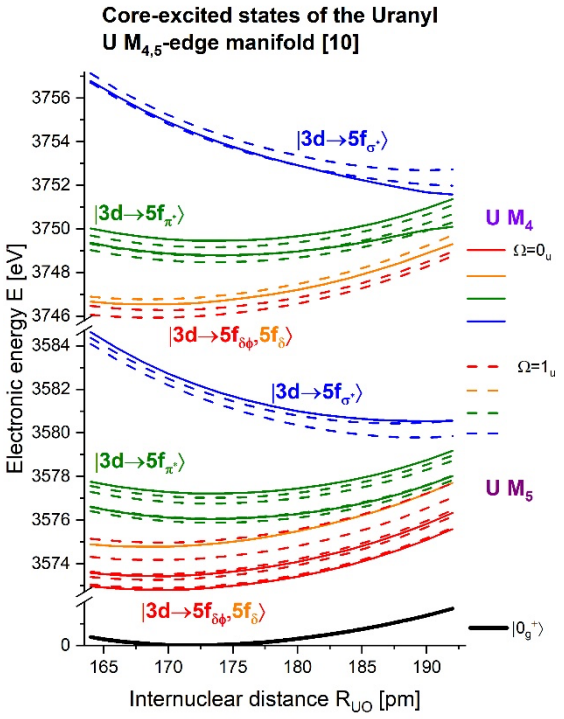

Fig. 6: Potential energy curves of core-excited states of uranyl belonging to the U $M_{4,5}$-edge manifold [10].

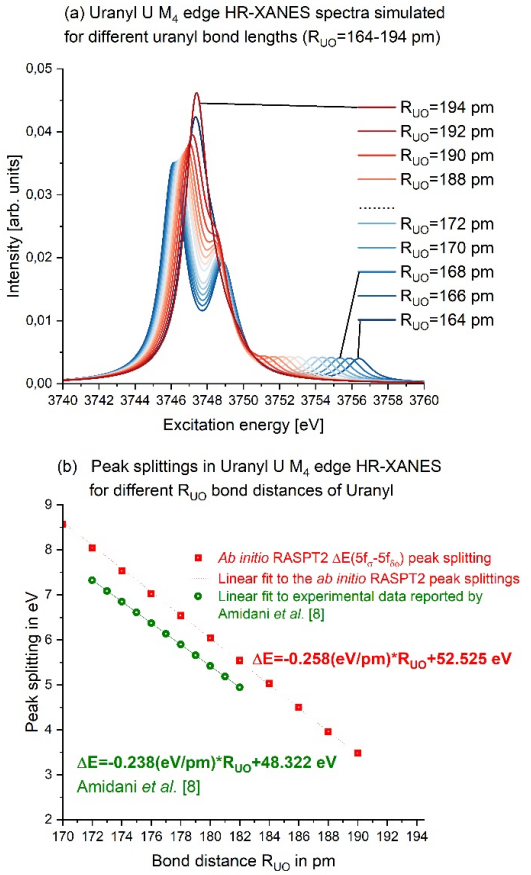

Fig. 7: Peak splittings in the uranyl U M4-edge for different bond distances.

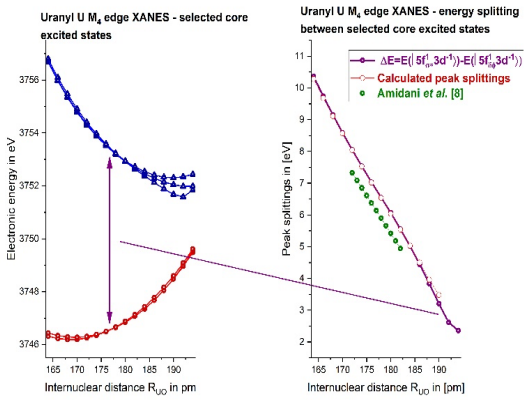

Fig. 8: Selected core excited states of Uranyl and comparison of the difference potential curve with the calculated and measured peak splittings.

Obviously, the potential energy curves of the core-excited states of the different uranyl systems [9] are only slightyl distorted when moving away from bare uranyl to uranyl in different chemical environments. Therefore, the peak splitting between the first and third peak can be used as sensitive test for the uranyl bond length in different uranyl systems.

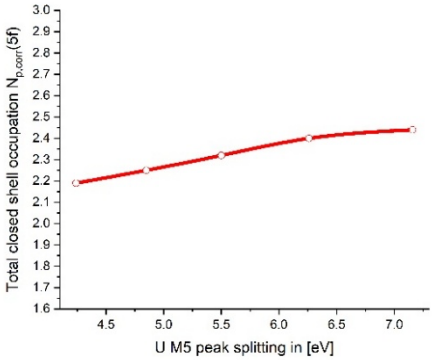

Fig. 9: Dependence of the projections $N_{p,corr}(5f)$ of the ground state on the peak splittings of the UO_2^{2+} U M_5 absorption edge XANES [9].

Recently [10] this study was extented to the U M_5 edge. In this new study we confirm the correlation of the peak splittings with the covalency postulated by Vitova *et al*. [6] and extend their work by considering the covalent character as a function of the bond distance. The covalency of the uranyl ground state measured with the $N_{p,corr}(5f)$ occupation [10] correlates linearly with the peak splitting in the U M_5 edge XANES (see Fig. 9). Although the variation of the covalency with the peak splitting is confirmed, the variation is very small.

Here we show how relativistic multiconfigurational *ab initio* calculations of U M_4-edge XANES spectra of uranyl substantially help to understand empirical spectoscopic observations, which otherwise lack a sound explanation. These results and the aforementioned successful *ab initio spectiation* of Tc(IV)-gluconate complexes strongly underlines the importance of accurate theoretical calculations in support of advanced X-ray spectroscopy methods.

References

[1] R. T. Cygan *et al.,* J. Phys. Chem. B 108, 1255, (2004)

[2] Y. An *et al*., J. Phys. Chem. A 104, 11243 (2000)

[3] J. Wang *et al.,* J. of Comp. Chem. 25, 1157 (2004)

[4] K. Dardenne *et al.*, Inorg. Chem. 60 (16), 12285, (2021)

[5] Polly *et al.*, Inorg. Chem. 2025, 64, 5412−5423

[6] T. Vitova *et al.*, Nature Communications, 8, 1-9, (2017)

[7] D.-C. Sergentu *et al.*, J. Phys. Chem. Lett. 9, 18, 5583 (2018)

[8] R. Polly *et al.*, Inorg. Chem. 2021, 60, 18764 (2021)

[9] L. Amidani *et al.*, Inorg. Chem. 60, 16286 (2021)

[10] R. Polly and B. Bagus, Inorg. Chem. (2026), https://doi.org/10.1021/acs.inorgchem.5c047

9 Advanced spectroscopy in f-element chemistry

The f-elements, specifically the lanthanides and the actinides, have fascinating but not well understood electronic structure and bonding properties that we explored in-depth by advanced X-ray spectroscopic approaches. Experimental and computational high-energy resolution X-ray spectroscopic tools were developed and applied for an in-depth characterization of bonding properties, specifically bond covalency, of actinide (An) and lanthanide (Ln) organic and inorganic compounds in solid and liquid states as well as Ln multimetallic clusters. A significant advancement in theoretical spectroscopy took place through the successful development and application of ligand field density function theory (LFDFT), which was utilized to calculate core-to-core and valence-band resonant inelastic X-ray scattering (CC-RIXS and VB-RIXS) spectra of An and Ln compounds. In a series of state-of-the art experimental and theoretical studies performed in collaborations with leading groups, it was demonstrated that each spectroscopic tool - HR-XANES, CC-RIXS, and VB-RIXS - is sensitive to An 5f valence electron density with different level of delocalization in a chemical bond. By combining them into a powerful tool, precise characterization of valence electron configurations and bond covalency can be achieved. This detailed description of electron density distribution in the chemical bond can be used to benchmark theoretical approaches. These developments and applications were carried out within the European Research Council (ERC) Consolidator Grant "THE ACTINIDE BOND properties in gas, liquid, and solid state" and the Collaborative Research Center (CRC) subprojects "Activation and Stabilization of Small Molecules by Rare Earth Compounds" (A1.2) and "Lanthanide-Based Multimetallic Clusters" (A3.2). The instrumentation developments of the NEXT X-ray emission spectrometer installed at the ACT station of the CAT-ACT beamline at the KIT Light Source are described in Chapter 8. An innovative experimental application exploring the energy resolution and efficiency of a Metal Magnetic Calorimeter (MMC) for γ spectroscopy was carried out. A MMC was applied in a broad collaboration to detect most of the daughter radionuclides of Ac-225, which was successfully achieved here for the first time; Ac-225 is one of the most promising short-lived radionuclides for targeted alpha therapy (TαT) of tumors.

9.1 Development of X-ray spectroscopies and radiochemical applications

B. Schacherl[1,2], K. Maurer, H. Kaufmann-Heimeshoff, S. Schenk, J. A. Branson, C. Reitz, C. Vollmer, T. Pruessmann, A. Beck, R. S. K. Ekanayake, T. Neill[1,7], D. Fellhauer, D. Schild, T. Sittel, H. Ramanantoanina, A. Tasi, D. Fellhauer, and T. Vitova

In co-operation with:

M. Tagliavini[3], J. Göttlicher[4], M. Mazzanti[5], K. Popa[6], O. Walter[6], D. Brager[8], C. Cahill[8], C. Windorff[9], M. Haverkort[3], D. Unger[10], M. Behe[11], A. Knecht[11]; K. von Schoeler[12], D. Hengstler[10], M. Benešová-Schäfer[13], A. Fleischmann[10], L. Gastaldo[10], C. Wängler[14], C. Enss[10,15]

[1] *Karlsruhe Institute of Technology (KIT), INE, P.O. Box 3640, 76021 Karlsruhe, Germany*
[2] *Lawrence Berkeley National Laboratory (LBNL), Chemical Sciences Division (CSD), Berkeley, CA, 97420, USA*
[3] *Heidelberg University, Institute for Theoretical Physics (ITP), Philosophenweg 19, 69120 Heidelberg, Germany.*
[4] *Karlsruhe Institute of Technology (KIT), IPS, P.O. Box 3640, 76021 Karlsruhe, Germany.*
[5] *Institut des Sciences et Ingénierie Chimiques, EPFL, CH-1015 Lausanne, Switzerland*
[6] *European Commission, Joint Research Centre Karlsruhe (JRC), Karlsruhe, Germany*
[7] *Research Centre for Radwaste Disposal and Williamson Research Centre, Department of Earth &Environmental Sciences, The University of Manchester, Oxford Road, Manchester M13 9PL, UK*
[8] *Department of Chemistry, George Washington University, 800 22nd Street, NW, Washington, DC, 20052, USA.*
[9] *Department of Chemistry and Biochemistry, NMSU, MSC 3C, P.O. Box 30001, Las Cruces, NM, 88003 USA*
[10] *Kirchhoff Institute for Physics, Heidelberg University, Im Neuenheimer Feld 227, 69120 Heidelberg, Germany*
[11] *Paul Scherrer Institute (PSI), Forschungsstraße 111, 5232 Villigen, Switzerland*
[12] *ETH Zürich, Institute for Particle Physics and Astrophysics, Otto-Stern-Weg 5, 8093 Zürich, Switzerland*
[13] *German Cancer Research Center (DKFZ), Research Group Translational Radiotheranostics, Im Neuenheimer Feld 223, 69120 Heidelberg, Germany*
[14] *Medical Faculty Mannheim of Heidelberg University, Clinic of Radiology and Nuclear Medicine, Biomedical Chemistry, Theodor-Kutzer-Ufer 1-3, 68167 Mannheim, Germany*
[15] *Karlsruhe Institute of Technology (KIT), Institute for Electronics and Data Processing (IPE), Hermann-von-Helmholtz-Platz 1, D-76344 Eggenstein-Leopoldshafen, Germany*

γ-Spectroscopy

Targeted alpha therapy (TαT) is a promising treatment method in which highly energetic alpha particles are selectively delivered to cancer cells, destroying them while minimizing damage to healthy surrounding tissues in the tumor environment. ^{225}Ac is one of the most promising short-lived radionuclides for application in targeted alpha therapy (TαT). However, during decay, the daughter nuclides such as ^{221}Fr, have altered chemical bonding interaction, suboptimal chelation and hence liberation of the ra-

diometal ion. Further, the energy released and the recoil effects during the alpha decay can break the chemical bonds. Thus, the liberated radionuclide can migrate to undesired locations in various organs, resulting in a significant dose burden to healthy organs and tissues.

In light of this, quantitative detection of ^{225}Ac and most of its daughter radionuclides is highly desirable. It has been unattainable by γ-spectroscopy so far. Achieving this would enable precise organ dosimetry and better targeting of the therapeutic potential of the ^{225}Ac decay series.

To date, only ^{221}Fr and ^{213}Bi are imageable in the decay chain of ^{225}Ac due to their suitable gamma lines (Fig. 1). However, quantitative detection of all radionuclides is desirable to precisely determine the distribution in the organism and thus the organ dose. Detectors used in Single Photon Emission Computed Tomography (SPECT) but also high purity germanium detectors lack energy resolution and sensitivity to distinguish between more than the above-mentioned radionuclides.[1]

In this study, a different kind of detector was employed. It is based on Metal Magnetic Calorimeter (MMC): A single MMC consists of a paramagnetic temperature sensor and a particle absorber in close thermal contact which are together weakly connected to a thermal bath at 20 mK. When energy is deposited by an incident γ- or X-ray, the temperature of the calorimeter increases and the temperature dependent magnetization of the sensor changes. The resulting change in the magnetization of the sensor, which is located in a small magnetic field, can be precisely measured using a highly sensitive Superconducting Quantum Interference Device (SQUID) magnetometer. The energy resolution of detectors that use MMC surpasses that of all previously mentioned technologies. An energy resolution of 10 eV Full Width at Half Maximum (FWHM) has been demonstrated at the 60 keV γ-line of an ^{241}Am source.[2]

In our study, a gamma and X-ray spectrum obtained using an 80 kBq source of ^{225}Ac, which was in equilibrium with its daughters was measured with an MMC detectors while a ^{55}Fe source for calibration was present. The resulting histogram was compared with simultaneously measured spectra from a silicon drift detector (SDD) which is visualized in Fig. 2. In addition, a theoretical gamma spectrum of ^{225}Ac (Nucleonica) was used to assign the various signals to the γs of actinium and its daughters (Fig. 3). Other sources of signal were discussed.

An ultra-high resolution (FWHM of 23 eV @ 5.9 keV) enabled the assignment of the γ-lines of ^{225}Ac, ^{221}Fr, ^{213}Bi, and ^{209}Tl. Additionally, the characteristic X-ray fluorescence lines of ^{221}Fr, ^{217}At, ^{213}Bi, ^{213}Po, and ^{209}Pb were recorded.

The resolution of the ^{225}Ac- γ- and X-ray spectrum presented in this work using the MMC detectors is the superior to available detectors, permitting to differentiate between the γ- lines of the individual daughters of ^{225}Ac in small energy ranges in the low

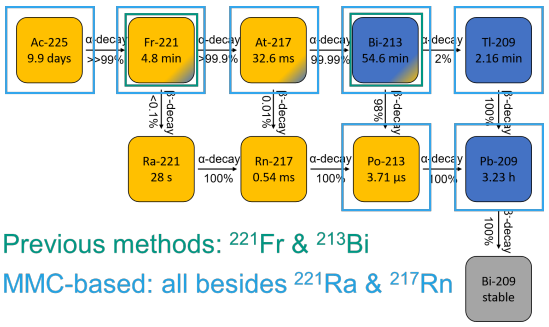

Fig. 1: Decay chain of ^{225}Ac with up to now imageable isotopes framed in green and using MMC detectors detectable isotopes marked in blue.

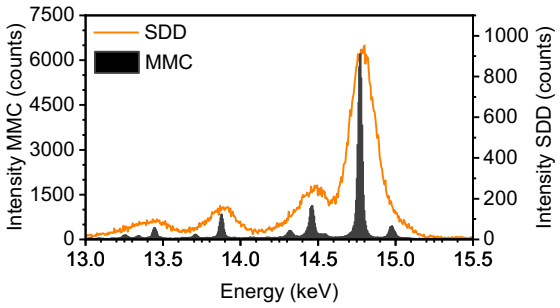

Fig. 2: Comparison of SDD and MMC detected spectra of the exact same 80 kBq ^{225}Ac solution.

energy region (<99 keV). This first MMC spectrum of ^{225}Ac demonstrates the detector's potential which could potentially be used to achieve better dose distribution in future applications.[3]

Advanced X-ray spectroscopy

The question of the participation of actinide (An) 5f and 6d electrons in bond covalency, and their role in the formation, bond stability, and chemical reactivity, as well as how this participation changes across the actinide series, is controversially discussed and a hot topic in actinide chemistry. By developing and applying state-of-the-art experimental and theoretical tools for in-depth studies of actinide-ligand bond covalency in various actinide systems we obtained advanced understanding. Several questions could be answer such as: How can An $M_{4,5}$ edge core-to-core resonant inelastic X-ray scattering (CC-RIXS), high energy resolution X-ray absorption near edge structure (HR-XANES) and valence band-RIXS (VB-RIXS) spectroscopic tools be useful to obtain advanced insights into the An-ligand chemical bonding and bond covalency?[4,5] An $M_{4,5}$ edge CC-RIXS and VB-RIXS are sensitive to the "effective" 5f electron occupation numbers. The former counts the number of 5f open-shell electrons that is localized on the actinide ion and constitutes a large part of the effective occupation number, and the latter determines the degree of delocalization of the 5f orbitals as results of donation effects to the surrounding ligands (i.e. 5f participation in the formation of covalent bonds).

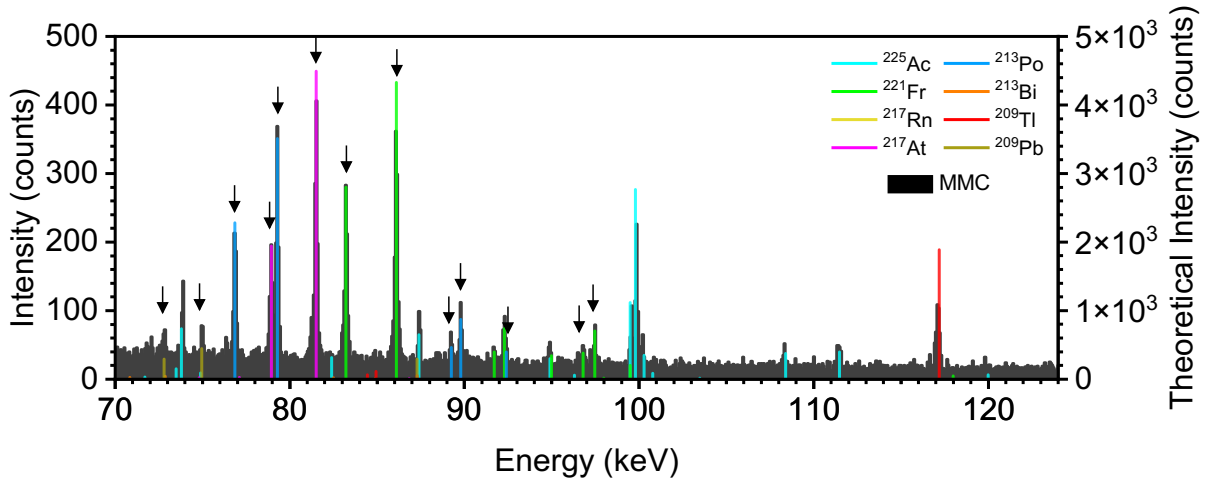

Fig. 3: Recorded γ- and X-ray-spectra of ^{225}Ac (black, left y-axis) and theoretically calculated γ- and X-ray-spectra of ^{225}Ac (Nucleonica, Hephaestus) with the efficiency of MMC detectors being taken into account (colored, right y-axis) (binsize:70 eV). The K_α-X-rays of the respective isotopes are marked with arrows

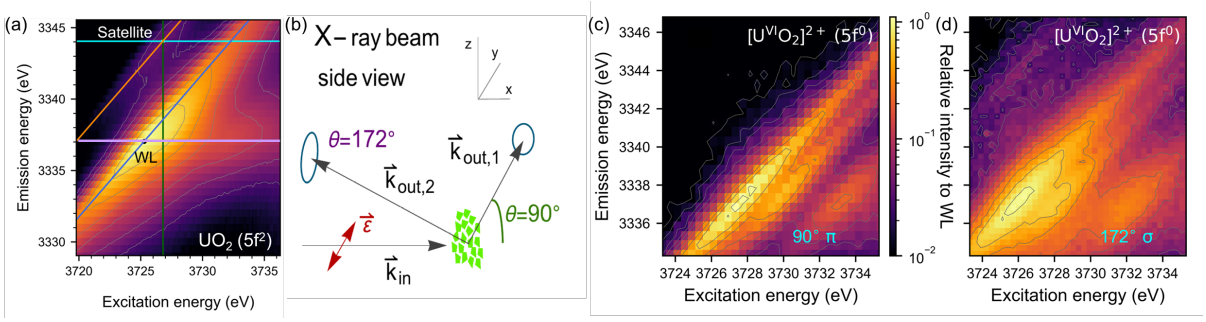

Fig. 4: (a) Experimental UO_2 M_4 edge CC-RIXS map depicting intensity changes of the Mβ characteristic fluorescence as a function of the excitation energy across the U M_4 absorption edge. (b) Side view of the experimental setup with denoted linear polarization of the incident X-ray beam in the plane of the synchrotron (ε). The considered scattering angles θ defined between the incoming and scattered X-rays are here 90° and 172° in the horizontal (the plane of the synchrotron) or vertical scattering plane with respect to the incident X-ray polarization vector (ε). The two different experimental geometries are denoted "90° π" and "172° σ". (c) experimentally recorded CC-RIXS maps for U^{VI} in ($[U^{VI}O_2$(Mesaldien)] at 90° π scattering geometry and (d) the same U^{VI} compound measured in 172° σ scattering geometry.

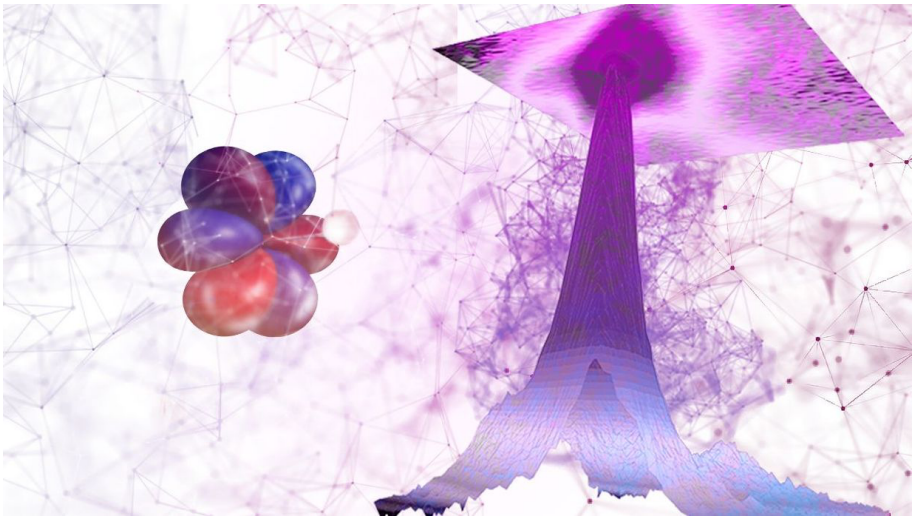

Fig. 5: Artist's concept of the signal (r.) occurring during measurement of resonant inelastic X-ray scattering in samples containing actinides, revealing the number of electrons in the 5f orbitals of the actinide (l.).[6]

We showed with this work that when combining HR-XANES, CC-RIXS and VB-RIXS experimental techniques and computations, a precise characterization of 5f valence electron density with different level of localization in a chemical bond is possible

and can be used to benchmark theoretical approaches.

Three new experimental tools based on a satellite peak in An M_4 edge CC-RIXS spectra for the characterization of the 5f electrons on the actinide atoms were developed.

1) When measured at 90° scattering geometry, the intensity of the satellite peak is sensitive to the number of 5f localized electron density on the An atom (Fig. 4 a-c).

2) Its intensity and energy position can be used to benchmark theoretical calculations.

3) Moreover, when recorded in near backscattering geometry, the intensity of this satellite peak increases and probes variations in bond covalency (Fig. 4 b + d).

This development was possible by CC-RIXS study of 21 different U, Np, Pu and Am compounds in solid and liquid state and novel quantum chemical computations based on multiplet ligand/crystal field theory and ligand field density function theory (LFDFT). [6]

References

[1] C. Apostolidis, R. Molinet, J. McGinley, K. Abbas, J. Möllenbeck, A. Morgenstern, Cyclotron production of Ac-225 for targeted alpha therapy *Appl. Radiat. Isot.* **2005**, *62*, 383–387, DOI 10.1016/j.apradiso.2004.06.013.

[2] T. Sikorsky, J. Geist, D. Hengstler, S. Kempf, L. Gastaldo, C. Enss, C. Mokry, J. Runke, C. E. Düllmann, P. Wobrauschek, K. Beeks, V. Rosecker, J. H. Sterba, G. Kazakov, T. Schumm, A. Fleischmann, Measurement of the Th 229 Isomer Energy with a Magnetic Microcalorimeter *Phys. Rev. Lett.* **2020**, *125*, 142503, DOI 10.1103/PhysRevLett.125.142503.

[3] K. Maurer, D. Unger, M. Behe, A. Knecht, K. von Schoeler, D. Hengstler, T. Vitova, M. Benešová-Schäfer, A. Fleischmann, L. Gastaldo, C. Wängler, C. Enss, B. Schacherl, Advancing towards cancer theragnostic by probing the 225Ac decay chain with ultra-high-resolution metallic mag-netic calorimeter based detectors *Nat. Med. Commun.* **n.d.**, DOI 10.26434/chemrxiv-2025-3591w.

[4] B. Schacherl, M. Tagliavini, H. Kaufmann-Heimeshoff, J. Göttlicher, M. Mazzanti, K. Popa, O. Walter, T. Pruessmann, C. Vollmer, A. Beck, R. S. K. Ekanayake, J. A. Branson, T. Neill, D. Fellhauer, C. Reitz, D. Schild, D. Brager, C. Cahill, C. Windorff, T. Sittel, H. Ramanantoanina, M. W. Haverkort3, T. Vitova, M. W. Haverkort, T. Vitova, Resonant inelastic X-ray scattering tools to count 5 f electrons of actinides and probe bond covalency *Nat. Commun.* **2025**, *16*, 1221, DOI 10.1038/s41467-024-54574-7.

[5] A. Bajaj, H. Ramanantoanina, B. Schacherl, S. Schenk, T. Pruessmann, A. Tasi, D. Fellhauer, A. Humiston, J. Terry, X. Wang, E. Zurek, T. Vitova, P. S. Bagus, J. Autschbach, Actinide 5f Occupations: The Case of PuO2 *Inorg. Chem.* **2025**, *64*, 12297–12312, DOI 10.1021/acs.inorgchem.5c01709.

[6] M. Heidelberger, "KIT Press release: New Measurement Technique Sheds Light on Bonding Properties of Actinides https://www.kit.edu/kit/english/pi_2025_007_new-measurement-technique-sheds-light-on-bonding-properties-of-actinides.php," **n.d.**

9.2 Theoretical spectroscopy

H. Ramanantoanina, C. Reitz, E. Reynolds, B. Schacherl, N. Palina, X. Gaona, D. Fellhauer, D. Schild, T. Prüssmann, T. Vitova

Introduction

Theoretical spectroscopy provides a fundamental bridge between electronic-structure theory and experiment, enabling the interpretation, prediction, and rationalization of complex spectroscopic features across molecular and solid-state systems. The localized and strongly correlated nature of lanthanide 4*f* and actinide 5*f* electrons, combined with their strong spin–orbit coupling and complex ligand-field interactions, gives rise to dense manifolds of multiplet states that dominate their electronic structures. As a result, optical, or X-ray absorption/emission, and other scattering techniques often probe transitions involving an admixture of multiple electron configuration, electron spin, orbitals, and even charge-transfer character. Extracting chemical information from such spectra, even the most obvious ones such as oxidation state or orbital occupations or metal–ligand bonding trends and covalency is then practically challenging and often requires theoretical tools capable of treating multi-electronic interactions with very good accuracy. Over the last decade, the increasing precision of high-energy resolution X-ray spectroscopies, that is also the state-of-the-art of our department "Advanced spectroscopy in *f*-element chemistry", has further amplified the demand for accurate theoretical models. Hereafter, some examples of systems that have been studied in the department within the last four years are highlighted.

Low-lying excited states of lanthanide organometallics

The divalent samarium complex [Sm(II)(η^9-C_9H_9)$_2$] (Figure 1a) has been studied due to its mixed ionic–covalent bonding character and the intricate multiplet structure associated with the Sm^{2+} $4f^6$ and $4f^5 5d^1$ configurations. Using ligand-field density-functional theory (LFDFT),[1] we computed the ground and low-lying excited states of this complex. The calculations show that [Sm(II)(η^9-C_9H_9)$_2$] is highly ionic, with the ground state dominated by the atomic $^7F_0$ (Sm(II) $4f^6$) term, indicating minimal 4*f*–ligand hybridization in the electronic ground-state configuration.[2] The subsequent spin–orbit counterparts $^7F_1$, $^7F_2$, $^7F_3$, $^7F_4$, $^7F_5$ and $^7F_6$ (Sm (II) $4f^6$) constitute the low-lying energy excited states, with also weak energy splitting induced by the ligand-field potential (Figure 1b).

Note that accurately resolving multiplet manifolds remains a major challenge for electronic-structure theory. *f*-element spectroscopy requires explicit treatment of strong electron–electron repulsion, exchange interactions, and near-degeneracy correlation, together with substantial spin–orbit coupling. Multireference wavefunction methods such as CASSCF/CASPT2 can, in principle, describe these effects rigorously, but the active spaces required for Sm(II) $4f^6$ and excited $4f^5 5d^1$ configurations rapidly become computationally prohibitive. On the other hand, conventional TDDFT and related DFT-based response methods struggle with dense multiplet manifolds, double excitations, and open-shell *f*-electron near-degeneracies. We have used

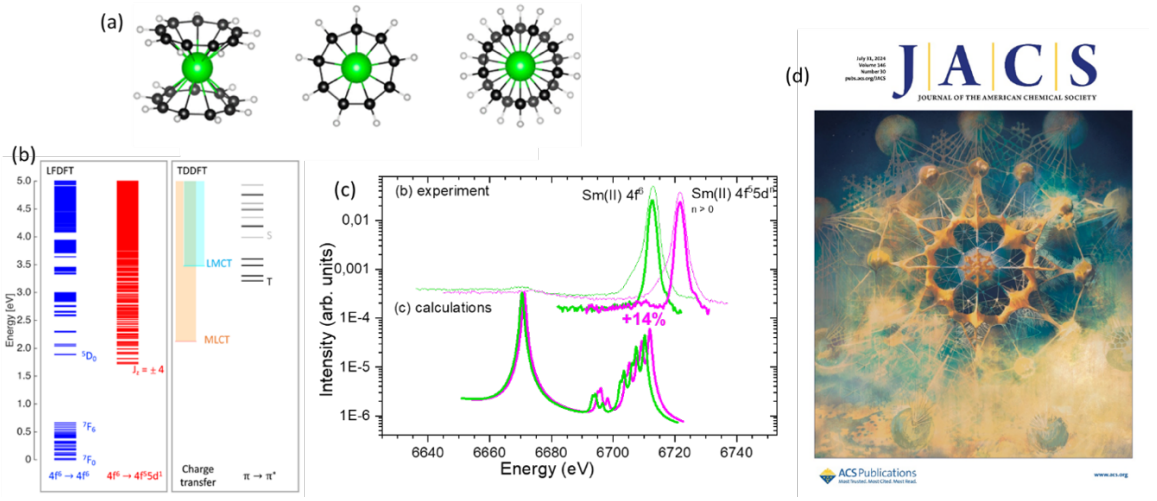

Fig. 1: (a) Representation of the molecular complex [Sm(II)(η^9-C_9H_9)$_2$] belonging to the D_{9h} and D_{9d} point groups via free rotation of the (η^9-C_9H_9) ligand; (b) ground and low-lying excited states of [Sm(II)(η^9-C_9H_9)$_2$] calculated with LFDFT; (c) experimental and calculated Sm L_3-edge VB-RIXS spectra of [Sm(II)(η^9-C_9H_9)$_2$]; (d) front cover of the J. Am. Chem. Soc. (see ref. [2]).

the LFDFT method since it circumvents these limitations by extracting ligand-field, inter-electron correlation, and spin–orbit parameters from DFT and reconstructing a compact many-electron Hamiltonian that retains the essential physics of the f-shell while remaining computationally efficient. In the present case, LFDFT reproduces the entire Sm(II) $4f^6$ and $4f^5 5d^1$ (Figure 1b) multiplet manifolds and their ligand-field splitting with good accuracy.

Beyond the intra-configurational 4f-4f excitations, LFDFT also identifies the next low-lying excited states of [Sm(II)(η^9-C_9H_9)$_2$] as belonging to the Sm(II) $4f^5 5d^1$ configuration, lying approximately 1.7 eV above the ground state (Figure 1b). Here the 5*d* ligand-field splitting is very large (in fact, it is 6 times larger than 4*f*), It is then possible that some Sm(II) $4f^5 5d^1$ states are found below $^5D_0$ (Sm(II) $4f^6$) level. These $4f^5 5d^1$ states exhibit markedly different bonding behavior: the DFT calculation shows that occupation of the Sm 5*d* orbitals leads to a noticeable contraction of the Sm–C bond distances, signaling significantly increased metal–ligand covalency relative to the ground-state $4f^6$ configuration.[2] That is, 5*d* orbitals are radially diffuse and capable of stronger overlap with ligand π-systems. We corroborated this prediction experimentally using Sm L_3-edge valence-band resonant inelastic X-ray scattering (VB-RIXS) (Figure 1c), which directly probes the Sm 5*d* orbitals. The spectra show enhanced intensity in features associated with 5*d* character upon population of the Sm(II) $4f^5 5d^1$ low-lying excited states, providing direct spectroscopic evidence for the increased covalency predicted by LFDFT. These findings have been highlighted in the front cover page of the *J. Am. Chem. Soc.* (Figure 1d).[2]

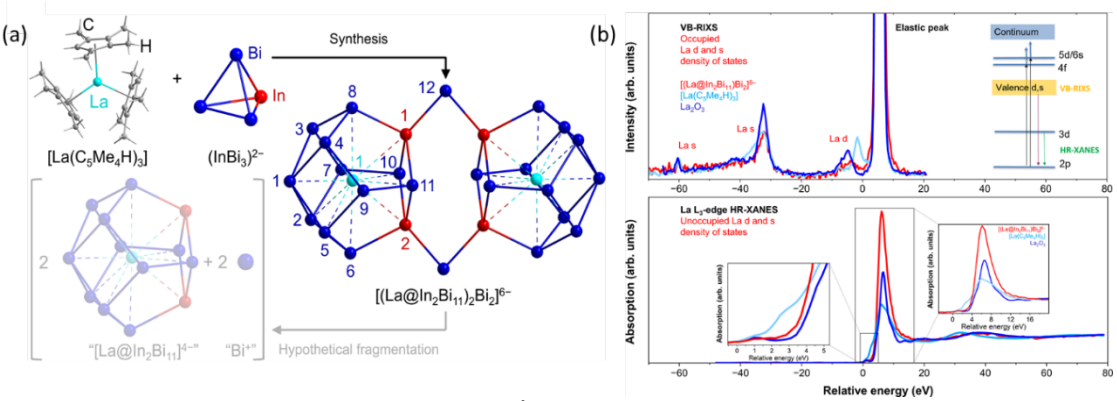

Fig. 2: (a) Representation of the cluster $[(La@In_2Bi_{11})_2Bi_2]^{6-}$ and its precursor $[La(C_5(CH_4)_4H)_3]$; (b) La L_3-edge HR-XANES and VB-RIXS spectra of $[(La@In_2Bi_{11})_2Bi_2]^{6-}$ $[La(C_5Me_4H)_3]$, and La_2O_3 as reference.

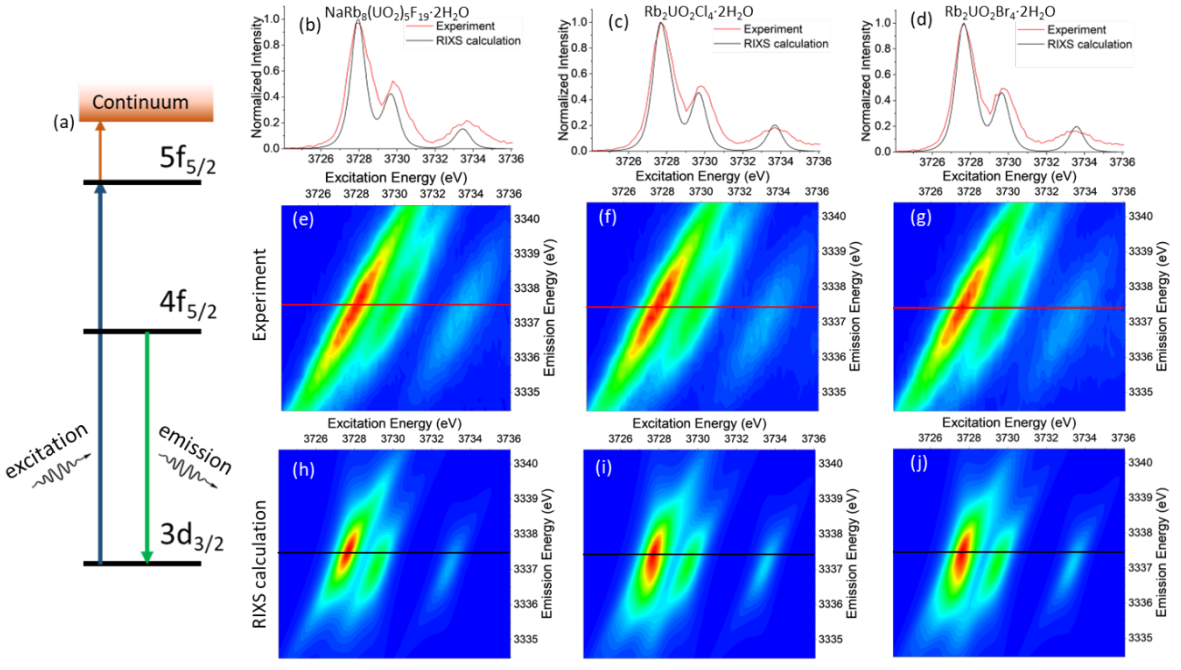

Fig. 3: (a) Mechanism of the U M_4-edge CC-RIXS; (b-d) Experimental and calculated HR-XANES spectra of $[UO_2F_5]^{3-}$, $[UO_2Cl_4]^{2-}$ and $[UO_2Br_4]^{2-}$; (e-g) Experimental CC-RIXS maps for $[UO_2F_5]^{3-}$, $[UO_2Cl_4]^{2-}$ and $[UO_2Br_4]^{2-}$; (h-j) Calculated CC-RIXS maps for $[UO_2F_5]^{3-}$, $[UO_2Cl_4]^{2-}$ and $[UO_2Br_4]^{2-}$.

Bonding interaction in multimetalloid cluster

The La–In–Bi cluster $[(La@In_2Bi_{11})_2Bi_2|^{6-}$ has been studied (Figure 2a) as a model system where ionic trapping, covalent interaction, and metallic delocalization can coexist in a single bonding motif.[3] The encapsulated lanthanide ion interacts with the highly electron-rich In/Bi cage, where the lanthanide 5*d* orbitals meaningfully participates in bonding, in stark contrast with the largely ionic character observed in its molecular precursor $[La(C_5(CH_4)_4H)_3]$ (Figure 2a).[3] High-energy-resolution X-ray absorption near edge structure (HR-XANES) and VB-RIXS spectra (Figure 2b) reveal a well-defined covalent La(5*d*)–Bi(6*p*) interaction (Figure 2b), superimposed on an overall ionic framework (localized 4*f* orbitals) that stabilizes the encapsulated La^{3+} center. The electronic structure of the Bi/In cage further introduces a metallic-like delocalization of electrons with mixed *p*/*d* character, reflected in the spectral line shapes and in the low-energy unoccupied angular momentum-projected density of states of the Bi and In elements.

The element- and orbital-selectivity of the advanced X-ray spectroscopies allowed us to disentangle the contributions of La 5*d*, In 5*p* and Bi 6*d* to the electronic structure. Direct comparison between the multimetalloid cluster and the precursor demonstrates that cage encapsulation activates La 5*d* participation, while preserving the largely atomic $4f^0$ configuration. These experimental observations were corroborated by theoretical modelling by using the GW and Bethe–Salpeter equation (GW-BSE) calculations,[3] which reproduce the spectroscopic features and confirm that La–Bi covalency is driven by overlap between extended La 5*d* functions and Bi 6*p* orbitals in a strongly reducing environment.

Modelling of core-to-core resonant inelastic x-ray scattering

The low-lying multiplet calculations presented in the first section highlighted the reliability of the LFDFT method[1] for describing the electronic structure of open-shell f-element systems. Motivated by these results, we extended the LFDFT formalism[1] toward the modelling of core-to-core resonant inelastic X-ray scattering (CC-RIXS) that probes core-excited states (exciton) and their associated fluorescence decay channels. The present section summarizes the new theoretical developments introduced to handle core-level multiplets, CC-RIXS polarization dependence, and scattering geometry, and showcases representative applications of the resulting LFDFT/CC-RIXS studies on U M_4-edge CC-RIXS in uranyl halides. Three systems are into consideration: $[UO_2F_5]^{3-}$, $[UO_2Cl_4]^{2-}$ and $[UO_2Br_4]^{2-}$ complexes (Figure 3).[4]

In the U M_4-edge 3*d*4*f* CC-RIXS, the excitation by an incident photon is accompanied by the emission of a second photon. This involves the ground state U(VI) $5f^0$ as the initial state, the core-excited state U(VI) $3d^9 5f^1$ as the intermediate state, and another core-excited state U(VI) $4f^{13} 5f^1$ as the final state (Figure 3a), giving rise to muli-electronic structure problem.

Experimental CC-RIXS data for the uranyl halides are shown in Figure 3(e–g), alongside RIXS calculations performed using LFDFT (Figure 3(h–j)), whereby the core holes in both intermediate (3d) and final state (4*f*) are explicitly considered. A comparison between experimental and theoretical HR-XANES spectra is shown in Figure 3(b-d), showing good agreements between them.

References

[1] H. Ramanantoanina, LFDFT - A Practical Tool for Coordination Chemistry, *Computation* **2022**, *10*, 70.

[2] T. Vitova, H. Ramanantoanina, B. Schacherl, L Münzfeld, A. Hauser, R. S. K. Ekanayake, C. Y. Reitz, T. Prüssmann, T. S. Neill, J. Göttlicher, R. Steiniger, V. A. Saveleva, M. W. Haverkort and P. W. Roesky, Photon-Modulated Bond Covalency of $[Sm(II)(\eta^9\text{-}C_9H_9)_2]$, *J. Am. Chem. Soc*. **2024**, *146*, 20577-20583.

[3] H. Ramanantoanina, J. Rienmüller, Y. R. Lohse, M. Rauwolf, M. Kehry, C. Reitz, E. M. Reynolds, T. Prüssmann, B. Schacherl, V. Saveleva, R. S. K. Ekanayake, J. Göttlicher, B. Weinert, W. Klopper, S. Dehnen and T. Vitova, Molecular-Metallic Binding Characteristics of the Intermetalloid *f*-/*p*-Block Cluster $[(La@In_2Bi_{11})_2Bi_2]^{6-}$, *Angew. Chem. Int. Ed*. **2025**, *64*, e202512019.

[4] T. S. Neill, H. Ramanantoanina, N. Palina, T. Prüssmann, J. Rothe, X. Gaona, D. Fellhauer, D. Schild, C. Wansorra, D. Hauschild, R. Steiniger, B. Schacherl, C. Heske, L. Weinhardt, O. Walter, F. Weigend and T. Vitova, The Role of Halides in the Bonding and Electronic Structure of Actinyl(VI) Halides - Energy Match Driven Stability, *J. Am. Chem. Soc.* **2025**, *147*, 35401-35412

10 (Radio-)chemical analysis

The task of the analysis team consists of the (radio)chemical analysis for the R&D projects of the INE, the analytical service for external customers, the development and adaptation of analytical methods, teaching and training of students and trainees, and finally the support of the INE infrastructure. A pool of instruments is available and is continuously adapted to the state of the art. Our staff is highly qualified and specialized in the analysis of radioactive samples. These include the handling of radioactive material, radiochemical separation processes for elemental and isotope analysis, and in the operation and maintenance of glove box compatible instruments. Our analytical service for external clients is in the areas of nuclear decommissioning, nuclear waste declaration, nuclear pharmacy and others. A particular focus is on mass spectrometry for trace element analysis and speciation studies of actinides and fission products. Composite techniques such as sector field or quadrupole ICP-MS coupled with a species-sensitive method, e.g. capillary electrophoresis (CE), are adapted and further developed. Another focus is accelerator mass spectrometry (AMS) for the sensitive determination of actinides and of ^{99}Tc in or even below the ppq range, which is carried out in close cooperation with international AMS institutions (see chapter 8.3).

M. Plaschke, M. Bachert, C. Beiser, M. Böttle, D. Fellhauer, A. Fried, M. Fröhlich, M. Fuss, F.W. Geyer, F. Heberling, T. Kisely, S. Kraft, S. Kuschel, C.M. Marquardt, S. Moisei-Rabung, P. Müller, F. Quinto, D. Rehhorn, J. Rentmeister, T. Roth, F. Steegborn, H. Geckeis

In co-operation with:

E. Hahn[a], S. Bahl[a], D. Lemmer[a], C. Troelenberg[a], A. Nothstein[b], P. Steinbach[b], T. Schäfer[c], A. Martin[d], R. Schneeberger[d]

[a] Kerntechnische Entsorgung Karlsruhe (KTE), Hermann-von-Helmholtz-Platz 1, 76344 Eggenstein-Leopoldshafen, Germany, [b] KIT-SUM, [c] Friedrich-Schiller-University Jena (FSU), Institute of Geosciences, Jena, Germany, [d] Nagra (National Cooperative for the Disposal of Radioactive Waste), Wettingen, Switzerland

Instrumentation

A number of new high-performance instruments were put into operation during the reporting period. Table 1 presents the spectrum of analytical techniques available at INE.

Table 1: Analytical techniques available at INE

Element and Isotope Analysis
Quadrupole Inductively Coupled Plasma (ICP) Mass Spectrometry (Q)-ICP-MS)
Triple Quadrupole (TQ)-ICP-MS
Sector-Field (SF)-ICP-MS
ICP Optical Emission Spectrometry (ICP-OES)
Nuclear Spectroscopic Methods
Alpha Spectrometry
Liquid Scintillation Counting (LSC, conventional/high sensitivity/TDCR)
Gamma Spectrometry (with auto-sampler)
Other Methods
Wavelength Dispersive X-ray Fluorescence (WDXRF)
(Capillary) Ion Chromatography (IC)
Capillary Electrophoresis (CE)
Gas Chromatography Mass Spectrometry (GC-MS)
Carbon Analysis (TOC, DOC, TIC, NPOC)
Specific Surface Area Analysis (BET)
Differential Thermal Analysis (DTA)
Dilatometry
Fusion and Microwave Digestions

NexION5000 ICP-MS: A state-of-the-art Triple Quadrupole (TQ)-ICP-MS is installed in our radioactive area. The triple-quadrupole technology is capable of analyzing trace elements in the ultra-trace range even in complex matrices. The standard reference material SLRS-6 was analyzed in different measurement modes, including single quadrupole (SQ), MS/MS (filtering and analyzing quadrupole) and KED (kinetic energy discrimination). While the measured intensities (cps) for ^{238}U decrease in the order SQ>MS/MS>KED, the background equivalent concentration (BEC) values (as a measure of the signal-to-background ratio) for all modes are relatively close at about 0.5 ng/L. As expected, the lowest instrument detection limits (IDL) for ^{238}U were achieved in the SQ mode in the range of 0.1 ng/L. Nevertheless, the stronger filtering measurement modes are advantageous for other nuclides or samples with more complex matrices. The instrument is meanwhile nuclearized.

Bruker Tiger S8 Series 2 WDXRF: A 4 kW Bruker Tiger S8 Series 2 WDXRF was put into operation, providing high analytical precision (generator stability), best excitation of light elements (high excitation current) and a small spot size (300 µm) for element mappings (µ-XRF). This instrument is ideal for geological and mineral applications as well as for cement and construction materials. A first application of µ-XRF is the spatially resolved study of the surface mineral composition of an Opalinus clay (OPA) sandy facies sample (see below).

Avio 550 Max ICP-OES: The Avio550 Max is a fully automated ICP-OES for simultaneous multi-element analysis over the entire wavelength range from 163-782 nm. The vertical design of the sample chamber makes the instrument more compact (width only 63 cm) and allows it to be placed completely in a glove box for radioactive measurements. The instrument is meanwhile nuclearized.

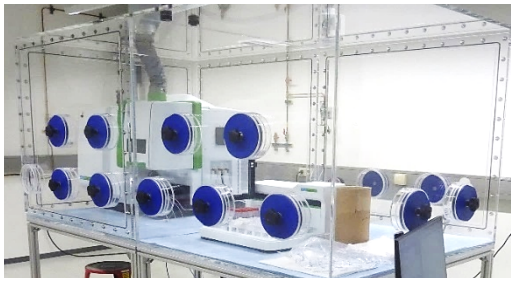

Fig. 1: Avio 550 ICP-OES adapted to a box (INE development)

A picture of the Avio 550 Max installed in a box is shown in Fig. 1. IDL for, e.g., Fe (238.204 nm), Sr (407.771 nm) and U (385.958 nm) have been determined to be 0.9, 0.01 and 19.6 µg/L, respectively, which are not affected by the box installation.

Hidex ULLA and 600 SL LSC: The Hidex ULLA is a ultra-low-level LSC counter with a special lead shielding, a guard detector and a detection unit consisting of three selected photomultiplier tubes. The determination of the triple-to-double coincidence ratio (TDCR) is a primary measurement method that allows an absolute measurement of radionuclides (RN) by LSC. The triple coincidences are much more affected by quench effects (especially color and chemical quench) than the double coincidences. The Hidex devices are also equipped with a very convenient alpha/beta discrimination technology.

The determination of certified ^{55}Fe and ^{63}Ni standards by different counting methods (TDCR, quench curve), instrumentation and in two different laboratories (KIT-INE and KIT-SUM) is summarized in Table 2, also demonstrating the capability of TDCR.

*Table 2: Certified and measured values (Bq/mL) of a ^{55}Fe and ^{63}Ni standard using different LSC counters**

		INE	SUM	
Nuclide Bq/mL	Certificate Value and Uncertainty	Hidex 600SL TDCR	Hidex 300SL TDCR	Packard 5 quench curve
^{55}Fe	127,1±5,5	126,8±6,3	128,0±6,4	121,2±6,1
^{63}Ni	74,71±2,2	77,2±3,7	74,6±3,7	74,2±3,9

**Assuming an uncertainty of 5% for all measurements*

In addition, a 3P micro 200B1 BET, a Mettler Toledo system for pipette calibration and a gas chromatography triple quadrupole mass spectrometry system (Thermo TSQ 9610 GC-MS/MS) were recently put into operation.

Method developments

Coupling of CE with SF-ICP-MS

Capillary Electrophoresis (CE) is an analytical technique that is used to separate atoms and molecules based on their charge and size. The basic setup of CE consists of a thin (ca. 50 µm internal diameter) silica capillary filled with an electrolyte (Fig. 2). The sample is injected at one end of the capillary as a small plug (multiple nL). A potential is applied to the ends of the capillary, which initiates the sample components to travel through the capillary with a speed that is based on their charge and size. After spatial separation, the analytes successively pass a detector. Most commercial CE instruments are equipped with a UV/VIS detector for identification and determination of species concentration. CE coupled with (ICP-)MS (CE-MS) combines the separation capability of CE with the high sensitivity of ICP-MS for elemental analysis.

An Agilent 7100 CE is successfully coupled with a Thermo Element XR SF-ICP-MS for the analysis of redox species (Fig. 2). The outlet side of the capillary is inserted into a low-volume nebulizer. Due to the low sample flow of the capillary, additional solution has to be provided via a syringe pump to operate the nebulizer (make-up solution). Sample solution, leaving the capillary, is converted into an aerosol that is passed on to the MS through polymer tubing. The spatial separation of the sample species based on their charge and size with CE (which makes the species arrive at the ICP-MS at different times) results in a time-resolved mass spectrum (electropherogram).

Fig. 3 shows the results of CE-MS analysis of multiple samples with distinct Pu oxidation states, as stacked electropherograms. The samples were heavily diluted with 1M acetic acid to ensure that Pu was quantitatively complexed with acetate. With knowledge of the electrophoretic mobilities (i.e. the speed of migration through the CE capillary) of the Pu-acetate complexes of each Pu oxidation state, the peaks in the electropherograms could be assigned. In this way, all relevant oxidation states of Pu could be successfully identified. The Pu(VI) sample in Fig. 3, however, shows one of

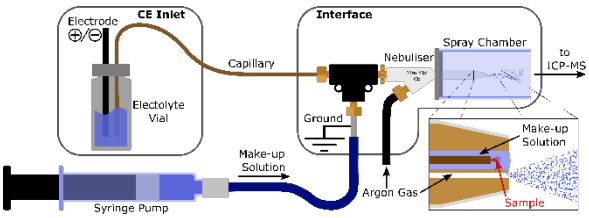

Fig. 2: Experimental setup of CE-MS, see text.

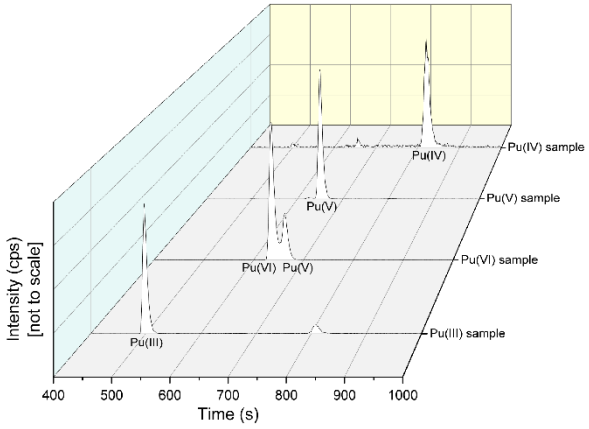

Fig. 3: CE-MS electropherograms of different Pu oxidation states in 1M acetic acid: c(Pu) ca. 2E-8 M; hydrodynamic injection: 20s / 100mbar; electrolyte: 1M acetic acid, pH 2.4; voltage: 30kV.

the limits of the currently employed CE-MS method. In the original sample, Pu was quantitatively present as Pu(VI), but in the time from dilution of the sample to the start of the CE-MS analysis, already 25% of Pu(VI) was reduced to Pu(V). Subsequent measurements showed this reduction reaction to be time-dependent. Thus, Pu(VI) seems to be unstable in 1M acetate, and only a lower limit of the Pu(VI) content of the original sample can be identified with the current method.

Contract analyses

Analytical service is offered to external clients, e.g., in the fields of nuclear waste declaration, decommissioning and nuclear pharmacy.

Nuclear pharmacy

Since 2018 we have a co-operation in the field of nuclear pharmacy with the Norwegian company *Oncoinvent AS*. *Oncoinvent* is committed to developing new innovative products to provide better treatment options for cancer patients. The radiopharmaceutical Radspherin® is a novel alpha-emitting radioactive microsphere suspension designed for treatment of metastatic cancers in body cavities. The active component ^{224}Ra is incorporated in inorganic microparticles of Ca_2CO_3 acting as carriers in the human body. This allows for a relatively slow degradation in the body and a regional retention of effective radiation dose. INE analyzed Radspherin® and technical samples with regard to toxic heavy metal trace impurities and matrix elements. Radspherin® is currently being evaluated in ongoing Phase 2 clinical trials (information taken from [1]). Since the end of 2024, Oncoinvent has its own laboratory capacities for elemental analysis and will only use INE's services occasionally.

Nuclear waste treatment and decommissioning of nuclear facilities (KTE)

For more than 25 years, INE has been performing contract analyses for waste declaration of low and intermediate level nuclear waste (LAW and MAW) and dismantling projects, for which the Kerntechnische Entsorgung Karlsruhe GmbH (KTE) is responsible. The samples are taken at the various waste treatment facilities at KTE, mainly the incineration facility (ashes) and the evaporation plant (liquid waste concentrates) including annually averaged samples. Samples from decommissioning of nuclear facilities include demolition waste, digested wipe tests or drying residues (see next paragraph). At INE, isotope concentrations and compositions are determined by the combination of radiochemical separations with nuclear and mass spectrometry techniques. The analyzed RN include neutron activation and fission products (^{55}Fe, ^{63}Ni, ^{90}Sr, ^{99}Tc), as well as actinides (U, Pu and Cm isotopes).

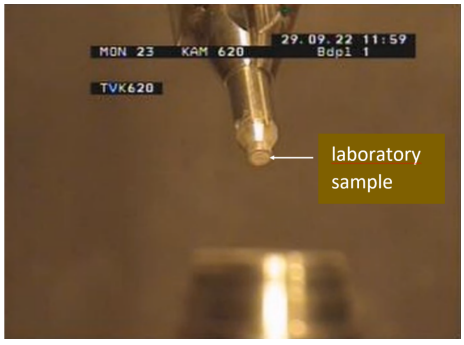

Fig. 4: Sample stamp filled with a laboratory sample of HAWC drying residue (image courtesy of KTE), see text.

Accompanying analyses for decommissioning of WAK HAWC storage tanks (KTE)

During the reprocessing process at the Karlsruhe Reprocessing Plant (WAK) in the 70s to 90s of the last century, nuclear fuel was separated and subsequently returned to the nuclear fuel cycle. The resulting liquid radioactive waste was temporarily stored in the form of so-called HAWC (High Active Waste Concentrate) in three storage tanks. KTE is responsible, among other things, for the dismantling of the WAK and disposal of its waste to the final repository Konrad. The dismantling of the first HAWC storage tank, named 210 B 02, with a residual activity of about $1.5*10^{15}$ Bq and a capacity of about 83 m^3 has carried out. Inside the storage tank, there are internals consisting of more than 500 m of cooling coils for the removal of the decay heat and six pulsators that provided continuous circulation of the HAWC during storage. Two types of waste are generated during the dismantling of 210 B 02: Metallic waste with contamination adhesions and solid residue materials from the dried HAWC rinsing solutions, which account for the majority of the total activity. In order to be able to declare the resulting residues radiologically, knowledge of the RN composition (nuclide vector) is necessary. Therefore, a disposal concept including a sampling strategy was prepared in the course of the dismantling planning for the storage tank. The sampling of material for analysis took place immediately after opening of the tank and removal of a part of the cooling coils in the presence of an expert for the disposal process. Material for one sample was scraped from the cooling coils and three samples were taken at different locations from the bottom area of the tank. All actions were performed remotely by manipulator technics. To ensure the representativeness of the sampling, approx. 60 g of the residual material were taken and ground. Of this, a laboratory sample of about 30 - 70 mg size was remotely obtained by pressing a sample stamp with a defined cavity of about 50 µl into the powder (Fig. 4).

The samples (contact dose rate of up to 260 mSv/h) were each transported in a shielded barrel to the MAW laboratory of KTE for radiological analysis. There, the samples were digested and the dose rate determining ^{137}Cs was separated. An aliquot of the diluted and Cs-separated digestion solution was transported to INE for analyses of the beta emitters ^{90}Sr, ^{63}Ni, and ^{55}Fe, as well as U, Pu, and Cm isotopes, with particular emphasis on the ^{90}Sr value. The analytical results available so far for the cooling coil sample and the first sample from the 210 B 02 bottom area are in good agreement with the assumed HAWC nuclide vector.

Analyses for INE R&D

The analytics group makes contributions to projects, theses and applied research, as shown here with selected examples:

Heterogeneity of OPA sandy facies

In this study, the sorption of ^{137}Cs on an intact Opalinus Clay (OPA) sandy facies surface is investigated. Due to the heterogeneity of the material, a quantitative, spatially resolved and at the same time non-destructive method for surface mineral analysis is advantageous, like µ-XRF. A bore core (named BDR-D1) was cut into discs out of which a cylinder with a diameter of 2 cm was drilled. The surface was polished and cleaned to remove any residue particles. The bulk mineral composition obtained by XRD and quantified by Rietveld refinement indicated Calcite (65.4%), Quartz (14.8%), Clay minerals (9.6%), Orthoclase (5.7%), Siderite (2.6%) and Pyrite (~2%).

Before starting the sorption experiment, the types and distributions of minerals present at the surface were examined by µ-XRF. A µ-XRF elemental mapping with a 300 µm spot size and the corresponding mineral assignments is shown in Fig. 6. It should be noted that features in the optical image (Fig. 5 a) are not necessarily mapped in the element distributions at the surface (Fig. 5 b and c). The distributions of major and minor elements are seen in Fig. 6 b and c.

The main minerals at the surface were assigned as follows: Calcite (mainly Ca), Quartz (mainly Si and no Al) and Clay minerals (Si, Al and partly Fe, Mg and K), see assignments in Fig. 5 b. Furthermore, some minor minerals like Rutile (indicated by Ti), Pyrite (indicated by Fe and S) and Apatite (indicated by P) could be identified (Fig. 5 c). The surface mineral composition detected by µ-XRF is in general agreement with the bulk XRD results. An interesting finding is, that the area covered in fossil remnants (the right ~80 surf%, yellow in Fig. 5 b) is dominated by Calcite and the left ~20 surf% is dominated by Clay minerals and Quartz.

^{233}U, ^{237}Np and ^{242}Pu breakthrough in CFM run 22-02

The concurrent determination of several long-lived actinides at the levels of ppt down to ca. 50 ppq can be achieved in low mineralized water samples without any previous chemical separation by SF-ICP-MS. An exemplary application of such an analytical method is the determination of the breakthrough curves of actinide tracers in the frame of the latest *in-situ* radionuclide tracer test performed at the Grimsel Test Site (GTS) underground laboratory [5], named CFM run 22-02 (for further details on the experiment, see chapters 5.3 and 8.3).). Briefly, a cocktail of Grimsel groundwater (GGW), Na-Febex bentonite and Ni-labelled Montmorillonite colloids, the conservative tracer fluorescence AminoG as well as radionuclide tracers, among which ^{233}U, ^{237}Np, ^{242}Pu and ^{243}Am, was prepared in the controlled area of KIT-INE. Such cocktail was then injected into a hydrological dipole intersecting a water conductive shear zone in the granodiorite rock of the

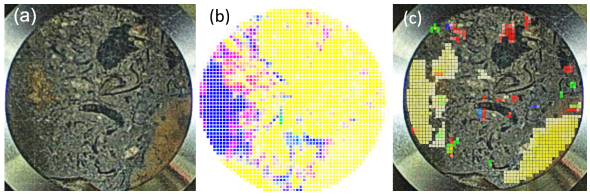

Fig. 5: OPA sample area (a) optical image, (b) µ-XRF mapping of the major elements and corresponding mineral assignments: Calcite (mainly Ca) colored in yellow, Clay minerals (Si associated with Al, Fe, Mg, K) colored in blue and Quartz (only Si) colored in pink, and (c) µ-XRF mapping of the minor elements Ti, Fe, S and P in blue, yellow, red and green, respectively; see text.

GTS. GGW samples were periodically collected and analyzed for their concentration of actinide tracers with SF-ICP-MS. Additionally, the concentration of Ni at the level of ppb was determined with Q-ICP-MS in the same GGW samples as proxy for the breakthrough of Ni-labelled Montmorillonite colloids as well as Na-Febex bentonite colloids.

Fig. 6 and Fig. 7 depict the breakthrough curves for ^{233}U, ^{237}Np and ^{242}Pu as well as for Ni, respectively. As shown in Fig. 7, the peak of the breakthrough curve for Ni (*i.e.*, for the clay colloids) resembles those of ^{242}Pu (in Fig. 6) and ^{243}Am (not shown here), pointing towards a colloid-mediated transport of ^{242}Pu (IV) and ^{243}Am (III) species. As it can be seen in Fig. 6, the breakthrough peak for ^{233}U is slightly retarded compared with that for ^{242}Pu, reflecting the expected stabilization of ^{233}U(VI) as soluble $CaUO_2(CO_3)_3^{2-}$ complexes in the geochemical conditions of GGW [6]. ^{237}Np shows a much higher retardation factor that is presently estimated as equal to ca. 1.8. While there is

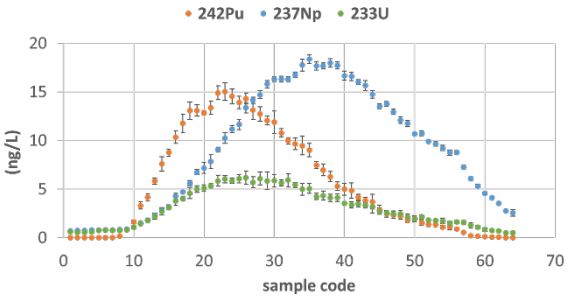

Fig. 6: ^{233}U (green dots), ^{237}Np (blue dots) and ^{242}Pu orange dots) breakthrough curves for CFM run 22-02 determined by SF-ICP-MS in GGW samples.

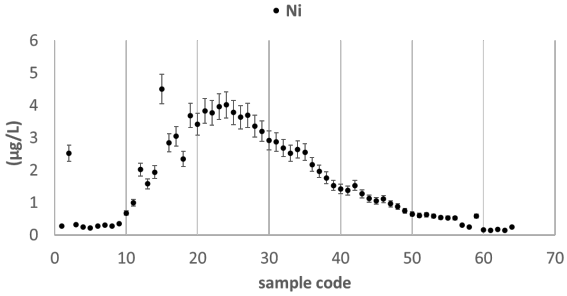

Fig. 7: Ni breakthrough curve (indicative of the Ni-labelled Montmorillonite colloids) for CFM run 22-02 determined by Q-ICP-MS in GGW samples.

no indication of a fraction of ^{237}Np migrating as colloid-bound species, the observed retardation of ^{237}Np suggests that there may have been *in-situ* some limited reduction from Np (V) to more adsorbing Np (IV) during Np transport through the shear zone.

For the analysis of the actinide tracers in GGW at levels below ca. 50 ppq, AMS is the technique of choice, providing the sensitivity to determine actinide tracer concentrations encompassing the long-term tailing of their breakthrough curves (see chapter 8.3).

References

[1] www.oncoinvent.com
[2] Keith-Roach et al., (2021), SKB Report R-20-04.
[3] Tasi et al., (2021), Appl. Geochem., 126, 104862.
[4] Szabo et al., (2022), Dalton Trans., 51, 943.
[5] https://www.grimsel.com/gts-projects/cfm-section/cfm-introduction
[6] Montoya et al., (2022), J. Hazard. Mater., 424, 12773351.

11 Geoenergy research

The Karlsruhe Institute of Technology (KIT) conducts an integrated research agenda on deep geothermal technologies within the program "Materials and Technologies for the Energy Transition" of the Helmholtz energy research field. Two large-scale research infrastructures are being established to conduct research into the two main areas of focus: EGS (Enhanced Geothermal Systems) and high-temperature heat storage. These are the planned underground research laboratory GeoLaB, and the pilot storage project on the KIT North Campus, DeepStor. Geoenergy research at INE focuses on the infrastructure development of these strategic research infrastructures. Special areas of expertise include geophysical monitoring and characterization methods and – newly built up – advanced digital methods.

T. Kohl, E. Schill et al.

Introduction

Achieving climate neutrality requires both the rapid expansion of renewable energy generation and the deployment of reliable energy storage technologies capable of balancing temporal mismatches between supply and demand. This challenge is particularly pronounced in the heating sector, where seasonal variability dominates consumption patterns and fossil fuels remain the primary energy source for space heating, district heating, and industrial process heat across Central Europe. Geoenergy technologies – including deep geothermal systems and subsurface thermal energy storage – have emerged as a key component of the transition toward low-carbon heat supply by utilizing the thermal capacity of the subsurface.

KIT geoenergy research adopts a systems-oriented perspective that integrates geological characterization, reservoir physics, numerical modeling, infrastructure development, and societal engagement. This approach incorporates multiple disciplines, ranging from geosciences and engineering to social sciences.

Within this strategic framework, two research infrastructures form the backbone of current activities: GeoLaB, a planned geothermal underground research laboratory in crystalline basement rocks, and DeepStor, an application-oriented infrastructure investigating high-temperature aquifer thermal energy storage (HT-ATES) in a sedimentary reservoir of the Upper Rhine Graben. Over the past two years, both infrastructures have progressed significantly, supported by advances in structural geology, numerical and stochastic modeling approaches, and multi-physics simulation workflows that strengthen the scientific basis for safe and efficient subsurface energy utilization. Integrated modelling workflows and stochastic geological representations were further advanced to support experiment planning at GeoLaB and reservoir evaluation at DeepStor. By embedding multiple geological scenarios into coupled simulations, these approaches strengthen the robustness of subsurface predictions and improve the transferability of results across different application contexts.

Societal integration has become an explicit pillar of research infrastructure development. Visualization tools, immersive digital environments, and participatory monitoring concepts were increasingly incorporated into project development processes (Fig. 1). These activities reflect the growing recognition that public acceptance, stakeholder engagement, and transparent communication are essential prerequisites for the successful implementation of large-scale subsurface energy projects.

Fig. 1: In a virtual elevator, stakeholders can explore the under-ground beneath their feet and learn about necessary conditions for deep geothermal storage.

GeoLaB: Development of a Geothermal Underground Research Laboratory

GeoLaB (Geothermal Laboratory in the Crystalline Basement)[1] is being developed as a large-scale underground research infrastructure designed to investigate geothermal processes in fractured crystalline rock under controlled conditions. Its principal scientific objective is to bridge the scale gap between laboratory experiments and reservoir-scale geothermal operations by facilitating controlled, long-term experiments under realistic geological conditions.

[1] https://geolab.helmholtz.de/

Crystalline basement rocks represent a substantial geothermal energy resource in Central Europe; however, they are also associated with elevated levels of uncertainty. The regulation of fluid flow is predominantly governed by fracture networks as opposed to matrix permeability. Furthermore, thermal, hydraulic, and mechanical processes exhibit a high degree of interconnection. GeoLaB has been developed to address these challenges by providing a specific, non-commercial research environment in which experiments can be designed flexibly.

The scientific scope of GeoLaB includes:

- Coupled THMC processes during fluid circulation and thermal loading,
- Targeted stimulation experiments in fractured crystalline rock,
- Stress redistribution, fracture transmissivity evolution, and induced seismicity,
- Wellbore and reservoir integrity under cyclic geothermal operation, and
- Advanced monitoring, data integration, and digital laboratory concepts.

A pivotal accomplishment during the reporting period was the start of the exploration phase. After conducting a thorough multi-criteria evaluation, the Tromm region in the Odenwald was identified as the primary candidate area for conducting site investigations. The region under consideration provides access to crystalline basement rock, which is representative of deep geothermal reservoirs in the Upper Rhine Graben. It also allows in situ investigations at comparatively shallow depth. In early 2025, the first deep exploration borehole, GeoLaB-1 (GLB-1), reached its final depth. GLB-1 provided essential data on lithology, fracture density, in situ stress conditions, and hydraulic properties. These data significantly reduced geological uncertainty and enabled refinement of site-specific geological and geomechanical models.

A second well (GLB-2) was drilled with the goal to complement and validate the findings from GLB-1 by providing additional structural constraints and improving the three-dimensional understanding of fracture networks and stress heterogeneity. GLB-1 and GLB-2 form the foundation for the scientific site assessment, and they are critical for the upcoming site decision, which is anticipated in 2026.

Concurrent with field exploration, significant advancements were made in numerical modeling and digital infrastructure development. Digitalization is a core element of the GeoLaB concept. Integrating geological models, monitoring data, and process simulations is essential to the development of a digital GeoLaB and a future digital twin. Virtual and immersive visualization tools support planning, interpretation, and communication. These digital components are designed to accompany the entire lifecycle of the infrastructure, from planning and construction to scientific operation. In this context, the BMBTR funded GeoDT project was successfully acquired, with UFZ serving as the coordinating institution.

A comprehensive communication strategy was developed and implemented for the complex GeoLaB project with differing stakeholders. It combines digital formats such as social media and website content with analogue materials including flyers and market stands. Hands-on activities, including offers for schools, were established to foster information transfer and dialogue. Local perspectives gathered through these activities are fed back into the planning and development of GeoLaB.

Experimental Platforms for Multi-Scale Process Investigations

To complement field-scale research at GeoLaB and DeepStor, KIT operates coordinated laboratory experiments addressing coupled thermo-hydro-mechanical-chemical processes across scales. The DFG large-scale research instrument F4aT Laboratory investigates fracture hydraulics and nonlinear flow behavior in controlled rough-fracture experiments, providing fundamental insight into fluid flow processes relevant for geothermal reservoirs [2]. Building on this work, RockBlockEx extends experimental research to the cm–m scale by studying hydro-fracturing and reactive flow in instrumented rock blocks representative of crystalline and sedimentary reservoir settings.

The RockBlockEx setup combines controlled pressure and temperature conditions with multi-parameter monitoring, including acoustic emission, geochemical sensors, and electric or electromagnetic measurements. This enables investigation of coupled hydraulic, mechanical, and electrochemical responses during fluid injection experiments, with particular emphasis on monitoring strategies and potential precursors of induced seismicity. Together, F4aT Laboratory experiments and RockBlockEx bridge the gap between microscale fracture physics and field-scale infrastructure research, supporting experimental design and monitoring concepts for GeoLaB and DeepStor.

DeepStor: Research Infrastructure for High-Temperature Aquifer Thermal Energy Storage

DeepStor[2] is a research infrastructure designed to investigate the high-temperature aquifer thermal energy storage (HT-ATES) for the heat supply of the KIT Campus North. The project is situated within the licensed exploration field KIT – Campus North, where a deep sedimentary reservoir has been thoroughly characterized in previous hydrocarbon exploration. DeepStor is conceptualized as an application-oriented infrastructure.

The objective of this project is to demonstrate and scientifically assess the technical, environmental, and societal acceptability of seasonal heat storage at

[2] https://www.geoenergiecampus.kit.edu/deepstor.php

Fig. 2: Public engagement event with a focus on seasonal geo-thermal storage in the deep underground (January 2025, Karlsruhe).

temperatures exceeding 100 °C in combination with geothermal heat production.

Parallel to the development of the DeepStor site, technology transfer towards the city of Karlsruhe was initiated with the GEOZeit project as part of the Helmholtz Zeitenwende initiative. A special focus was dedicated to public engagement. Within the GEOZeit project and the Helmholtz climate initiative HiCAM, information and dialogue events were carried out, e.g., in the KIT open space Triangel (Fig. 2).

The utilization of visualization tools and virtual-reality environments enables stakeholders to explore subsurface processes interactively, thereby enhancing transparency and facilitating knowledge transfer between research, industry, and the public. These approaches are indicative of the expanding role of digital communication tools in fostering societal acceptability for subsurface energy technologies.

Structural geology and geophysical characterization and monitoring methods

Recent structural analyses have yielded novel insights into the geological evolution of the central Upper Rhine Graben and its implications for reservoir behavior. Integrated seismic interpretation and structural modelling demonstrate that intra-rift basin development was strongly influenced by a late Oligocene stress-field change, leading to the superposition of younger basin structures onto earlier fault systems [1]. These findings underscore the importance of inherited faults and en-echelon structures for reservoir compartmentalization, fluid flow pathways, and geothermal doublet performance.

Studies of geothermal analogues further emphasize the role of deep structural controls. Joint gravity–magnetic inversion workflows reveal that intrusive bodies and fault intersections govern permeability distribution and heat transport, providing methodological advances for reducing geological uncertainty in geothermal exploration [5]. Similarly, morpho-structural analyses of superhot geothermal systems demonstrate how regional tectonics influence fracture porosity and stress distribution near the brittle–ductile transition zone [3]. These insights contribute to a refined geological understanding and inform monitoring strategies.

Recent research applying joint three-dimensional inversion of gravity and magnetic data provides new insights into the deep structural framework of superhot geothermal systems using the Acoculco field (Fig. 3). By integrating terrestrial gravity measurements with airborne magnetometry, the study resolves density and magnetization distributions within a regional 3D model, revealing semicircular intrusive structures interpreted as mafic magma bodies controlling heat supply and volcanic evolution.

The results indicate that fault intersections and intrusive complexes can regulate permeability distribution.

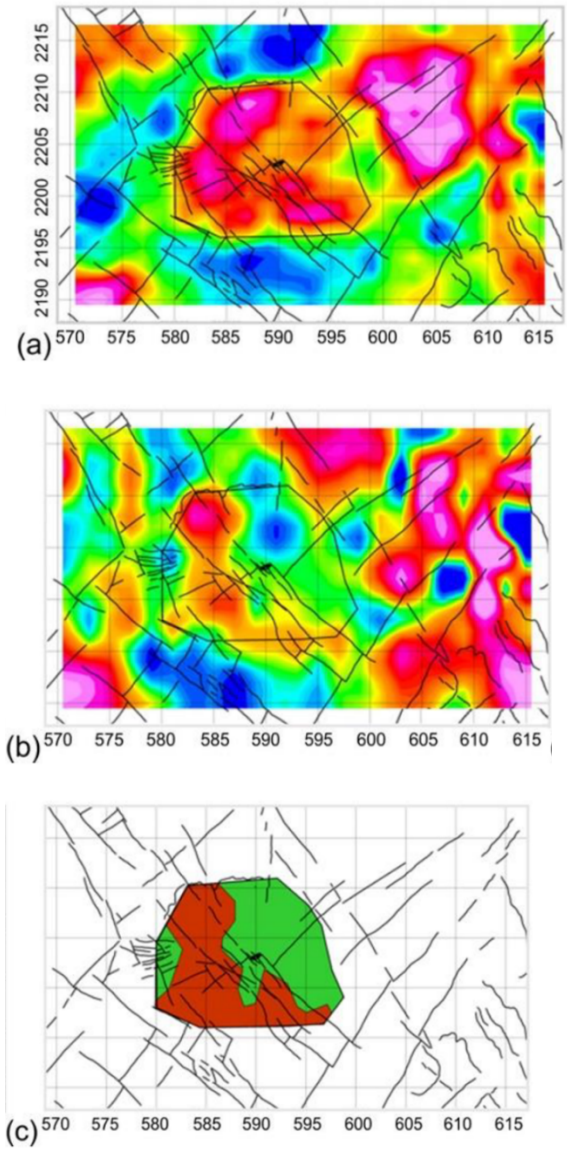

Fig. 3: (a) The deepest magnetization slice of the 3D model (1000 m.b.s.l.). With a dark line is contoured the semicircular shape of Acoculco. (b) the deepest density slice of the 3D model and the contoured shape (1000 m.b.s.l.). (c) A composition image showing with red a large magnetized body with large density. Green color with lower density and slightly lower magnetization.

Joint inversion notably enhances depth resolution compared to single-method approaches. Cross-sections of the model reveal the presence of dense and magnetized bodies in proximity to exploratory wells, indicating that past hydrothermal circulation and mineral sealing may be responsible for the observed lack of permeability, despite temperatures exceeding 250 °C [5]. The workflow illustrates how integrating geophysical inversion and petrophysical coupling can reduce geological uncertainty and support exploration strategies for enhanced geothermal and subsurface energy storage systems, providing methodological advances relevant to DeepStor-type infrastructures.

Modeling Advances and Reservoir Processes

Numerical modeling has played a central role in supporting DeepStor development. Automated meshing workflows based on open-source simulation tools allow for rapid evaluation of alternative geological scenarios (Fig. 5). This efficient assessment of reservoir performance during development phases enables informed decision-making [4]. Sensitivity analyses indicate that sub-seismic faults may locally modify pressure evolution and heat plume geometry, while thermal recovery remains relatively robust against small-scale structural variability.

Coupled thermo-hydro-mechanical simulations provide new insights into reservoir deformation and surface uplift risks. According to the findings of the modeling, thermoelastic stress redistribution is the primary factor in deformation at reservoir depth (Fig. 4). In contrast, surface uplift remains significantly reduced and is primarily influenced by poroelastic effects [6]. Even at injection temperatures exceeding 100 °C, predicted vertical displacements at the surface remain negligible

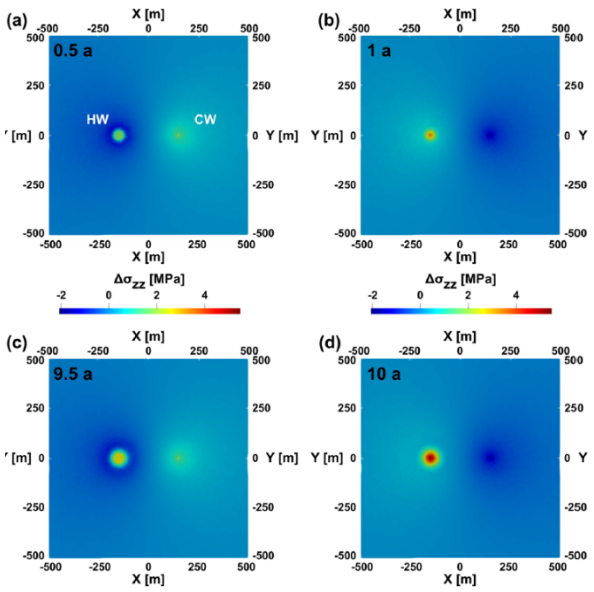

Fig. 4: Distribution of stress changes at the reservoir top around the two wells (CW: cold well; HW: hot well) after a one charging period, b one full charging and discharge cycle, c the tenth charging period (i.e., after 9.5 years), and d the full simulation duration of ten charging and discharge cycles.

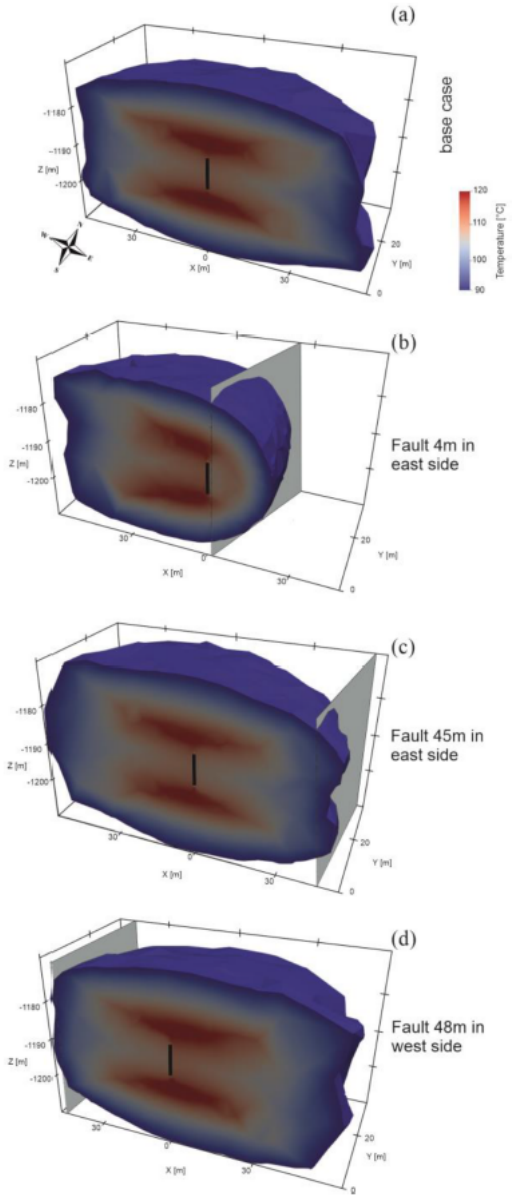

Fig. 5: Heat accumulation in four different scenarios of the DeepStor model at the end of the last production cycle. The planned well is shown as a solid black line. Subplots from (a) to (d) represent different scenarios including the base case and arbitrary faults (shown with a grey surface) at 4 and 45m to the east of the well and 48m to the west. The temperature scale is also the same and shown only once in subplot (a) to avoid repetition.

compared to reservoir-scale deformation. This supports risk-informed designs, monitoring concepts and regulatory assessments.

Recent reactive-transport simulations within the VESTA framework have yielded novel perspectives on the hydrogeochemical processes that govern high-temperature aquifer thermal energy storage (HT-ATES) at the DeepStor site. The study utilizes coupled flow, heat transport, and kinetic mineral reactions to assess the performance of seasonal doublet operation with injection temperatures reaching up to 140°C. The findings indicate that mineral dissolution plays a predominant role in the vicinity of the heated well, resulting in an

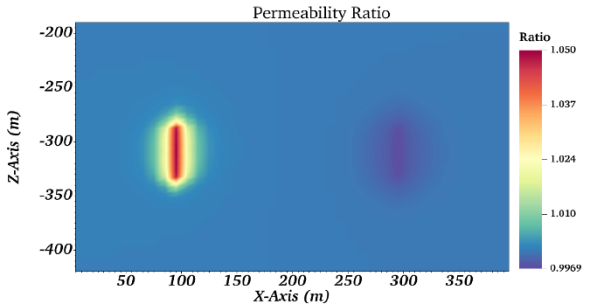

Fig. 6: Permeability ratio in the XZ-plane (Y=145 m) after 5 years of seasonal injection and production cycles.

estimated porosity enhancement of approximately 1.5%. In contrast, minimal precipitation and negligible permeability reduction occur in the vicinity of the chilled well (Figs. 6) [7].

Geochemical analyses further reveal temperature-dependent pH shifts (Fig. 7) and elevated iron species concentrations around the hot well. These findings indicate potential scaling and corrosion risks under oxidizing conditions that must be considered in future monitoring concepts. Notably, the simulations indicate an absence of substantial thermal short-circuiting between the hot and cold plumes, thereby validating the long-term viability of cyclic heat storage operations [7]. Integrating kinetic geochemistry with thermo-hydraulic modeling provides a technological basis for predicting mineralogical evolution, optimizing operational strategies, and improving risk assessment for DeepStor-type HT-ATES infrastructures.

Conclusions and Outlook

Geoenergy research at KIT has transitioned into the infrastructure implementation phase, in which reservoir characterization, advanced numerical modeling, lab experiments, and digital innovation converge while the research infrastructures are being constructed.

With the Main Operations Plan approved, preparatory activities for DeepStor are underway, including the completed installation of groundwater monitoring wells. The following activities are planned or already in progress: laying the conductor pipes in the first quarter of 2026, completing the drilling sites and infrastructure connections, and carrying out the DeepStor-1

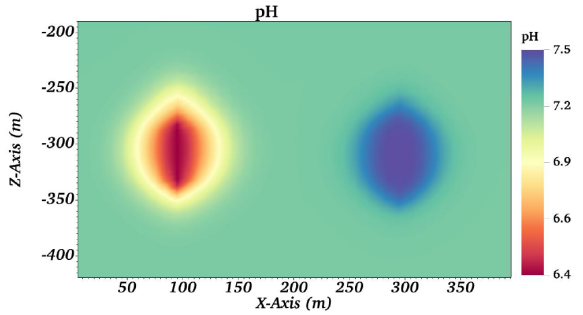

Fig. 7: pH distribution in the XZ-plane (Y=145 m) after 5 years of seasonal injection and production cycles.

Fig. 8: Drilling of GLB-1. The borehole reached a depth of more than 500 m and was fully cored. The drilling results form the basis for the site evaluation and assessment of whether the Tromm location is suitable for the planned underground research lab GeoLaB.

exploration drilling. The drilling campaign will be accompanied by an extensive core drilling, logging, and testing program, as well as continuous seismic and hydrogeological monitoring. DeepStor has achieved significant milestones in regulatory approval and technical prepa-ration, supported by advancements in THMC modeling, reactive transport simulations, and risk assessment.

The completion of GLB-1 and GLB-2 marked a significant milestone in the GeoLaB project, which is in the final stages of the exploration phase (Fig. 8).

Recent scientific contributions demonstrate that structural uncertainty, thermoelastic stress redistribution, and geochemical evolution are critical factors for the safe deployment of HT-ATES systems. At the same time, structural analyses of the Upper Rhine Graben provide essential geological context for both infrastructures. GeoLaB and DeepStor are combining controlled underground experimentation with application-oriented research to unlock the unexploited potential of the crystalline bedrock and seasonal underground heat storage. Collectively, these initiatives provide a cohesive framework for advancing geoenergy technologies as a fundamental component of a climate-neutral energy system.

References

[1] Bauer, F. et al., *Tectonics,* 44 (4), (2025).
[2] Buness, C. M. et al., *Scientific Reports*, **16 (1)**, (2026).
[3] Cornejo-Triviño, N. et al., *Geothermal Energy*, 12 (1), (2024).
[4] Dashti, A. et al., *Geoscientific Model Development,* 17 (8), (2024).
[5] Perez-Flores, M. A. et al., *Geothermics*, **117** (2024).
[6] Stricker, K. et al., *Geothermal Energy*, **12**, (2024)
[7] Kumar, R. et al., *2024 Geothermal Rising Conference*, (2024).

12 Publications

2024

ISI/SCOPUS

1. Bagus, P. S.; Nelin, C. J.; Rosso, K. M.; Schacherl, B.; Vitova, T. (2024). Electronic Structure of Actinyls: Orbital Properties. *Inorganic Chemistry*, 63 (4), 1793–1802. doi:10.1021/acs.inorgchem.3c03158
2. Bagus, P. S.; Nelin, C. J.; Schacherl, B.; Vitova, T. (2024). Actinyl Electronic Structure Probed by XAS: The Role of Many-Body Effects. *Inorganic Chemistry*, 63 (29), 13202 – 13213. doi:10.1021/acs.inorgchem.4c00270
3. Bagus, P. S.; Nelin, C. J.; Schacherl, B.; Vitova, T.; Polly, R. (2024). Bonding and Interactions in UO 2 2+ for Ground and Core Excited States: Extracting Chemistry from Molecular Orbital Calculations. *The Journal of Physical Chemistry A*, 128 (38), 8024–8034. doi:10.1021/acs.jpca.4c03555
4. Brown, A. R.; Molinas, M.; Roebbert, Y.; Faizova, R.; Vitova, T.; Sato, A.; Hada, M.; Abe, M.; Mazzanti, M.; Weyer, S.; Bernier-Latmani, R. (2024). The isotopic signature of UV during bacterial reduction. *Geochemical Perspectives Letters*, 29, 45–50. doi:10.7185/geochemlet.2411
5. Comins, M. B.; Shang, C.; Polly, R.; Skerencak-Frech, A.; Altmaier, M.; Hixon, A. E.; Gaona, X. (2024). Cm(III) speciation in the presence of citrate from neutral to hyperalkaline conditions and the effect of calcium. *Chemosphere*, 364, Art.-Nr.: 143233. doi:10.1016/j.chemosphere.2024.143233
6. Cornejo-Triviño, N.; Liotta, D.; Piccardi, L.; Brogi, A.; Kruszewski, M.; Perez-Flores, M. A.; Carrillo, J.; Calcagno, P.; Sass, I.; Schill, E. (2024). Gravimetric and morpho-structural analyses in the superhot geothermal system Los Humeros: an example from central Mexico. *Geothermal Energy*, 12 (1), Art.-Nr.: 7. doi:10.1186/s40517-024-00285-7
7. Dashti, A.; Grimmer, J. C.; Geuzaine, C.; Bauer, F.; Kohl, T. (2024). Developing meshing workflows in Gmsh v4.11 for the geologic uncertainty assessment of high-temperature aquifer thermal energy storage. *Geoscientific Model Development*, 17 (8), 3467–3485. doi:10.5194/gmd-17-3467-2024
8. Ehrman, J. N.; Shumilov, K.; Jenkins, A. J.; Kasper, J. M.; Vitova, T.; Batista, E. R.; Yang, P.; Li, X. (2024). Unveiling Hidden Shake-Up Features in the Uranyl M 4 -Edge Spectrum. *JACS Au*, 4 (3), 866–1249. doi:10.1021/jacsau.3c00838
9. Faden, L.-P.; Reiß, A.; Popescu, R.; Donsbach, C.; Göttlicher, J.; Vitova, T.; Gerthsen, D.; Feldmann, C. (2024). Sc, Zr, Hf, and Mn Metal Nanoparticles: Reactive Starting Materials for Synthesis Near Room Temperature. *Inorganic Chemistry*, 63 (2), 1020–1034. doi:10.1021/acs.inorgchem.3c03074
10. Ferrari, P.; Venturi, G.; Campani, L.; Mariotti, F.; Becker, F.; Jansen, J.; Jovanović, Z.; Krstić, D.; Teles, P. (2024). Medical staff monitoring in interventional cardiology: over apron dosemeter placement based on measurements and simulations. *Radiation Protection Dosimetry*, 200 (8), 802–807. doi:10.1093/rpd/ncae125
11. Fouquet-Métivier, P.; Medyk, L.; Lebreton, F.; Guéneau, C.; Hunault, M. O. J. Y.; Solari, P.-L.; Dardenne, K.; Rothe, J.; Martin, P. M. (2024). Insight into the Cationic Charge Distribution in U Pu Am O Mixed Oxides. *Inorganic Chemistry*, 63 (43), 20482–20491. doi:10.1021/acs.inorgchem.4c03084
12. Geckeis, H. (2024). Obituary: Jae-Il Kim (1936–2023). *Radiochimica Acta*, 112 (2), 139. doi:10.1515/ract-2023-2001
13. Golshadi, Z.; Dinari, M.; Knebel, A.; Lützenkirchen, J.; Monjezi, B. H. (2024). Metal organic and covalent organic framework-based QCM sensors for environmental pollutant detection and beyond. *Coordination Chemistry Reviews*, 521, Art.-Nr. 216163. doi:10.1016/j.ccr.2024.216163
14. Greif, G.; Sauerwein, F. S.; Weßling, P.; Duckworth, T. M.; Patzschke, M.; Gericke, R.; Sittel, T.; März, J.; Wilden, A.; Modolo, G.; Panak, P. J.; Roesky, P. W. (2024). 6-(6-Methyl-1,2,4,5-Tetrazine-3-yl)-2,2′-Bipyridine: A N-Donor Ligand for the Separation of Lanthanides(III) and Actinides(III). *Inorganic Chemistry*, 63 (33), 15259–15269. doi:10.1021/acs.inorgchem.4c01793
15. Grosse, M.; Boldt, F.; Herm, M.; Roessger, C.; Stuckert, J.; Weick, S.; Nahm, D. (2024). The SPIZWURZ project – Experimental investigations and modeling of the behavior of hydrogen in zirconium alloys under long-term dry storage conditions. *Nuclear Engineering and Technology*, 56, 824–831. doi:10.1016/j.net.2023.09.027
16. Guidone, R. E.; Gaona, X.; Altmaier, M.; Lothenbach, B. (2024). Gluconate and formate uptake by hydrated cement phases. *Applied Geochemistry*, 175, Art.-Nr.: 106145. doi:10.1016/j.apgeochem.2024.106145
17. Guidone, R. E.; Gaona, X.; Winnefeld, F.; Altmaier, M.; Geckeis, H.; Lothenbach, B. (2024). Citrate sorption on cement hydrates. *Cement and Concrete Research*, 178, Art.-Nr.: 107404. doi:10.1016/j.cemconres.2023.107404

18. Hattem, A. van; Dankelman, R.; Colineau, E.; Griveau, J.-C.; Dardenne, K.; Rothe, J.; Couweleers, S.; Konings, R. J. M.; Smith, A. L. (2024). Experimental investigations and thermodynamic modelling of the ternary system Pb-Mo-O. *Journal of Alloys and Compounds*, 1003, Art.-Nr. 175588. doi:10.1016/j.jallcom.2024.175588

19. Jo, Y.; Lothenbach, B.; Çevirim-Papaioannou, N.; Blochouse, B. de; Altmaier, M.; Gaona, X. (2024). Uptake of chloride and isosaccharinic acid by cement paste with high slag content (CEM III/C). *Cement and Concrete Research*, 180, Art.-Nr.: 107509. doi:10.1016/j.cemconres.2024.107509

20. Karwadiya, J.; Lützenkirchen, J.; Darbha, G. K. (2024). Retention of ZnO nanoparticles onto polypropylene and polystyrene microplastics: Aging-associated interactions and the role of aqueous chemistry. *Environmental Pollution*, 352, Art.-Nr.: 124097. doi:10.1016/j.envpol.2024.124097

21. Kim, K.; Duckworth, S. B.; Altmaier, M.; Um, W.; Gaona, X. (2024). Solubility, complexation and thermodynamics of the Tc(IV)–isosaccharinic acid system: Trends in the M(IV) series. *Chemosphere*, 364, Art.-Nr.: 143140. doi:10.1016/j.chemosphere.2024.143140

22. Köhnke, F.; Steuri, B.; Baetcke, L.; Borchers, M.; Brinkmann, T.; Dittmeyer, R.; Dornheim, M.; El Zohbi, J.; Förster, J.; Gawel, E.; Görl, K.; Herbst, M.; Heß, D.; Kalhori, A.; Korte, K.; Li, Z.; Markus, T.; Mengis, N.; Monnerie, N.; Oschlies, A.; Prats-Salvado, E.; Reusch, T. B. H.; Rhoden, I.; Sachs, T.; Schaller, R.; Schill, E.; Simon, S.; Stevenson, A.; Thoni, T.; Thrän, D.; Xiao, M.; Jacob, D. (2024). A storyline approach: integrating comprehensive, interdisciplinary research results to create narratives – in the context of the net-zero target in Germany. *Frontiers in Environmental Science*, 12. doi:10.3389/fenvs.2024.1433491

23. Lessing, J.; Neumann, J.; Lützenkirchen, J.; Bok, F.; Moisei-Rabung, S.; Schild, D.; Brendler, V.; Stumpf, T.; Schmidt, M. (2024). Natural and synthetic plagioclases: Surface charge characterization and sorption of trivalent lanthanides (Eu) and actinides (Am, Cm). *Colloids and Surfaces A: Physicochemical and Engineering Aspects*, 688, Art.-Nr.: 133529. doi:10.1016/j.colsurfa.2024.133529

24. Lüth, S.; Steegborn, F.; Heberling, F.; Beilecke, T.; Bosbach, D.; Deissmann, G.; Geckeis, H.; Joseph, C.; Liebscher, A.; Metz, V.; Rebscher, D.; Rink, K.; Ryberg, T.; Schennen, S. (2024). Characterization of heterogeneities in the sandy facies of the Opalinus Clay (Mont Terri underground rock laboratory, Switzerland). *Geophysical Journal International*, 236 (3), 1342–1359. doi:10.1093/gji/ggad494

25. Lux, C.; Kerz, S.; Ribeiro, C. C.; Bareuther, J.; Lützenkirchen, J.; Stock, S.; Tsintsaris, M.; Rehahn, M.; Stark, R. W.; Klitzing, R. von. (2024). Conceptualizing flexible papers using cellulose model surfaces and polymer particles. *Soft Matter*, 20 (6), 1333–1346. doi:10.1039/D3SM01461D

26. Marsac, R.; Catrouillet, C.; Pédrot, M.; Benedetti, M. F.; Dia, A.; van Hullebusch, E. D.; Davranche, M.; Sivry, Y.; Pierson-Wickmann, A.-C.; Tharaud, M.; Heberling, F. (2024). Equilibrium surface complexation modeling with metastable natural colloids: The key to predict the oxidation state distribution of trace elements?. *Current Opinion in Colloid & Interface Science*, 72, Article no: 101820. doi:10.1016/j.cocis.2024.101820

27. Mennecart, T.; Iglesias, L.; Herm, M.; König, T.; Leinders, G.; Cachoir, C.; Lemmens, K.; Verwerft, M.; Metz, V.; González-Robles, E.; Meert, K.; Vandoorne, T.; Gaggiano, R. (2024). Effect of hydrogen gas and leaching solution on the fast release of fission products from two PWR fuels. *Journal of Nuclear Materials*, 588, 154811. doi:10.1016/j.jnucmat.2023.154811

28. Morelová, N.; Finck, N.; Lützenkirchen, J.; Schild, D.; Dardenne, K.; Geckeis, H. (2024). Corrigendum to "Sorption of americium / europium onto magnetite under saline conditions: Batch experiments, surface complexation modelling and X-ray absorption spectroscopy study" [J. Colloid Interface Sci. 561 (2020) 708–718]. *Journal of Colloid and Interface Science*, 656, 125–126. doi:10.1016/j.jcis.2023.11.048

29. Muñoz, A. G.; Abdelouas, A.; Alonso, U.; Fernández, A. M.; Bernier-Latmani, R.; Cherkouk, A.; Gaggiano, R.; Hesketh, J.; Smart, N.; Padovani, C.; Mijnendonckx, K.; Montoya, V.; Idiart, A.; Pont, A.; Riba, O.; Finck, N.; Singh, A. R.; King, F.; Diomidis, N. (2024). WP15 ConCorD state-of-the-art report (container corrosion under disposal conditions). *Frontiers in Nuclear Engineering*, 3, Art.-Nr.: 1404739. doi:10.3389/fnuen.2024.1404739

30. Perez-Flores, M. A.; Carrillo, J.; Schill, E.; Lopéz-Hernández, A.; Sosa-Ceballos, G.; Cornejo-Triviño, N.; Jiménez-Haro, A.; Boijseauneau-López, M. E. (2024). Density and magnetization models for the Acoculco geothermal field by joint 3D inversion. *Geothermics*, 117, 102869. doi:10.1016/j.geothermics.2023.102869

31. Sakai, A.; Weisenburger, S.; Pegg, I. L.; Ishida, S. (2024). Issues Associated with Yellow Phase Formation and Other Disruptions in Japanese High-Level Waste Vitrification and Their Improvement. *Nuclear Technology*, 210 (6), 1054–1077. doi:10.1080/00295450.2023.2266612

32. Santos, P. F. dos; Gaona, X.; Lassin, A.; Skerencak-Frech, A.; Fellhauer, D.; Altmaier, M.; Madé, B. (2024). Thermodynamics of the Eu(iii)–Mg–SO –HO and Eu(iii)–Na–SO–HO systems. Part II: spectroscopy experiments, complexation and Pitzer/SIT models. *Dalton Transactions*, 53 (14), 6323–6332. doi:10.1039/d3dt04323a

33. Santos, P. F. dos; Lassin, A.; Gaona, X.; Garbev, K.; Altmaier, M.; Madé, B. (2024). Thermodynamics of the Eu(iii)–Mg–SO_4 –H_2O and Eu(iii)–Na–SO_4 –H_2O systems. Part I: solubility experiments and the full dissociation Pitzer model. *Dalton Transactions*, 53 (14), 6289–6299. doi:10.1039/d3dt04322c

34. Schacherl, B.; Maurer, K.; Schäfer, M.; Remde, Y.; Geyer, F.; Fried, A.; Happel, S. A.; Benešová-Schäfer, M. (2024). Concept validation of separations for thorium-based radionuclide generator systems for medical application. *Frontiers in Nuclear Engineering*, 3. doi:10.3389/fnuen.2024.1379996

35. Shang, C.; Gaona, X.; Oher, H.; Polly, R.; Skerencak-Frech, A.; Duckworth, S.; Altmaier, M. (2024). Experimental and computational evidence of U(VI)–OH–Si(OH)₄ complexes under alkaline conditions: Implications for cement systems. *Chemosphere*, 350, Art.-Nr.: 141048. doi:10.1016/j.chemosphere.2023.141048

36. Sittel, T.; Becker, K.; Geist, A.; Panak, P. J. (2024). Cs^+ Extraction from Chloride-Rich Brine Solutions Using the Calixarene Crown Ether MAXCalix. *Solvent Extraction and Ion Exchange*, 42 (2), 118–132. doi:10.1080/07366299.2024.2349528

37. Sittel, T.; Meißner, M.; Keller, M.; Geist, A.; Panak, P. J. (2024). Spectroscopic Study on the Complexation of trivalent Actinide and Lanthanide ions with TEDGA in Solution. *European Journal of Inorganic Chemistry*, 27 (10), Art.-Nr.: e202300720. doi:10.1002/ejic.202300720

38. Stracke, J.; Weßling, P.; Sittel, T.; Adam, C.; Rominger, F.; Geist, A.; Panak, P. J. (2024). 2,6-Bis(5-(tert-butyl)-1H-pyrazol-3-yl)pyridine: Effects of the Peripheral Aliphatic Side Chain on the Coordination of Actinides(III) and Lanthanides(III). *Inorganic Chemistry*, 63 (29), 13214–13222. doi:10.1021/acs.inorgchem.4c00396

39. Stracke, J.; Weßling, P.; Sittel, T.; Meiners, P.; Geist, A.; Panak., P. J. (2024). Extraction and complexation studies with 2,6-bis(5-(tert -butyl)-1 H -pyrazol-3-yl)pyridine in the presence of 2-bromohexanoic acid. *RSC Advances*, 14 (39), 28415–28422. doi:10.1039/d4ra05630b

40. Stricker, K.; Egert, R.; Schill, E.; Kohl, T. (2024). Risk of surface movements and reservoir deformation for high-temperature aquifer thermal energy storage (HT-ATES). *Geothermal Energy*, 12, Art.-Nr.: 4. doi:10.1186/s40517-024-00283-9

41. Tasi, A.; Szabo, P.; Gaona, X.; Bouby, M.; Sittel, T.; Schild, D.; Maier, A. C.; Hedström, S.; Altmaier, M.; Geckeis, H. (2024). Degradation of the polyacrylonitrile-based UP2W material under cementitious conditions. *Applied Geochemistry*, 169, Art.-Nr.: 106015. doi:10.1016/j.apgeochem.2024.106015

42. Thumm, A. K.; Skerencak-Frech, A.; Gaona, X.; Altmaier, M.; Geckeis, H. (2024). Uptake of Cm (III) and Eu (III) by C–S–H phases under saline conditions in presence of EDTA: A batch sorption and TRLFS study. *Applied Geochemistry*, 170, 106087. doi:10.1016/j.apgeochem.2024.106087

43. Vitova, T.; Ramanantoanina, H.; Schacherl, B.; Münzfeld, L.; Hauser, A.; Ekanayake, R. S. K.; Reitz, C. Y.; Prüßmann, T.; Neill, T. S.; Göttlicher, J.; Steininger, R.; Saveleva, V. A.; Haverkort, M. W.; Roesky, P. W. (2024). Photon-Modulated Bond Covalency of [Sm(II)(η -CH)]. *Journal of the American Chemical Society*, 146 (30), 20577–20583. doi:10.1021/jacs.3c13934

44. Warmuth, L.; Steurer, M.; Schild, D.; Zimina, A.; Grunwaldt, J.-D.; Pitter, S. (2024). Reversible and Irreversible Structural Changes in Cu/ZnO/ZrO_2 Catalysts during Methanol Synthesis. *ACS Applied Materials & Interfaces*, 16 (7), 8813–8821. doi:10.1021/acsami.3c17383

45. Yan, Y.; Çevirim-Papaioannou, N.; Gaona, X.; Fellhauer, D.; Altmaier, M. (2024). Thermodynamic description of U(IV) solubility and hydrolysis in chloride systems: Pitzer activity model for the system U–Na–Mg–Ca–H–Cl–OH–HO(l). *Applied Geochemistry*, 171, 106091. doi:10.1016/j.apgeochem.2024.106091

46. Yu, Y.; Hao, Y.; Xiao, B.; Langer, E.; Novikov, S. A.; Ramanantoanina, H.; Pidchenko, I.; Schild, D.; Albrecht-Schoenzart, T. E.; Eichel, R.-A.; Vitova, T.; Alekseev, E. V. (2024). U(V) Stabilization via Aliovalent Incorporation of Ln(III) into Oxo-salt Framework. *Chemistry – A European Journal*, 30 (40), Art.-Nr.: e202401033. doi:10.1002/chem.202401033

47. Zhang, Y.; Zhuang, Y.-B.; Liu, X.; Cheng, J.; Lützenkirchen, J.; Lu, X. (2024). Physical adsorption of OH^- causes anomalous charging at oxide–water interfaces. *Chemical Communications*, 60 (68), 9113–9116. doi:10.1039/d4cc01833h

Oral and poster presentations

1. Börner, C.; Müller, K.; Schild, D.; Seewald, F.; Stumpf, T.; Mayordomo, N. (2024, August 26). *Interaction of Tc with iron(ll) phosphate*. 10th International Conference on Nuclear and Radiochemistry (NRC 2024), Brighton, United Kingdom, August 25–30, 2024.

2. Bouby, M. (2024, July 31). *Colloid influence on the Radionuclide Migration from a Nuclear Waste Repository: Brief overview of on-going activities at KIT-INE following the way opened by Professor Jae-Il KIM*. 16th Europe-Korea Conference on Science and technology (EKC 2024), Coventry, United Kingdom, July 30–August 2, 2024.

3. Çevirim-Papaioannou, N.; Orucoglu, E.; Grangeon, S.; Lützenkirchen, J.; Franke, K.; Fuss, M.; Agnel, M.; Altmaier, M.; Gaona, X. (2024, November 5). *Aqueous speciation and sorption properties of Be(II) in Aptian Sands*. Jahrestagung der Fachgruppe Nuklearchemie (2024), Karlsruhe, Germany, November 5–7, 2024.

4. Chaillou, M.; Bouby, M.; Geckeis, H.; Nivesse, A.-L.; Montavon, G.; Catherine, L.; travis, colin; benalcazar, soraya; mallet, clarisse; lebault, catherine. (2024, November 25). *Colloidal vectors of Uranium in an Aqueous Environment as determined by using the LC-OCD-OND-UVD-ICP-MS: Application to the Former Uranium Mining Site of Rophin (Puy-de-Dôme, France)*. 6th International Conference on Radioecology & Environmental Radioactivity (ICRER 2024), Marseille, France, November 24–29, 2024.

5. Dardenne, K.; Herm, M.; König, T.; Lin, T.-Y.; Metz, V.; Pruessmann, T.; Rothe, J.; Schild, D.; Walschburger, A.; Geckeis, H. (2024). *Spectroscopic investigation on the behavior of irradiated light water reactor fuels during prolonged dry interim storage and final disposal*. ATAS-AnXAS 2024 - 2nd Joint Workshop - 6th International Workshop on Advanced Techniques in Actinide Spectroscopy - 10th International Workshop on Speciation, Techniques and Faculties for Radioactive Material at Synchrotron Light Sources (ATAS-AnXAS 2024), Karlsruhe, Germany, October 7–11, 2024.

6. Duckworth, S. B.; Shang, C.; Gaona, X.; Altmaier, M. (2024, August 29). *Impact of silicate and citrate on the solubility of U in weakly alkaline to hyperalkaline saline systems*. 10th International Conference on Nuclear and Radiochemistry (NRC 2024), Brighton, United Kingdom, August 25–30, 2024.

7. Duckworth, S. B.; Shang, C.; Gaona, X.; Altmaier, M. (2024, November 6). *Solubility of Uranium in the presence of silicate and citrate under intermediate ionic strength conditions*. Jahrestagung der Fachgruppe Nuklearchemie (2024), Karlsruhe, Germany, November 5–7, 2024.

8. Fellhauer, D.; Walter, O.; Schild, D.; Neill, T.; Rothe, J.; Altmaier, M. (2024, August 29). *Synthesis, characterization and solubility of M-Pu(VI)-O(H) solid phases*. 10th International Conference on Nuclear and Radiochemistry (NRC 2024), Brighton, United Kingdom, August 25–30, 2024.

9. Fürst, P. Q.; Cevirim-Papaioannou, N.; Gaona, X.; Altmaier, M.; Geckeis, H. (2024, April 19). *Löslichkeit, Redoxverhalten und Speziation von Fe unter endlagerrelevanten Bedingungen = Solubility, redox behavior and speciation of Fe under repository-relevant conditions*. 4. Tage der Standortauswahl (2024), Goslar, Germany, April 18–19, 2024.

10. Fürst, P. Q.; Cevirim-Papaioannou, N.; Gaona, X.; Altmaier, M.; Geckeis, H. (2024, August 21). *Thermodynamic description of Fe(II) solubility and hydrolysis in dilute to concentrated KCl systems*. Goldschmidt (2024), Chicago, IL, USA, August 18–23, 2024.

11. Geist, A. (2024, February 28). *Actinide separations by solvent extraction — nitrogen donor ligands do it better*. FENABIUM II Spring School "The Chemistry of f-Elements" (2024), Leipzig, Germany, February 27–March 1, 2024.

12. Guidone, R. E.; Huber, N.; Heberling, F.; Sittel, T.; Brassinnes, S.; Altmaier, M.; Gaona, X. (2024, August 21). *Retention of $^{14}CO_3^{2-}$ by hydrated cement and calcite: impact of ISA and chloride*. Goldschmidt (2024), Chicago, IL, USA, August 18–23, 2024.

13. Guidone, R. E.; Huber, N.; Sittel, T.; Brassinnes, S.; Altmaier, M.; Gaona, X. (2024, November 6). *Impact of ISA and chloride on the retention of 14^CO 3^2– by cement and calcite*. Jahrestagung der GDCh-Fachgruppe Nuklearchemie (2024), Karlsruhe, Germany, November 5–7, 2024.

14. Haaf, N.; Jougnot, D.; Guarracino, L.; Niemz, P.; Schill, E. (2024, February 14). *Electric self-potential during hydraulic fracturing (HF) in the Äspö Hard Rock Laboratory, Sweden*. 49th Workshop on Geothermal Reservoir Engineering (2024), Stanford University, Stanford, CA, USA, February 12–14, 2024.

15. Huber, N.; Cevirim-Papaioannou, N.; Gaona, X.; Garbev, K.; Dardenne, K.; Altmaier, M.; Geckeis, H. (2024, October 8). *Retention of Sn in reducing cement systems*. ATAS-AnXAS 2024 - 2nd Joint Workshop - 6th International Workshop on Advanced Techniques in Actinide Spectroscopy - 10th International Workshop on Speciation, Techniques and Faculties for Radioactive Material at Synchrotron Light Sources (ATAS-AnXAS 2024), Karlsruhe, Germany, October 7–11, 2024.

16. Huber, N.; Gaona, X.; Dardenne, K.; Altmaier, M.; Geckeis, H. (2024, November 6). *Solubility, redox behavior and sorption of Sn(II) and Sn(IV) in cement systems*. Jahrestagung der Fachgruppe Nuklearchemie (2024), Karlsruhe, Germany, November 5–7, 2024.

17. Huber, N.; Guidone, R. E.; Gaona, X.; Garbev, K.; Brassinnes, S.; Altmaier, M.; Geckeis, H. (2024, August 26). *Impact of ISA and chloride on the uptake of Nb(V) by calcite and carbonated cement paste*. 10th International Conference on Nuclear and Radiochemistry (NRC 2024), Brighton, United Kingdom, August 25–30, 2024.

18. Joseph, C.; Schacherl, B.; Vitova, T.; Lavrova, P.; Hennig, T.; Kühn, M. (2024, November 25). *Diffusion of Np through Illite du Puy*. 9th International Clay Conference (2024), Hanover, Germany, November 25–28, 2024.

19. Kaufmann-Heimeshoff, H.; Schacherl, B.; Tagliavini, M.; Göttlicher, J.; Mazzanti, M.; Popa, K.; Walter, O.; Prüßmann, T.; Vollmer, C.; Beck, A.; Ekanayake, R. S. K.; Branson, J. A.; Neill, T.; Reitz, C. Y.; Schild, D.; Brager, D.; Cahill, C.; Windorff, C.; Sittel, T.; Ramanantoanina, H.; Haverkort, M.; VItova, T. (2024, October 7). *Counting 5f electrons in actinide compounds*. ATAS-AnXAS 2024 - 2nd Joint Workshop - 6th International Workshop on Advanced Techniques in Actinide Spectroscopy - 10th International Workshop on Speciation, Techniques and Faculties for Radioactive Material at Synchrotron Light Sources (ATAS-AnXAS 2024), Karlsruhe, Germany, October 7–11, 2024.

20. Kiefer, C.; Gaona, X.; Fellhauer, D.; Altmaier, M. (2024, November 5). *Development of a Pitzer activity model for the solubility and hydrolysis of Tc(IV) in dilute to concentrated NaCl, KCl, MgCl and CaClsystems*. Jahrestagung der GDCh-Fachgruppe Nuklearchemie (2024), Karlsruhe, Germany, November 5–7, 2024.

21. Kiefer, C.; Gaona, X.; Suzuki-Muresan, T.; Schild, D.; Garbev, K.; Kobayashi, T.; Dardenne, K.; Dieste Blanco, O.; Altmaier, M.; Grambow, B.; Geckeis, H. (2024, November 5). *Solubility and structural characterization of Zr(IV) hydrous oxides*. Jahrestagung der GDCh-Fachgruppe Nuklearchemie (2024), Karlsruhe, Germany, November 5–7, 2024.

22. König, T.; Dagan, R.; González-Robles, E.; Herm, M.; Metz, V.; Walschburger, A.; Geckeis, H. (2024). *Long-term dissolution experiments with medium and high burn-up spent UOX and MOX fuels under conditions expected in a deep geological repository*. Neutron Resonance Analysis School (2024), Geel, Belgium, May 13–17, 2025.

23. König, T.; Gaggiano, R.; Herm, M.; Meert, K.; Metz, V.; Walschburger, A. (2024). *Determination of the residual radionuclide inventory of internal and distal specimens of a leached spent nuclear fuel rod segment*. 32nd Spent Fuel Workshop (2024), Nîmes, France, November 5–7, 2024.

24. Kovac, N.; Bauer, F.; App, T. E.; Bornschein, B.; Vincenz, D. de; Glück, F.; Heyns, S.; Kempf, S.; Langer, M.; Müller, M.; Sack, R.; Schlösser, M.; Steidl, M.; Valerius, K. (2024, May). *ELECTRON - Development of High Resolution Metallic Microcalorimeters for a Future Neutrino Mass Experiment with Tritium*. 16th Pisa Meeting on Advanced Detectors (2024), La Biodola, May 26–July 1, 2024.

25. Maurer, K.; Schacherl, B.; Schäfer, M.; Remde, Y.; Taş, H.; Geyer, F.; Fried, A.; Happel, S.; Benešová-Schäfer, M.; Vitova, T.; Geckeis, H. (2024, October 7). *Investigation of thorium-based generator concepts – improvements, labeling and speciation*. ATAS-AnXAS 2024 - 2nd Joint Workshop - 6th International Workshop on Advanced Techniques in Actinide Spectroscopy - 10th International Workshop on Speciation, Techniques and Faculties for Radioactive Material at Synchrotron Light Sources (ATAS-AnXAS 2024), Karlsruhe, Germany, October 7–11, 2024.

26. Maurer, K.; Schacherl, B.; Schäfer, M.; Remde, Y.; Taş, H.; Geyer, F.; Fried, A.; Happel, S.; Benešová-Schäfer, M.; Vitova, T.; Geckeis, H. (2024, November 5). *Investigation of thorium-based generator concepts – improvements, labeling and speciation*. Jahrestagung der GDCh-Fachgruppe Nuklearchemie (2024), Karlsruhe, Germany, November 5–7, 2024.

27. Müller, P.; David, F.; Dieter, S.; Marcus, A.; Xavier, G.; Horst, G. (2024, November 7). *Solubility, speciation and thermodynamics of $PuCO_3OH(cr)$ in carbonate containing NaCl solutions*. Jahrestagung der Fachgruppe Nuklearchemie (2024), Karlsruhe, Germany, November 5–7, 2024.

28. Müller, P.; David, F.; Dieter, S.; Marcus, A.; Xavier, G.; Horst, G. (2024, September 12). *Solubility, Speciation and Thermodynamics of $PuCO_3OH(cr)$ in Carbonate Containing Solutions*. Plutonium Futures - The Science (2024), Charleston, SC, USA, September 8–12, 2024.

29. Müller, P.; Fellhauer, D.; Schild, D.; Dardenne, K.; Rothe, J.; Altmaier, M.; Gaona, X.; Geckeis, H. (2024, October 10). *Solubility, speciation and thermodynamics of PuCO3OH(cr) in carbonate containing NaCl solutions*. ATAS-AnXAS 2024 - 2nd Joint Workshop - 6th International Workshop on Advanced Techniques in Actinide Spectroscopy - 10th International Workshop on Speciation, Techniques and Faculties for Radioactive Material at Synchrotron Light Sources (ATAS-AnXAS 2024), Karlsruhe, Germany, October 7–11, 2024.

30. Ramanantoanina, H.; Celis-Barros, C.; Vitova, T. (2024, October 7). *A practical computational tool for actinide coordination chemistry (LFDFT): study of M4,5-edge core-to-core and valence-band resonant inelastic x-ray scattering*. ATAS-AnXAS 2024 - 2nd Joint Workshop - 6th International Workshop on Advanced Techniques in Actinide Spectroscopy - 10th International Workshop on Speciation, Techniques and Faculties for Radioactive Material at Synchrotron Light Sources (ATAS-AnXAS 2024), Karlsruhe, Germany, October 7–11, 2024.

31. Ramanantoanina, H.; Schenk, S.; Reitz, C. Y.; Fellhauer, D.; Ekanayake, R. S. K.; Kaufmann-Heimeshoff, H.; Zhang, X.; Prüssmann, T.; Vitova, T. (2024, September 8). *Theoretical Study of Electronic Structure of Pu(III-VI) Aqua Ions Using M4,5-Edge Resonant Inelastic X-Ray Scattering and High-Energy Resolution Spectroscopies*. Plutonium Futures - The Science (2024), Charleston, SC, USA, September 8–12, 2024.

32. Reitz, C. Y.; Ekanayake, R. S. K.; Ramanantoanina, H.; Reynolds, E.; Frick, D.; Lohse, Y.; Weinert, B.; Roesky, P.; Dehnen, S.; Vitova, T. (2024, June 9). *Developing x-ray spectroscopic method for f-element bond covalency*. Center for Rare Earth and Actinides Research - Science and Outreach Association for the f-elements (CS2FE 2024), Aussois, France, June 9–14, 2024.

33. Reitz, C. Y.; Zhang, X.; Vollmer, C.; Dardenne, K.; Prüßmann, T.; Sittel, T.; Panak, P.; Vitova, T. (2024, November 5). *Complexation of U(VI) with N-donor ligands studied by high energy resolution X- ray spectroscopy and computations*. Jahrestagung der Fachgruppe Nuklearchemie (2024), Karlsruhe, Germany, November 5–7, 2024.

34. Reitz, C. Y.; Zhang, X.; Vollmer, C.; Dardenne, K.; Prüßmann, T.; Sittel, T.; Panak, P.; Vitova, T. (2024, October 7). *Complexation of U(VI) with N-donor ligands studied by high energy resolution X-ray spectroscopy and computations*. ATAS-AnXAS 2024 - 2nd Joint Workshop - 6th International Workshop on Advanced Techniques in Actinide Spectroscopy - 10th International Workshop on Speciation, Techniques and Faculties for Radioactive Material at Synchrotron Light Sources (ATAS-AnXAS 2024), Karlsruhe, Germany, October 7–11, 2024.

35. Reynolds, E.; Ekanayake, R. S. K.; Kim, C.; Gaona, X.; Kaufmann-Heimeshoff, H.; Steininger, R.; Göttlicher, J.; Prüßmann, T.; Benešová-Schäfer, M.; Geckeis, H.; Schacherl, B.; Vitova, T. (2024, October 7). *Development and Application of a Microfluidic Set-Up for In-Situ Studies of Formation Kinetics of La- and U-Complexes Using High Resolution Spectroscopic Methods*. ATAS-AnXAS 2024 - 2nd Joint Workshop - 6th International Workshop on Advanced Techniques in Actinide Spectroscopy - 10th International Workshop on Speciation, Techniques and Faculties for Radioactive Material at Synchrotron Light Sources (ATAS-AnXAS 2024), Karlsruhe, Germany, October 7–11, 2024.

36. Reynolds, E.; Ekanayake, R. S. K.; Kim, C.; Gaona, X.; Kaufmann-Heimeshoff, H.; Steininger, R.; Göttlicher, J.; Prüßmann, T.; Benešová-Schäfer, M.; Geckeis, H.; Vitova, T.; Schacherl, B. (2024, November 5). *Development and Application of a Microfluidic Set-Up for In-Situ Studies of Formation Kinetics of La- and U-Complexes Using High Resolution Spectroscopic Methods*. Jahrestagung der Fachgruppe Nuklearchemie (2024), Karlsruhe, Germany, November 5–7, 2024.

37. Rudolph, B.; Neuwirth, N.; Schätzler, K.; Kohl, T.; Kolditz, O.; Sass, I.; Schüth, C.; the GeoLaB Team. (2024, November 13). *GeoLaB – an URL for Geothermal Energy is on its way*. European Geothermal Workshop (EGW 2024), Stavanger, Norway, November 13–14, 2024.

38. Sittel, T.; Becker, K.; Polly, R.; Geist, A.; Panak, P. J. (2024, November 6). *How to extract Cs+ from chloride-rich brine solutions? An Extraction, NMR and DFT study*. Jahrestagung der GDCh-Fachgruppe Nuklearchemie (2024), Karlsruhe, Germany, November 5–7, 2024.

39. Sittel, T.; Geist, A.; Panak, P. J. (2024, September 5). *Probing the metal ion-ligand interaction in An(III) and Ln(III) complexes: an overview about recent advancements*. 6th Nuclear Chemistry for Sustainable Fuel Cycles (ATALANTE 2024), Avignon, France, September 1–6, 2024.

40. Vitova, T. (2024, December 1). *Counting the 5f electrons of the actinides*. Materials Research Society: MRS Fall-Meeting and Exhibit (2024), Boston, MA, USA, December 1–6, 2024.

41. Vitova, T.; Blankenship, M.; Dardenne, K.; Ekanayake, R. S. K.; Geckeis, H.; Göttlicher, J.; Hauschild, D.; Schacherl, B.; Steininger, R.; Wansorra, C.; Heske, C.; Weinhardt, L. (2024, August 26). *High Resolution X-ray Spectroscopy of Actinides at the KIT Light Source*. 15th International Conference on Synchrotron Radiation Instrumentation (SRI 2024), Hamburg, Germany, August 26–30, 2024.

42. Vitova, T.; Schacherl, B.; Ramanantoanina, H.; Kovács, A.; Benesova, M.; Göttlicher, J.; Steininger, R.; Haverkort, M.; Geckeis, H. (2024, November 6). *Towards New Spectroscopic Tools for Detection of Bonding Properties in Radiopharmaceuticals: Application on La Used as a Homolog of Ac*. Jahrestagung der Fachgruppe Nuklearchemie (2024), Karlsruhe, Germany, November 5–7, 2024.

43. Vitova, T.; Schacherl, B.; Tagliavini, M.; Ramanantoanina, H.; Kaufmann-Heimeshoff, H.; Fellhauer, D.; Prüßmann, T.; Popa, K.; Walter, O.; Haverkort, M.; Autschbach, J.; Bagus, P. (2024, September 8). *Probing Bonding Properties of Pu by High Resolution X-ray Spectroscopy and Computations*. Plutonium Futures - The Science (2024), Charleston, SC, USA, September 8–12, 2024.

44. Vitova, T.; Yao, J.; Schacherl, B.; McNamara, B.; Ilton, E.; Heo, J.; Vollmer, C.; Schenk, S.; Tripathi, S.; Ramanantoanina, H.; Buck, E. (2024, December 1). *Real-time tracking of oxidation states of nano particulate UO2 electrode using HR-XANES at Uranium M4 edge and a microfluidic technique*. Materials Research Society: MRS Fall-Meeting and Exhibit (2024), Boston, MA, USA, December 1–6, 2024.

45. Zhang, X.; Vollmer, C.; Ramanantoanina, H.; Schreckenbach, G.; Haverkort, M.; Vitova, T. (2024, June 4). *Probing actinide bonding properties by computations and advanced X-ray spectroscopy*. Canadian Chemistry Conference and Exhibition (CSC 2024), Winnipeg, Canada, June 2–6, 2024.

Proceedings

1. Altmaier, M. (2024). *2021 Annual Workshop Proceedings of the CORI WP in EURAD*. Karlsruher Institut für Technologie (KIT). doi:*10.5445/IR/1000173343*

2. Fanghänel, S. (2024). *ATAS - AnXAS 2024 – 2nd Joint Workshop : KIT Campus North, Karlsruhe, Germany, October 7 – 11, 2024 Proceedings*. (J. Rothe, Ed.), Karlsruher Institut für Technologie (KIT). doi:*10.5445/IR/1000175765*

3. Haaf, N.; Guarracino, L.; Jougnot, D.; Schill, E. (2024). Estimation of electrochemical and electrothermal coupling effects on self-potential data obtained during Hydraulic Fracturing in the Äspö Hard Rock Laboratory, Sweden. *49th Workshop on Geothermal Reservoir Engineering 2024 : Stanford, California, USA, 12-14 February 2024*, Curran Associates.

4. Kumar, R.; Neupane, G.; Jin, W.; Atkinson, T.; McLing, T.; Smith, R.; Zhang, Y.; Dobson, P.; Schill, E.; Kohl, T.; Bauer, F.; Nitschke, F.; Bremer, J. (2024). Development of Reactive Transport Models for Very High Temperature Heat Aquifer Storage (VESTA) at a Pilot Site in Germany. *2024 Geothermal Rising Conference: Using the Earth to Save the Earth, Waikoloa, 27th - 30th October2024*, 1168 – 1183, Geothermal Resources Council (GRC).
5. Schill, E.; Bauer, F.; Zhang, Y.; Rutqvist, J.; Dobson, P.; Atkinson, T.; Jin, W. (2024). DeepStor - District Heating From High-Temperature Heat Storage In A Depleted Hydrocarbon Reservoir In The Upper Rhine Graben. *2024 Geothermal Rising Conference: Using the Earth to Save the Earth, Waikoloa, 27th - 30th October 2024*, 3066 – 3075, Geothermal Resources Council (GRC).

Reports / Books

1. Becker, F.; Berg, M. (2024). Ungewissheiten und Narrative im Kontext der Entsorgung hochradioaktiver Abfälle – eine schwierige Beziehung?. *Entscheidungen in die weite Zukunft : Ungewissheiten bei der Entsorgung hochradioaktiver Abfälle. Hrsg.: A. Eckhardt*, 361–382, Springer Fachmedien Wiesbaden. doi:10.1007/978-3-658-42698-9_17
2. Dagan, R.; Herm, M.; Konobeev, A.; König, T. (2024). *Characteristics of selected irradiated material, irradiation history, methodology of experimental / analytical procedures and inventory calculations*. doi:*10.5445/IR/1000171624*
3. Eckhardt, A.; Becker, F.; Mintzlaff, V.; Scheer, D.; Seidl, R. (2024). Das Unbekannte vorausdenken : Entscheidungen unter Ungewissheit und zum Umgang mit Ungewissheiten. *Entscheidungen in die weite Zukunft : Ungewissheiten bei der Entsorgung hochradioaktiver Abfälle. Hrsg.: A. Eckhardt*, 383–403, Springer Fachmedien Wiesbaden. doi:10.1007/978-3-658-42698-9_18
4. Eckhardt, A.; Becker, F.; Mintzlaff, V.; Scheer, D.; Seidl, R. (Eds.). (2024). *Entscheidungen in die weite Zukunft : Ungewissheiten bei der Entsorgung hochradioaktiver Abfälle*. Springer Fachmedien Wiesbaden. doi:*10.1007/978-3-658-42698-9*
5. Heberling, F.; Lützenkirchen, J.; Gil-Díaz, T. (2024). Thermodynamic models of solid-liquid-interface chemistry - free surfaces and charge regulation boundary conditions. *Encyclopedia of Solid-Liquid Interfaces*, 215–229, Elsevier. doi:10.1016/B978-0-323-85669-0.00087-8
6. König, T.; Herm, M.; Metz, V.; Villagra, N. R.; Elorrieta, J. M.; Milena-Pérez, A.; Bonales, L. J.; Gutiérrez, L.; Fernández-Carretero, S.; Núñez, A.; Galán, H.; Király, M.; Bertsch, J.; Duarte, L. I.; Goutam, K.; Schneider, C. (2024). *Deliverable 8.10: Chemical and structural / crystallographic properties of simulated fuel pellets and irradiated fuel pellets at the cladding / fuel interface; Work Package 8 SFC*. doi:*10.5445/IR/1000188890*
7. Oschlies, A.; Mengis, N.; Rehder, G.; Schill, E.; Thomas, H.; Wallmann, K.; Zimmer, M. (2024). Mögliche Beiträge geologischer und mariner Kohlenstoffspeicher zur Dekarbonisierung. *Klimawandel in Deutschland. Hrsg.: G.P. Brasseur*, 449–460, Springer Spektrum.
8. Scheer, D.; Becker, F.; Hassel, T.; Hocke, P.; Leusmann, T.; Metz, V. (2024). Trittsicherheit auf Zukunftspfaden? Ungewissheitsbewältigung bei der Entsorgung hochradioaktiver Abfälle. *Entscheidungen in die weite Zukunft : Ungewissheiten bei der Entsorgung hochradioaktiver Abfälle. Hrsg.: A. Eckhardt*, 113–140, Springer Fachmedien Wiesbaden. doi:10.1007/978-3-658-42698-9_7
9. Seidl, R.; Becker, F.; Eckhardt, A.; Mintzlaff, V.; Scheer, D. (2024). Die Vielfalt der Ungewissheit bei der Entsorgung hochradioaktiver Abfälle. *Entscheidungen in die weite Zukunft : Ungewissheiten bei der Entsorgung hochradioaktiver Abfälle. Hrsg.: A. Eckhardt*, 1–12, Springer Fachmedien Wiesbaden. doi:10.1007/978-3-658-42698-9_1
10. Thrän, D.; Edenhofer, O.; Pahle, M.; Schill, E.; Wilts, H.; Steubing, M. (2024). Minderungsansätze in der Energie- und Kreislaufwirtschaft. *Klimawandel in Deutschland : Entwicklung, Folgen, Risiken und Perspektiven. Ed.: G. Brasseur*, 430–437, Springer Spektrum. doi:10.1007/978-3-662-66696-8

Dissertations

1. Guidone, R. E. (2024, April 19). *Impact of formate, citrate and gluconate on the retention behavior of Pu(III/IV), Cm(III) and Eu(III) by cement phases*. PhD dissertation. Karlsruher Institut für Technologie (KIT). doi:10.5445/IR/1000170098
2. Kiefer, C. (2024, December 4). *Fundamental investigation of Zr(IV) solubility and surface processes in alkaline systems: a combined solubility, spectroscopic and theoretical study*. PhD dissertation. Karlsruher Institut für Technologie (KIT). doi:10.5445/IR/1000176745
3. Steegborn, F. M. (2024, December 10). *Impact of the heterogeneity of the sandy facies of Opalinus Clay on the retention of Cs, Co and Eu*. PhD dissertation. Karlsruher Institut für Technologie (KIT). doi:10.5445/IR/1000172114

4. Thumm, A. K. (2024, October 2). *Sorption of Eu(III) and Cm(III) on C-S-H phases and bentonite in presence of oxalate and EDTA at low to intermediate ionic strength conditions*. PhD dissertation. Karlsruher Institut für Technologie (KIT). doi:10.5445/IR/1000174523

Research Data

1. Schacherl, B.; Tagliavini, M.; Kaufmann-Heimeshoff, H.; Göttlicher, J.; Mazzanti, M.; Popa, K.; Walter, O.; Pruessmann, T.; Vollmer, C.; Beck, A.; Ekanayake, R. S. K.; Branson, J. A.; Neill, T.; Fellhauer, D.; Reitz, C. Y.; Schild, D.; Brager, D.; Cahill, C.; Windorff, C.; Sittel, T.; Ramanantoanina, H.; Haverkort, M. W.; Vitova, T. (2024, November 11). *Research Data to publication "Resonant inelastic X-ray scattering tools to count 5f electrons of actinides and probe bond covalency"*. doi:10.35097/5qqht0vfqrktvccj

2025

ISI/SCOPUS

1. Abdelmonem, A.; Glikman, D.; Gong, Y.; Braunschweig, B.; Saathoff, H.; Lützenkirchen, J.; Fawey, M. H. (2025). Surface–bulk photochemical coupling of nonanoic acid and 4-benzoylbenzoic acid: the dual role of the photosensitizer and environmental influences. *Atmospheric Chemistry and Physics*, 25 (20), 13019–13035. doi:10.5194/acp-25-13019-2025

2. Abram, U.; Roca Jungfer, M. (2025). Cyclopentadienyl Complexes of Technetium. *Molecules*, 30 (24), 4813. doi:10.3390/molecules30244813

3. Almendros-Ginestà, O.; Duckworth, S.; Fürst, P. Q.; Missana, T.; Altmaier, M.; Gaona, X. (2025). Thermodynamic description of the Ni(II)-citrate system in alkaline, dilute to concentrated NaCl solutions. Formation of quaternary complexes with ca. *Applied Geochemistry*, 180, 106290. doi:10.1016/j.apgeochem.2025.106290

4. Androniuk, I.; Guidone, R. E.; Altmaier, M.; Gaona, X. (2025). Sorption of Eu(III) on C–S–H phases in the presence of gluconate: A molecular dynamics study. *Applied Geochemistry*, 193, 106579. doi:10.1016/j.apgeochem.2025.106579

5. Androniuk, I.; Thumm, A. K.; Skerencak-Frech, A.; Altmaier, M.; Gaona, X. (2025). Uptake of Eu(III) by C-S-H phases in CaCl2 solution in presence of EDTA: A molecular dynamics study. *Computational and Theoretical Chemistry*, 1250, 115271. doi:10.1016/j.comptc.2025.115271

6. Baccelli, D.; Stracke, J.; Gullo, M. C.; Weßling, P.; Grivas, S.; Rispoli, F.; Volpi, S.; Mele, A.; Geist, A. G.; Panak, P. J.; Sansone, F.; Sittel, T.; Macerata, E.; Casnati, A. (2025). A preorganized triarmed bis-triazolylpyridine-calix[4]arene with high affinity and selectivity for minor actinides for nuclear waste treatment. *Chemical Communications*, 61 (73), 13968–13971. doi:10.1039/D5CC02948A

7. Bagus, P. S.; Nelin, C. J.; Trumm, M.; Schacherl, B.; Vitova, T. (2025). Origins of NpO+ XAS features: Hydrated compared to isolated NpO^+. *The Journal of Chemical Physics*, 162 (20), Art.-Nr.: 204706. doi:10.1063/5.0263322

8. Bajaj, A.; Ramanantoanina, H.; Schacherl, B.; Schenk, S.; Pruessmann, T.; Tasi, A.; Fellhauer, D.; Humiston, A.; Terry, J.; Wang, X.; Zurek, E.; Vitova, T.; Bagus, P. S.; Autschbach, J. (2025). Actinide 5f Occupations: The Case of PuO_2. *Inorganic Chemistry*, 64 (24), 12297–12312. doi:10.1021/acs.inorgchem.5c01709

9. Bauer, F.; Grimmer, J. C.; Houpt, L.; Hertweck, T.; Schill, E. (2025). Development of Intra-Rift Basins During Stress Field Change in the Central Upper Rhine Graben (SW Germany). *Tectonics*, 44 (4), e2024TC008721. doi:10.1029/2024TC008721

10. Coutelot, F.; Riss, M.; Wang, D. L.; Olive, D. T.; Schnurr, A.; Powell, B. A. (2025). Examination of Np(V) sorption to montmorillonite as a function of temperature (25–55 °C) and ionic strength. *Applied Geochemistry*, 190, 106466. doi:10.1016/j.apgeochem.2025.106466

11. Dagan, R.; König, T.; Herm, M.; Alvarez, F.; Dorval, E.; Häkkinen, S.; Vlassopoulos, E.; Shama, A.; Smaizys, A.; Schillebeeckx, P. (2025). Investigation of nuclide inventory of cladding material irradiated in the Goesgen PWR core. *Annals of Nuclear Energy*, 212, 111061. doi:10.1016/j.anucene.2024.111061

12. Dagan, R.; Danon, Y.; Konobeev, A. (2025). Open issues on scattering kernels of compound nuclear reactors. (P. Dimitriou, R. Capote & G. Schnabel, Eds.) *EPJ Web of Conferences*, 322, 10005. doi:10.1051/epjconf/202532210005

13. Eun, H.; Szabo, P. G.; Rehhorn, D.; Lee, S.; Jo, Y.; Altmaier, M.; Lee, J.; Gaona, X.; Yun, J.-I. (2025). Uptake of Eu, Th, U, and Pu by granite and biotite gneiss in Korean fresh groundwater under oxidizing and reducing conditions. *Radiochimica Acta*, 113 (3), 181–194. doi:10.1515/ract-2024-0331

14. Ferrari, P.; Becker, F.; Dabin, J.; Eakins, J.; Jovanović, Z.; Krstić, D.; Michaś-Majewska, E.; Tymińska, K.; Benali, A.; Bouwman, R.; McCann, A.; Hürkamp, K.; Fioroni, F. (2025). Monte Carlo study of the eye lens exposure of medical staff administering Sc-47 and Cu-67 labelled radiopharmaceuticals. *Physica Medica*, 137, 105077. doi:10.1016/j.ejmp.2025.105077

15. Fürst, P. Q.; Çevirim-Papaioannou, N.; Gaona, X.; Garbev, K.; Roth, T.; Hagemann, S.; Altmaier, M.; Geckeis, H. (2025). Solubility, speciation and thermodynamics of Fe in reducing aqueous KCl solutions. *RSC Advances*, 15 (54), 46308–46319. doi:10.1039/D5RA07073B

16. Glückman, D.; Quinto, F.; Joseph, C.; Metz, V.; Hain, K.; Steier, P.; Geckeis, H. (2025). Diffusion of U(VI) in Opalinus Clay Studied down to Ultratrace Levels. *Environmental Science & Technology*, 59 (17), 8694–8702. doi:10.1021/acs.est.4c12739

17. Guidone, R. E.; Huber, N.; Heberling, F.; Sittel, T.; Palina, N.; Bocchese, F.; Brassinnes, S.; Altmaier, M.; Gaona, X. (2025). Uptake of H CO/CO by calcite: impact of ISA and chloride. *RSC Advances*, 15 (46), 38762–38773. doi:10.1039/d5ra05547d

18. Hattem, A. van; Geus, L. de; Sacristán, A.; Dankelman, R.; Couweleers, S.; Hennig, C.; Griveau, J.-C.; Colineau, E.; Dardenne, K.; Rothe, J.; Pruessmann, T.; Konings, R. J. M.; Smith, A. L. (2025). Elucidation of the Off-Center Displaced Mo in Octahedral Coordination in BaMoO. *Inorganic Chemistry*, 64 (1), 674–681. doi:10.1021/acs.inorgchem.4c03617

19. Hiemstra, T.; Lützenkirchen, J. (2025). Development and Modus Operandi relating Surface Structure and Ion Complexation Modeling for Important Metal (Hydr)oxides. *Reviews in Mineralogy and Geochemistry*, 91A (1), 13–84. doi:10.2138/rmg.2025.91A.02

20. Hosseini Monjezi, B.; Lützenkirchen, J. (2025). Comment on Zhou et al. Adsorption Behaviors of Lanthanum (III) and Yttrium (III) Ions on Gibbsite. Minerals 2023, 13, 1530. *Minerals*, 14 (11), 1137. doi:10.3390/min14111137

21. Huber, N.; Guidone, R. E.; Gaona, X.; Garbev, K.; López-García, M.; Alcubierre, L.; Bocchese, F.; Brassinnes, S.; Altmaier, M.; Geckeis, H. (2025). Retention of niobium(V) by calcite and carbonated cement paste: quantitative description and impact of isosaccharinic acid and chloride. *Cement and Concrete Research*, 197, 107952. doi:10.1016/j.cemconres.2025.107952

22. Jordan, N.; Heberling, F.; Kelling, J.; Lützenkirchen, J. (2025). History, Algorithms, Model Uncertainty, and Common Pitfalls of Traditional SCM Fitting Procedures. *Reviews in Mineralogy and Geochemistry*, 91A (1), 383–411. doi:10.2138/rmg.2024.91A.12

23. Kaufhold, S.; Kahra, C.; Hassel, T.; Finck, N.; Munoz, A. G. (2025). Screening of Six Different Potential HLRW Canister Materials Surrounded by Bentonite. *Journal of nuclear materials management*, 52 (2), 4–15.

24. Kiefer, C.; Fellhauer, D.; Altmaier, M.; Gaona, X. (2025). Improved Pitzer activity model for Tc(iv) solubility and hydrolysis in the Tc(iv)–Na–K–Ca–Mg–H–Cl–OH–HO(l) system. *RSC Advances*, 15 (45), 37816–37823. doi:10.1039/d5ra04721h

25. Kiefer, C.; Gaona, X.; Suzuki-Muresan, T.; Schild, D.; Garbev, K.; Kobayashi, T.; Dardenne, K.; Blanco, O. D.; Altmaier, M.; Grambow, B.; Geckeis, H. (2025). Structural characterization of amorphous hydrous Zr(IV) oxide and the transformation occurring under hydrothermal conditions. *Applied Geochemistry*, 182, 106302. doi:10.1016/j.apgeochem.2025.106302

26. Lützenkirchen, J.; Monjezi, B. H.; Kosmulski, M. (2025). Comments on “Part I: determination of a structure/property transformation mechanism responsible for changes in the point of zero change of anatase titania with decreasing particle size” by M. Leffler, A. Mirich, J. Fee, S. March and S. L. Suib, RSC Adv. , 2024, 14, 30543. *RSC Advances*, 15 (22), 17248–17254. doi:10.1039/d5ra01865j

27. Molinas, M.; Lederballe Meibom, K.; Brown, A.; Abriata, L. A.; Prüßmann, T.; Bernier-Latmani, R. (2025). Speciation-dependent molecular mechanism of electron transfer from the c -type cytochrome MtrC to U(VI)-ligand complexes. *Geo-Bio Interfaces*, 2, e2. doi:10.1180/gbi.2024.10

28. Müller, P.; Fellhauer, D.; Schild, D.; Gaona, X.; Dardenne, K.; Rothe, J.; Altmaier, M.; Geckeis, H. (2025). Solubility, Speciation and Thermodynamics of $PuCO_3OH(cr)$ in Carbonate Containing NaCl Solutions. *Angewandte Chemie International Edition*, 64 (50), e202515522. doi:10.1002/anie.202515522

29. Muñoz, A. G.; Schild, D.; Kaufhold, S.; Dobrev, D.; Viebranz, V. F.; Hassel, T. (2025). Effects of γ-radiation on the interfacial chemistry of spheroidal graphite cast iron in contact with Wyoming bentonite slurry. *Surfaces and Interfaces*, 75, Art.-Nr.: 107773. doi:10.1016/j.surfin.2025.107773

30. Muñoz, A. G.; Schild, D. (2025). Corrosion of Spheroidal Graphite Cast Iron GGG40 in Anoxic Opalinus-Clay Water: Influence of Hydrostatic Pressure. *Materials and Corrosion*. doi:10.1002/maco.202414761

31. Murphy, G. L.; Gilson, S.; Popa, K.; Prieur, D.; Schenk, S. M.; Valu, S.-O.; Ramanantoanina, H.; Prüßmann, T.; Vitova, T.; Dardenne, K.; Rothe, J.; Colle, J.-Y.; Walter, O.; Huittinen, N. (2025). Structural and chemical insights on the incorporation of americium into zircaloy-derived monoclinic zirconia. *Communications Chemistry*, 9 (1), 50. doi:10.1038/s42004-025-01857-9

32. Neill, T. S.; Ramanantoanina, H.; Palina, N.; Prüßmann, T.; Rothe, J.; Gaona, X.; Fellhauer, D.; Schild, D.; Wansorra, C.; Hauschild, D.; Steininger, R.; Schacherl, B.; Heske, C.; Weinhardt, L.; Walter, O.; Weigend, F.; Vitova, T. (2025). The Role of Halides in the Bonding and Electronic Structure of Actinyl(VI) Halides─Energy Match Driven Stability. *Journal of the American Chemical Society*, 147 (39), 35401–35412. doi:10.1021/jacs.5c08999

33. Noli, F.; Papadopoulou, L.; Palina, N.; Schild, D.; Heberling, F.; Geckeis, H. (2025). Sorption studies of cesium and cobalt in single and binary systems using Greek Petrota zeolite. *Journal of Radioanalytical and Nuclear Chemistry*. doi:10.1007/s10967-025-10296-8

34. Özyagan, S.; Gillmeister, R. E.; Sittel, T.; Skerencak-Frech, A.; Panak, P. J. (2025). Complexation of Eu3+ with a polycarboxylate based concrete superplasticizer in chloride media. *Results in Chemistry*, 16, 102399. doi:10.1016/j.rechem.2025.102399

35. Özyagan, S.; Sittel, T.; Skerencak-Frech, A.; Panak, P. J. (2025). Interaction of Trivalent An(III) with Glenium 51: The Effect of Ionic Strength. *Inorganic Chemistry*, 64 (44), 22073–22081. doi:10.1021/acs.inorgchem.5c03814

36. Özyagan, S.; Warth, K. J.; Sittel, T.; Panak, P. J. (2025). Complexation of Cm(III) with monosilicic acid in chloride media. *Applied Geochemistry*, 190, 106465. doi:10.1016/j.apgeochem.2025.106465

37. Polly, R.; Dardenne, K.; Duckworth, S.; Gaona, X.; Pruessmann, T.; Rothe, J.; Altmaier, M.; Geckeis, H. (2025). Ab Initio Speciation of Tc-Gluconate Complexes in Aqueous Systems. *Inorganic Chemistry*, 64 (11), 5412–5423. doi:10.1021/acs.inorgchem.4c05115

38. Prieur, D.; Vigier, J.-F.; Baumann, V.; Popa, K.; De Bona, E.; Hein, H.; Dardenne, K.; Rothe, J.; Beck, A.; Vitova, T.; Cologna, M. (2025). Synthesis and oxidation of Ru-doped UO2. *MRS Advances*, 10 (18), 2188–2192. doi:10.1557/s43580-025-01391-9

39. Rajak, J. K.; Khandelwal, N.; Ganie, Z. A.; Schild, D.; Darbha, G. K. (2025). Reactive transport and sorption behavior of pollutants in presence of redox-sensitive nano Fe0 impregnated graphene: Advancing towards continuous water filtration. *Environmental Nanotechnology, Monitoring & Management*, 23, Article no: 101053. doi:10.1016/j.enmm.2025.101053

40. Ramanantoanina, H.; Rienmüller, J.; Lohse, Y. R.; Rauwolf, N.; Kehry, M.; Reitz, C.; Reynolds, E. M.; Prüßmann, T.; Schacherl, B.; Saveleva, V. A.; Ekanayake, R. S. K.; Göttlicher, J.; Weinert, B.; Klopper, W.; Dehnen, S.; Vitova, T. (2025). Molecular-Metallic Binding Characteristics of the Intermetalloid f-/p-Block Cluster [(La@InBi)Bi]. *Angewandte Chemie*, 137 (37), Art.-Nr.: e202512019. doi:10.1002/ange.202512019

41. Ramanantoanina, H.; Rienmüller, J.; Lohse, Y. R.; Rauwolf, N.; Kehry, M.; Reitz, C.; Reynolds, E. M.; Prüßmann, T.; Schacherl, B.; Saveleva, V. A.; Ekanayake, R. S. K.; Göttlicher, J.; Weinert, B.; Klopper, W.; Dehnen, S.; Vitova, T. (2025). Molecular-Metallic Binding Characteristics of the Intermetalloid f-/p-Block Cluster $[(La@In_2Bi_{11})_2Bi_2]^{6-}$. *Angewandte Chemie International Edition*, 64 (37), e202512019. doi:10.1002/anie.202512019

42. Ratnayake, S.; Lützenkirchen, J.; Schild, D.; Finck, N.; Eiche, E.; Gil-Díaz, T.; Weerasooriya, R.; Geckeis, H. (2025). Solid phase speciation and mobility of thorium in soil samples from a case study in Sri Lanka. *Radiochimica Acta*, 113 (4), 277–298. doi:10.1515/ract-2024-0334

43. Reiß, A.; Göttlicher, J.; Vitova, T.; Feldmann, C. (2025). Semiconducting Manganese-Bipyridyl Coordination Polymer via a Manganese–Metal-Nanoparticle Approach. *Inorganic Chemistry*, 64 (19), 9469–9476. doi:10.1021/acs.inorgchem.5c00080

44. Sadeghnejad, S.; Hupfer, S.; Pingel, J.; Lanyon, B.; Schneeberger, R.; Blechschmidt, I.; Alonso, U.; Hauser, W.; Kraft, S.; Geckeis, H.; Schäfer, T. (2025). Bentonite mass loss in fractured crystalline rock quantified from CT scans using digital rock physics and machine learning: case study from the Grimsel Test Site (Switzerland). *Applied Clay Science*, 276, 107915. doi:10.1016/j.clay.2025.107915

45. Sauerwein, F. S.; Sittel, T.; Geist, A.; Panak, P. J.; Wilden, A.; Modolo, G. (2025). Selective Americium Separation: New Insights into the Complexation of Trivalent f -Elements with SO3 -Ph-BTBP. *EPJ Web of Conferences*, 317, Article no: 01012. doi:10.1051/epjconf/202531701012

46. Schacherl, B.; Tagliavini, M.; Kaufmann-Heimeshoff, H.; Göttlicher, J.; Mazzanti, M.; Popa, K.; Walter, O.; Pruessmann, T.; Vollmer, C.; Beck, A.; Ekanayake, R. S. K.; Branson, J. A.; Neill, T.; Fellhauer, D.; Reitz, C.; Schild, D.; Brager, D.; Cahill, C.; Windorff, C.; Sittel, T.; Ramanantoanina, H.; Haverkort, M. W.; Vitova, T. (2025). Resonant inelastic X-ray scattering tools to count 5 f electrons of actinides and probe bond covalency. *Nature Communications*, 16 (1), Article no: 1221. doi:10.1038/s41467-024-54574-7

47. Schmidt, M.; Skerencak-Frech, A.; Panak, P. J.; Huittinen, N. (2025). Curium(iii) luminescence spectroscopy as a tool for species determination. *Chemical Society Reviews*, 54 (23), 10880–10939. doi:10.1039/d5cs00764j

48. Shelyug, A.; Pauna, H.; Springer, H.; Souza Filho, I. R. (2025). Puppet Strings of Hydrogen Plasma Reduction of Iron Ores: The Impact of Process Parameters on Plasma Properties and Reduction Kinetics. *Metallurgical and Materials Transactions B*, 56 (5), 5232–5245. doi:10.1007/s11663-025-03698-2

49. Sittel, T.; Becker, K.; Polly, R.; Müllich, U.; Geist, A.; Panak, P. J. (2025). The Role of Ion Size and π-Interaction in Stabilizing Calix[4]arene Crown Ether Metal Complexes. *Chemistry – A European Journal*, 31 (40), Art.-Nr.: e202501065. doi:10.1002/chem.202501065

50. Urbanek, M.; Gil-Díaz, T.; Lützenkirchen, J.; Castelvetro, V. (2025). Nano-Zirconia as a Protective and Consolidant Material for Marble in Architectural Surfaces. *Buildings*, 15 (3), Art.-Nr.: 492. doi:10.3390/buildings15030492

51. Vanel, V.; Wilden, A.; Modolo, G.; Geist, A.; Montuir, M. (2025). Flowsheets for the Validation of the Reference AmSEL System. (P. Guilbaud, Ed.) *EPJ Web of Conferences*, 317, Article no: 01013. doi:10.1051/epjconf/202531701013

52. van Hattem, A.; Popa, K.; Wallez, G.; Boshoven, J.; Colineau, E.; Dahms, E.; Griveau, J.-C.; Hein, H.; Walter, O.; Schacherl, B.; Vitova, T.; Dardenne, K.; Pruessmann, T.; Rothe, J.; Smith, A. L.; Konings, R. J. M. (2025). Structural and physical investigation of ordered BaO-deficient Ba3PuO6. *Communications Chemistry*, 8 (1), Art.-Nr.: 270. doi:10.1038/s42004-025-01669-x

53. Wang, B.; Yu, Z.; Chen, S.; Da Roit, N.; Schild, D.; Zimmermann, M.; Wang, Y.; Behrens, S. (2025). Single-Step Synthesis of Dimethyl Ether from Syngas over Nanoparticle-Derived Bifunctional Pd/CeO2/Al2O3 Catalysts. *Angewandte Chemie International Edition*, 64 (16), Art.-Nr.: e202423273. doi:10.1002/anie.202423273

54. Xia, Q.; Joshi, P.; Pan, Z.; Lazarov, M.; Bartova, B.; Xu, X.; Prüssmann, T.; Kappler, A.; Dong, H.; Weyer, S.; Bernier-Latmani, R. (2025). Mineral Dynamics Revealed by Fe^{2+}-Catalyzed Recrystallization of U-Incorporated Goethite. *Environmental Science & Technology*, 59 (48), 25900–25910. doi:10.1021/acs.est.5c11748

55. Yassin, G.; Pönitz, E.; Huittinen, N. M.; Schild, D.; Konheiser, J.; Müller, K.; Barkleit, A. (2025). Phase Characterization of (Mn, S) Inclusions and Mo Precipitates in Reactor Pressure Vessel Steel from Greifswald Nuclear Power Plant. *Journal of Nuclear Engineering*, 6 (2), Art.-Nr.: 12. doi:10.3390/jne6020012

56. Zarzycki, P.; Lützenkirchen, J.; Gilbert, B. (2025). Preface. *Reviews in Mineralogy and Geochemistry*, 91A (1), v. doi:10.2138/rmg.2025.91A.00

Oral and poster presentations

1. Amr Talaat Tolba. (2025, April 10). *Enhancing Crystalline Basement Characterization Using 3D Seismic Attributes and Spectral Decomposition: Unveiling Small-Scale Features and Complex Structures*. 1st GeoLaB Scientific Conference (2025), Potsdam, Germany, April 9–11, 2025.

2. Bouby, M.; Lunz, A.; Geyer, F. W.; Kaplan, U.; Geckeis, H.; Brassines, S. (2025, September 22). *Characterization of Boom Clay (BC) Dissolved Organic Matter (DOM) and associated naturally abundant trace*. 19th International Conference on the Chemistry and Migration Behavior of Actinides and Fission Products in the Geosphere (Migration 2025), New Orleans, LA, USA, September 21–27, 2025.

3. Branson, J. A.; Schacherl, B.; Schenk, S.; Reynolds, E.; Kaufmann-Heimeshoff, H.; Tim Pruessman; Minasian, S. G.; Vitova, T. (2025, March 18). *Evaluating 5f Orbital Covalency in $UX6^{-}$ (X = F, Cl) with U M-edge Resonant Inelastic X-ray Scattering*. 54èmes Journées des Actinides (JdA 2025), Annecy, France, March 18–21, 2025.

4. Chaillou, M.; Bouby, M.; Geyer, F. W.; Müller, N.; Nivesse, A.-L.; Catherine, L.; Montavon, G. (2025, September 24). *Colloidal Vectors of Uranium as Determined by Size-based Fractionation Techniques: Case of the Wetland from the Former Mining Site of Rophin (France)*. 19th International Conference on the Chemistry and Migration Behavior of Actinides and Fission Products in the Geosphere (Migration 2025), New Orleans, LA, USA, September 21–27, 2025.

5. Chen, Z.; Bouby, M.; Fried, A.; Kuschel, S.; Moisei-Rabung, S.; Kraft, S.; Geckeis, H. (2025, September 23). *Effects of groundwater composition and accessory minerals on bentonite erosion*. 19th International Conference on the Chemistry and Migration Behavior of Actinides and Fission Products in the Geosphere (Migration 2025), New Orleans, LA, USA, September 21–27, 2025.

6. Dickbreder, T.; Heberling, F.; Backus, E. H. G. (2025, March). *Investigating the Water Organization at the Calcite (10.4)-Water Interface at High pH*. European Geosciences Union General Assembly (EGU 2025), Vienna, Austria, April 27–May 2, 2025.

7. Fellhauer, D.; Walter, O.; Meier, R.; Rothe, J.; Dardenne, K.; Schild, D.; Jo, Y.; Schramm, T.; Kuzenkova, A.; Schorer, M.; Müller, P.; Gaona, X.; Altmaier, M.; Geckeis, H. (2025, September 22). *Pu(VI) hydrolysis in aqueous NaCl-NaOH solutions*. 19th International Conference on the Chemistry and Migration Behavior of Actinides and Fission Products in the Geosphere (Migration 2025), New Orleans, LA, USA, September 21–27, 2025.

8. Fürst, P. Q.; Cevirim-Papaioannou, N.; Gaona, X.; Prüßmann, T.; Dardenne, K.; Rothe, J.; Altmaier, M.; Geckeis, H. (2025, September 22). *Chemistry of iron in cementitious systems : impact of Calcium and particle size on Iron(III) solubility and speciation*. 19th International Conference on the Chemistry and Migration Behavior of Actinides and Fission Products in the Geosphere (Migration 2025), New Orleans, LA, USA, September 21–27, 2025.

9. Fürst, P. Q.; Cevirim-Papaioannou, N.; Gaona, X.; Roth, T.; Hagemann, S.; Garbev, K.; Altmaier, M.; Geckeis, H. (2025, September 22). *Iron(II) in repository systems : a thermodynamic study of solubility and hydrolysis in dilute to concentrated chloride systems*. 19th International Conference on the Chemistry and Migration Behavior of Actinides and Fission Products in the Geosphere (Migration 2025), New Orleans, LA, USA, September 21–27, 2025.

10. Fürst, P. Q.; Hagemann, S.; Bischofer, B.; Cevirim-Papaioannou, N.; Gaona, X.; Altmaier, M.; Geckeis, H. (2025, November 10). *STAMINA: Stabilität von Mineralphasen des Eisens im Nahfeld eines Endlagers*. Projektstatusgespräch "Entsorgung radioaktiver Abfälle" (2025), Karlsruhe, Germany, November 10–11, 2025.

11. Geist, A. (2025, October 1). *30+ years of solvent extraction development for minor actinide separations in Europe*. International Solvent Extraction Conference (ISEC 2025), Melbourne, Australia, September 29–October 3, 2025.

12. Guidone, R. E.; Huber, N.; Heberling, F.; Bocchese, F.; Brassinnes, S.; Altmaier, M.; Gaona, X. (2025, May 22). *Retention of $^{14}CO_3^{2-}$ by hydrated cement and calcite: impact of ISA and chloride*. 5th International Symposium on Cementation of Nuclear wastes (NUWCEM 2025), Avignon, France, May 20–22, 2025.

13. Haaf, N.; Häfner, V.; Schill, E. (2025, February). *RockBlockEx - A laboratory scale hydraulic fracturing experiment at differential stress of up to 20 MPa*. 50th Workshop on Geothermal Reservoir Engineering (2025), Stanford, CA, USA, February 10–12, 2025.

14. Haaf, N.; Tolba, A. T.; Bauer, F. (2025, March 12). *GEOZeit: Analyse von Schwerefelddaten zur Bewertung von lokalen Wärmeanomalien nördlich von Karlsruhe, Deutschland*. Workshops für terrestrische Gravimetrie in Deutschland (2025), Hanover, Germany, March 11–12, 2025.

15. Hattem, A. van; Popa, K.; Wallez, G.; Benes, O.; Boshoven, J.; Colineau, E.; Dahms, E.; Griveau, J.-C.; Hein, H.; Valu, O.; Walter, O.; Schacherl, B.; Vitova, T.; Dardenne, K.; Prüßmann, T.; Rothe, J.; Smith, A. L.; Konings, R. J. M. (2025, September 16). *Experimental study into ordered BaO-deficient Ba3PuO6*. 6th NuFuel workshop (NuFuel 2025), Delft, Netherlands, September 16–18, 2025.

16. Heberling, F.; Zunftmeister, L.; Müller, N.; Kutzschbach, M.; Gill, N. M.; Schild, D.; Prüßmann, T.; Dardenne, K.; Geckeis, H. (2025, March). *Calcite interactions with selenite and neptunyl, from surface complexation to solid-solution formation*. American Chemical Society (ACS) National Meeting & Exposition (2025), San Diego, CA, USA, March 23–27, 2025.

17. Huber, N.; Guidone, R. E.; Gaona, X.; Garbev, K.; Prüßmann, T.; López-Garcia, M.; Alcubierre, L.; Bocchese, F.; Brassinnes, S.; Altmaier, M.; Geckeis, H. (2025, September 23). *Impact of ISA and chloride on the uptake of Nb(V) by calcite and carbonated cement paste*. 19th International Conference on the Chemistry and Migration Behavior of Actinides and Fission Products in the Geosphere (Migration 2025), New Orleans, LA, USA, September 21–27, 2025.

18. Huber, N.; Guidone, R. E.; Gaona, X.; Heberling, F.; Bocchese, F.; Brassinnes, S.; Altmaier, M.; Geckeis, H. (2025, September 22). *Impact of ISA and NaCl on the uptake of Ra(II) by calcite*. 19th International Conference on the Chemistry and Migration Behavior of Actinides and Fission Products in the Geosphere (Migration 2025), New Orleans, LA, USA, September 21–27, 2025.

19. Kim, K. (2025, September 23). *Chemistry of Tc(IV) in cementitious environments: uptake by C-S-H phases and complexation with EDTA*. 19th International Conference on the Chemistry and Migration Behavior of Actinides and Fission Products in the Geosphere (Migration 2025), New Orleans, LA, USA, September 21–27, 2025.

20. König, T.; Gaggiano, R.; Herm, M.; Meert, K.; Metz, V.; Walschburger, A.; Geckeis, H. (2025). *Leaching behaviour of medium and high burn-up spent UOX and (U, Pu)OX fuels under anoxic and reducing conditions*. 3. Internationale Forschungssymposium für die Sicherheit der nuklearen Entsorgung (safeND 2025), Berlin, September 17–19, 2025.

21. Martin, A. J.; Diomidis, N.; Behazin, M.; Keech, P.; Reddy, B.; Suzuki, S.; Nagata, S.; Ogawa, Y.; Finck, N.; Philipp, T. (2025). *In-situ testing the corrosion performance of candidate HLW/SF canister materials in contact with bentonite in a crystalline rock environment*. 9th International Workshop on Long-Term Prediction of Corrosion Damage in Nuclear Waste Systems (LTC 2025), Sendai, Japan, November 3–7, 2025.

22. Maurer, K.; Unger, D.; Behe, M.; Knecht, A.; von Schoeler, K.; Fleischmann, A.; Gastaldo, L.; Benešová-Schäfer, M.; Vitova, T.; Wängler, C.; Enss, C.; Schacherl, B. (2025, May 15). *Ultra high-resolution γ-spectroscopy of 225Ac and its daughter radionuclides using MMC detectors*. 26th International Symposium on Radiopharmaceutical Sciences (iSRS 2025), Gold Coast, Australia, May 11–15, 2025.

23. Mottram, L. M.; Seufert, D.; Pachl, C.; Braun, J.; N'Diaye, A. T.; Minasian, S. G.; Powell, A. K.; Schacherl, B. (2025, October 8). *X-Ray Magnetic Circular Dichroism of Dinuclear Cobalt Dyprosium Compounds*. 33. Terrae Rarae - Tage der Seltenen Erden (2025), Karlsruhe, Germany, October 7–9, 2025.

24. Panjiyar, L.; Finck, N.; Stephan-Scherb, C. (2025, November 4). *Early anaerobic corrosion of potential canister material in compacted bentonite*. 9th International Workshop on Long-Term Prediction of Corrosion Damage in Nuclear Waste Systems (LTC 2025), Sendai, Japan, November 3–7, 2025.

25. Polly, R.; Dardenne, K.; Duckworth, S.; Gaona Martinez, J.; Pruessmann, T.; Rothe, J.; Altmaier, M.; Geckeis, H. (2025, September 23). *Ab initio speciation of Tc-gluconate complexes in aqueous systems*. 19th International Conference on the Chemistry and Migration Behavior of Actinides and Fission Products in the Geosphere (Migration 2025), New Orleans, LA, USA, September 21–27, 2025.

26. Reynolds, E. M.; Günther-Schmidt, N.; Steininger, R.; Reitz, C. Y.; Göttlicher, J.; Wansorra, C.; Blankenship, M.; Hauschild, D.; Heske, C.; Weinhardt, L.; Ramanantoanina, H.; Roesky, P. W.; VItova, T. (2025). *Influence of Oxidation State on Bonding Properties of [CeIII (PhC(Nt Bu) 2) 3] and [CeIV (PhC(Nt Bu) 2) 3] + [Al(OC4F9) 4] - Probed by High-Resolution X-Ray Absorption*. 33. Terrae Rarae - Tage der Seltenen Erden (2025), Karlsruhe, Germany, October 7–9, 2025.

27. Reynolds, E. M.; Reitz, C. Y.; Günther-Schmidt, N.; Göttlicher, J.; Steininger, R.; Schacherl, B.; Ramanantoanina, H.; Roesky, P. W.; VItova, T. (2025). *A Toolbox for Probing Bonding Properties in Lanthanide Metalorganic Systems via X-Ray Spectroscopic Methods*. 2nd RAC (2025), Tallinn, Estonia, December 4–7, 2025.

28. Rothe, J.; Dardenne, K.; Prüssmann, T. (2025, November 26). *XAS based speciation of technetium and long-lived fission products*. 1st Joint TecRad-RULET Autumn School on Technetium and other Fission Products (2025), Dresden, Germany, November 24–27, 2025.

29. Schacherl, B. (2025, September 29). *Shedding light on the hidden world of actinide bonding and behavior using photon spectro-microscopy*. Jahrestagung der Fachgruppe Nuklearchemie (GDCh 2025), Karlsruhe, September 29–October 1, 2025.

30. Schacherl, B.; Maurer, K.; Unger, D.; Behe, M.; Knecht, A.; Schoeler, K. von; Hengstler, D.; Gastaldo, L.; Benešová-Schäfer, M.; Vitova, T.; Fleischmann, A.; Wängler, C.; Enss, C. (2025, September 18). *Ultra-high-resolution γ- and X-ray spectroscopy of 225Ac and its daughter radionuclides using MMC-based detectors*. 31. Jahrestagung der AGRR / 3. Jahrestagung der grpw (2025), Davos, Switzerland, September 18–20, 2025.

31. Schacherl, B.; Mottram, L. M.; Chen, Y.; Seufert, D.; Pachl, C.; Klyatskaya, S.; Braun, J.; Ghiami, A.; Schuppler, S.; Nagel, P.; Ramanantoanina, H.; Powell, A. K.; Ruben, M.; Minasian, S. G.; N'Diaye, A. T. (2025, October 7). *XMCD Investigations of Lanthanide Magnetic Molecular Systems*. 33. Terrae Rarae - Tage der Seltenen Erden (2025), Karlsruhe, Germany, October 7–9, 2025.

32. Schacherl, B.; Tagliavini, M.; Göttlicher, J.; Mazzanti, M.; Popa, K.; Walter, O.; Prüssmann, T.; Vollmer, C.; Beck, A.; Ekanayake, R. S. K.; Branson, J. A.; Neill, T.; Fellhauer, D.; Reitz, C. Y.; Schild, D.; Brager, D.; Cahill, C.; Windorff, C.; Sittel, T.; Ramanantoanina, H.; Haverkort, M.; Vitova, T.; Kaufmann-Heimeshoff, H. (2025, March 18). *Resonant inelastic X-ray scattering tools to count 5f electrons of actinides and probe bond covalency*. 54èmes Journées des Actinides (JdA 2025), Annecy, France, March 18–21, 2025.

33. Schenk, S.; Ramanantoanina, H.; Fellhauer, D.; Schacherl, B.; Prüßmann, T.; Vitova, T. (2025, August 25). *Investigation of Pu Bonding Properties using X-ray Spectroscopic and Computational Methods*. RÅC International Summer School (2025), Tallin, Estonia, August 24–31, 2025.

34. Sittel, T.; Becker, K.; Polly, R.; Müllich, U.; Geist, A.; Panak, P. J. (2025, October 1). *Cs-137 extraction from chloride brines using calixarene crown ethers – selectivity explained by coordination chemistry*. International Solvent Extraction Conference (ISEC 2025), Melbourne, Australia, September 29–October 3, 2025.

35. Vitova, T. (2025, December 20). *Detecting Localized and Delocalized 5f Electron Density in Actinide Bonding by Experimental and Theoretical X-ray Spectroscopy*. Pacifichem (2025), Honolulu, HI, USA, December 15–20, 2025.

36. Vitova, T. (2025, June 19). *X-ray Spectroscopic Probing and Tuning of Lanthanide Binding Properties*. 30th Rare Earth Research Conference (RERC 2025), Chicago, IL, USA, June 15–19, 2025.

37. Vitova, T. (2025, August 29). *Multispectral X-ray Spectroscopy of Actinide Compounds*. RÅC International Summer School (2025), Tallin, Estonia, August 24–31, 2025.

38. Vitova, T.; Schacherl, B.; Ramanantoanina, H.; Kaufmann, H.; Schenk, S.; Prüßmann, T.; Tagliavini, M.; Haverkort, M. W.; Bajaja, A.; Autschbach, J.; Bagus, P. (2025, September 21). *Advanced X-Ray Spectroscopic Tools for Probing 5F Electron Participation in Actinide Bonding*. 19th International Conference on the Chemistry and Migration Behavior of Actinides and Fission Products in the Geosphere (Migration 2025), New Orleans, LA, USA, September 21–27, 2025.

39. Wolf, J.; Fürst, P. Q.; Cevirim-Papaioannou, N.; Duckworth, S.; Gaona, X.; Altmaier, M.; Geckeis, H. (2025, November 25). *Retention of Tc by Fe(II) solid phases: Combining wet chemistry experiments and spectroscopic data*. 1st Joint TecRad-RULET Autumn School on Technetium and other Fission Products (2025), Dresden, Germany, November 24–27, 2025.

Proceedings

1. Becker, F. B. E.; Biswas, S.; Dagan, R. (2025). Bewertung von Strahlenfeldern in tiefengeologischen Endlagern für abgebrannte Brennelemente im Hinblick aufverschiedene Neutronenstreuungsformalismen. *Strahlung - natürlich! Natürlich mit Strahlenschutz!*, 135–138, TÜV Media.

2. Becker, F. B. E.; Biswas, S.; Dagan, R. (2025). Monte-Carlo-Simulationen von Strahlungsfeldern in tiefengeologischen Endlagern für abgebrannte Brennelemente und zugehörige dosimetrische Aspekte. *Strahlung - natürlich! Natürlich mit Strahlenschutz!*, 110–113, TÜV Media.

3. Bremer, J.; Azzola, J.; Schätzler, K.; Bauer, F.; Kohl, T. (2025). *Engaging Schools and Communities in Geothermal Monitoring: Theoretical Framework and Case Studies from the DeepStor Research Infrastructure (Germany)*. Copernicus. doi:10.5194/egusphere-egu25-16396

4. Deon, F.; Lüth, S.; Sass, I.; Giese, R.; Milsch, H.; Hoffert, U.; Grimmer, J. C.; Neuwirth, N.; Haaf, N.; Schüth, C.; Rudolph, B.; Zimmermann, G. (2025). GeoLaB exploration in the Odenwald: towards the realization of an underground geothermal laboratory. *European Geothermal Congress 2025*.

5. Haaf, N.; Häfner, V.; Schill, E. (2025). RockBlockEx - A laboratory scale hydraulic fracturing experiment at differential stress of up to 20 MPa. *50th Workshop on Geothermal Reservoir Engineering 2025 : Stanford, California, USA, 10-12 February 2025*, Curran Associates.

6. Haaf, N.; Tolba Talaat, A.; Pavez, M.; Bauer, F.; Cornejo-Trivino, N.; Schill, E. (2025). Characterizing Structural Elements in the Heat Anomalies of the Upper Rhine Graben using Gravimetric and Seismic Data. *European Geothermal Congress 2025*.

7. Häusler, F.; Gaona, X.; Lassin, A.; Garbev, K.; Skerencak-Frech, A.; dos Santos, P.; Touzelet, S.; Cartigny, Y.; Altmaier, M.; Madé, B. (2025). Solubility and thermodynamics of the Eu(III)-Na/Mg-NO-HO systems. *Goldschmidt2025 abstracts*, European Association of Geochemistry. doi:10.7185/gold2025.29720
8. Huber, N.; Guidone, R. E.; Gaona, X.; Garbev, K.; Lopez-Garcia, M.; Alcubierre, L.; Bocchese, F.; Brassinnes, S.; Altmaier, M.; Geckeis, H. (2025). Uptake of Nb(V) by calcite and carbonated cement systems: impact of isosaccharinic acid and chloride. *5th International Symposium on Cementation of Nuclear Wastes (NUWCEM 2025)*.
9. Kiefer, C.; Gaona, X.; Altmaier, M.; Fellhauer, D. (2025). *Thermodynamic Reference Database (THEREDA): Updated Pitzer activity model for Tc(IV) solubility and hydrolysis in the Tc(IV)–NaK –Mg –Ca –H–Cl–OH–HO(l) system*. European Association of Geochemistry. doi:10.7185/gold2025.29751
10. Lassin, A.; Häusler, F.; Gaona, X.; Madé, B.; Altmaier, M.; Shang, C.; Greb, F. (2025). Solubility and thermodynamics of the systems. *Goldschmidt2025 abstracts*, European Association of Geochemistry. doi:10.7185/gold2025.28165
11. Neles, J. M.; Becker, F.; Hassel, T.; Leusmann, T.; Metz, V.; Scharf, I. (2025). 40 plus X years interim storage of high active waste. *safeND 2025 | 17–19 September 2025, Berlin, Germany*, Copernicus. doi:10.5194/safend2025-128
12. Panjiyar, L.; Finck, N.; Stephan-Scherb, C. (2025). Early anaerobic corrosion of potential canister material in compacted bentonite. *safeND 2025*, Copernicus. doi:10.5194/safend2025-95
13. Rudolph, B.; Neuwirth, N.; Schätzler, K.; Kohl, T.; Olaf, K.; Sass, I. (2025). GeoLaB – the URL for Geothermal Energy. *EGC 2025 - European Geothermal Congress, Zürich, 6th - 10th October 2025*.
14. Tolba, A. T.; Bauer, F.; Grimmer, J. C.; Dashti, A.; Kohl, T. (2025). First identification of fluvial channels by advanced spectral decomposition in Chattian syn-rift successions of the central Upper Rhine Graben: Implications for subsurface energy storage. *EGU General Assembly 2025*, 10539, Copernicus. doi:10.5194/egusphere-egu25-10539

Reports

1. Bremer, J.; Kohl, T.; Sass, I.; Kolditz, O.; Rudolph, B.; Rühaak, W.; Köbe, W.; Dehmer, D.; Schamp, J.; Grimmer, J. C.; Scheuvens, D.; Schüth, C.; Deon, F.; Lüth, S.; Haaf, N.; Hoffert, U.; Milsch, H.; Giese, R.; Zimmermann, G.; Könitz, D.; Rink, K.; Şen, Ö. O.; Goldstein, S.; Jahn, M.; Steinhülb, J.; Bauer, F.; Selzer, M.; Schätzler, K. (2025). *GeoLaB Annual Report 2024*. GeoLab. doi:*10.5445/IR/1000184950*
2. Neles, J.; Becker, F.; Hassel, T.; Leusmann, T.; Metz, V.; Scharf, I. (2025). *Aspekte im Hinblick auf eine Neugenehmigung von Zwischenlagern für hochradioaktive Abfälle und abgebrannte Brennelemente nach 40 Jahren Betriebslizenz*. Technische Universität (TU Clausthal). doi:*10.21268/20241213-0*

Dissertations

1. Alzaydan, M. A. (2025, January 21). *Influence of Carbonate on the Radium Uptake by Barite and Witherite*. PhD dissertation. Karlsruher Institut für Technologie (KIT). doi:10.5445/IR/1000177635
2. Singh, A. R. (2025, October 9). *Metallic corrosion at the steel/bentonite interface under anoxic and water saturated conditions*. PhD dissertation. Karlsruher Institut für Technologie (KIT). doi:10.5445/IR/1000184722
3. Zunftmeister, L. (2025, July 21). *Kinetics and interfacial processes during the recrystallization of calcite and barite, and their influence on radionuclide incorporation*. PhD dissertation. Karlsruher Institut für Technologie (KIT). doi:10.5445/IR/1000180379

Research Data

1. Wang, B.; Da Roit, N.; Schild, D.; Zimmermann, M.; Wang, Y.; Yu, Z.; Chen, S.; Behrens, S. (2025, February 13). *Research data to "Single-Step Synthesis of Dimethyl Ether from Syngas over Nanoparticle-Derived Bifunctional Pd/CeO2/Al2O3 Catalysts"*. doi:10.35097/4jh897ny0tvjsa2e
2. Gill, N. M.; Heberling, F.; Göttlicher, J.; Finck, N.; Metz, V.; Geckeis, H. (2025, July 30). *Iron Induced Alteration of Bentonite to Serpentine Minerals at 90°C*. doi:10.35097/8h72ev2htzrt4hgb

Audio/Video

1. Bremer, J.; Schwald, R.; Schätzler, K. (2025). GeoLaB - Forschungslabor Geothermie: Die Erkundungsphase (Kurzfilm). doi:10.5445/IR/1000185406
2. Bremer, J.; Schwald, R.; Schätzler, K.; Rudolph, B.; Kamrani, S. (2025). GeoLaB – Geothermal Research Laboratory: The Exploration Phase. doi:10.5445/IR/1000185722
3. Bremer, J.; Schwald, R.; Schätzler, K.; Rudolph, B.; Kamrani, S. (2025). GeoLaB - Forschungslabor Geothermie: Die Erkundungsphase. doi:10.5445/IR/1000185495
4. Fuchs, S.; Geckeis, H. (2025). „70 Jahre Entsorgungsforschung in Karlsruhe“ – Das Institut für Nukleare Entsorgung des KIT und die schwierige Suche nach einem Endlager - Campus-Report am 10.06.2025. doi:10.5445/IR/1000182361

INE Scientific Working Documents
ISSN 2701-262X

www.kit.edu